Structural studies of integral membrane GPCR accessory proteins

Barbara Sladek

Department of Biochemistry and St John's College,

University of Oxford

A thesis submitted in partial fulfilment of the requirements for the degree of

Doctor of Philosophy at the University of Oxford

Oxford, Trinity Term 2013

ABSTRACT

Structural studies of integral membrane GPCR accessory proteins

Department of Biochemistry and St John's College, University of Oxford
Submitted for the degree of Doctor of Philosophy, Trinity 2013

GPCR accessory proteins regulate the strength, efficiency and specificity of signal transfer upon receptor activation. Due to the inherent difficulties of studying membrane proteins *in vitro* and *in vivo*, little is known about the structure and topology of these small accessory proteins. Two examples of GPCR accessory proteins are the Melanocortin-2 receptor accessory protein (MRAP) and the Receptor-activity-modifying protein (RAMP) family. MRAP and RAMP1 are the main focus of this thesis in which they are thoroughly characterised by solution-state NMR and further biophysical techniques.

The single-pass transmembrane domain protein MRAP regulates the class A GPCR melanocortin receptors. It is specifically required for trafficking the melanocortin-2-receptor from the endoplasmic reticulum to the cell surface and subsequent receptor activation. A remarkable characteristic of MRAP is its proposed native dual-topology, which leads to an antiparallel homodimeric conformation. Investigation of the biochemical and biophysical properties of MRAP revealed an α-helical transmembrane domain, and an α-helical N-terminal LD(Y/I)L-motif. Further efforts concentrated on establishing the homodimeric conformation of MRAP *in vitro*.

RAMP1 facilitates receptor trafficking and alters the ligand specificity of the GPCR Class B receptors calcitonin receptors and calcitonin receptor-like receptors. Moreover, RAMP1 is required to act as a Calcitonin-gene-related peptide (CGRP) receptor (RAMP1). RAMP1 has been shown to form stable parallel homodimers in the absence of its cognate receptor. Its dimerisation and the possible dimerisation motif PxxxxP-motif were studied extensively.

With the goal of understanding the mechanism of dimerisation and the role of GPCR accessory proteins I have used solution-state NMR in detergent micelles as my main technique. NMR provides unique possibilities for understanding the structure and dynamics of such small membrane proteins.

This thesis is dedicated to my family

"Everybody thinks of changing the world, but no one thinks of changing himself."

(Leo Tolstoy - Three Methods Of Reform)

ACKNOWLEDGEMENTS

I would first wish to express my warmest thanks for the enormous support, encouragement and advice I have received from my supervisor, Dr Jason R. Schnell. His leadership, intellect and scientific rigour served me as an excellent example and motivation. Jason's attention to detail, hard work and openness to new ideas allowed me to learn many methodologies, which added significantly to my scientific development. Without his patience and understanding this thesis would have not been possible.

I also would like to express my sincerest thanks to Dr. Jolyon Claridge, Dr. Jose Luise Ortega-Roldan and Jacob Brady, from whom I benefited greatly from the input and discussion on a daily basis in the laboratory. Special thanks goes to Amanda Buyan, who shared her knowledge on molecular dynamic simulation with me. They all contributed to some great memories in the lab, pub, or while punting.

Dr. Michele Erat, Dr. John Vakonakis and Dr. George Hatzopoulos as well as Dr. Camilla Oxley in the New Department of Biochemistry, Oxford, shared not only their knowledge on NMR and protein biochemistry with me, but also many thoughts (whether they were about science or life in general). Dr. Christina Redfield and Dr. Jonathan Boyd were of constant help and advice when it came to NMR. Dr. David Staunton taught me multiple biophysical techniques and helped me so much through my first steps at Oxford. Moreover, I would like to thank Professor Iain D. Campbell for the initial introduction to Oxford in 2007/08.

My thesis was generously founded by the New Department of Biochemistry, Oxford. I wish to acknowledge additional travel funding from St John's College Oxford, which allowed me to attend several conferences, and thus allowed me to meet and learn from countless researchers at several interesting places.

Special thanks goes to Benjamin Oestringer and Christina Mayer, for their friendship, endless support and encouragement. I further wish to thank Gregory Wyatt for supporting me over the last few months and for giving me strength to stay positive. Many friends outside the lab deserved to be thanked, too. Hannah, Thomas, Julia, Maria, Leigh, Andreas, Michael and Tatjana are just some of the most important ones. My dear parents and immediate family have always supported me and have been a great help throughout my student years - DANKE.

TABLE OF CONTENTS

Abstract..... i
Acknowledgements..... ii
List of Figures..... iii
List of Equations..... iv
List of Abbreviations..... v

CHAPTER 1: Introduction to membrane, membrane proteins and intra-membrane dimerisation..... 1
1.1 From Organisms to Protein Structures..... 2
1.2 The Tools of Structural Biology..... 3
1.2.1 X-ray crystallography..... 5
1.2.2 Electron microscopy..... 6
1.2.3 Molecular dynamic simulations..... 6
1.2.4 NMR spectroscopy..... 7
1.3 Biological Membrane Structure..... 11
1.3.1 Composition of lipid membranes..... 12
1.3.2 Glycerol backbone and headgroup structures of lipids..... 13
1.3.3 Biophysical properties of lipid membranes..... 14
1.4 Membrane Proteins..... 16
1.4.1 Small integral transmembrane proteins prefer α-helical formation..... 17
1.4.2 Amino acid distribution and architecture of integral transmembrane..... 17
1.4.3 Membrane insertion and topology of integral transmembrane proteins..... 20
1.4.4 Interaction between transmembrane helices..... 22
1.4.5 Shape complementarity between transmembrane helices..... 29
1.5 Introduction to G-Protein Coupled Receptors..... 30
1.5.1 Classification of GPCRs..... 30
1.5.2 Signalling pathways of GPCRs..... 32
1.5.3 Structural features of GPCRs..... 33
1.5.4 GPCR maturation and regulation..... 36
1.5.5 GPCR accessory proteins..... 37
1.6 Aims of the Thesis Work..... 40

CHAPTER 2: The use of NMR for studying membrane proteins..... 41
2.1 Membrane mimetics for the study of membrane proteins..... 42
2.1.1 Micelles..... 43
2.1.2 Mixed micelles and bicelles..... 45
2.1.3 Liposomes and Nanodiscs..... 46
2.2 Introduction to the basic principles of protein NMR..... 48
2.2.1 The basic NMR experiment..... 48
2.2.2 One-dimensional ^{1}H NMR experiments..... 53
2.2.3 Two-dimensional NMR experiments..... 53

2.2.4 Nuclear Overhauser Effect Spectroscopy…….. 59
2.2.5 3D Triple-resonance Experiments……... 60
2.2.6 Strategies for determining membrane protein structures by solution- state NMR……..... 62
2.2.7 Increasing the structure quality with additional restraints…… 65

CHAPTER 3: Methods and Materials……. 70
3.1 Protein Production……... 71
3.1.1 DNA sub-cloning and mutagenesis…… 72
3.1.2 Protein expression and uniform isotope labelling…… 73
3.1.3 Protein Purification……... 75
3.2 Protein Identification and Analysis…… 77
3.2.1 Sodium dodecyl sulphate polyacrylamide gel electrophoresis (SDS-PAGE)…… 77
3.2.2 Mass spectrometry (MS)…….. 77
3.2.3 Protein concentration determination…… 78
3.3 NMR sample detergent reconstitution…… 79
3.3.1 Reconstitution of MRAP……... 79
3.3.2 Reconstitution of RAMP1tm constructs…… 79
3.3.3 Alternative reconstitution methods…… 80
3.4 NMR Methods…….. 81
3.4.1 NMR spectrometers and spectral analysis…… 81
3.4.2 Sequential resonance assignments…….. 82
3.4.3 Chemical shift perturbation……..……... 84
3.4.4 Residual dipolar couplings…….. 84
3.4.5 NMR-based structure calculations…….. 85
3.4.6 NMR-based dynamics analyses of MRAP and RAMP1tm…… 86
3.4.7 Site-specific paramagnetic relaxation enhancement experiments for MRAP(2-67) ……... 87
3.4.8 Water-soluble paramagnetic broadening enhancement…….. 89
3.4.9 Hydrogen-deuterium exchange measurements in RAMP1tm……... 90
3.4.10 Hydrodynamic radius determination by pulse gradient field experiments…… 90
3.5 Biochemical methods…….. 92
3.5.1 Chemical crosslinking with DSP and glutaraldehyde…… 92
3.5.2 Studies of MRAP dimerisation via disulphide bonds formation……... 93
3.5.3 Circular dichroism…… 95
3.5.4 Dynamic light scattering……... 96
3.5.5 Analytical ultracentrifugation (AUC) …… 97
3.6 Computational studies of MRAP…….. 99
3.6.1 Theoretical background…… 99
3.6.2 MD software and practical choices…… 103

CHAPTER 4: Structural and biophysical characterisation of monomeric MRAP.. 106
4.1 INTRODUCTION…… 107
4.1.1 Melanocortin system and the Melanocortin Receptors…… 107
4.1.2 Melanocortin Receptor Accessory Proteins……... 113
4.1.3 Aims of studying MRAP on a molecular level…….. 120
4.2 RESULTS……... 122
4.2.1 Secondary structure prediction and transmembrane insertion prediction... 122
4.2.2 Construct design rationale…….. 124
4.2.3 Expression and purification of MRAP(2-67) ……. 126
4.2.4 Establishing suitable conditions for MRAP(2-67) …… 128
4.2.5 Circular Dichroism of MRAP(2-67) …… 136
4.2.6 Spectroscopical characterisation and structure determination……... 137
4.2.7 The structure of MRAP is robust and detergent-independent……... 174

CHAPTER 5: Investigations into MRAP dimerisation…… 177
5.1 INTRODUCTION…… 178
5.1.1 What governs membrane topology? …….. 178
5.1.2 Evidence for dual topology and antiparallel homodimerisation……... 180
5.1.3 Aim of studying the MRAP antiparallel dimer……. 182
5.2 RESULTS……..… 184
5.2.1 Anomalous gel mobility of MRAP(2-67) in SDS……... 184
5.2.2 Chemical crosslinking of MRAP(2-67) ……..…… 185
5.2.3 Biochemical analysis of the dimeric interface of MRAP(2-67) via disulphide bonds in membranes…… 186
5.2.4 Attempts to acquire intermolecular NOEs for a dimeric MRAP(2-67)…….. 189
5.2.5 Concentration dependence and peak doubling of MRAP(2-67)…… 190
5.2.6 Investigation of the transmembrane domain of MRAP……... 195
5.2.7 Investigation of the roles of post-translational modifications in MRAP(2-67) ……... 198
5.2.8 Biophysical investigation of MRAP(2-67) …… 200
5.2.9 Molecular dynamic (MD) studies of MRAP intermolecular interactions…. 203
5.3 DISCUSSION……... 219
5.3.1 Investigation of the monomeric MRAP…….. 219
5.3.2 What could drive dimerisation? …… 219

CHAPTER 6: Towards a structural understanding of the transmembrane domain of Receptor Activity Modifying Protein 1……... 221
6.1 INTRODUCTION…….. 222
6.1.1 Function of RAMPs and their interaction with GPCRs……... 223
6.1.2 Expression and disease relevance of RAMPs…… 226
6.1.3 The structure of RAMP1……... 228
6.1.4 A likely interaction pathway of RAMP1 with CLR…….. 230
6.1.5 Current knowledge about dimerisation of RAMP1…… 231
6.1.6 Aims of studying RAMP1 on a molecular level…… 232

6.2 RESULTS..... 233
6.2.1 Construct design rationale and amino acid distribution..... 233
6.2.2 Prediction of RAMP1tm secondary structure and possible dimerisation..... 234
6.2.3 Expression and purification of RAMP1tm constructs..... 236
6.2.4 Establishing suitable reconstitution conditions for RAMP1tm constructs... 237
6.2.5 Circular dichroism of RAMP1tm constructs..... 240
6.2.6 Spectroscopic characterisation and structure determination..... 242
6.2.7 Comparison of chemical shift perturbation between two RAMP1tm constructs..... 252
6.2.8 Establishing a dimeric interface..... 253
6.2.9 Structure calculation of the parallel dimeric RAMP1tm(116-148)..... 258
6.2.10 Dynamics of RAMP1tm constructs in 40 mM SDS..... 260
6.2.11 Investigation of the depth of insertion of RAMP1tm(102-148) in 40mM SDS micelles..... 266
6.2.12 Mutational studies and close examination of the dimeric interface..... 269
6.3 DISCUSSION..... 276
6.3.1 How robust is the transmembrane region of RAMP1? 276
6.3.2 What is the impact of the N-terminal domain on dimerisation? 277
6.3.3 What is the role of the PxxxxP-motif? 277
6.3.4 What drives dimerisation? 277

CHAPTER 7: Conclusion and Outlook..... 279
7.1 Findings concerning MRAP in general..... 280
7.2 Findings concerning RAMP..... 282
7.3 Future directions and experiments in progress..... 282
7.3.1 Future directions for studies of MRAP..... 283
7.3.2 Future directions for studies of RAMP..... 285

BIBLIOGRAPHY..... 287

APPENDIX..... 324
Appendix I: Additional Experiments..... 325
Investigation of the N-terminal domain of MRAP(2-67) by solution NMR..... 325
Interaction of MRAP(2-67) with the ligand ACTH..... 326
Towards a PRE-based method for measuring MRAP dimerisation..... 328
Study of a plausible dimeric interface by mutational studies..... 330
Appendix II: Cloning protocols and primers..... 338
Primers for MRAP..... 339
Primers for RAMP..... 342

LIST OF FIGURES

1.1: Schematic representation of an eukaryotic cell..... 2
1.2: Numbers of protein structures solved..... 4
1.3: Schematic representation of an eukaryotic cell membrane..... 11
1.4: Common glycerophospholipids..... 12
1.5: Schematic representation of typical motions in a cell membrane..... 15
1.6: Variations in the association of membrane proteins with the lipid bilayer..... 16
1.7: Insertion of transmembrane helices..... 21
1.8: Schematic illustration of factors that can influence helix-helix interactions..... 23
1.9: Examples for dimerisation motifs..... 23
1.10: Activation of GPCRs..... 32
1.11: Structural outline of GPCRs..... 35
1.12: GPCR regulation..... 37
1.13: GPCR accessory proteins RAMPs and MRAP..... 39

2.1: Schematic representation of micelles and bicelles. 44
2.2: NMR pulses..... 50
2.3: 1D ^{1}H-NMR spectrum of MRAP..... 53
2.4: The HSQC experiment..... 55
2.5: HMQC and SOFAST-HMQC pulse sequence..... 56
2.6: Magnetisation transfer during a TOCSY experiment..... 58
2.7: Magnetisation transfer of experiments..... 60
2.8: Typical NMR-derived structural restraints..... 64
2.9: Residual dipolar coupling..... 66
2.10: Schematic illustration of conformational events in membrane proteins..... 68

3.1: Vector map of pMM-LR6 (Kan^{R}) vector with the trpΔLE gene..... 72
3.2: Schematic model of PRE measurements..... 88
3.3: Chemical structures of Glutaraldehyde and DSP..... 92
3.4: Atomistic vs. coarse-grained representations of DPPC..... 102

4.1: Sequence alignment of human melanocortin receptors..... 109
4.2: Schematic overview of interaction between MRAP and MC2R..... 111
4.3: Hypothetical model of the interaction between MRAP and MC2R..... 114
4.4: Schematic representation of essential MRAP regions..... 117
4.5: Schematic representation of MRAP and MRAP2..... 118
4.6: Secondary structure predication of MRAP..... 122
4.7: MRAP(2-67) sequence analysis..... 123
4.8: Alignment of human MRAP..... 124
4.9: Alignment of MRAPα in different species..... 125
4.10: Expression and Purification of MRAP(2-67) 126
4.11: Properties of detergents..... 131
4.12: MRAP(2-67) characterisation..... 132
4.13: The impact of DMPG on MRAP(2-67) 134

4.14: Temperature dependence of MRAP(2-67) 135
4.15: Circular dichroism spectra of MRAP(2-67) 136
4.16: Intramolecular NOEs of MRAP(2-67) 138
4.17: Sidechain assignment of MRAP (2-67) 139
4.18: Dipolar wave analysis..... 142
4.19: Investigation of the structure of MRAP(2-67) 145
4.20: Ramachandran plot of MRAP(2-67) 146
4.21: Correlation plots of ^{15}N-$^{1}H_N$ RDC data sets of MRAP(2-67) 149
4.22: Correlation plots of ^{15}N-$^{1}H_N$ RDC data sets of MRAP (2-67) 151
4.23: Correlation plots of ^{15}N-$^{1}H_N$ RDC data sets of MRAP(2-67) 151
4.24: {^{1}H}-{^{15}N} heteronuclear NOEs of MRAP(2-67) in different detergents..... 153
4.25: R_1 of MRAP(2-67) in different detergents..... 155
4.26: R_2 of MRAP(2-67) in different detergents..... 156
4.27: Dynamics of MRAP(2-67) in 100mM DHPC..... 160
4.28: Dynamics of MRAP(2-67) in 50 mM SDS..... 161
4.29: Dynamics of MRAP(2-67) in mixed micelles..... 162
4.30: Interaction of MRAP(2-67) with the detergent..... 165
4.31: Chemical shift perturbation difference of MRAP(2-67) 167
4.32: Paramagnetic broadening enhancement in 100 mM DHPC..... 169
4.33: Paramagnetic broadening enhancement in 50 mM SDS..... 170
4.34: Paramagnetic broadening enhancement in mixed micelles..... 171
4.35: Further investigation of the N-terminal domain..... 173
4.36: Electrostatic potential for MRAP(2-67) 175

5.1: MRAP(2-67) anomalous gel mobility on SDS-PAGE..... 184
5.2: Crosslinking of MRAP(2-67)P66KQ67K..... 186
5.3. Monomerising of MRAP(2-67) and solubility in solvent..... 187
5.4: Membrane assay of MRAP(2-67) 189
5.5: Concentration dependence of MRAP (2-67) in DHPC..... 191
5.6: Concentration dependence of MRAP (2-67) in 50 mM SDS..... 193
5.7: Concentration dependence of MRAP(2-67) in mixed micelles..... 194
5.8: The transmembrane domain of MRAP(2-67) 197
5.9: Mimicking of phosphorylation of MRAP (2-67) 199
5.10: Dynamic light scattering of MRAP (2-67)..... 201
5.11: Analytical Ultracentrifugation of MRAP(2-67) 203
5.12: Initial set up for CG-MD simulations..... 205
5.13: Coarse-grain simulation of MRAP(13-67) in BOND..... 206
5.14: Coarse-grain simulation of MRAP(13-67) in MARTINI2.2..... 208
5.15: Coarse-grain simulation of Glycophorin A in MARTINI2.2..... 209
5.16: Simulation of a right-handed antiparallel MRAP(13-67) homodimer..... 211
5.17: Simulation of a left-handed antiparallel MRAP(13-67) homodimer..... 212
5.18: Interface of an antiparallel MRAP (13-67) homodimer..... 214
5.19: Simulation of a parallel right-handed MRAP(13-67) homodimer..... 215
5.20: Atomistic simulation of a parallel MRAP (13-67) homodimer..... 216
5.21: Atomistic simulation of a parallel MRAP(13-67) homodimer..... 218

6.1: Sequence alignment of human RAMP family members…….. 222
6.2: Heterodimerisaion of CLR and RAMPs……. 224
6.3: Physiological function of CLR/RAMP1…….. 227
6.4: Schematic representation of essential RAMP1 regions…… 228
6.5: Structural features of the molecular surface of RAMP1……... 229
6.6: Schematic representation of a proposed cycle of RAMP1/CLR complex…….. 231
6.7: Alignment of RAMP1tm(102-148) in multiple organisms……... 233
6.8: Predication of transmembrane domain topology of RAMPtm……... 235
6.9: Secondary structure prediction of the transmembrane domains…… 236
6.10: Flowchart for the production and purification of RAMP1tm……... 238
6.11: Detergent screening for RAMPtm1(102-148) …….. 240
6.12: Circular dichroism spectra of RAMP1tm(116-148) …… 241
6.13: Intramolecular NOEs of RAMP(102-148) in 40 mM SDS…….. 243
6.14: Characterisation of RAMP1tm(102-148) and RAMP1tm(116-148) …….. 244
6.15: Dipolar wave analysis……. 245
6.16: Investigation of the structure of RAMP1tm…… 248
6.17: Ramachandran plot of RAMP1tm constructs…….. 249
6.18: Correlation plots of ^{15}N-$^{1}H_N$ Residual Dipolar Coupling data sets…….. 251
6.19: Difference between long RAMP1tm constructs……... 253
6.20: Crosslinking of RAMP1tm(116-148) …… 254
6.21: Concentration dependency of RAMP1tm…… 257
6.22: Dimeric RAMP1tm(116-148) structure in 40 mM SDS…….. 259
6.23: Dynamics of RAMP1tm(102-148) and RAMP1tm(116-148) …….. 263
6.24: Motional Anisotropy of RAMP1tm …….. 265
6.25: Water-soluble paramagnetic broadening enhancement…… 267
6.26: Hydrogen/deuterium exchange…… 268
6.27: Dimeric RAMP1tm(116-148) structure…….. 269
6.28: Circular dichroism spectra of RAMP1tm(116-148) …… 270
6.29: Crosslinking of V133A, V137A……... 271
6.30: Mutational studies of RAMP1tm(116-148) by NMR……... 272
6.31: Crosslinking of P121A/L and P126A/L…… 273
6.32: Mutational studies of RAMP1tm(116-148) by solution NMR……... 274

Appendix 1: Investigation of the N-terminal domain of MRAP(2-67) …… 325
Appendix 2: MRAP(2-67) - ACTH titration in mixed micelles…….. 327
Appendix 3: Paramagnetic relaxation enhancement experiments on MRAP(2-67) in mixed micelles……. 329
Appendix 4: Mutations in MRAP(2-67) …… 331
Appendix 5: Mutations in MRAP(2-67) in 100mM DHPC…….. 333
Appendix 6: Mutations in MRAP(2-67) in 50mM SDS…… 335
Appendix 7: Mutations in MRAP(2-67) in mixed micelles……. 336
Appendix 8: Further investigation of the N-terminal domain……... 337

LIST OF EQUATIONS

Eq.1: Larmor frequency……... 49
Eq.2: Gyromagnetic ratio……. 49
Eq.3: Resonance frequency…… 50
Eq.4: Chemical shift scale..…….. 51
Eq.5: Karplus equation……..……... 52
Eq.6: relationship between T2 and linewidth……... 52
Eq.7: Residual Diploar Coupling…… 65
Eq.8: correlation time…….…... 69
Eq.9: Chemical shift perturbation……... 85
Eq.10: Mean Residue Weight……... 96
Eq.11: Mean Residue Ellipticity…….. 97
Eq.12: MD force field…… 101

ABBREVIATION LIST

ACTH – adenocorticotropic hormone
AGRP – agouti-related proteins
AM – adrenomedullin
AMRX – adrenomedullin receptor X
ASP – agouti signalling protein
AT – atomistic
BTL – Brain Total Lipids
cAMP – cyclic adenosine monophosphate
CasR - calcium^{2+}-sensing receptor
CD – circular dichroism
CG – coarse grain
CGRP – calcitonin gene related peptide
CHAPS - 3-[(3-cholamidopropyl)dimethylammonio]-1-propanesulfonate
CL – cardiolipin
CLR – Calcitonin-like receptor
CMC – Critical micelle concentration
CNBr – cyanogen bromide
CPMG – Carr-Purcell-Meiboom-Gill
CSA – chemical shift anisotropy
CSP – chemical shift perturbation
CTR – calcitonin receptor
DAG – diacylglycerol
DDM – n-dodecyl β-D-maltopyranoside
DHPC – 1,2-dihexanoyl-*sn*-glycero-3-phosphocholine
diC7PC – 1,2-diheptanoyl-sn-glycero-3-phosphocholine
DLS – dynamic light scattering
DMPC – 1,2-dimyristol-sn-glycero-3-phosphocholine
DMPG – 1,2-dimyristoyl-sn-glycero-3-phospho-(1'-rac-glycerol (sodium salt)
DMSO – dimethylsulfoxide
DPPC – 1,2-dipalmitoyl-*sn*-glycero-3-phosphocholine
DPPG – 1,2-dipalmitoyl-*sn*-glycero-3-phospho-(1'-*rac*-glycerol) (sodium salt)
DSS – disuccinimidyl suberate
DTT – dithiothreitol
EDDA – ethylendiamindiacetat
EDTA – ethylenediaminetetraacetic acid
ERK – extracellular signal-regulated kinases
FID – free-induction decay
FT – Fourier transformation
GpA – glycophorin A
GPCR – G-protein coupled receptor
HFIP – 1,1,1,3,3,3-hexafluoro-2-propanol

HMQC – heteronuclear multiple-quantum correlation
HPLC – high-pressure liquid chromatography
HSQC – heteronuclear single-quantum correlation
INEPT – intensive nuclei enhanced by polarisation transfer
IPTG – Isopropyl-β-D-thiogalactopyranoside
LMPG - 1-myristoyl-2-hydroxy-sn-glycero-3-[phospho-RAC-(1- glycerol)]
LPPG - 1-palmitoyl-2-hydroxy-sn-glycero-3-[phospho-RAC-(1-glycerol)]
MAPK – mitogen-activated protein kinases
MCXR – melanocortin-X-receptor
MD – molecular dynamics
MM – molecular mechanics
MRAP – melanocortin-2-receptor accessory protein
MSH – melanocyte-stimulating hormone
MTSL – (S-(2,2,5,5-tetramethyl-2,5-dihydro-1H-pyrrol-3-yl)methyl-methanesulfonothioate
MWCO – molecular weight cut-off
NMR – nuclear magnetic resonance
NOE – nuclear Overhauser effect
NOESY - nuclear Overhauser effect spectroscopy
OD – optical density
OMIM – Online Mendelian Inheritance in Man
PA –phosphatidic acid
PC – phosphatidylcholine
PCR – polymerase chain reaction
PDB – protein data dank
PE - phosphatidylethanolamine
PFG – pulse field gradient
PG-SLED - pulse gradient stimulated echo longitudinal encode-decode
POMC – proopiomelanocortin precursor
POPC – 1-palmitoyl-2-oleoyl-sn-glycero-3-phosphocholine
ppm – parts per million
PRE – paramagnetic relaxation enhancement
PS – phophatidylserine
PTHRX - parathyroid hormone receptor X
QM-MM – quantum mechanical molecular mechanic
RAMPX – receptor-Activity-Modifying Protein X
RDC – residual dipolar coupling
rf – radiofrequency
RMSD – root-mean square deviation
SCTR – secretin receptor
SDS – sodium dodecyl sulphate
SDS-PAGE – sodium dodecyl sulphate polyacrylamide gel electrophoresis

SOFAST-HMQC – band-selective optimized flip-angle short-transient heteronuclear multiple quantum coherence
SM – sphingmyolin
SDSL – site-directed spin labelling
StAR – steroidogenic acute regulatory gene
TCEP – tris(2-carboxyethyl)phosphine
TFE – 2,2,2-trifluoroethanol
TOCSY – total correlation spectroscopy
TROSY – transverse relaxation optimised spectroscopy
VPAC1 – vasoactive intestinal polypeptide receptor 1
YPL – yeast polar lipids

CHAPTER 1

INTRODUCTION TO MEMBRANES, MEMBRANE PROTEINS AND INTRA-MEMBRANE DIMERISATION

"Nothing in life is to be feared, it is only to be understood. Now is the time to understand more, so that we may fear less."

(Marie Curie)

1.1 FROM ORGANISMS TO PROTEIN STRUCTURES

Living organisms are extraordinarily diverse, nonetheless they all have a principle unit of life in common: the cell. Each cell contains the machinery necessary for the basic functions of life that includes harnessing energy from the environment and reproduction (Alberts 2008). All cells are surrounded by cell membranes, which create a barrier between the intracellular and extracellular compartments. Plasma membranes have the crucial function of creating selective permeability, enabling exchange of only certain molecules, energy and information across the membranes. More complex organisms, such as eukaryotes, contain membrane-enclosed organelles within a cell that enable further compartmental specialisation. Examples of intracellular organelles include the endoplasmic rediculum (ER), Golgi vesicles, and mitochondria (Figure 1.1.).

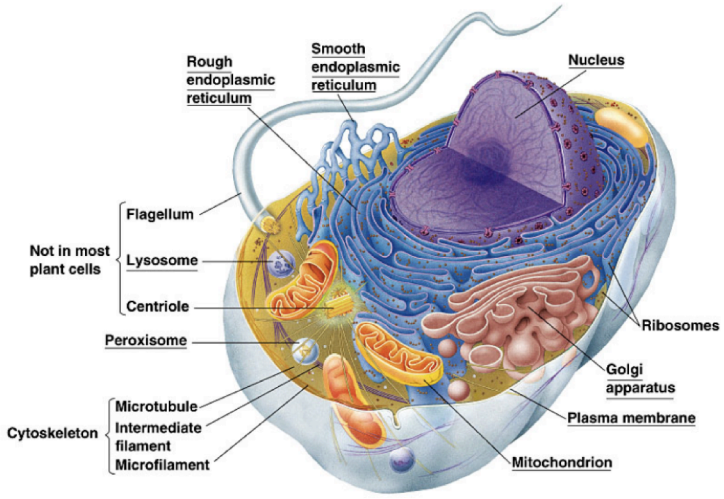

Figure 1.1: Schematic representation of an eukaryotic cell
(Image copyright Pearson Education Inc.; published by Benjamin Cummings)

Proteins are often referred to as the "workhorses" of a cell, and mediate a variety of different functions both within a cell and at the cell membrane. Flexibility allows proteins to provide molecular level microenvironments, such as enzyme active sites, or give shape and stability to communities of cells, such as some extracellular matrix

proteins. Proteins that are integral to the cell membrane play pivotal roles in a large number of cellular processes. They mediate the transport of specific molecules across the membrane or catalyse membrane-associated reactions, such as ATP synthesis. Additionally, some membrane proteins are structural links connecting the cytoskeleton through the lipid bilayer to either the extracellular matrix or an adjacent cell, while others act directly as receptors to detect and transduce chemical signals from the environment (Alberts 2008).

Mutations in membrane proteins are involved in many common diseases, like heart disease, cancer, neurodegenerative disorders, congenital conditions, obesity and many more. It is therefore not surprising that over 50 % of small molecule drugs interact with membrane proteins (Adams et al. 2012). In particular, ion channels and G-protein coupled receptors (GPCR) are of major pharmacological interest. Therefore, gaining accurate insights into the structure of these proteins and how they are regulated on the molecular level, which can lead to a more accurate understanding of the relationship between protein structure and function, may facilitate development of more effective treatments and offer possibilities for the design of specifically targeted drugs.

1.2 THE TOOLS OF STRUCTURAL BIOLOGY

Several techniques exist to determine the structure of proteins. In 1958, myoglobin was the first protein structure to be solved (Kendrew et al. 1958), and was determined using X-ray crystallography. Since then, nuclear magnetic resonance (NMR) and electron microscopy (EM) have been developed to the point at which they also can be used to determine protein structures to high resolution. In addition, molecular dynamic (MD) simulations can be used as a complementary approach to assess motion and dynamics

and to build structural models of experimentally challenging proteins. In some cases, data from one or more experimental techniques are integrated into MD simulations to further understand and extend the structural insights. X-ray crystallography remains the most widely used experimental approach, with more than 80,000 structures having been determined to date (RSCB Protein Data Bank statistics, accessed 18 September 2013). This compares with ~10,000 structures by NMR, and ~650 by EM. Figure 1.2 highlights the phenomenal growth of available protein structures, starting from year 1976, and the contributions of different structural biology techniques. The growth in the number of deposited structures has increased exceptionally over the last 20 years.

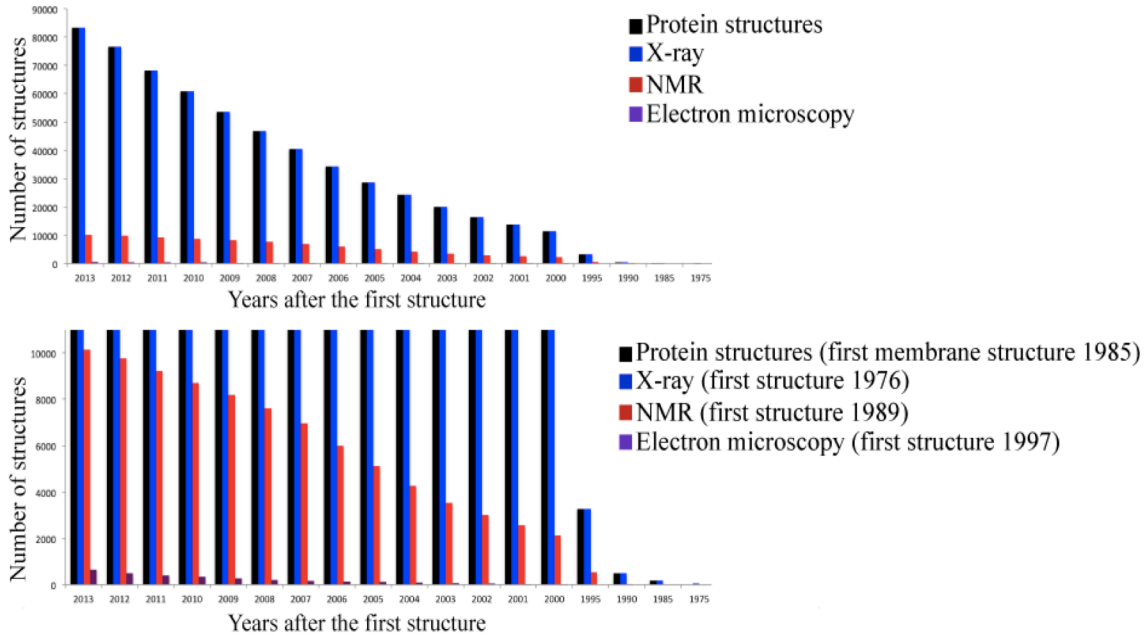

Figure 1.2: Numbers of protein structures solved by different experimental methods. Data was collected from the RCSB PDB database.

Understanding the atomic level structure of membrane proteins and their orientation within the membrane environment can reveal factors that drive the molecular interactions leading to functions such as transport and signalling (Brändén & Tooze 1999). However, the structural and functional properties of membrane proteins originate

from heterogeneous interactions with molecules like amphipathic lipids, polysaccharides, cholesterol, proteins, and water. The complex environment of native membranes makes the task of understanding their structure and function extremely challenging, and determination of high-resolution structures of membrane proteins is one of the most challenging areas of structural biology nowadays. All methods used to determine protein structures encounter similar problems when targeting membrane proteins: (i) the requirement to obtain sufficient (~milligram) quantities of purified protein, and (ii) the tendency for membrane proteins to rapidly unfold during the purification process as they are removed from the natural lipid bilayer environment (Lacapère et al. 2007).

While the number of known membrane protein structures is growing, it lags greatly behind that of water-soluble membrane proteins: ~1300 membrane protein structures have been deposited in the PDB out of >90,000 total depositions. This is even more striking considering that ~30 % of the proteins encoded in an average genome are membrane proteins (Alberts 2008).

1.2.1 X-ray crystallography

X-ray crystallography uses diffraction patterns from macroscopic crystals of protein molecules. The construction of atomic protein coordinates, which matches the electron density is performed by Fourier transform (Brändén & Tooze 1999). X-ray crystallography is a highly successful tool to study the structure of proteins and, in theory, there are no limitations to protein size. However, a major challenge is that the studied molecule must be coated into a crystal lattice containing a regular array of lattice contacts. This can be exceedingly difficult to achieve with membrane proteins

since they need to be solubilised into a dynamic coating of detergents or lipids (Carpenter et al. 2008). In addition, once formed, the crystal lattice can lead to difficulties during the interpretation of the results since the determined structure represents a single structural snapshot of the protein "locked" in a single conformation, and that conformation may be influenced by the crystal contacts. In addition, although evidence of protein flexibility can be extracted from X-ray diffraction data, its interpretation is complicated by the potential presence of static disorder within the crystal lattice (Brändén & Tooze 1999).

1.2.2 Electron Microscopy

Electron microscopy (EM) has great potential for determining structures of proteins and especially macromolecular assemblies, however it is not yet fully exploited. To determine an atomistic resolution protein structure using EM is difficult due to specimen damage during the application of the sample to the support grid, and also by the electron beam (Orlova & Saibil 2011). Further obstacles include specimen hydration, problems related to the thickness of the specimen, a "missing cone" of data in tilt series imaging, and estimating non-linearity in the so-called contrast transfer process (Frank 2006). However, over the last few years macromolecular structure determination on a near-atomic resolution level was achieved using single particle analysis of electron cryo-microscopy (Bai et al. 2012). Recently, the first structure of the mammalian transient receptor potential channel V1 was solved at a resolution of 3.4 Å (Liao et al. 2013).

1.2.3 Molecular Dynamics simulations

MD simulations are a powerful tool for complementing experimental studies, providing insights in biological processes at the molecular and atomistic level and offer the

possibility to evaluate structure and dynamics of proteins using theoretical methods. This does require that the simulation setup allows assessment of the question addressed. Two different methods are mainly used to elucidate large conformational changes in proteins: coarse-grained (CG) representations and atomistic (AT) resolution (Pluhackova et al. 2012). The CG-MD approach is especially suited to study orientation and interactions of large systems such as membrane proteins within lipid bilayers, however it lacks the atomistic details (Shelley et al. 2001; Marrink et al. 2004). AT-MD approaches allow more detailed analyses of the properties of a system, but are limited to smaller systems and shorter simulation times due to the required computation time; this limitation means that the approach might not fully sample all dynamic processes that exist in reality (Stansfeld & Sansom 2011). In a typical membrane protein simulation, the experiment starts with either an experimentally determined or hypothetical protein structure, to which water, lipids (membrane), and ions are added. To mimic ambient experimental conditions, MD simulations are often conducted either under constant temperature (310 K) and constant pressure (1 atm), while keeping the total number of particles in the system constant or under conditions in which the volume of the system is kept constant (Shaikh et al. 2013).

1.2.4 NMR spectroscopy

NMR spectroscopy has played an important role in the structure determination of bio-macromolecules, ranging from proteins to nucleic acids, for nearly three decades. A key strength of NMR spectroscopy is that atomic-level structural and dynamical details of proteins can be observed under native conditions of temperature and hydration. This has enabled detailed structural and dynamical insights that are inaccessible through

other biophysical means. Nowadays, NMR spectroscopy is an alternative as well as a complementary technique to X-ray crystallography (Levitt 2013).

NMR spectroscopy makes use of the nuclear spins of atoms in the protein. Some of the useful properties of nuclear spins are: (i) in the presence of an applied external magnetic field they have preferred orientations that can be perturbed by radiofrequency radiation, (ii) the magnitude of the external magnetic field at a particular nuclear spin depends on the chemistry and environment of that spin ('chemical shift'), (iii) they 'couple' via electrons to other bonded nuclear spins in a conformational dependent manner ('J-coupling'), and (iv) nuclear spins interact through space in dipole-dipole interactions ('nuclear Overhauser enhancements' or NOE) (Cavanagh 2007; Keeler 2011). Protein structure determination by solution-state NMR has traditionally depended heavily on distance restraints from NOEs and bond angle restraints from 3-bond J-couplings. Increasingly, residual dipolar couplings and extensive heavy atom chemical shift measurements are being used to provide additional structural constraints related to bond angles and secondary structures, respectively.

Two NMR methods developed over the years are solution and solid-state NMR spectroscopy. In solution-state NMR studies the protein is not confined to a single conformation by a crystal lattice, and a more straightforward interpretation of protein dynamics is thus possible. Measuring different solution-state NMR parameters enables the collection of motion information from the picosecond to nanosecond and microsecond to millisecond time scales (Dürr et al. 2012). Indeed, solution-state NMR is without parallel in its ability to quantify dynamics over a wide range of timescales. Small collections of atoms can undergo restricted motion on fast time scales (picosecond

- nanosecond), while larger elements of structure can undergo large amplitude motions with slower correlation times (Rösner & Kragelund 2011).

In addition, NMR chemical shifts are highly sensitive to chemical environment and molecular conformation, and are thus often used to probe for intermolecular interactions or changes in structure during biological processes such as ligand or protein-protein binding, or upon changes in other solution conditions. Recent developments in fast data acquisition methods are resulting in the ability to monitor even very rapid changes. Such studies help to narrow the gap between structural and functional understanding and are often highly complementary to X-ray crystallographic studies.

A major limitation within the field of solution-state NMR is molecular size, which affects the tumbling time of the protein resulting in broad signals that lowers sensitivity and also increases spectral overlap. Narrowing spectral lines at high magnetic field strengths and developing new sources of restraints for the structure calculation however can extend the size limit. The upper limit of molecular weight for full structure determination using standard NOESY-based approaches is currently ~50 kDa, but is constantly being pushed higher with techniques such as heteronuclear direct detection, higher magnetic field strengths, the development of new types of restraints for structure calculations, and the use of selective labeling (particularly for methyl groups). For targeted studies of local interactions or dynamics, proteins of nearly 1 megaDalton have been studied by solution NMR (Mainz et al. 2013).

Over the last decade, solid-state NMR has developed rapidly and showed its potential as technique for determining structural properties of membrane proteins and

characterising their ligand binding and dynamics. Magic-angle spinning and static-oriented solid-state NMR are the two main solid-state methods. Solid-state NMR offers the possibility to directly examine membrane proteins in a bilayer environment (Korukottu et al. 2008; Ader et al. 2010). The resolution and sensitivity of solid-state NMR however, is lower than that of solution-state NMR, since the signals are affected by the size and orientation-dependence of the nuclear spin interactions, i.e. the chemical shielding and the homonuclear and heteronuclear dipolar spin–spin couplings (Tapaneeyakorn et al. 2011).

1.3 BIOLOGICAL MEMBRANE STRUCTURE

A typical biological membrane is a complex structure that is composed of a bilayer of lipids, incorporated proteins and small amounts of carbohydrates (Alberts 2008; Giraldo & Pin 2011). The hydrophobic core of the lipid bilayer is about 30 ± 10 Å thick, while the membrane-water interfacial region adds another ~15 Å thick region on both sides of the membrane (White & Wimley 1999). Since Singer *et al*. (Singer & Nicolson 1972) first proposed the "fluid mosaic model", new biophysical properties such as membrane density, permeability and flexibility, have been introduced to describe a membrane. Recent studies suggested that biomembranes often have distinct domains that are in either 'lipid-ordered' (i.e. lipids rafts, which are glycolipoprotein microdomains) and 'lipid-disordered' states (Lingwood & Simons 2009).

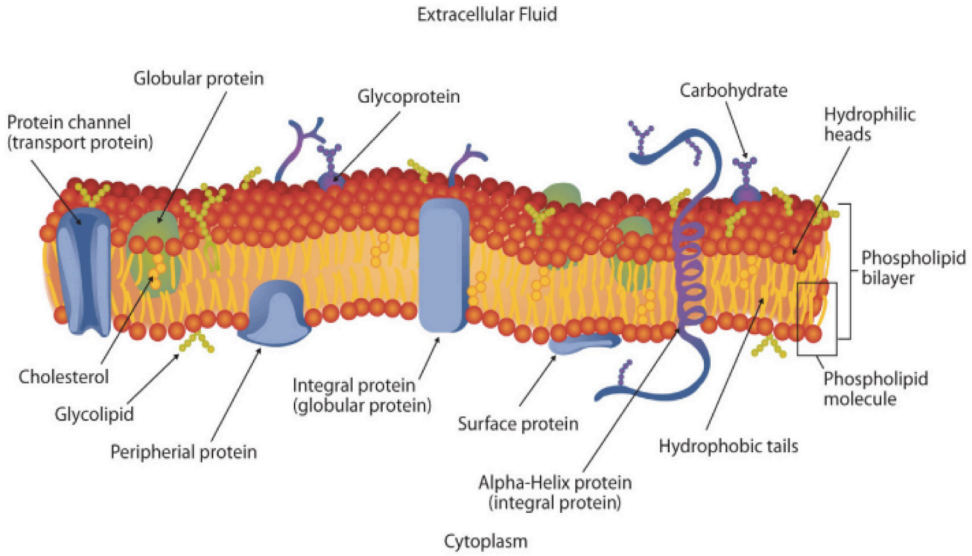

Figure 1.3: Schematic representation of an eukaryotic cell membrane (Figure taken from David W. Ball, John W. Hill, and Rhonda J. Scott)

1.3.1 Composition of lipid membranes

The importance of lipids is shown by the fact that ~5 % of the entire cell genome is used to specify lipid synthesis (van Meer et al. 2008). Besides forming a structural barrier, lipids can also serve as energy stores in form of triacylglycerol esters and sterol esters (van Meer & de Kroon 2011), or function as second messengers in signal transduction and molecular recognition processes (van Meer et al. 2008; van Meer & de Kroon 2011). Lipid-lipid, protein-lipid and protein-protein interactions within a biomembrane are responsible for cell segregation, compartmentalisation and specification of membrane micro-domains (van Meer et al. 2008; Alberts 2008). The major lipid components of plasma membranes are glycerophospholipids, sphingolipids and cholesterol, with glycerophospholipids being most abundant (Griffiths 2007; Feigenson 2007) (shown in Figure 1.4).

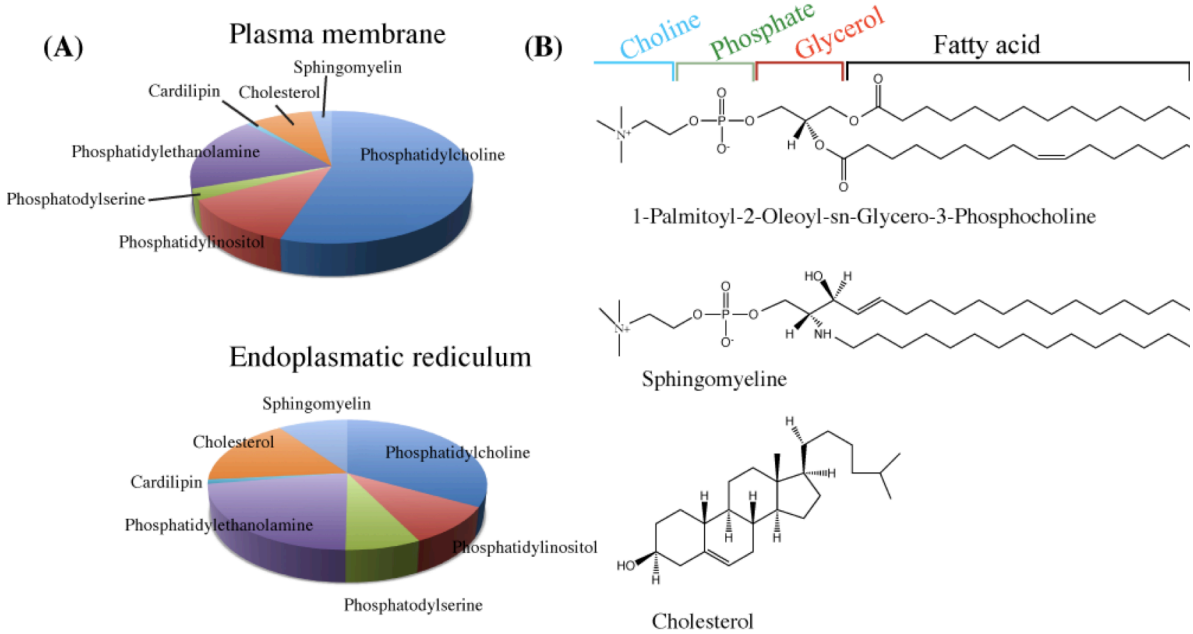

Figure 1.4: Common glycerophospholipids found in biomembranes
(A) Distribution of phospholipids and cholesterol in eukaryotic membranes. (B) Chemical structure of the three most common lipids. (Figure adapted from van Meer et al. 2011)

This class of lipids are amphipathic hydrocarbon polymers, with hydrophobic tails of varying lengths (C8-C30). Sphingolipids are the second major component in eukaryotic biological membranes and have a long saturated fatty acid chain (C16–C32) with an amide linkage to the sphingoid base. Sphingomyelins are often closely associated with cholesterol to form segregated lipid micro-domains, or lipid rafts (Lingwood & Simons 2009). Figure 1.4 depicts the distribution of some of the main components in the plasma membrane and the ER as well as their chemical structure.

1.3.2 Glycerol backbone and headgroup structures of lipids

Glycerophospholipids comprise a *sn*-glycero-3-phosphate backbone that is bound via ester bonds to two hydrophobic hydrocarbon chains at carbons numbers one and two of the glycerol backbone (Figure 1.4 (B)). Their phosphate group is bound to a polar, relatively rigid headgroup, which defines the phospholipid class.

Phosphatidylcholines, which make up ~50 % of phospholipids in most eukaryotic membranes, are located mainly in the outer leaflet together with sphingomyelin and glycosphingolipids. Aminophospholipids, phosphatidylserine and phosphatidylethanolamine lipids, as well as minor lipids containing phosphatidylinositol or phosphatidic acid, are actively concentrated in the cytosolic leaflet (Ikeda et al. 2006; van Meer et al. 2008). This composition of five to ten major lipid classes, with different lengths of saturated or unsaturated fatty acids, enables the flexibility and curvature observed within eukaryotic biological membranes.

Lipid phases are generally classified by the packing of acyl chains and the curvature of the membrane surface. These characteristics arising from the complex composition of bilayers facilitates vesicle formation, fusion, membrane sorting and signal transduction

as well as accommodating proteins with different sized hydrophobic transmembrane regions (Giraldo & Pin 2011; Pan et al. 2012; Ikeda et al. 2006; van Meer & de Kroon 2011).

Importantly, headgroup diversity modulates electrostatic potential in and near the membrane surface, a feature many central biological processes rely on (Dowhan 1997). Each headgroup undergoes steric interactions with a hydrophobic diacylglycerol (DAG) domain, which comprises saturated or *cis*-unsaturated fatty acyl chains of varying lengths (van Meer et al. 2008).

1.3.3 Biophysical properties of lipid membranes

Membranes are highly dynamic and their biophysical features are important controlling elements in cell signalling. Membrane protein function can be strongly modulated by membrane lipid composition and organisation. Glycerophospholipids spontaneously self-assemble into a planar bilayer structure, which is dictated by lateral attractive and repulsive forces, including hydrophobic, van der Waals, steric, dipole–dipole and electrostatic interactions (Marsh 2013). In an aqueous environment, lipids shield their hydrophobic tails from the surrounding polar fluid, exposing the hydrophilic heads to water. This arrangement minimises the free energy of the water-lipid system (Griffiths 2007), and efficiently prevents polar solutes from diffusing across the membrane and simultaneously allows hydrophobic molecules to passively diffuse across (Giraldo & Pin 2011). The fluidity of the membrane is modulated by the acyl-chain length and saturation with the van der Waals interactions, which are countered by the packing defects and steric clashes introduced by *cis*-double bonds (Pan et al. 2012; Alberts 2008).

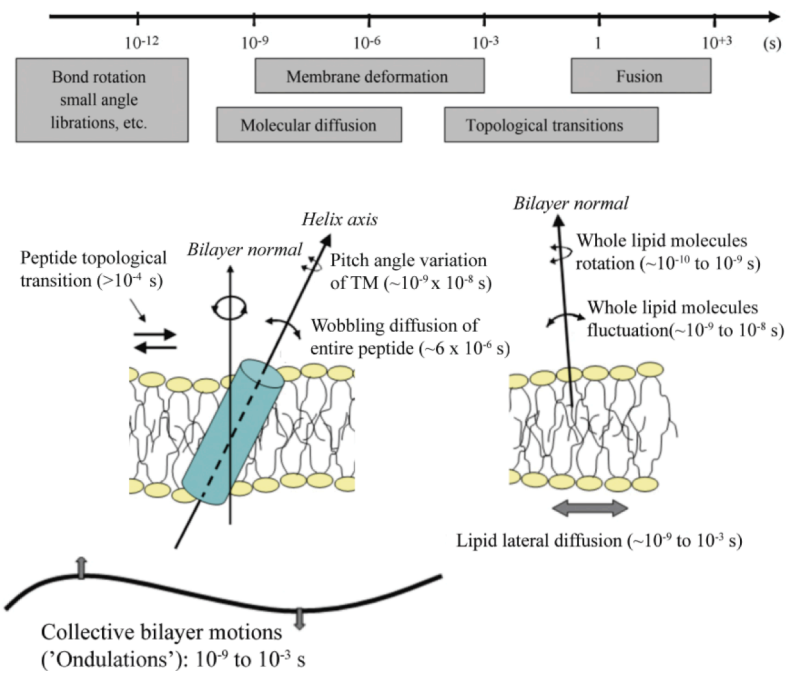

Figure 1.5: Schematic representation of typical motions and their characteristic time-scales in a cell membrane. Peptide helices are shown in blue in a transmembrane. (Adapted from B. Bechinger and E. S. Salnikov, 2012)

However, membrane fluidity can be heterogeneous within the same membrane, with highly ordered lipid rafts forming adjacent to more disordered regions of membrane. Typically, membrane components have considerably large motional freedom depending on the timescale. Lateral movements include rotations and translations of individual lipid molecules, collective motions of several lipid molecules together, as well as local movements of parts of a lipid molecule. These motions can be described by their amplitude and frequency, and are influenced by curvature-induced stresses and the packing of different lipids. In contrast, axial movement of lipids between the leaflets of the bilayer is a slow process, but ATP-dependent transporter kinases, flippases can catalyse this process (Devaux 1988). Thus, while the lipid bilayer is dynamic, it contains both axial and lateral asymmetry, which can be rapidly modulated to allow for bidirectional information transfer (Grecco et al. 2011). Figure 1.5 is a schematic representation of membrane motion types and the time scales over which they occur.

1.4 MEMBRANE PROTEINS

Membrane proteins account for ~30 % of the proteins encoded in the human genome (Stevens et al. 2008; Almén et al. 2009) and perform most of the highly specific functions of a membrane, such as signal transduction, immune recognition and cell adhesion. They are therefore major drug targets.

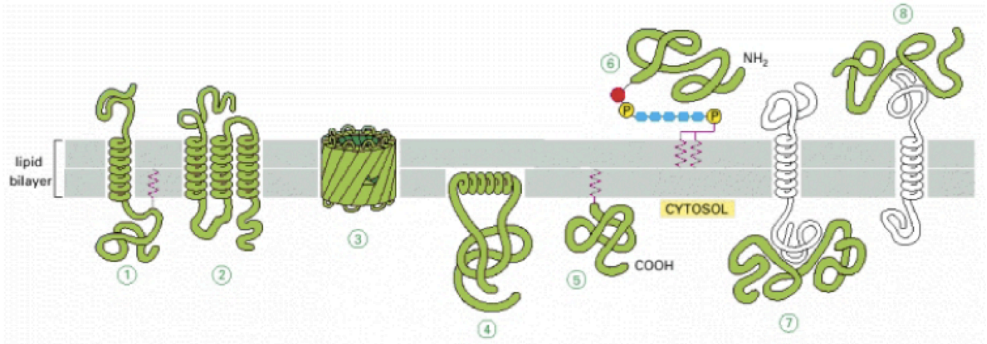

Figure 1.6: Variations in the association of membrane proteins with the lipid bilayer. (Taken from Alberts, 2008)

Five classes of membrane proteins can be distinguished (Figure 1.6) (Alberts 2008):

1. Integral membrane proteins span both bilayer leaflets (e.g. transporters, channels, receptors) (Figure 1.6; 1 & 2).
2. Peripheral proteins that interact with only one leaflet of the cell membrane surface (Figure 1.6; 4).
3. Proteins that bind to the membrane via the lipid head groups (Figure 1.6; 5).
4. Proteins that tether to the membrane via a covalent hydrophobic anchor that inserts into the membrane (Figure 1.6; 6).
5. Proteins that are water-soluble, whilst able to integrate into the membrane (Figure 1.6; 7 & 8).

Integral membrane proteins are further subdivided into two families according to their secondary structure: α-helical and β-barrel. The work in this thesis focuses on α-helical integral membrane proteins. The membrane-embedded helices can be short (with a

minimum of ~15 residues), long (up to ~30 residues, but possibly longer), kinked or interrupted in the middle of the membrane, they can cross the membrane at oblique angles, or possibly even span only a part of the membrane and then turn back, forming so-called re-entrant loops.

1.4.1 Small integral transmembrane proteins prefer α-helical formation

In general, both α-helices and β-sheets satisfy the requirement to shield the polarity of the protein backbone. However, the vast majority of known integral membrane-spanning domains are α-helical. α-helical transmembrane regions have the ability to satisfy all backbone hydrogen bonds locally (within 4 residues) within a single transmembrane helix. Driven by the hydrophobic effect and main-chain hydrogen bonding, α-helices additionally allow a modular nature resulting in a great architectural diversity (Popot & Engelman 2000; Beevers & Dixon 2010). In comparison, β-barrels require long-range interactions between multiple β-strands (at least 8) to fold correctly (Fairman et al. 2011). β-barrels are exclusively found in the outer membrane of bacteria and mitochondria possibly because the barrel architecture allows non-selective movement of ions across the membrane.

1.4.2 Amino acid distribution and architecture of integral transmembrane

The separation of the residues along the axis of an α-helix is ~1.5 Å per residue. Thus, a membrane-spanning α-helix requires ~20 residues or more to traverse the hydrophobic core of a typical lipid bilayer (White & Wimley 1999). However, transmembrane domains can also tilt within the membrane. Driving forces for tilting are hydrophobic

mismatch, depending on the length of helix, as well as helix self-association (de Planque et al. 2003). A further reason for a helix-tilt is the variation in chain length of different lipids, which changes the depth of the membrane. In order to accommodate all hydrophobic amino acids within the transmembrane region helical tilt angles can increase in membranes with shorter lipid chains (Beevers & Dixon 2010). Statistical comparison of 45 known membrane proteins indicated an average tilt angle of 22.0º ± 11.6° in transmembrane helices (Ulmschneider & Sansom 2001).

α-helical transmembrane domains comprise two structural features: a central region spanning the membrane acyl-chain region and a high percentage of hydrophobic amino acids (e.g. valine, leucine, isoleucine, and phenylalanine). Flanking regions often contain a mixture of positively charged residues (i.e., arginine and lysine) and amphipathic aromatic amino acids such as tryptophans and tyrosines. These residues act as anchoring residues to stabilise the helix within the bilayer and to discourage peptide aggregation (van der Wel et al. 2000; Huschilt et al. 1989).

Most hydrophobic amino acids distribute unsystematically along the transmembrane region, however, alanine has a preference for the interior of α-helical regions in multispanning proteins (Ulmschneider & Sansom 2001). Similarly, glycine residues are fairly common in transmembrane α-helices, where they may facilitate tight helix-packing (MacKenzie et al. 1997). Overall, polar residues are relatively rare in the transmembrane domain. However, threonine and serine residues are the most frequently found polar residues within the hydrophobic segment and can be important for helix-helix association, and are often involved in the folding of multispan membrane proteins (Arkin & Brunger 1998; Dawson et al. 2002; Nyholm et al. 2007). Their

distribution might be explained by their ability to form hydrogen bonds with adjacent carbonyl oxygens (Eilers et al. 2000).

Prolines are located infrequently within transmembrane domains. Though, when located in the core of transmembrane proteins they do not break the helix, but rather induce kinks and bends or form molecular hinges in the helical backbone (Senes et al. 2004). Prolines thus influence the torsional angle preference of the residues preceding it in the sequence (the pre-Pro position), which can lead to stabilisation of more extended conformations relative to the helical conformation. Moreover, this amino acid can function as a conformational switch in helices within receptors and channels (Lu et al. 2001; Tieleman et al. 2001). Prolines also have a high packing propensity in transmembrane domains, which can lead to further stabilisation of helix–helix packing (Senes et al. 2004).

In general, hydrophobic amino acids in the transmembrane region favour free energy of transfer from water to bilayer and hence stabilise helices within the membrane. Although polar amino acids have unfavourable free energies of transfer, they are often required for protein function to be placed in the membrane (Popot & Engelman 2000; Granseth et al. 2005). Compared to the hydrophobic acyl-chain region of the bilayer, the interfacial region presents a chemically complex environment with its carbonyl phosphate groups, lipid headgroups, and water molecules (Wallin et al. 1997). Aromatic residues, such as tryptophan and tyrosine, and the hetero-aromatic residue histidine often enrich the interfacial region as a consequence of their hydrogen bond forming ability and their dipolar but still hydrophobic character (Wallin et al. 1997; van der Wel et al. 2000; de Planque et al. 2003). Tryptophan side chains at the interfacial region tend

to be orientated towards the interface while residues located further out tend to direct their side chains toward the bilayer core (Granseth et al. 2005). Moreover, tryptophans frequently flank the transmembrane region in phospholipid bilayers and resist displacement either toward the aqueous phase or toward the membrane interior (Braun & von Heijne 1999).

The charged residues arginine, lysine, aspartate and glutamate are frequently found in bordering non-translocated cytoplasmic segments, and the distribution of arginine and lysine residues can be up to two to four times higher on the cytoplasmic side than the lumen or extracellular side of the membrane (von Heijne 1986; Ulmschneider et al. 2005; Nilsson et al. 2005). These residues are crucial for creating specific topology of membrane proteins (von Heijne 1986). When newly synthesised membrane proteins insert into a membrane, the lysine and arginine residues prefer a *cis*-side orientation, while aspartate and glutamate residues are found more frequently at the *trans*-side of the membrane (Wallin et al. 1997).

1.4.3 Membrane insertion and topology of integral transmembrane proteins

The thermodynamic process of topology is mainly determined during the initial insertion of the polypeptide chain into the membrane. In cells, transmembrane helix insertion is mediated by the translocon. Two prominent translocons are the prokaryotic SecYEG (Driessen et al. 1998) system and the eukaryotic homolog, the Sec61 translocon in the rough ER (Greenfield & High 1999; Berg et al. 2003). The Sec61 translocon forms a protein-conducting channel across the ER membrane and is used by all secretory proteins to gain entry into the secretory pathway. It is also used by membrane proteins,

however transmembrane helices are not translocated all the way across the membrane, but rather shunted sideways into the lipid bilayer, presumably through a 'lateral gate' in the wall of the translocon (Alder & Johnson 2004).

The attributes tilt angle, topology and orientation are thought to be interlinked in the translocation process (Figure 1.7). Single helical transmembrane segments can span across the membrane in three possible ways:

- Class I: an N-terminal cleavable signal peptide and an internal apolar stop-transfer sequence (Kuhn 1987).
- Class II: an N-terminal or internal uncleaved signal.
- Class III: an N-terminal start-stop transfer sequence peptide (von Heijne & Gavel 1988).

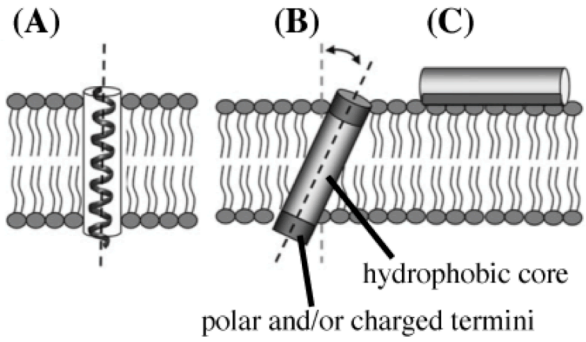

Figure 1.7: Insertion of transmembrane helices
(A) Whether a transmembrane helix spans across the lipid membrane is dependent on the thickness membrane and the length of the protein.
(B)Transmembrane proteins can be forced to 'tilt' in order to bury the hydrophobic amino acid groups in the apolar core of the bilayer.
(C) Amphipathic helices can interact with both head groups and lipid chains.
(Figure adapted from A. Beevers and A. Dixon, 2010)

To predict the overall orientation of a membrane-spanning protein, one can use the 'charge-difference' rule, which uses net charge difference and the orientation of transmembrane segments (Hartmann et al. 1989). A more elegant strategy to defining the topology of transmembrane domains is the 'positive-inside' rule (von Heijne &

Gavel 1988; von Heijne 1992; Sipos & von Heijne 1993). According to this rule, positively charged amino acids, such as arginine and lysine, primarily flank the cytoplasmic side of the transmembrane domain and dictate the orientation of the single-spanning segments.

The vast majority of membrane proteins are inserted into the membrane with a single topology. However, a growing number of 'dual topology' proteins have been discovered, as described further in Chapter 5. Integral membrane proteins can adopt a dynamic topology. Multiple membrane proteins have the ability to re-orientate one or more of their transmembrane helices post-translationally until they reach their final (stable) topology (von Heijne 2006). Examples include many viral proteins, such as hepatitis B virus (Lambert & Prange 2001) and hepatitis C virus (Cocquerel 2002) envelope glycoproteins. Dynamic topology is linked to their multifunctionality. Both proteins initially insert into the ER with their N-terminal so-called pre-S domains located in the cytoplasm. During the post- translational maturation process, the pre-S domain is then translocated across the membrane in about 50% of the molecules, resulting in a mixed topology with either three or four transmembrane helices for this protein. Finally, it has been shown that the composition of the surrounding lipids can alter insertion orientation of membrane proteins (Bay & Turner 2013).

1.4.4 Interaction between transmembrane helices

A monomeric transmembrane helix can be described as one that interacts more favourably with lipids than with itself or other helices in the membrane (Li et al. 2012). Likewise, helical self-assembly happens when helix–helix or lipid–lipid interactions are slightly favoured over helix–lipid interactions. Several possibilities can shift the

preference towards helix-helix interaction, which are described in the following subchapters (Popot & Engelman 2000; Nyholm et al. 2007; Li et al. 2012).

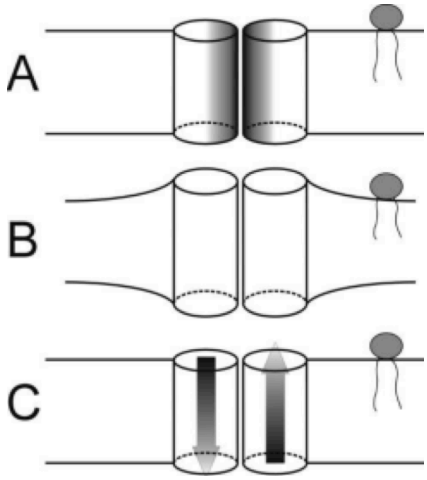

Figure 1.8: Schematic illustration of factors that can influence helix-helix interactions in membranes
(A) Presence of specific recognition motifs or polar residues on one side of the helix promotes association between helices.
(B) Unfavourable interaction between helices and lipids can promote helix self-association (e.g.: effect of positive mismatch between bilayer thickness and the hydrophobic length of the helices).
(C) Favourable interactions between helix dipole moments may promote formation of antiparallel helices. (Figure taken from Nyholm et al. 2007)

1.4.4.1 Interaction between transmembrane helices due to dimerisation motifs

"Helix-helix recognition motifs", also called "dimerisation motifs", drive specific association within transmembrane segments. These motifs favour a helix-helix interaction over helix-lipid interactions in given lipid environment.

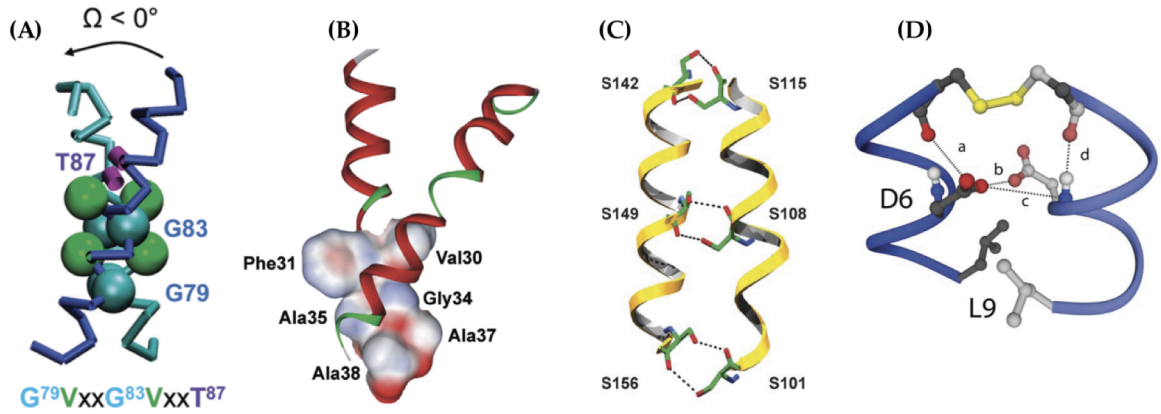

Figure 1.9: Examples for dimerisation motifs
(A)MD representation of the GxxxG-motif of the GpA transmembrane helix dimer, showing the negative helix crossing angle (Ω) and key interfacial residues (Psachoulia et al. 2008).
(B) Structural model of the cytochrome b5590, where dimerisation occurs based on close packing and hydrogen bonding (Weber et al. 2009)
(C) Structures of serine zipper from cytochrome c oxidase (North et al. 2006).
(D) Structural Arrangement of the D6 side chains of the ζζ dimer (call et al. 2006)

1.4.4.1.1 The GxxxG-motif

One of the most well characterised dimerisation motifs is the GxxxG-motif (Russ & Engelman 2000; Doura et al. 2004). Homodimerisation of the membrane-spanning protein sialoglycoprotein, called glycophorin A (GpA), is a prominent example in which dimerisation occurs due to the GxxxG-recognition motif. In several studies, it has been shown that the sequence contribution to dimerisation is best described by the seven amino acid motif LIxxGVxxGVxxT (Lemmon et al. 1992; Treutlein et al. 1992). In this motif the two glycine (Gly79 and Gly83) residues, which are on the same helical face at position *i* and *i+4*, appear to form a "groove" that allows tight helical packing in a so-called "ridges-into-grooves" manner. The GpA dimer adopts a right-handed helix packing, and all seven amino acids are directly involved in helix–helix interactions and align at the contact surface (Figure 1.9) (MacKenzie et al. 1997). This formation was shown to be of special importance for dimerisation, tight packing and dimer stability (MacKenzie & Prestegard 1996; Doura & Fleming 2004).

The presence of the GxxxG-motif has been observed in dimerisation of other membrane proteins. A further example for a membrane protein with such motif is carnitine palmitoyltransferase-1A. Jenei *et al*. (Jenei et al. 2011) showed that dimerisation of carnitine palmitoyltransferase-1A is disrupted by a single glycine mutation in a GxxxG-motif to a bulky isoleucine (Gly107/Ile113) resulting in non-specific self-association.

1.4.4.1.2 The (Sm)xxx(Sm)-motif

Other dimerisation motifs with short side chains separated by three residues, such as the GxxxG-motif, were found to be over-represented in membrane proteins (Senes et al. 2000). Thus, the (Sm)xxx(Sm)-motif, where "Sm" is a small residue (glycine, alanine,

serine or threonine), is often referred to as a "GxxxG-like motif" and was proposed as a general interaction motif for transmembrane helices.

Cytochrome b single-span protein PsbF, containing a GxxxA-motif, is an example of a dimeric membrane protein with one GxxxG-like motif (Figure 1.9) (Weber & Schneider 2013). Though recent findings highlighted that in complex pattern multiple amino acids within the dimerisation motif are needed to determine sequence-specificity of transmembrane dimerisation and helix–helix interactions, which are driven by close packing and inter-helical hydrogen bonding (Weber & Schneider 2013). For instance, several human receptor tyrosine kinase transmembrane domains contain more than one dimerisation motif, which may be involved in the formation of alternative dimer conformations that are involved in the signalling mechanism (Finger et al. 2009; Li et al. 2012). (shortened)

1.4.4.2 Interaction between transmembrane helices due to heptad motifs

Alternative examples of close packing and induced dimerisation include the well-known 'leucine-zipper' motif and other repetitive heptad motifs. This motif has been studied extensively in water-soluble proteins and occurs when hydrophobic amino acids, such as isoleucine and leucine residues, are found at positions *i, i+3 and i+7* which are on the same face of the helix. The increased hydrophobicity and complementary shapes of the sidechains lead to strong helix-helix contacts (Figure 1.9) (Lupas 1996; Qin et al. 2007; Sanders & Mittendorf 2011). The potential for leucine zipper motifs in membrane proteins is high, since the percentage of leucine and isoleucine amino acids in transmembrane regions is high.

Heptad repeats with serine residues have been described as 'serine-zippers' (Adamian & Liang 2002). In this motif serine side chains are spaced at seven-residue increments (SxxLxxx) and shown to form both parallel and antiparallel dimers (Figure 1.9) (North et al. 2006). They were used to design ion channel peptides (Lear et al. 1988) and are known to drive dimerisation in natural proteins, such as erythropoietin receptors (Kubatzky et al. 2001).

1.4.4.3 Interaction between transmembrane helices via polar residues

In comparison to a hydrophobic side chain, a polar side chain in a transmembrane helix creates a thermodynamically unfavourable situation due to exposure to the lipid hydrocarbon chain (White & Wimley 1999). Peptide- and protein-based hydrophobicity scales showed that the cost of placing polar groups into a bilayer can be between 0.3 and 1.0 kcal/mol for a simple polar group (Wimley & White 1996; White & Wimley 1999). Salt bridges and hydrogen bonds between polar groups within the hydrophobic environment can reduce the energetic cost of burial and thereby drive helix dimerisation (Wimley et al. 1996). Thus, polar residues, such as asparagine, glutamine, aspartate, or glutamate residues, strongly promote oligomerisation so that the polar groups can bury within the dimer interface (Gratkowski et al. 2001; Zhou et al. 2001).

The bovine papillomavirus E5 protein is stabilised both by interhelical hydrogen bonding between polar glutamate residues and by the tight packing of leucine residues (King et al. 2011). The ζζ dimer that is necessary for T-cell receptor signalling is stabilised to a large extent by the formation of a tyrosine-threonine interhelical hydrogen bond (Call et al. 2006). A further example is the polar QxxS dimerisation motif in bacterial aspartate receptor (Tar) transmembrane domain (Sal-Man et al. 2004). There

it was shown that interchanging the two polar residues had no effect, whereas mutation of one or the other nonpolar residues reduced dimerisation drastically. Moreover, exchange of the QxxS-motif with the GxxxG-motif disrupted the dimer (Sal-Man et al. 2004).

1.4.4.4 Interaction between transmembrane helices due to hydrophobic mismatch

Protein-lipid interactions result from a balance of forces, which can be sensitive to the deformability of the lipid environment. Hydrophobic mismatch between helices and the membrane can lead to deformation of the lipid bilayer. Deformation of the lipid bilayer is unfavourable since boundaries between the deformed lipids and bulk lipids can lead to strain or exposure of the hydrophobic acyl chains to water. Some of the energetic cost of the deformation can be recovered if helices with similar hydrophobic mismatch are clustered. In this way, hydrophobic mismatch can drive helix association within the membrane (Nyholm et al. 2007) (Figure 1.8). For small, single-span transmembrane proteins, the length of mismatch of lysine- and tryptophan-flanked regions are sufficient to control helix-helix interactions (Mall et al. 2001; Sparr et al. 2005).

1.4.4.5 Interaction between transmembrane helices due to lipid packing and cholesterol

Oligomerisation of integral membrane proteins can be promoted either by the lipophobic effect, which depends on acyl-chain flexibility and a change in lipid packing (Naarmann et al. 2005) or through the presence of cholesterol. Cholesterol impacts the bilayer thickness and its chain ordering (Baier et al. 2010; Loura et al. 2010), resulting in proteins being expelled from sterol-rich domains (Kruijff et al. 2006; Nyholm et al. 2007).

The lipophobic effect decreases toward the bilayer centre since acyl-chain flexibility increases in the vicinity of the terminal methyl groups (Holte et al. 1995). Moreover, more loose packing of the bilayer interior, modulated by the addition of small alcohols and change of lipid–water interface, can affect protein oligomerisation. Overall, physical bilayer matrix alterations can influence peptide association accordingly. However, this contribution influences dimerisation in an opposite direction to that of polar effects (described in subchapter 5.1). An example is the specific interaction of transmembrane domains with the headgroup and backbone of exclusively one sphingolipid spicies (SM18) via the signature sequence VxxxTLxxIY within the helix (Contreras et al. 2012).

1.4.4.6 Interaction between transmembrane helices due to juxtamembrane sequence and transmembrane domain boundaries

The juxtamembrane regions of membrane proteins can have dramatic effects on dimerisation. This can occur directly by specific interfacial interactions, or indirectly by influencing the local bilayer properties, the depth of transmembrane domain membrane insertion, or the allowed rotational angles of transmembrane segments (Broughman et al. 2002). Examples for dimerisation through juxtamembrane sequences is the ErbB family of receptor tyrosine kinases (Muthuswamy et al. 1999; Brewer et al. 2009, Lemmon 2009).

1.4.4.7 Interaction between transmembrane helices due to dipolar-dipolar interactions

In addition, some evidence for the role of favourable helix dipole-dipole interactions helix-helix association has been reported. Dimer formation of a transmembrane helix

was observed when increasing the length of phosphocholine acyl-chains from 14 to 22 carbons. Spelbrink *et al*. (Spelbrink 2005) argued that the reason for an increase in dimerisation was due to an increase in strength of interactions between the helix macro-dipoles as the partial charges are moving into a more hydrophobic environment (Spelbrink 2005; Nyholm et al. 2007).

Furthermore, Sparr *et al*. (Sparr et al. 2005) found that a single transmembrane domain flanked by tryptophans would adopt antiparallel conformation as a result of change in electrostatic environment.

1.4.5 Shape complementarity between transmembrane helices

Helix-helix interactions within transmembrane proteins often contribute to stabilisation of individual helices. Specific helix-helix association can result in closely packed right- and left-handed contacts. Packing is dictated by the spacing of side chains at their surfaces (Chothia et al. 1977). A simple crossing or wrapping around each other of the helices may cause left-handed pairing of two helices. This packing usually creates contacts between every third or fourth amino acid, resulting in a repeat every 7 amino acids ('the heptad repeat'). In a right-handed packing orientation, the contacts occur approximately every four amino acids (Cohen & Parry 1986). An example of a left-handed packing is spectrin (Pascual et al. 1997) and for a right-handed one it is the homodimer GpA (Treutlein et al. 1992). Helix interaction can be again broken by steric clashes at helix-helix interfaces and restrictions of side-chain rotamers.

1.5 INTRODUCTION TO G-PROTEIN COUPLED RECEPTORS

G-protein coupled receptors (GPCR) are one of the largest membrane protein families encoded by the genome and contains approximately 800 members (Stevens et al. 2008). GPCRs exhibit much structural and functional diversity and are responsive to a plethora of endogenous (biogenic amines, cations, lipids, peptides, and glycoproteins) and exogenous (therapeutic drugs, photons, tastants, and odorants) stimuli. They are thus involved in a myriad of cellular processes, and mutations in GPCRs can lead to a wide range of diseases like retinitis pigmentosa (rhodopsin receptor) (Mendes et al. 2005), hypogonadotropic hypogonadism (gonadotropin releasing hormone receptor) (Mendes et al. 2005), familial glucocorticoid deficiency (FGD) (melanocortin 2 receptor) (Chan et al. 2008) and X-linked nephrogenic diabetes insipidus (V2 vasopressin receptor) (van den Ouweland et al. 1992; Heng et al. 2013; Harrison 2013) to name just a few. Approximately 40 % of clinically approved drugs target GPCR signalling, and thus are good targets for drug screening and discovery. The pace of research into new GPCR-based drug discovery has recently accelerated due to rapid advancements in high-resolution structure determination, high-throughput screening technology and *in silico* computational modelling of GPCR binding interactions with potential drug molecules (Heng et al. 2013).

1.5.1 Classification of GPCRs

GPCRs are typified by a seven-transmembrane α-helical bundle (Perez 2005; Kroeze et al. 2003). Despite no shared sequence homology across the superfamily, GPCRs can be grouped into six classes. The classification criteria include phylogeny, sequence

similarity, structural motifs and mechanisms of signal transduction (Schiöth & Fredriksson 2005; Fredriksson et al. 2003). The International Union of Basic and Clinical Pharmacology defined the following classes (Kolakowski LF 1994; Attwood & Findlay 1994; Schiöth & Fredriksson 2005; Sharman et al. 2012):

- Class A: Rhodopsin-like GPCRs
- Class B: Secretin-like GPCRs, including the vasoactive intestinal peptide receptors, calcitonin and parathyroid hormone receptors and receptors for secretin (Hoare 2005; Sexton & Wootten 2013)
- Class C: Glutamate family GPCRs, including the metabotropic glutamate receptors (Chun et al. 2012)
- Class D: Fungal mating pheromone GPCRs, including receptors of fungal mating pheromones (Alberts 2008)
- Class E: Cyclic AMP receptors, including those for chemotactic migration of slime mold (Klein et al. 1988; Goncalves et al. 2010)
- Class F: Frizzles/Smoothened GPCRs, including the Wnt signalling pathway receptors (Fredriksson et al. 2003)

GPCR classes C to F are beyond the scope of this thesis and are not further discussed, but are reviewed in detail by Chun *et al*. (Chun et al. 2012).

Class A has the largest number of members. Rhodopsin-like GPCRs account for ~85 % of all known GPCR genes (>20,000 Class A sequences are listed at (Gautier et al. 2010)). Members of this GPCR class respond to the presence of diverse stimuli ranging from light absorption to the binding of various ligands, including small molecule amines and hormones. Class B GPCRs include several peptide hormone receptors, which are

involved in functions like bone maintenance, glucose regulation, immune function and pain transmission (Sexton & Wootten 2013).

1.5.2 Signalling pathways of GPCRs

In GPCR signalling, an extracellular ligand binds to the receptor and induces a conformational change that is transmitted to the cytoplasmic face of the receptor. GPCRs can then bind one or more cytoplasmic proteins from the four G protein classes Gαs, Gαi/o, Gαq/11, Gα12/13) (Gilman 1987). The GPCR interactions with the hetero-trimeric G proteins catalyse exchange of guanine nucleotides bound to the Gα protein. This in turn results in dissociation of the Gα and Gβγ subunits from each other, as well as the receptor. Depending on the specific subtype, the activated Gα protein subunit can in turn either activate RhoGEF (Gα12/13) or lead to changes in intracellular levels of secondary messengers like cAMP (Gαs & Gαi/o), diacylglycerol (DAG), inositol-1,4,5-triphosphate (IP3) and Ca^{2+} (Gαq/11).

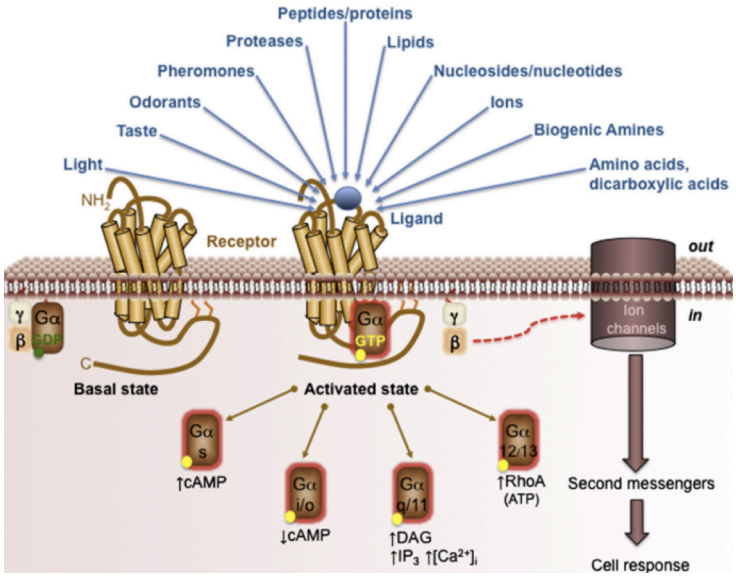

Figure 1.10: Activation of GPCRs GPCRs can be activated by a diverse range of ligands and stimuli. The four major classes of G-proteins (Gαs, Gαi/o, Gαq/11, and Gα12/13) and their associated secondary messengers account for the canonical model of GPCR signalling. (Figure taken from Heng BC et al. 2013)

The dissociated Gβγ subunit is able to bind and activate other downstream effectors such as ion channels. The overall process amplifies the original signal in a cascade (Figure 1.9) (Giraldo & Pin 2011; Heng et al. 2013; Alberts 2008).

1.5.3 Structural features of GPCRs

The first structure of a GPCR to be determined was that of rhodopsin, which was solved by X-ray crystallography in 2000 (bovine rhodopsin (2.8 Å) (Palczewski et al. 2000). Other rhodopsin structures that have been solved include squid rhodopsin (2.5 Å) (Murakami & Kouyama 2008)) and sensory rhodopsin II, which was the first structure of a GPCR solved using solution-state NMR (Gautier et al. 2010). In 2013, the first GPCR class B structure, the human corticotropin-releasing factor 1 (CRF1), was determined by X-ray crystallography (3 Å) (Hollenstein et al. 2013).

GPCRs have highly conserved structural motifs required for receptor biogenesis, protein stability or functionality. GPCRs have one N-glycosylation site at the N-termini, phosphorylation recognition sites for protein kinases A (PKA) and C (PKC) and conserved cysteines near their C-termini (Urwyler 2011). Small and weakly polar amino acids such as glycines, serines, threonines, alanines and cysteines are highly conserved among the GPCR superfamily. These residues are important for mediating transmembrane helix-helix contacts within GPCRs that stabilise the receptors in an inactive conformation in the absence of bound ligand. Strongly polar amino acids, such as aspartate, asparagine, glutamate, glutamine, arginine, lysine and histidine, are necessary for the structure and function of the receptor in the hydrophobic interior of GPCRs (Eilers et al. 2005). Prolines are extremely important for the conformational flexibility of GPCRs as well as the exposure of a free carbonyls to mediate interhelical

interactions (Goncalves et al. 2010). This effect is possible due to the lack of amide protons and results in a non-hydrogen-bonded carbonyl at the *i-4* position in the helix. Pro215 on helix 5, Pro267 on helix 6 and Pro303 on helix 7 (rhodopsin numbering) are highly conserved throughout Class A GPCRs (Eilers et al. 2005).

Topologically GPCRs are arranged with an extracellular, glycosylated N-terminus and a cytoplasmic C-terminus (Venkatakrishnan et al. 2013). The seven GPCR transmembrane helices (TM1-TM7) are connected by alternating extracellular (ECL1–ECL3) and intracellular (ICL1–ICL3) loop regions. In addition, they contain an intracellular amphipathic helix (H8) at the C-terminus. The extracellular (EC) regions vary in length and are responsible for ligand binding (Figure 1.10) (Lagerström & Schiöth 2008). The seven-transmembrane helical bundle is the most highly conserved component of GPCRs and acts as communication link between the extracellular ligand-binding pocket and the cytoplasmic G-protein coupling region.

The extracellular domain is responsible for ligand modulation and receptor activation (Venkatakrishnan et al. 2013; Katritch et al. 2012), which leads to conformational changes in the transmembrane core. The highly conserved disulphide bridge between TM3 and ECL2 anchors the extracellular side of the helix near the ligand binding site and is essential for limiting conformational changes of this region during receptor activation (Cherezov et al. 2007; Wu et al. 2010).

The intracellular (IC) region is involved in binding to G-proteins, arrestins and downstream signal transduction through mechanisms that are believed to be similar across the entire GPCR superfamily (Gurevich & Gurevich 2006). The N-terminal domain and the extracellular loops vary not only in size but also in sequence and

frequently contain a 'lid' that folds down over the ligand-binding pockets (Lagerström & Schiöth 2008; Murakami & Kouyama 2008).

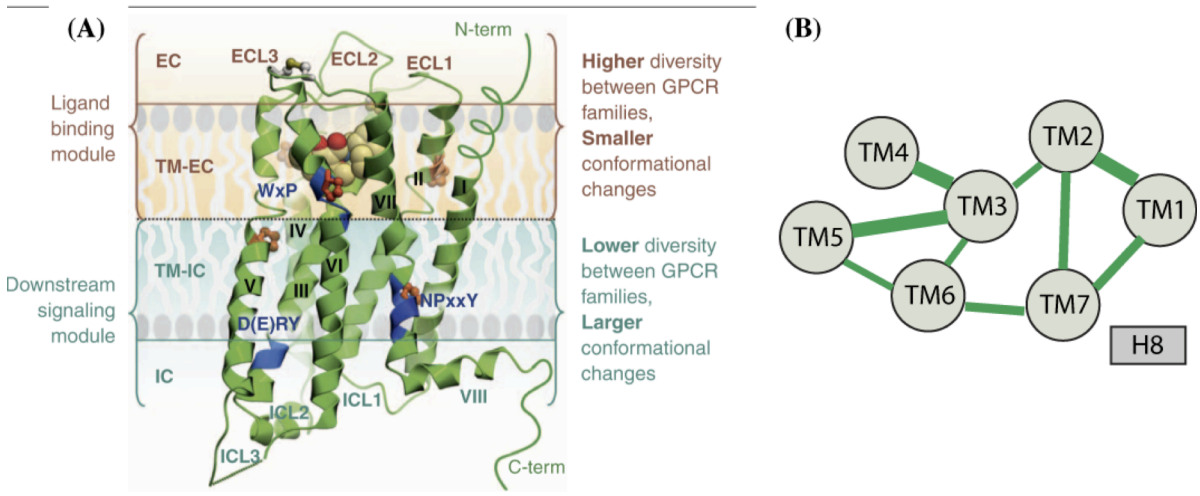

Figure 1.11: General structural outline of GPCRs
(A) General architecture and modularity of GPCRs (shown on the example of PDB ID 3PBL). The EC region includes three ECLs and the N-terminus, which may be represented by a short unstructured peptide or a longer globular-like domain. The seven transmembrane helical bundle contains proline-dependent kinks (orange) that approximately divide the receptor into two modules. The EC module (EC and TM–EC regions) is responsible for binding diverse ligands and has much higher structural diversity. By contrast, the IC module (IC and IC–TM regions), involved in binding downstream effectors including G proteins and arrestins, is more conserved between GPCRs, but undergoes larger conformation changes upon receptor activation. Blue ribbon patches highlight highly conserved, functionally relevant motifs within transmembrane helices of class A GPCRs. The C-terminus in most GPCRs is comprised of helix VIII, and in many receptors also has a palmitoylation site anchoring helix VIII to the membrane (not shown) (Figure taken from Katritch et al. 2013).
(B) General schematic representation of the inter-transmembrane tertiary contact network in which transmembrane helices. Each 25 to 35 amino acid long transmembrane segments are independently stable within the surrounding lipid environment. The consensus contacts are primarily clustered at the interfaces of TM1–TM2, TM3–TM4, TM3–TM5 and TM3–TM4–TM7. The lines between a pair of circles (TM) are proportional to the number of contacts between the TM helices. (Figure adapted from Venkatakrishnan et al. 2013).

The long C-terminal domain is hypothesised to be involved in regulation of interactions with cytosolic proteins, and involved in targeting, trafficking and signalling of GPCRs in specialised cells (Bockaert et al. 2010; Unal & Karnik 2012). Further structural analysis of GPCRs are well reviewed by Katritch *et al*. (Katritch et al. 2012), Venkatakrishnan *et al*. (Venkatakrishnan et al. 2013) and Eilers *et al*. (Eilers et al. 2005).

1.5.4 GPCR maturation and regulation

All GPCR members are synthesised in the ER and are properly folded before insertion into the cell membrane at defined sites (Jean-Alphonse & Hanyaloglu 2010). Multiple quality control systems and molecular chaperones for correct folding, maturation and transport sense membrane insertion and disulphide bond formation as well as correct association with other chaperone proteins are present throughout this process (Ellgaard & Helenius 2003). In case of defective GPCR synthesis or folding, degradation is executed through the proteasome pathway. After passing the ER and the Golgi, GPCRs have to reach the plasma membrane, before they can fulfil their function. Homo-and heterodimerisation between GPCRs and/or with accessory proteins can positively or negatively regulate GPCR signalling (Bulenger et al. 2005). If the binding of one ligand molecule improves the overall binding, a second molecule can then bind to a second receptor, leading to positive cooperativity (Franco et al. 2007; Jean-Alphonse & Hanyaloglu 2010). Heterodimerisation between different GPCR subtypes significantly modifies functional characteristics of the individual protomers.

Hetero-dimerisation can be obligatory or non-obligatory (Figure 1.11). In obligatory hetero-dimerisation, one GPCR promotes the efficient transport of a second GPCR through the endoplasmic reticulum to the cell surface (Salahpour et al. 2004). However, only one of two GPCRs is able to interact and bind to the ligand. During non-obligatory hetero-dimerisation, the two different GPCRs can selectively interact with either one of the two possible ligands, or with even both (Alberts 2008; Achour et al. 2008; Heng et al. 2013).

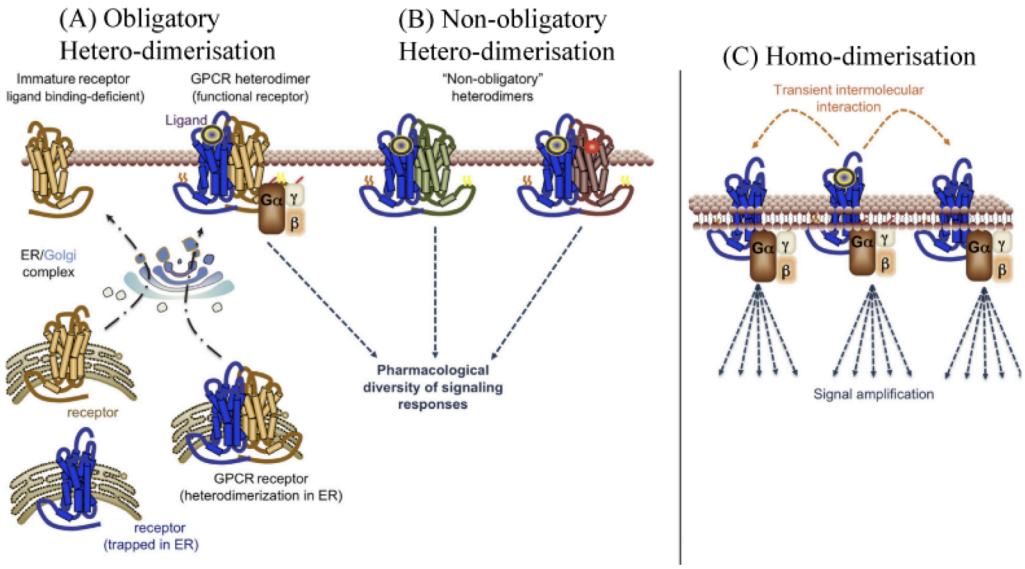

Figure 1.12: GPCR regulation
GPCR signalling can be regulated through homomeric or heteromeric interactions with other GPCR receptors.
(A) Obligatory hetero-dimerisation described that one GPCR promotes the efficient transport of a second GPCR through the ER to the cell surface. However, only one of them is able to interact and bind ligand in the functional hetero-dimer.
(B) In non-obligatory hetero-dimerisation, the two different GPCRs can selectively interact with either one of the two possible ligands, or both.
(C) Signal amplification at low ligand concentrations might be achieved through homo-dimerisation of GPCRs.
(Figure taken from Heng BC et al. 2013)

1.5.5 GPCR accessory proteins

Membrane trafficking coordinates signalling by directing ligands, receptors, and effectors at a precise time to specific microdomains where required. Thus, it is possible for membrane trafficking to initiate or stop and accelerate or attenuate signalling by engaging or disengaging signalling cascades (Swiatecka-Urban 2012). Specifically, membrane trafficking may regulate net signalling output and can be determined by:

- controlling accessibility of ligands, receptors, accessory proteins and accessory-protein-like proteins at the plasma membrane;
- targeting ligand-receptor complexes to different endocytic routes;
- sorting internalised ligand-receptor complexes for either recycling or degradation;
- recruiting different signalling pathways to the same vesicular compartment to orchestrate cross-talk (Swiatecka-Urban 2012; Magalhaes et al. 2012).

In general, accessory proteins and accessory-protein-like proteins are defined as proteins other than GPCR, G protein, or classical effectors that regulate the strength, efficiency, or specificity of signal transfer upon receptor activation or position these entities in the right microenvironment, contributing to the formation of a functional signal transduction complex (Sato et al. 2006). Accessory-protein-like proteins such as arrestin and glycogen synthase kinase (GSK) are universal regulators and interact with a diverse range of GPCRs. Arrestin is involved in a two-step mechanism, where a GPCR kinase phosphorylates an active receptor, converting it into a target for high affinity binding to arrestin. Bound arrestin then shields the cytoplasmic surface of the receptor and initiates G-protein binding and activation (Gurevich & Gurevich 2006). The small protein terminates the receptor interaction with the G-protein, redirects the signalling to a variety of alternative pathways, and orchestrates receptor internalisation and subsequent intracellular trafficking. Similar to arrestin, GSK is a multifunctional serine/threonine kinase that regulates numerous signalling pathways (Welsh 1993; Chen et al. 2011). In contrast, accessory proteins are highly specific for each receptor or receptor class. They further help position three core signalling components in the right microenvironment, and/or contribute to the formation of a functional signal transduction complex. These interactions and functions can also exist in the absence of a stimulus and their formation can be initiated by receptor activation. Two examples of GPCR accessory proteins are the Melanocortin-2 receptor accessory protein (MRAP) and the family of Receptor activity modifying proteins (RAMP). The Introduction sections of Chapters 4 and 6 describe both accessory protein families in detail and elaborate on the interaction with the receptor and their dependency on each other.

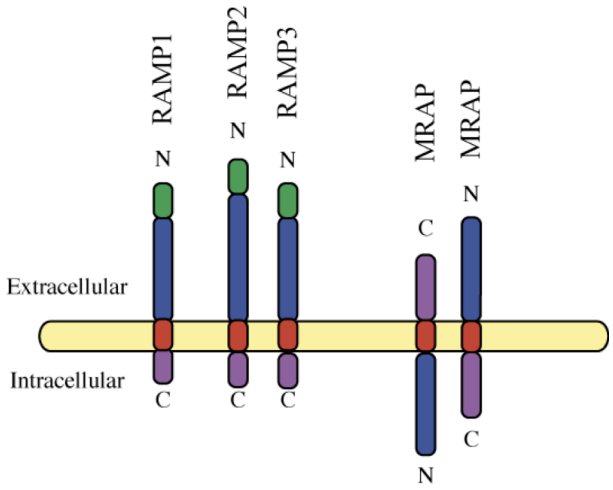

Figure 1.13: GPCR accessory proteins RAMPs and MRAP
(A) Receptor activity modifying proteins (RAMP) are a group of three proteins that are required for CLR and CTR, class B GPCRs, to act as a calcitonin gene-related peptide receptor (RAMP1), or adrenomedullin receptor (RAMP2 and 3).
(B) The melanocortin-2-receptor-accessory protein (MRAP) is a further accessory proteins that is required for melanocortin-2 receptor maturation, intracellular trafficking and ACTH-dependent signalling and is furthermore likely to modulate other GPCR class A melanocortin receptors. It has been shown that MRAP has dual topology as well as the ability to form antiparallel homodimers. The RAMPs and MRAP have similar functions but act on different receptors, and have no sequence similarities.

1.6 AIMS OF THE THESIS WORK

Knowledge of membrane protein structure is key to understanding the molecular basis of their function. The unique physical demands placed on membrane proteins by their native environment have made both *in vivo* and *in vitro* studies challenging. Even though the field has rapidly evolved over the last decade, our understanding of structure-function relationships of most membrane proteins is still limited. The aim of this thesis was to investigate the structural properties of homodimerising transmembrane GPCR accessory proteins in order to better understand their role in regulating GPCRs.

The first aspect of the presented studies was to determine the structure and biophysically characterise the melanocortin-2 receptor accessory protein (MRAP) by mainly solution-state NMR. In addition, further biophysical techniques, such as dynamic light scattering and circular dichroism, were used.

The next aim was to investigate MRAP dimerisation *in vitro*, with the hope of identifying an antiparallel homodimeric interface. Besides experimental approaches, computational methods were explored.

The investigation of the dimerisation of the accessory protein receptor-activity-modifying protein 1 (RAMP1) was an additional central point in this thesis. The focus was on the transmembrane domain. Since the ectodomain of RAMP1 does not dimerise, the transmembrane domain has been proposed to form the dimeric interface.

G-protein coupled receptor accessory proteins that are embedded in the membrane, such as MRAP and RAMP1, are essential for their cognate GPCR signalling, but still remain structurally uncharacterised. These proteins are relatively small membrane proteins, and therefore suitable for study by solution state NMR. Since solution-state NMR on membrane proteins is still a challenging field, this thesis has an additional methodological perspective. Comparison of multiple membrane-mimicking environments, as well as the combination of a wide range of different biophysical techniques with computational approaches can extend the boundaries of current studies and open up possibilities for studies of similar systems.

CHAPTER 2

THE USE OF NMR FOR STUDYING MEMBRANE PROTEINS

"In every branch of knowledge the progress is proportional to the amount of facts on which to build, and therefore to the facility of obtaining data."

(James Maxwell)

2.1 MEMBRANE MIMETICS FOR THE STUDY OF MEMBRANE PROTEINS

Due to the complexity of natural bilayers, membrane proteins must be removed from this environment to enable high quality structural and biophysical characterisation (Rösner & Kragelund 2011). Unfortunately, membrane proteins can be exceedingly difficult to characterise biophysically since their highly hydrophobic nature routinely causes misfolding and aggregation when they are removed from membranes (Lacapère et al. 2007). Therefore, one of the first goals in any membrane protein structural or biophysical study is to suitably mimic the cellular membrane environment in vitro so that the protein of interest can be studied in its native conformation. The aim is to find conditions closely resembling the natural membrane environment that also enable collection of high quality experimental data. In some cases, this can be achieved by careful screening of the protein in different detergents, or in mixtures of detergents and lipids. This search for an *in vitro* environment is a highly empirical and time-consuming process. The small number of membrane protein structures that have been determined largely reflects the challenges in finding conditions that both stabilise the protein's native state and are compatible with experimental data collection. This is a particular challenge for complex membrane proteins that cannot be refolded, since conditions that stabilise the native state must be maintained at all stages of the sample preparation process including membrane extraction, purification, and detergent exchange.

The assembly of lipids into bilayers occurs spontaneously in a manner that maximises the interactions between hydrophobic acyl chains and those between the hydrophilic headgroups and water, while at the same time minimising the interactions of the acyl

chains and water molecules. This results in a highly amphipathic environment in which membrane proteins have evolved to fold and function. The exact physical nature of a bilayer also depends on other energetic considerations such as charges on the headgroup, the saturation level of the acyl chains, and the ratio of the volumes between the head group and the hydrophobic tail. A more detailed description of lipid membranes is provided in Chapter 1. Since this thesis focuses on the use of solution NMR for the study of integral membrane proteins, I describe the systems that are typically used to mimic the membrane environment for studies of membrane proteins by solution NMR in the next section.

2.1.1 Micelles

For conventional data collection approaches, high quality solution NMR data requires tumbling times that are less than ~25 ns. As a result, detergent systems are most often used for NMR studies of membrane proteins. Above a critical micelle concentration (cmc) that is specific to the detergent and the solvent conditions, detergent molecules aggregate into micelles, in which the hydrophobic tails of the detergent are oriented towards the interior of the sphere, whilst the polar head groups form the micelle surface and water interface (Seddon et al. 2004). Increases in the detergent concentration above the cmc characteristically result in formation of more micelles rather than larger micelles (Raschle et al. 2010). Thus micelle sizes are largely fixed for a particular detergent, and the size is known as the aggregation number, which ranges from 50 to 100 detergent molecules per micelle for the detergents most commonly used in NMR studies (Figure 2.1). Micelle characteristics such as cmc, aggregation number, and shape can depend strongly on pH, ionic strength, temperature, acyl-chain length, headgroup size and the

presence of protein and other surfactants (le Maire et al. 2000; Oliver et al. 2013). Micelles are typically quite dynamic. Thus the protein undergoes motion within the micelle in addition to the overall tumbling of the protein/micelle complex, resulting in tumbling times that are short enough to permit acquisition of high resolution solution NMR spectroscopy (Luchette et al. 2001).

A major drawback of micelles as membrane-mimics is the high degree of surface curvature, which would not typically be observed in native membranes (van den Brink-van der Laan et al. 2004; Cantor 1999). Additionally, micelles are highly dynamic assemblies, and exhibit lateral pressure that would be observed in membranes. As a result, micelles can induce membrane protein unfolding and aggregation. Therefore, although detergent micelles have favourable experimental properties, they are considered to only poorly mimic the architecture and physical properties of a cellular membrane (le Maire et al. 2000; Lichtenberg et al. 2013b).

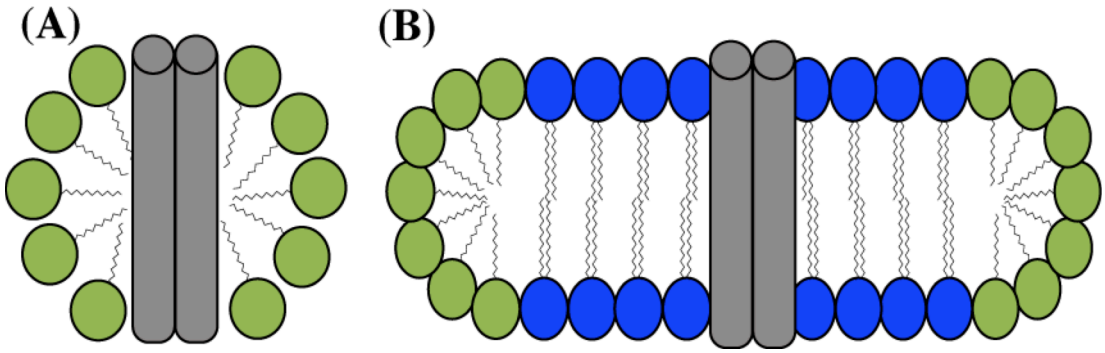

Figure 2.1: Schematic representation of (A) micelles and (B) bicelles
(A) Micelles consist of one detergent type. Whereas mixed micelles are defined by a mixture of at least two different detergents.
(B) Bicelles refer to mixtures of detergent with lipids or mixtures of short and long-chain phospholipids. The terms "mixed micelles" and "bicelles" are used interchangeably. The membrane protein is shown in grey, detergents are coloured in green and lipids in blue.

2.1.2 Mixed micelles and bicelles

Particularly useful has been the discovery that mixtures of lipids and detergents can spontaneously form patches of lipid bilayers surrounded by a ring of detergent molecules (Sanders & Landis 1995; Whiles et al. 2002; Luchette et al. 2001; Glover et al. 2001). These mixtures of lipids and detergents, or mixtures of short and long-chain phospholipids are termed 'bilayered micelles', or bicelles. They provide a powerful medium for studying peptide orientation, phospholipid packing, and membrane-peptide interactions since the disc-shaped bicelles can provide a patch of lipid bilayer that is small enough to tumble rapidly in solution and are thus amenable to solution NMR studies (Figure 2.1). A q-value is used describe the molar ratio between lipid and detergent, which dictates the bicelle size. The q-value is defined as: q = [lipid]/[detergent] (Sanders & Landis 1995).

Values of q, as well as hydration level, temperature and ionic strength determine the microscopic morphology. A further factor to consider when working with mixed micelles or bicelles is detergent solubilisation. Solubilisation is the result of a balance between the energy associated with bending of phospholipid monolayers into a curved micellar surface, and the energy associated with filling the void in the centre of the resultant mixed micelle (Lichtenberg et al. 2013b). Thus, a higher q-value, which implies a greater proportion of lipid, is expected to form a more properly ordered lipid bilayer. However, bicelles with large q values can result in 10 to 100-fold increases in rotational tumbling time and the associated large NMR spectral linewidths (Henry & Sykes 1994). Such large bicelles may also adopt an isotropic phase or form an aligned phase in magnetic fields depending on morphology, composition, phospholipid concentration

and temperature (Gabriel & Roberts 1984; Sanders & Landis 1995; Luchette et al. 2001). Such alignment can further decrease the spectral quality by solution NMR. Thus, for solution NMR studies, commonly used q-values range from ~0.25 - 0.4, which exhibit relatively short tumbling times and are sometimes referred to as 'isotropic bicelles'.

A drawback of bicellar lipid bilayers is their restricted location within the phase diagram, which is bound by limiting temperatures and hydration levels (Rösner & Kragelund 2011). However, in the context of NMR studies of membrane proteins, lipid bicelles have opened completely new ways of preparing samples for NMR studies (Raschle et al. 2010; Dürr et al. 2012; Cantor 1999), and solution-state NMR shows great promise for the characterisation of protein–protein and protein–ligand interactions in membrane-like environments.

Mixtures of micelle-forming detergent molecules can be also highly useful for tuning micelle conditions for protein stability, since varying the molar fractions of two or more detergents in a mixture enables generation of a continuous range of micelle properties (e.g., shape and charge) (Dürr et al. 2012; Columbus et al. 2009; Call et al. 2006).

2.1.3 Liposomes and Nanodiscs

In some cases, it is desirable to completely remove detergent, as it can interfere with proper protein folding and/or complicate biophysical measurements. Liposomes are systems in which membrane proteins can be studied under conditions that are completely detergent free. Phospholipids form 'edgeless', spherical liposomes when dissolved in water and allowed to spontaneously self-assemble. Spheres are the lowest energy state for a continuous bilayer and are an excellent tool to study protein function and are compatible with some biophysical approaches to studying protein structure.

Small liposomes of ~100 nm can permit biophysical measurements such as far UV circular dichroism, but have high membrane curvature (Lichtenberg et al. 2013a; Seddon et al. 2004) that can induce artefacts, and are still much too large to permit solution-state NMR studies.

Recently, new membrane-mimicking systems have appeared, most notably nanodiscs, which show very promising features for structural studies of membrane proteins in solution. They were initially developed in the Sligar laboratory based on the physiochemical properties of lipid transport proteins (Bayburt & Sligar 2002) Like bicelles, nanodiscs contain a central lipid bilayer, but rather than being surrounded by a rim of detergent, they are surrounded by a protein such as the membrane scaffolding protein. The right ratio of individual components, leads to spontaneous assembly of the nanodiscs. Although they are typically larger, and therefore tumble more slowly than isotropic bicelles, a major advantage of nanodiscs is that they allow for solution NMR studies under conditions completely free of detergent, and they may also provide a more native like packing and lateral pressure for the lipid bilayer (Gluck et al. 2011; Baas et al. 2004).

2.2 INTRODUCTION TO THE BASIC PRINCIPLES OF PROTEIN NMR

NMR is a fundamentally quantum mechanical phenomenon, which has proven invaluable in providing molecular details for the biological functions of proteins. This biophysical technique manipulates and detects nuclear spin reorientations within proteins to acquire the desired information (Wüthrich 1989). Only isotopes with odd nuclear mass or an odd number of protons, such as ^{1}H, ^{13}C and ^{15}N have a non-zero nuclear spin and are detectable by NMR. The spin properties of several nuclei are listed in table 2.1.

Nucleus	Spin	Frequency at 11.74 T [MHz]	Frequency at 22.3 T [MHz]	Natural abundance [%]
^{1}H	$^{1}/_{2}$	~500.00	~950.00	99.98
^{2}H	1	76.75	145.75	1.5×10^{-2}
^{13}C	$^{1}/_{2}$	125.72	238.72	1.10
^{14}N	1	36.12	68.62	99.63
^{15}N	$^{1}/_{2}$	50.66	96.25	0.37

Table 2.1: Relevant nuclei characteristics in protein NMR (Table adapted from Campbell 2012).

2.2.1 The basic NMR experiment

During a standard NMR experiment, the applied static, or external, magnetic field B_0 (ranging between 2-23 tesla (T)), created by a magnet, generates the net nuclear magnetisation. A spin with a magnetic moment, μ_N, can interact with B_0, leading to a nucleus with a spin quantum number *I*, with *2I+1* possible quantised energy levels – either with or against the applied field B_0. Movements between these energy levels can only occur when atoms absorb or emit a photon of energy that matches the difference in energy levels (Levitt 2013). Nuclei prefer to be aligned along the direction of the

magnetic field B_0, which is a lower energy state (spin m=+1/2) and is often given the notation α, whereas the higher energy anti-parallel orientation (spin m=-1/2) is referred to as β. Thus, a B_0 creates a bulk magnetisation vector along the z-axis. However, the rotational axis of the spinning nucleus cannot be orientated exactly parallel (or anti-parallel) with the direction of the applied field $\mathbf{B_0}$ (defined in our coordinate system as about the *z* axis), but must precess (motion similar to a gyroscope) about this field at an angle, with an angular momentum similar to a spinning gyroscope. This can be described as

$$\omega_o = \gamma \mathbf{B_0} \qquad \text{(Eq. 1)}$$

Where ω_o is the precession rate, called the Larmor frequency. The constant g is called the gyromagnetic ratio and relates the magnetic moment m and the spin number I for any specific nucleus:

$$\gamma = 2\pi\mu/hI \qquad \text{(Eq. 2)}$$

The energy difference between the spins aligned with or against the field is small, and therefore the population difference between the spins with different orientations is small. As a result, the sensitivity of NMR is very low compared with other spectroscopies like electronic absorbance spectroscopy (Campbell 2012).

The static magnetic field, B_0, is typically designated as M_z. Application of a short radio frequency pulse, perpendicular to B_0, results in a tilt of the bulk magnetisation away from the z-axis and towards the xy-plane resulting in a net M_{xy} component (Figure 2.2). The magnetisation in the xy-plane relaxes back to equilibrium via two mechanisms.

The first one is called T_1, or longitudinal, relaxation. Magnetisation is detected by T_1 via release of photons, which is an enthalpic process. The second form of relaxation is T_2, or

spin-spin relaxation, in which the NMR signal is modified by the influence of nearby spins. T_2 relaxation results in a loss of coherence without an energy release. T_2 relaxation is an entropic process. Chemical exchange, which happens when a nucleus experiences two or more different chemical environments, contributes to T_2.

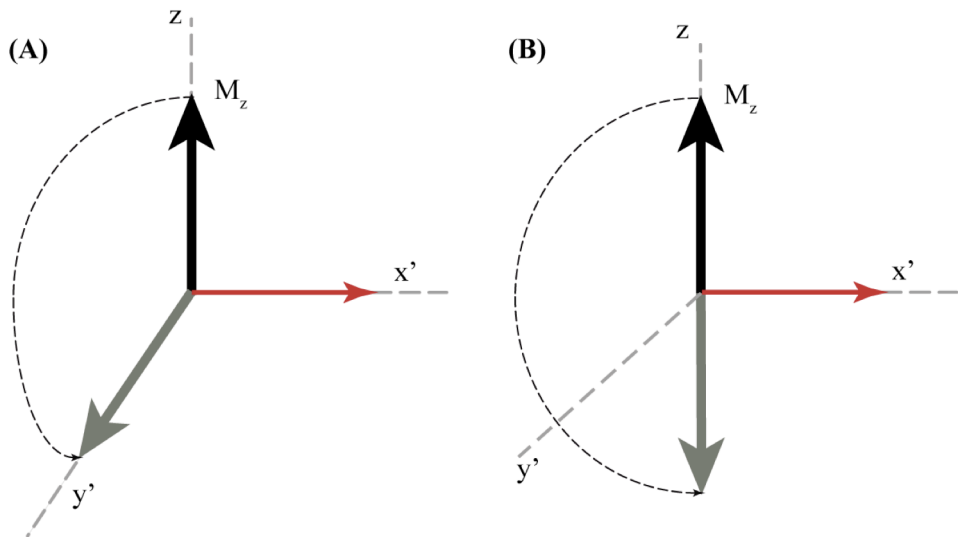

Figure 2.2: NMR pulses
(A) 90º pulse: A radio frequency pulse (red) applied along the rotating axis x' causes precession of the equilibrium magnetisation M, around x'. If applied for time t, M is rotated to the y' axis.
(B) 180º pulse: f the pulse is applied for 2t, M is inverted by rotation, to the –z axis. (Figure adapted from Campbell 2012)

In simple terms, an NMR experiment involves application of a series of radiofrequency 'pulses', or equivalently magnetic field gradient pulses, applied to a sample within a static magnetic field B_0. The resulting time-dependent free-induction decay (FID) is then detected by metal coils placed close to the sample. The FID is a time-dependent representation of the signal, which can be processed by a Fourier transformation (FT) into a frequency-dependent spectrum.

For given nuclei in the same environment, this so-called resonance frequency is given by

$$\nu = \gamma B_0/2\pi, \qquad \text{(Eq. 3)}$$

where γ is a constant for a particular isotope. However, in reality, the local environment influences the magnetic field at the nucleus, and therefore the observed resonance

frequency (ν). As a result, the same isotopic nuclei in different environments (either due to chemistry, conformation, or non-bonded environment) can give rise to signals with distinctive resonance frequencies. These differences are commonly referred to as chemical shifts (Figure 2.7) (Pascal 2008; Levitt 2013; Rösner & Kragelund 2011; Keeler 2011), and enable not only simultaneous observation of multiple nuclei, but also provide information on the structure and environment of those nuclei (Cavanagh 2007; Keeler 2011). The common chemical shift scale in NMR can be described as

$$\delta = (\nu - \nu_{reference})/\nu_0 , \quad \text{(Eq. 4)}$$

where $(\nu - \nu_{reference})$ is the frequency difference between the line of interest and the reference line in Hz; ν_0 is the applied frequency [MHz]. δ has the dimensionless unit of parts per million [ppm] (Campbell 2012).

Spin-spin interactions occur either directly through dipole-dipole coupling or indirectly through scalar coupling mediated by bonding electrons. Direct interactions are useful for structural studies since they only depend on known physical constants and provide information about the geometrical form of a molecule. In molecules that are tumbling isotropically, they average to zero. However, spin dipoles can still affect the relaxation properties of nearby spins, which is the basis of the nuclear Overhauser effect (NOE). NOEs can be used to determine spin-spin distances of up to 5 Å and are a critical tool in structural studies of proteins. In addition, dipole-dipole couplings find application in residual dipolar coupling, which are described in the Subchapter 2.2.7.1.

Indirect spin-spin coupling, or J-coupling is present between spins that are chemically bonded. For bonded nuclei with spin, coupling of the spin states is mediated via electrons. The coupling resulting in a set of resonances for each spin depending on the

spin state of the bonded nuclei. The size of split of such a doublet is defined by a field-independent spin-spin coupling constant [Hz]. The so-called scalar or J-coupling is an important experimental observable since it provides information about the connectivity within a protein and dihedral bond angles (Keeler 2011; Campbell 2012). The Karplus equation describes the correlation between scalar coupling constants and dihedral torsion angles: $J(\phi) = A\,cos^2\phi + Bcos\phi + C$ (Eq. 5)

Where J is the ^{3}J coupling constant and ϕ is the dihedral angle. This relationship is between local geometry and coupling constants used for comparison of ^3J values measured in solution with dihedral angles and is highly important for determining the backbone torsion angles.

Over time, the magnetisation returns back to equilibrium via a combination of T_1 and T_2 relaxation. For proteins, this happens in the millisecond (ms) to second (s) time range. T_2 is the time constant of that M_{xy} decay. Inhomogeneity of B_0 and the intrinsic T_2 arising from spin-spin interactions affect the observed linewidth. The spread of effective B_0 fields due to fluctuations in the local magnetic field produces a spread of precession frequencies, which results in decay of M_{xy}. For proteins tumbling on the nanosecond timescale, this effect increases with tumbling time and results in signal broadening The linewidth, W, of one peak or one nucleus at half-height of an NMR signal is thus related directly to the relaxation time T_2 of the corresponding nucleus and can be described as followed:

$$W_{1/2} = \frac{1}{\pi T_2} \quad \text{(Eq. 6)}$$

During an experiment, limitations on the rate of pulsing are set by the acceptable linewidth $W_{1/2}$ for the signal and nuclear spin-lattice relaxation time T_1: the pulse

repetition rate should be less than 1/4 T_1 to compare peak areas quantitatively (Pervushin et al. 1997; Campbell 2012). In samples containing membrane proteins, the linewidth may be broader than the scalar splitting, so the latter may not be apparent.

2.2.2 One-dimensional ^{1}H NMR experiments

The simplest possible NMR experiment is the one-dimensional (1D) NMR experiment, where a single nucleus, usually ^{1}H, is excited. Because of the natural abundance of ^{1}H and the relatively high sensitivity of ^{1}H (i.e., a large γ value), this experiment is ideal for looking at wide range of sample types. However, the abundance and diversity of ^{1}H sites can also be a disadvantage: due to signal or peak overlap, it can be difficult to resolve all peaks in a 1D spectrum and thus it is usually used only for preliminary analyses of protein samples. Nonetheless, 1D experiments are well suited to establish the signal to noise ratio of a sample and to check its structural integrity, which is particularly useful in comparisons with previously collected spectra are available (Figure 2.3) (Keeler 2011; Rösner & Kragelund 2011).

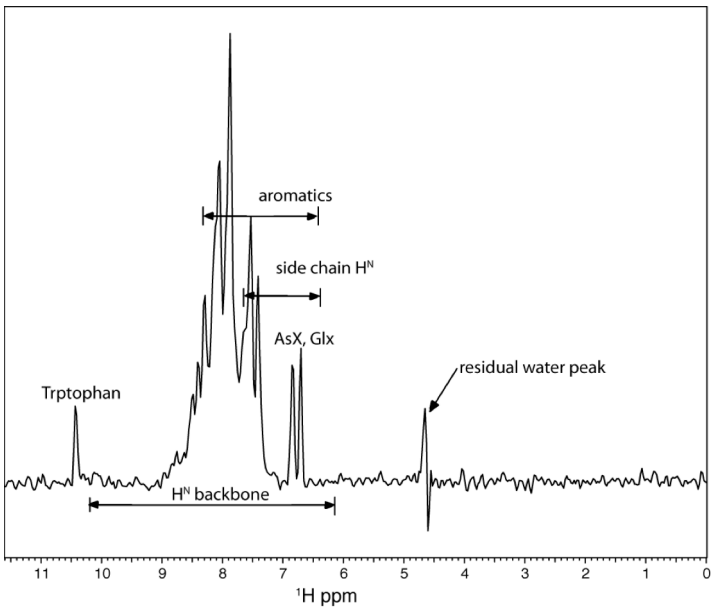

Figure 2.3: 1D ^{1}H-NMR spectrum of MRAP with the chemical shifts of the NMR signals on the x-axis. The large overlap between signals demands for extraction into more dimensions.

2.2.3 Two-dimensional NMR experiments

Because of the large number of protons, a 1D proton experiment of a protein contains all chemical shift data in an inaccessible form - due to overlap. Therefore, two-dimensional (2D) NMR experiments were introduced. These experiments "spread" the resonances out over a second dimension, which increases resolution and decreases overlap. 2D experiments thus allow a more specific assignment of peaks to specific amino acids in small peptides (Turner 1980; Keeler 2011). The most commonly used 2D experiment for proteins is the ^{1}H-^{15}N Heteronuclear Single Quantum Coherence (HSQC) experiment.

2.2.3.1 ^{1}H-^{15}N HSQC experiment

The HSQC experiment provides a map that correlates the chemical shifts of ^{15}N atoms with peaks of the chemical shifts of their covalently attached ^{1}H (Bodenhausen & Ruben 1980; Bodenhausen et al. 1984). This experiment provides a distinctive "fingerprint" of a protein, with unique chemical shifts for each amino acid (except proline, which lacks an amide hydrogen). During the HSQC experiment, magnetisation is transferred from amide protons to their attached nitrogen atoms via an INEPT (Insensitive Nuclei Enhanced by Polarisation Transfer) sequence (Figure 2.4).

The experiment is started at the amide proton, since protons are more sensitive to their environment than amide. At this point the chemical shift of the nitrogen nucleus is encoded via a delay that is incremented with every point collected in the second dimension. Then the magnetisation is returned to the proton via a reverse INEPT sequence, and the detector is turned on and the FID is recorded. The ^{1}H-^{15}N HSQC forms

the basis of further experiments such as three-dimensional through-bond (e.g. HNCO, HNCA) or through-space (^{1}H-^{15}N-NOESY-HSQC) experiments (Cavanagh 2007).

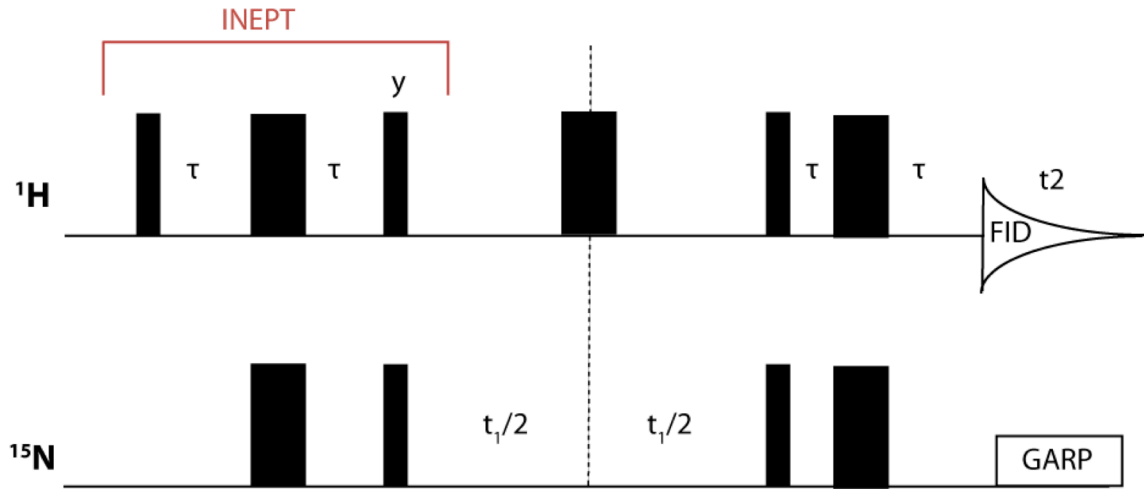

Figure 2.4: The HSQC experiment
The basic HSQC pulse sequence can be subdivided into INEPT + echo + INEPT. The first INEPT step improves sensitivity of low magnogyric ratio nuclei; during the defocus delay - or echo - the magnetisation evolves and the coupling is being refocused. In the finally reverse INEPT step, inverse detection is performed and the magnetisation is transferred to the proton plane again.

2.2.3.2 SOFAST-HMQC

Heteronuclear Multiple Quantum Correlation (HMQC) experiments (Mueller 1979) give essentially the same information as decoupled HSQC experiments. However, magnetisation can be transferred via the multiple-quantum pathway with fewer radio frequency pulses and a shorter overall pulse sequence duration than HSQC-based sequences. The resulting B_1-field inhomogeneities and pulse imperfections reduce signal loss and also reduce the loss of resolution in the indirect dimension (Figure 2.5 (A)).

The band-Selective Optimized Flip-Angle Short-Transient Heteronuclear Multiple Quantum Coherence (SOFAST-HMQC) experiment records ^{1}H-X (X = ^{15}N or ^{13}C) correlation spectra of proteins and relies on standard data sampling in the indirect dimension (Schanda et al. 2005), but is designed to allow for short inter-scan delays.

Inter-scan delays are required for relaxation processes to re-establish equilibrium that provides bulk magnetisation along the z-axis.

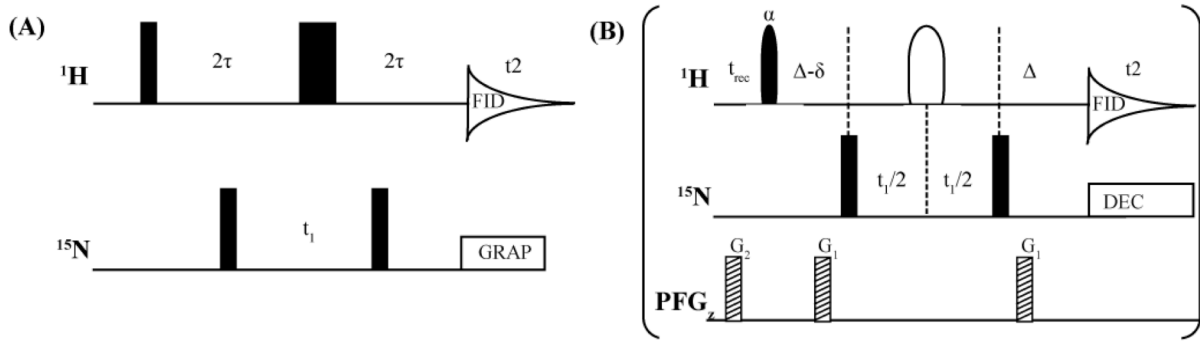

Figure 2.5: HMQC and SOFAST-HMQC pulse sequence
(A) The HMQC pulse experiment permits to obtain 2D heteronuclear chemical shift correlation map between directly bound ^{1}H and X (X = ^{15}N or ^{13}C) heteronuclei.
(B) SOFAST-HMQC experiment records ^{1}H-X (where X is ^{15}N or ^{13}C) correlation spectra of proteins.
The transfer delay Δ is set to 1/(2JHX), the delay δ accounts for spin evolution during the pulse, and t_{rec} is the recycle delay between scans. (Figure adapted from Schanda et al. 2005)

However, in conventional experiments the relaxation rates are such that inter-scan delays on the order of a second are required. In the SOFAST-HMQC approach, short inter-scan delays are achieved via incomplete flipping of the magnetisation into the x-y plane; the so-called Ernst angle is used, which results in optimal signal-to-noise over a fixed period of experimental time. The Ernst angle describes the flip angle for a particular spin that gives the maximal signal in the least amount of time when signal averaging over many transients. In addition, only the amide protons are excited by the use of shaped pulses. This results in shorter T_1 relaxation times due to the large number of unperturbed spins in the local environment. With the SOFAST-HMQC, inter-scan delays of as short as 50 ms can be used, resulting in a large increase in sensitivity for a given unit of acquisition time, and is very useful for low concentration samples. Conversely, when high sample concentrations are possible, this experiment permits very fast acquisition times and site-resolved NMR studies of kinetic processes in proteins on a time scale of seconds can be achieved (Figure 2.5. (B)) (Schanda et al. 2005).

2.2.3.3 Transverse Relaxation Optimised Spectroscopy (TROSY)

The TROSY experiment is a through-bond 2D experiment that can greatly improve the resolution and sensitivity in larger systems (Pervushin et al. 1997). The basis of this experiment is that the interference of two relaxation effects, dipolar-dipolar coupling and chemical shift anisotropy (CSA) can be either constructive – leading to an increased T_2 relaxation rate, an increased linewidth, and a decreased signal-to-noise ratio – or it can be destructive where the components partially cancel each other leading to a decreased relaxation rate, a decreased line-width, and an increased signal- to-noise ratio. For nuclei strongly coupled to another, whether the relaxation rate is constructive or destructive depends on the spin state of the coupled nuclei. Thus, in essence, all TROSY pulse sequences allow separation of the nuclei according to the spin state of their neighbours, and this can be achieved quite simply by leaving out the decoupling pulses that are normally used in each dimension for observation of a single uncoupled spin. The spectral components with favourable relaxation rates are selectively observed via phase cycling.

The longer relaxation times result in sharper peaks and therefore less peak overlap and improved resolution (Cavanagh 2007). This effect can be very important when working with membrane proteins, since the slow tumbling time of the protein/micelle or protein/bicelle complexes result in fast relaxation times. In addition, the transmembrane domains of proteins often have similar chemical shifts due to the low variation in amino acid composition (Rösner & Kragelund 2011). CSA is field dependent and dipole-dipole coupling is field independent. Theoretically the maximum TROSY effect should be observed at a ~1 GHz (^{1}H frequency) external magnetic field.

2.2.3.4 Total correlation spectroscopy (TOCSY)

The homonuclear TOCSY experiment creates correlations between all protons within a given spin system by obtaining information about coupling between two spins, indicated by the presence of a cross-peak multiplet (Caravatti et al. 1983). Correlations can be seen between distant protons as long as there are couplings between every intervening protein (Figure 2.6). It is so also possible to record crosspeaks between spins, which are connected by an unbroken chain of couplings. Thus, TOCSY is a useful technique to identify inter-residual spins, which belong to an extended network of couplings, such as large proteins. Its main parameter is the isotropic mixing time τ_{mix}, which causes evolution of the z-magnetisation (Keeler 2011). To detect only directly coupled spins relatively short mixing times, in the order of $1/(2J)$, are applied on the system. Large mixing times, of amplitudes between ~30 ms and ~70 ms, are used for obtaining information crosspeaks due to transfer through two or more couplings.

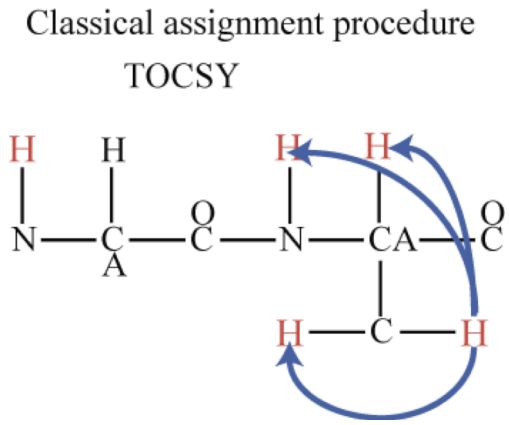

Figure 2.6: Magnetisation transfer of the TOCSY.
***Red Atoms** are those ones whose chemical shifts are going to be measured or observed in a TOCSY experiment.*

2.2.4 Nuclear Overhauser Effect Spectroscopy

One of the most important pieces of information required to elucidate protein structure comes from the nuclear Overhauser effect (NOE). As previously discussed, this effect is based on through-space dipolar coupling and offers a method for measuring short inter-nuclear distances up to ~5 Å, which are essential to define protein folds and protein-protein contacts. NOESY is the complementary method to TOCSY, where intra-residual information is obtained. The 2D NOESY experiment consists of three 90º pulses with the second and third pulse separated by a delay τ_{mix} (mixing time), corresponding to the stage during which magnetisation is transferred through space, in a distance-dependent manner, via cross-relaxation. Phase cycling filters all but the desired zero quantum coherence, while magnetisation is "stored" on the z-axis. The length of τ_{mix} must be chosen carefully as at longer mixing times a process occurs known as "spin diffusion", which corresponds to indirect transfers of magnetisation via intervening spins. Spin diffusion can generate strong cross-peaks between nuclei more than 5 Å apart.

2.2.4.1 The 3D ^{1}H-^{15}N NOESY-HSQC and 3D ^{1}H-^{15}N NOESY-TOCSY

The NOESY pulse sequence can be combined with the ^{1}H-^{15}N HSQC, where the preparatory 90º pulse in the HSQC is replaced by the 2D NOESY sequence. This experiment detects NOEs to the amide protons from any other protons in the molecule. Thus it provides information on chemical shifts between the two protons as well as a correlation to the chemical shift of the ^{15}N nucleus that is attached to the amide proton. The stronger the intensity, the closer the protons. Typically the distances are binned according to the intensity of the NOE crosspeak: 1.8 to 2.4 Å (strong peak), 1.8 to 3.8 Å (medium), and 1.8 to 5.0 Å (weak peak) (Rösner & Kragelund 2011).

Similar to the 3D ^{1}H-^{15}N-NOESY-HSQC, the 3D ^{1}H-^{15}N-NOESY-TOCSY is specifically designed to obtained homonuclear ^{1}H-^{1}H-NOE and J-coupling information in a single experiment. This experiment consists of a 2D TOCSY followed by a 2D HSQC pulse sequence (Pascal 2008; Cavanagh 2007).

2.2.5 3D Triple-resonance Experiments

3D triple resonance experiments use ^{1}H, ^{15}N and ^{13}C pulses. The additional dimension provides the possibility to resolve additional peaks and provide additional structural or chemical information. In addition, the magnetisation transfer is achieved via one-bond scalar couplings (^{1}J), which in many cases permits unambiguous identification of the observed resonances. Triple resonance has become especially important for the sequential assignment of proteins larger than ~10 kDa (Pascal 2008; Levitt 2013).

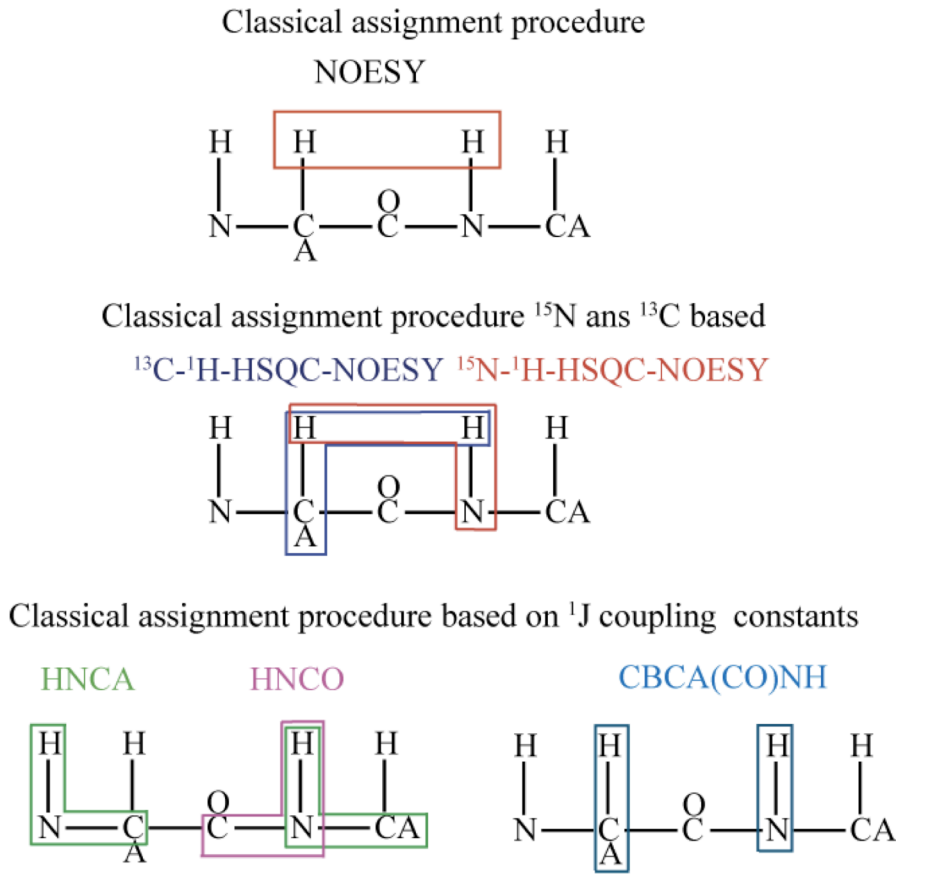

Figure 2.7: Magnetisation transfer of experiments used for classical assignment procedure

Three triple resonance experiments primarily were used in this thesis: HNCA, HNCO and CBCA(CO)NH. Figure 2.6 described the heteronuclear coupling as well as the transfer pathways. The name for each sequence derived from its magnetisation pathway.

The 3D HNCA experiment transfers magnetisation from the N_H to the ^{15}N and then to the Cα of the starting and the previous residue within an amino acid sequence. Chemical shifts with the intra- and inter-residue Cα shift are correlated through the $^{1}J(N_H)$ and $^{1,2}J(N,C\alpha)$ coupling constants.

The 3D HNCO experiment connects sequential backbone connectivities between ^{15}N-^{1}H pair of each residue with the carbonyl CO resonances of the preceding residue via the $^{1}J(N_H)$ and $^{1}J(N,CO)$ coupling constants. Due to the large values of the $^{1}J(N_H)$ coupling constants, the HNCO experiment is the most sensitive of all triple-resonance experiments.

3D CBCA(CO)NH experiments correlate the ^{1}H and ^{15}N amide resonances of the one residue with the Cα and Cβ resonance of its preceding residue via the intervening CO spin using the $^{1}J(N_H)$, $^{1}J(N,CO)$, $^{1}J(C\alpha,CO)$ and optional $^{1}J(C\alpha,C\beta)$ coupling constants.

2.2.6 Strategies for determining membrane protein structures by solution-state NMR

Thanks to the development of many sophisticated NMR techniques, NMR-based structure determination of small- and medium- sized soluble proteins has become a standard biophysical tool over the past two decades. Many of the methods developed for application to large proteins are becoming particularly useful for membrane proteins due to the slow tumbling of the protein and micelle or bicelle complexes (Krueger-Koplin et al. 2004). However, making sequence-specific assignments of backbone and

side-chain resonances in α-helical membrane proteins is particularly challenging due to a (i) small number of different amino acids within the transmembrane regions, and (ii) a narrow chemical shift dispersion due to the repeating helical conformational. Both lead to peak overlap and thus, increased difficulty in spectral interpretation (Rösner & Kragelund 2011). Deuteration and selective labelling strategies of the target protein help to improve the experimental resolution. Additionally, deuteration of detergents helps decrease relaxation rates, allows for observation of the much weaker protein signals in carbon-based experiments, and decreases spin-diffusion of magnetisation away from the protein. Experiments with long coherence transfer pathways such as the 3D experiments necessary for assigning and obtaining structural restraints are also difficult due to the fast relaxation rates of the slowly tumbling protein/micelle or protein/bicelle complexes (Löhr et al. 2012). Thus, to date, the most sensitive backbone NMR experiments are the 3D TROSY-HNCO and 3D TROSY-HNCA (Löhr et al. 2012; Krueger-Koplin et al. 2004; Maslennikov et al. 2007).

For helical transmembrane proteins the use of three- and four-dimensional NOESYs can permit observation of medium- to long-range NOEs and gives additional information due to hydrogen bonds between residues *i*, *i-3* and even *i-4* residues (Hiller et al. 2009). Especially useful is the observation of methyl groups, which exhibit high signal-to-noise due to the three-fold degenerate protons and relaxation properties that are superior to the backbone due to increased flexibility. Methyls are also frequently found in long-range or intermolecular packing interfaces, and therefore help to acquire long-range NOE information. Thus, assignment of side-chain resonances is especially important, because the helix–helix distances are too long for observation of backbone-backbone

NOEs and side-chain protons are thus the major source of long- range NOE information in helical membrane proteins. Kay *et al*. established the specific labelling of methyl groups of isoleucines, leucines and valines (Tugarinov et al. 2006), which exploits the methyl-TROSY effect to enable detection of nuclei in very large protein systems (Tugarinov & Kay 2005).

In addition to ^{1}H-^{1}H NOEs, chemical shift assignments are fast becoming powerful restraints in structure determinations. Although they have been used for several years to calculate the likelihood for the backbone dihedral angles to be in a particular region of ϕ/ψ-space, it has been shown recently that chemical shifts can even be used in the absence of other experimental information to determine protein structures (Shen et al. 2008).

After obtaining all experimentally available information about the system, including NOE-derived distance restraints, dihedral angles restraints, coupling constants and, if possible, PREs and RDCs (explained in the following subchapter), the constraints are fed into a computational simulation that employs force fields to describe bond lengths, atom dimensions and mass, and bond angles. The calculation output is a set of structures that are consistent with the experimental data. The process of structure calculation is iterative, with experimental data being revisited, based on analysis of the predominant restraint violations, followed by re-refinement (Rösner & Kragelund 2011). RDCs are most usefully implemented at a late stage of the refinement process, when convergence is already quite high.

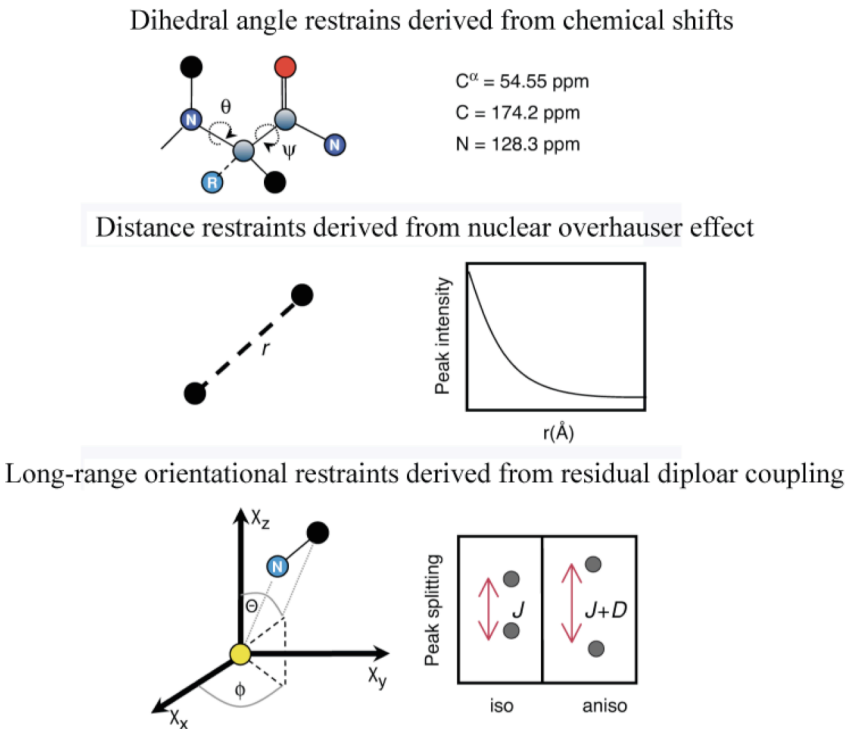

Figure 2.8: Typical NMR-derived structural restraints (Figure adapted from Roesner et al. 2011)

In the final stage, the quality of the structures is evaluated. The root mean square deviation (RMSD) for any atom is a measurement for the quality of a superimposed ensemble of structures and can be calculated as the square root of the sum of squares of distances between the atom in all models in a computes ensemble and the average position for that atom in the ensemble. Programs, such as iCing (Doreleijers et al. 2012), can be used to quickly validate experimentally obtained structures.

2.2.7 Increasing the structure quality with additional restraints

2.2.7.1 Residual dipolar coupling

Residual dipolar couplings (RDCs) have recently grown in significance as a new tool to study bio-macromolecular structures in solution. RDCs provide bond vector information relative to a molecular alignment tensor. Thus, under the same set of conditions the bond vectors of multiple interacting nuclei can be related irrespective of their position within

the protein. As a result, RDCs provide long-range information and are highly complementary to NOE-derived distances (Prestegard et al. 2004). Dipolar couplings are through-space interactions between the spin dipoles. If a molecule is allowed to tumble freely in solution, all possible orientations are sampled equally and the dipolar coupling will be averaged to zero. To measure dipolar coupling one has to introduce partial alignment of the media. Common mechanisms to introduce partial alignment include filamentous phage particles (Hansen et al. 1998), lipid bicelles (Ottiger & Bax 1998), stretched or compressed polyacrylamide gels (Chou et al. 2001) and DNA-nanotubes (Douglas et al. 2007; Bellot et al. 2013). In a partially aligned sample, molecules tumble anisotropically, and the dipolar interaction no longer vanishes, as motion is restricted. Residual coupling can be observed as apparent changes to the scalar (J) coupling. The RDC δ(θ, ϕ) between two directly coupled nuclei with different orientation can be expressed as follows (Lipsitz & Tjandra 2004):

$$\delta(\theta,\phi) = A_a\{(3cos^2\theta - 1) + \frac{2}{3}A_r(sin^2\theta cos^2\phi)\} \quad \text{(Eq. 7)}$$

where A_a and A_r are the axial and rhombic components of the alignment tensors and the orientation of the inter-nuclear vector with respect to the alignment tensor is defined by θ and φ. More accurately, θ describes the angle between the interatomic vector and the z-axis of the alignment tensor, whereas φ is the angle describing the position of the projection of the inter-atomic vector on the xy-plane, relative to the x-axis (Clore et al. 1998) (Figure 2.8.(A)). From a change in the J-coupling of the NMR signal, either to larger (positive RDC) or smaller (negative RDC) splitting, the angles, and thus the orientation, relating the N-H vector to the laboratory frame can be determined for each vector of the molecule.

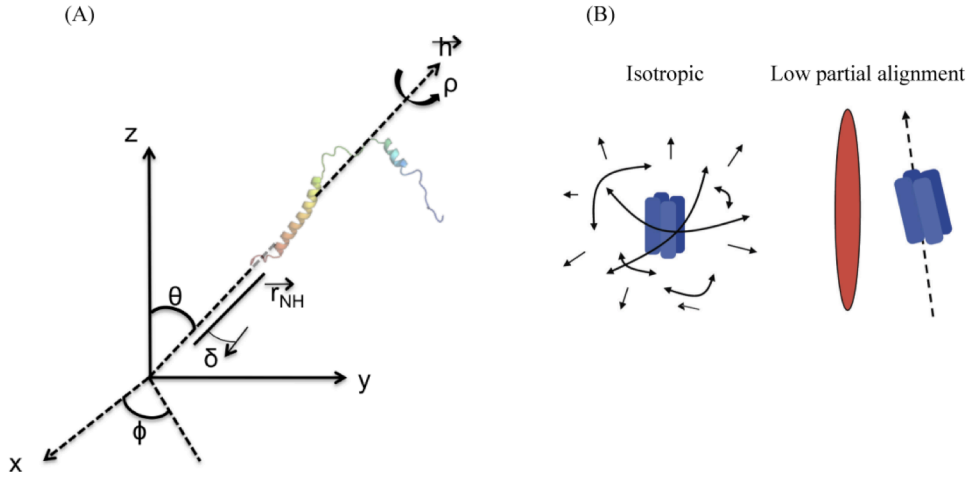

Figure 2.8: Residual Dipolar Coupling
(A) Schematic representation of the geometric parameters, which are used to define the dipolar coupling as a function of the secondary structure element orientation (Adapted from A. Mascioni and G. Veglia 2002)
(B) Under isotropic conditions, the protein is free to tumble in solution and the dipolar coupling is averaged to 0. In an anisotropic scenario, where submolar fractions of a suitable alignment media has been added to the NMR-sample, the splitting of the two peaks changes as a function of the sum of the J-coupling and the residual dipolar coupling D (Figure adapted from Roessner et al., 2011).

2.2.7.2 Paramagnetic Broadening Enhancement

The magnetic moment of an unpaired electron is 658-fold larger than that of a proton and therefore results in higher signal-to-noise and longer range information. Including a paramagnetic centre in a solution can give information about molecular motion, distance from the paramagnetic centre to the observed nucleus, and binding of the paramagnetic ion to the macromolecule. The interaction between a paramagnetic centre (e.g., a nitroxide or certain lanthanides) and a nucleus enhances the relaxation process and thus broadens the signals and lowers the intensity of the NMR signals of nearby nuclei (Jeannin et al. 2005). This effect arises primarily from dipolar interactions (Campbell 2012). The obtained restraints are long-range (> 5 Å), and therefore complementary to NOEs. The combination of site-directed spin labelling in which reagents such as the organic nitroxide radical S-(2,2,5,5-tetramethyl-2,5-dihydro-1H-pyrrol-3-yl)methyl-

methanesulfonothioate (MTSL) are reacted with a free cysteine enables measurement of distances between a large number of amide protons and the unpaired electron in a single set of 2D experiments (Gaponenko et al. 2000; Van Horn et al. 2009).

Compounds like the transition ion Mn^{2+} in complex with $EDDA^{2-}$ can be used to determine depth of insertion of peptide residues in a lipid bilayer. $Mn^{2+}EDDA^{2-}$ is water-soluble, and therefore regions of the protein that are embedded in detergent micelles or bicelles are protected from its PRE effects. Thus, measurement of crosspeak intensities in 2D HSQC spectra in the presence and absence of $Mn^{2+}EDDA^{2-}$ provides an indication of the protein insertion depth (Rösner & Kragelund 2011; Lau et al. 2009; Altenbach et al. 1994).

2.2.7.3 Dynamics

Proteins are dynamic, and the motions can have important functions in promoting catalysis or allowing rapid responses to the presence of allosteric modulators or variations in the environment. Solution-state NMR is a unique structural biological technique since it permits measurement of atomic-level dynamics over a very large range of timescales (Baskaran et al. 2010). Dynamics can be especially important for membrane receptors, which transmit ligand binding on one side of a membrane by altering its conformation on the other side of the membrane. Figure 2.9 schematically illustrates the timescale of conformational events in membrane proteins. Librations and vibrations of covalent bonds and fast side-chain rotations occur on a picosecond to nanosecond timescale, whereas protein-ligand dissociation may happen over hours.

The most common approach to quantifying protein fast timescale dynamics of a nucleus by solution-state NMR on the picosecond to nanosecond timescale is to measure

longitudinal (T_1) and transverse (T_2) ^{15}N relaxation rates and $\{^1H\}$-^{15}N heteronuclear NOE values (Figure 2.9).

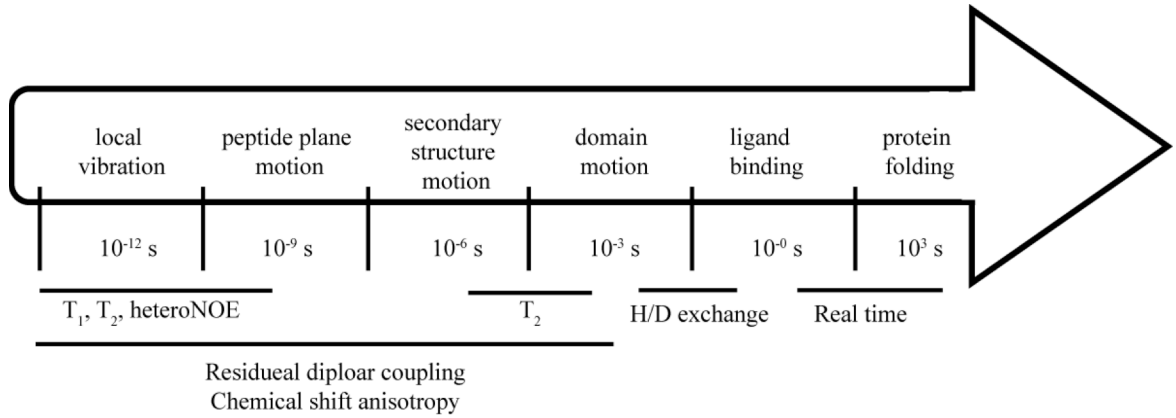

Figure 2.9: Schematic illustration of conformational events in membrane proteins
The motions that change a protein conformation occur with time-constants between picoseconds to several minutes. The fastest motions, vibrations and librations around covalent bonds, result in atoms moving only a fraction of one Å. Ligand binding may involve only subtle motions like rearrangement of amino-acid residues in the binding site or larger movements over several Å.

The underlying principal mechanisms for ^{15}N relaxation measurements are the random fluctuations in dipolar coupling between the ^{15}N and amide ^1H and chemical shift anisotropy, produced by molecular motion (Pascal 2008). The transverse relaxation time T_2 is closely correlated with tumbling times on the nanosecond timescale, whereas for proteins the longitudinal relaxation time T_1 is most closely correlated with faster intramolecular dynamics. T_1 and T_2 are also often expressed as their reciprocal, which gives relaxation rates R_1 and R_2, respectively (Keeler 2011). In the absence of chemical exchange, the molecular tumbling time in solution can be characterised by an overall correlation time τ_c, which relates to the molecular size of a protein, and can be estimated from the following calculation:

$$\tau_c \approx \frac{1}{4\pi\nu_N}\sqrt{6\frac{T_1}{T_2} - 7} \qquad \text{(Eq. 8)}$$

where ν_N is the ^{15}N resonance frequency in Hz. τ_c relates to the molecular size of a protein.

In addition, comparison of the ratio of R_2/R_1 and the product of R_1*R_2 can reveal motions that are fast or slow relative to the molecular tumbling time (Kneller et al. 2002). R_2/R_1 is frequently used to estimate global correlation times, but is skewed to high values in residues that are sensitive to rotational diffusion anisotropy. By using both R_2/R_1 and R_1*R_2 one can distinguish between motional anisotropy and chemical exchange.

The $\{^1H\}$-^{15}N heteronuclear NOE exploits the heteronuclear dipole-dipole interaction between the amide proton and amide nitrogen. The intermolecular distance can be regarded as constant since it is defined by the chemical bond length (Opella & Marassi 2004). Since the NOE transfer rate depends also on dynamics, the magnitude of the heteronuclear NOE can be used to identify flexible residues. When the motion of the internuclear vector is faster than the overall tumbling times of the protein, the NOE peak intensity decreases, indicating flexibility (Rösner & Kragelund 2011).

Another important measure of protein dynamics are Carr-Purcell-Meiboom-Gill (CPMG) (Meiboom & Gill 1958) relaxation dispersion experiments, which monitor dynamics in the microsecond to millisecond time scale. This time scale frequently corresponds to biologically important processes such as ligand binding and catalysis, and has been used to correlate dynamics and function in detail (Doreleijers et al. 2012; Kay & Prestegard 1986; Religa & Sprangers 2010).

CHAPTER 3

METHODS AND MATERIALS

"Truth is ever to be found in simplicity, and not in the multiplicity and confusion of things."

(Isaac Newton)

3.1 PROTEIN PRODUCTION

3.1.1 DNA sub-cloning and mutagenesis

3.1.1.1 DNA sub-cloning for MRAP

The chosen construct to investigate MRAP was 67 amino acids long (MRAP(2-67)), containing the N-terminus (residues Ala2 to Ser37), the predicted transmembrane domain (Ile38 to Trp62), and five C-terminal residues. The MRAP gene was inserted between the HindIII (5′) and BamHI (3′) site of the pMM-LR6 vector (J P Staley 1992; North & Blacklow 1999). pMM-LR6 (Kan^R) vector includes the *trpΔLE* gene with an N-terminal $(His)_9$ tag and a single methionine residue at the C-terminus of *trpΔLE*. *TrpΔLE* comprises the leader sequence of the trp operon of E.coli fused to a 97 amino acid sequence, which is located near the C-terminus of the anthranilate synthase gene. The protein product is referred to as trpLE and is used to drive the construct of interest into inclusion bodies. The MRAP sequence was thus expressed as a C-terminal in-frame fusion to the $(His)_9$-trpLE. A short construct of MRAP, without the N-terminal domain, comprised 38 amino acids. This construct was produced according to the protocol for MRAP(2-67). Clones containing the correct insert were identified by colony PCR and verified by DNA sequencing (Source Bioscience Oxford, Department of Biochemistry).

Site-specific mutations of the MRAP constructs were generated using the *QuikChange II Site-Directed Mutatgensis Kit* (Agilent Technologies) according to the manufacturer's protocol. In brief, complementary synthetic oligonucleotide primers containing the nucleotide substitutions were used to replicate both

plasmid strands. The incorporation of these primers produced a mutated, nicked plasmid. The endonuclease *Dpn*I (target sequence: 5′-Gm^{6}ATC-3′), which is specific for methylated and hemimethylated DNA was used to digest the parental DNA template, thereby enriching the mutated plasmid DNA. The plasmid DNA was transformed into DH5α cells (New England Biolabs), and nucleotide substitutions were verified by DNA sequencing.

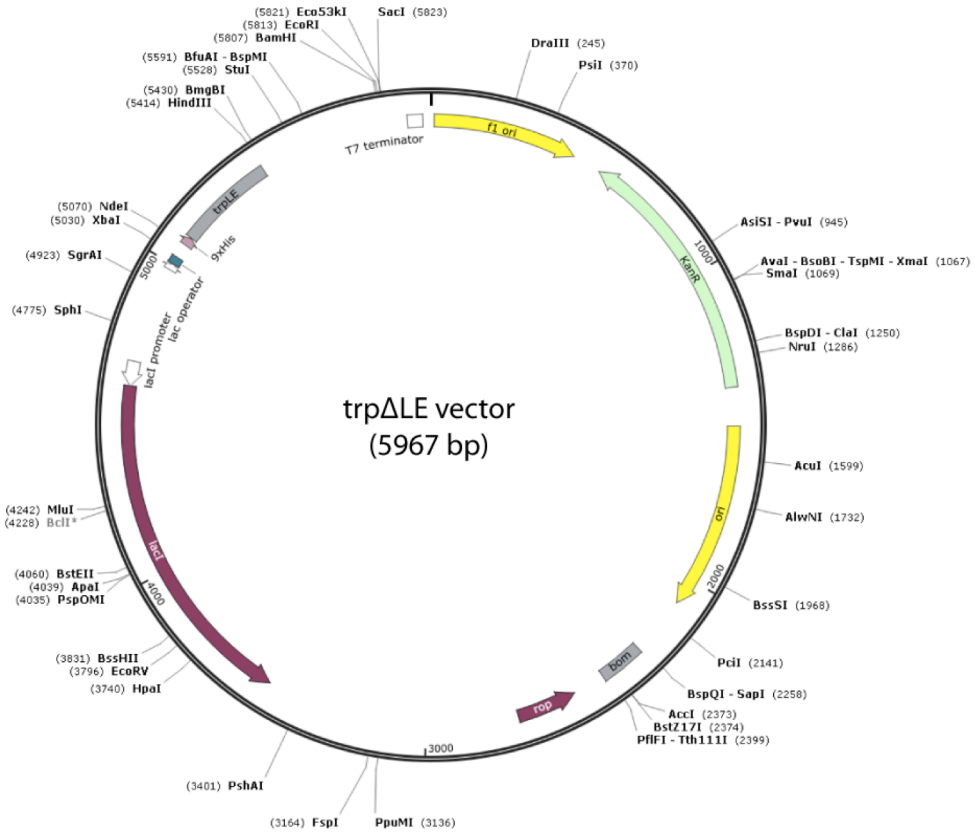

Figure 3.1: Vector map of pMM-LR6 (Kan^{R}) vector with the trpΔLE gene. SnapGene version 2.01 was used to generate the vector map.

3.1.1.2 DNA sub-cloning for RAMP1tm

To study the transmembrane domain of human RAMP1 two specific constructs were produced. The first one began at residue 116 and comprised the transmembrane domain (predicted to include residues Gly116 to Trp139) as well

as the short C-terminal region (Gln140 to Val148) for a total of 32 residues (RAMPtm(116-148)). The second construct was 47 amino acids long and included an additional extended N-terminal domain (Arg102 to Val148) (RAMPtm(102-148)). Both constructs were inserted into the pMM-LR6 vector as a *trpΔLE*-fusion using the same approach as for MRAP (see above).

3.1.2 Protein expression and uniform isotope labelling

NMR studies of proteins require large amounts of pure, isotopically enriched (e.g., ^{13}C, ^{15}N and ^{2}H) samples. The most effective way to achieve these requirements is by using recombinant DNA techniques and *Escherichia coli* (*E. coli*) as expression system. High level expression of MRAP and RAMP1 constructs was achieved by directing the proteins into inclusion bodies, which reduce toxicity and protease sensitivity (Staley & Kim 1994). Typically, ~70 % of the target protein was expressed within the first three hours after induction with 1 mM IPTG (Figure 4.10 (B)). Protein expression and uniform isotope labelling were carried out in an identical manner for all constructs. DNA plasmids carrying the correct sequence were transformed into *E. coli* Codon Plus BL21 (DE3, (Chloramphenicol^{R}) pLysS cells, taken from the agar plate and inoculated into 100 ml Luria Broth (LB) media over night at 310 K. For unlabelled growth the cells were transferred into three litres of LB media and split into 300 ml each in 2.0 litre baffled flasks and grown to an optical density of OD_{600} = 0.6 at 310 K. When the desired OD_{600} was reached, protein target expression was induced by

addition of 1 mM isopropyl β-D-1-thiogalactopyranoside (IPTG) and incubated overnight at 310 K.

Uniform isotope labelling was achieved by expression in isotope-enriched M9 minimal media. For ^{15}N-labelled protein, $^{15}NH_4Cl$ (1 g/L) was used as the only nitrogen source. For uniform carbon labelling, ^{13}C-glucose (2-4 g/L) was used as carbon source. To achieve partial deuteration, H_2O was substituted with D_2O (98-99 %). To achieve perdeuteration, D_2O (99.9 %) and perdeuterated glucose (D_7) was used. Isotope-enriched chemicals were obtained from Cambridge Isotope Laboratories, Cortecnet, or SigmaAldrich. To achieve a high yield per litre of isotope-labelled media a 4-fold condensation technique was used. For that bacterial cells containing the appropriate expression vector were grown in LB media at 310 K until they reached an optical density of OD_{600} = ~ 0.6. Three and four litres of LB media were used per growth. The cells were spun down at 3350 g for 20 minutes at 277 K, washed in 200 ml of 1 x M9 salts and subsequently centrifuged again at 3350 g for 20 min. The cells were then resuspended in 1 L M9 media, containing the appropriate nitrogen, carbon and/or hydrogen sources, incubated for 1 hour at 310 K and then protein expression was induced by the addition of 1 mM IPTG. Protein expression was allowed to precede overnight at 310 K before harvesting. For ^{2}H labelling cells were expressed for 24 hours at 310 K before harvesting.

3.1.3 Protein Purification

Protein purification was carried out in an identical manner for MRAP, RAMP1 and ACTH constructs. Figure 6.10 in Chapter 6 comprises all steps graphically. Fusion of the target proteins to *trpΔLE* resulted in the constructs being directed to inclusion bodies. Following expression, all constructs were purified according to Claridge *et al.* (Claridge & Schnell 2011). The protein of interest was primarily located in inclusion bodies. The cells were centrifuged at 3350 g for 20 min at 277 K and dissolved in 100 ml lysis buffer (50 mM Tris pH 8.0, 200 mM NaCl). For constructs containing cysteines, all buffers were supplemented with 5 mM β-mercaptoethanol. After sonication, lysates were centrifuged at 27,200 g for 15 min at 297 K. The pellet was washed with lysis buffer to remove water-soluble contaminants. Inclusion bodies were extracted with guanidine buffer (6 M guanidine HCl, 50 mM Tris (pH 8.0), 200 mM NaCl) and centrifuged at 18,000 g for 1.5 hours at 277 K to remove cellular debris. To separate the protein of interest from the crude lysate, the sample was bound to a Ni^{2+}-NTA affinity column (Sigma) and washed with six volumes guanidine buffer before elution with buffer containing 400 mM imidazole. After over night dialysis against H_2O the precipitated protein was centrifuged at 1500 g for 30 min and digested with cyanogen bromide (CNBr) (0.2 g/mL) in 70 % formic acid for 2 hours under a low-pressure stream of nitrogen gas to separate the protein from the *trpΔLE* fusion protein. CNBr cleaved at the single methionine residues that were introduced between the *trpΔLE* and target protein. The digested peptide of

interest was dialysed solely against H_2O for 1 hour, using a 3.5 kDa MWCO dialysis cassettes, and lyophilised over night. For the final purification step, reverse-phase HPLC was performed. The cleaved protein was dissolved in 50 % 2,2,2-triflouroethanol (TFE) and 25 % formic acid and loaded onto a C4 column (Grace-Vydac). Fragments were separated on a gradient from buffer A (5 % acetonitrile, 95 % H_2O, 0.1 % TFA) to buffer B (40 % acetonitrile, 60 % isopropanol, 0.1 % TFA).

3.2 PROTEIN IDENTIFICATION AND ANALYSIS

3.2.1 Sodium dodecyl sulphate polyacrylamide gel electrophoresis (SDS-PAGE)

SDS-PAGE was performed to estimate the molecular weight and to evaluate sample purity (Raymond & Weintraum 1959; Shapiro et al. 1967). In particular, precast 4 - 12 % Bis-Tris NuPAGE gels in MES buffer (Invitrogen) were used according to the manufacturer's protocol. An advantage of using these gels are their neutral pH environment and the Bis-Tris gradient throughout the gel, which allows for better separation of small mixed proteins. Coomassie Simply Blue Safe Stain (Invitrogen) was used to visualise the peptides at higher concentrations, while silver staining was used to develop gels containing lower protein concentrations. Apparent molecular weights were estimated based on migration rates of SeeBlue® Plus2 Pre-Stained Standard (Invitrogen). Gels were further analysed by the program ImageJ (Abràmoff et al. 2004).

3.2.2 Mass spectrometry (MS)

The correct sequence and size of the peptide preparations were confirmed by MS using an ESI-TOF mass spectrometer in Oxford's Biochemistry Department, Biophysics facility. Similarly, ESI-TOF MS was used to evaluate the efficiency of specific isotope labelling.

3.2.3 Protein concentration determination

Concentrations of peptide samples were determined by absorbance measurements at 280 nm using an UV/VIS BioPhotometer (Eppendorf). The theoretical protein extinction coefficient was calculated using the Expasy ProtParam tool (http://web.expasy.org/protparam/), which estimates extinction coefficients based on amino acid composition. ε(MRAP) is 21430 and ε(RAMP) is calculated to be 6990.

3.3 NMR SAMPLE DETERGENT RECONSTITUTION

3.3.1 Reconstitution of MRAP

For evaluation of the quality of NMR data, solutions of detergent were added to lyophilised samples of MRAP. All solutions contained 50 mM sodium phosphate buffer at pH 6.5 and 7 % D_2O. Samples typically contained 250 μM peptide in 100 mM Fos-Choline-10, 20 mM 1,2-dimyristoyl-*sn*-glycero-3-phosphocholine (DMPC) and 5 mM 1,2-dimyristoyl-*sn*-glycero-3-phospho-glycerol (DMPG). Further NMR samples were prepared in 50 mM SDS or 100 mM 1,2-dihexanoyl-*sn*-Glycero-3-Phosphocholine (DHPC). To ensure complete solubilisation and homogeneity within the sample each sample was freeze-thawed multiple times before usage. MRAP samples were typically stable up to three weeks at room temperature.

3.3.2 Reconstitution of RAMP1tm constructs

Lyophilised RAMP1 constructs were reconstituted by addition of buffered solution containing 40 mM SDS. All solutions contained 50 mM sodium phosphate (pH 6.5) and 7 % D_2O. Observation of the NMR spectra of RAMP1tm over the range of protein concentrations between 50 μM to 700 μM of peptide indicated that protein concentration was important for RAMP1tm(116-148) oligomerisation, and aggregation was observed when the protein concentration exceeded ~500 μM. Therefore, samples of RAMP1tm(116-148) typically contained 300 μM protein. The samples were stable for 1-2 weeks at room temperature.

3.3.3 Alternative reconstitution methods

3.3.3.1 Reconstitution from 6 M guanidine

The detergent of choice was dissolved in 6 M guanidine and 50 mM sodium phosphate buffer (pH 6.5) followed by addition of peptide. After the solution clarified, guanidine was dialysed out over night against 50 mM sodium phosphate buffer (pH 6.5). Dialysis was carried out at low stirring speed so that peptide refolding was gradual.

3.3.3.2 Reconstitution from thin films

For this method, the detergent of choice was dissolved in a fluorinated organic solvent in a glass vial. Depending on the detergent and the protein, 1,1,2,2-triflouroethanol (TFE) or 1,1,1,3,3,3-hexaflouro-2-propanol (HFIP) were used as solvents, since MRAP and RAMP1tm constructs did not dissolve in chloroform or methanol. A thin film of detergent was produced by rotating the solution under a weak nitrogen flow. The obtained detergent thin film was then re-dissolved in 400 μl of the same solvent, and lyophilised peptide was added. A second thin film containing detergent and peptide was formed at the bottom of the glass tube under weak nitrogen flow. This process was repeated until the thin film was clear. The thin film was then lyophilised to remove all remaining solvents and re-hydrated into the buffer of choice.

3.4 NMR METHODS

3.4.1 NMR Spectrometers and spectral analysis

All NMR experiments were performed on spectrometers with Oxford Instruments superconducting magnets (operating ^{1}H frequencies: 500 MHz, 600 MHz, 750 MHz and 950 MHz) equipped with either home built triple resonance probes with triple axis gradients (Battiste 2000; Soffe et al. 1995) (500, 600, 750, and 950 MHz) or with Bruker TCI Cryoprobes with single Z-axis gradients (500 and 600 MHz). Triple resonance probes allow for pulsing on ^{1}H, ^{13}C, and ^{15}N in one experiment, in addition to ^{2}H on the lock channel. TCI Cryoprobes are equipped with cooled preamplifiers for the ^{1}H, ^{13}C, and ^{2}H channels giving more sensitivity for double and triple resonance NMR experiments. NMR measurements were made on 350 µl samples in Shigemi microcells (5x17.5 mm). Unless otherwise indicated experiments were performed at 303 K. Spectra were routinely referenced to the water proton resonance frequency at 303 K (4.65 ppm). For chemical shift-based prediction of backbone ϕ and ψ angles using TALOS+, spectra were referenced to 4,4-dimethyl-4-silapentane-1-sulfonic acid (DSS) at 0 ppm (^{1}H). NMR data was processed using NMRPipe (Liang et al. 2006; Delaglio et al. 1995) and analysed using NMRDraw (Fanucci 2006; Delaglio et al. 1995). Chemical shifts were assigned using CARA (Delaglio et al. 1995; Keller R and Wuthrich K 2004).

3.4.2 Sequential resonance assignments

To assign MRAP(2-67) 3D ^{1}H-^{15}N- NOESY-HSQC (Kumar et al. 1981) and ^{1}H-^{15}N-TOCSY-HSQC (Davis & Bax 1985) spectra were recorded. A list for all obtained experiments is displayed in Table 3.1. 3D ^{1}H-^{13}C-HSQC-NOESY on uniformly ^{13}C-labelled samples were collected to achieve a large number of side-chain ^{1}H and ^{13}C assignments. For MRAP(2-67) stereospecific assignment of γ-methyls of valyl and δ-methyls of leucyl and isoleucyl residues were obtained by collecting a constant-time ^{1}H-,^{13}C-HSQC with 28 ms carbon evolution on 10% ^{13}C-labeled protein in deuterated SDS and protonated DHPC (Wilkins et al. 1999; Szyperski et al. 1992). This experiment enables assignment based on the presence or absence of ^{13}C-^{13}C couplings in the stereospecifically incorporated labels (Neri et al. 1989). Side-chain χ_1 and χ_2 rotamers for valyl, leucyl and isoleucyl residues were determined from methyl-based 3-bond *J*-coupling measurements (Grzesiek et al. 1993; Vuister & Wang 1993) in deuterated SDS or deuterated DHPC. Side chain χ_1 rotamers were extracted from $^{3}J_{C'C_\gamma}$ and $^{3}J_{NC_\gamma}$ coupling constants. Side chain χ_2 rotamers for leucine and isoleucines were determined from $^{3}J_{C_\alpha C_\gamma}$ coupling constants.

Triple-resonance experiments HNCA, HNCO, and CBCA(CO)NH in all three environments were used to obtain information on intramolecular and intermolecular $^{13}C\alpha$ and/or $^{13}C\beta$ resonances and to verify backbone amide assignments. Triple resonance experiments rely on transfer of magnetisation via heteronuclear J-coupling and the sensitivity of the experiments depends strongly

on the sizes of the J coupling required for magnetisation transfer. HNCA experiments were used to obtain correlation of the amide ^{1}H and ^{15}N resonances with the intra- and inter-residue $^{13}C\alpha$. CBCACONH experiments were collected to confirm backbone amide assignments and extend assignments to the $^{13}C\beta$ resonances. HNCO experiments were collected to assign $^{13}C'$ resonances.

Similarly, RAMP1tm(101-148) resonance assignments were completed using 3D ^{1}H-^{15}N-NOESY-HSQC and 3D ^{1}H-^{13}C-NOESY-HSQC, combined with HNCA, HNCO and CBCA(CO)NH experiments, collected on uniformly ^{15}N- and ^{13}C-labelled samples in deuerated SDS.

Sample	Environment	Experiment	Mixing time
^{15}N-labelled MRAP(2-67)	prot. DHPC	^{1}H-^{15}N-HSQC-NOESY	60 ms, 110 ms
^{15}N-labelled MRAP(2-67)	deut. DHPC	^{1}H-^{15}N-HSQC-NOESY	90 ms, 110 ms, 160 ms
^{15}N-labelled MRAP(2-67)	deut.SDS	^{1}H-^{15}N-HSQC-NOESY	100 ms, 140 ms, 200 ms
^{15}N-labelled MRAP(2-67)	Mixed micelles	^{1}H-^{15}N-HSQC-NOESY	120 ms and 180 ms
^{2}H-^{15}N-labelled MRAP(2-67)	deut. SDS	^{1}H-^{15}N-HSQC-NOESY	180 ms
^{2}H-^{15}N-labelled MRAP(28-67)	Mixed micelles	^{1}H-^{15}N-HSQC-NOESY	170 ms
^{13}C-^{15}N -labelled MRAP(2-67)	deut. DHPC	^{1}H-^{13}C-HSQC-NOESY	160 ms
^{13}C-^{15}N -labelled MRAP(2-67)	deut. SDS	^{1}H-^{13}C-HSQC-NOESY	160 ms, 200 ms, 250 ms
^{13}C-^{15}N -labelled MRAP(2-67)	deut. DHPC	HNCA, HNCO, CBCA(CO)NH	
^{13}C-^{15}N -labelled MRAP(2-67)	deut. SDS	HNCA, CBCA(CO)NH	
^{15}N-labelled RAMP1tm(116-148)	deut. SDS	^{1}H-^{15}N-HSQC-NOESY	110 ms
^{15}N-labelled RAMP1tm(101-148)	deut. SDS	^{1}H-^{15}N-HSQC-NOESY	110 ms
^{13}C-labelled RAMP1tm(101-148)	deut. SDS	^{1}H-^{13}C-HSQC-NOESY	200 ms
^{13}C-labelled RAMP1tm(101-148)	deut. SDS	HNCA, HNCO, CBCA(CO)NH	

Table 3.1: Obtained experiments to achieve assignment of MRAP(2-67), RAMP1tm(101-148) and RAMP1tm(116-148) in different environments

3.4.3 Chemical shift perturbation

For analysis of the backbone $^{1}H_N$ and ^{15}N chemical shift perturbation, the weighted average chemical shift differences were calculated using the equation

$$\Delta\delta_{AVE} = \sqrt{(\Delta\delta_{HN})^2 + \left(\frac{\Delta\delta_N}{5}\right)^2}, \quad \text{(Eq. 9)}$$

where $\Delta\delta_{HN}$ is the proton chemical shift and $\Delta\delta_N$ is the ^{15}N chemical shift changes.

3.4.4 Residual dipolar couplings

For residual dipolar coupling (RDC) measurements, weak alignment of the protein-mixed-micelle complex was accomplished using the strain-induced alignment in a gel (SAG) method (Chou & Bax 2001; Sass et al. 2000). The protein and surfactant solution was soaked into a cylindrically shaped 4.2 % - 4.4 % polyacrylamide gel, initially of a 5.4 mm diameter and 9 mm length. The polyacrylamide gel was dried for a few hours to decrease sample dilution. The protein-micelle mixture was then incubated with the dried gel for three days and subsequently stretched to fit within the 4.2 nm inner diameter of a NMR tube with open ends (http://newera-spectro.com), thereby increasing its length to 18 mm. $^{1}D_{NH}$ couplings were measured from a pair of ^{1}H-^{15}N correlation spectra recorded using a regular gradient-enhanced ^{1}H-^{15}N-HSQC and a gradient-selected $^{1}H^{15}N$ TROSY at 600 MHz. Dipolar wave analysis was performed using the previously published methods of Mesleh and Opella (Mesleh et al. 2002). QTIplot was used to analyse the sinusoidal function for helical regions of each protein. RDC refinement and back-calculation was performed using the program MODULE (Sebag & Hinkle 2007; Dosset et al. 2001).

3.4.5 NMR-based structure calculations

Structure calculations were performed using XPLOR-NIH 2.21 (Schwieters et al. 2003), with python-based scripting. The canonical parameter set provided in XPLOR-NIH was used to describe bond lengths, atom sizes and mass, and bond angles. Experimental data consisted of distance restraints from NOEs, side-chain χ_1 and χ_2 angles from $^3J_{C'C_\gamma}$ and $^3J_{NC_\gamma}$ scalar couplings. Distance restraints were derived from 3D ^{1}H-^{15}N-NOESY-HSQC and 3D ^{1}H-^{13}C-NOESY-HSQC spectra. Starting from a random coil initial structure, the simulation protocol comprised an initial high-temperature annealing step (1000 K) with low restraint energies to enable conformational sampling. The bath was then cooled from an initial high-temperature annealing step (1000 K) to 300 K with temperature steps of 20 K, during which experimental restraint energies and some canonical force field energies were ramped up: distances, 5 to 100 k cal mol^{-1} Å^{-2}; van der Waals, -0.002 → 4 kcal mol^{-1} Å^{-2}; improper = 0.1 → 1.0 k cal mol^{-1} degree^{-2}; and bond angles, 0.4 → 1.0 k cal mol^{-1} degree^{-2}. In addition, a weak database-derived 'rama'-potential function (Claridge & Schnell 2011; Kuszewski et al. 1997) was ramped from 0.02 to 0.2 (dimensionless force constant) for the general treatment of side chain rotamers. The calculation output was a set of 200 calculated structures. A set of twenty structures was selected based on lowest overall energies. These structures where then used as the starting model for the subsequent RDC refinement from 300 K to 20 K. The force constants used during the RDC refinement were identical to those values at the end of the high-temperature annealing run.

The open-source molecular viewer PYMOL (http://www.pymol.org/) was used for visualisation purposes. iCing (Doreleijers et al. 2012), an integrated residue-based structure validation program for NMR data was used to compare the experimental data with the NMR-derived structural models in each detergent. This program combines the programs WHATIF (Arsham & Kahn 1990), PROCHECK (Laskowski et al. 1996) and ShiftX (Neal et al. 2003).

3.4.6 NMR-based dynamics analyses of MRAP and RAMP1tm

{^{1}H}-^{15}N heteronuclear NOE spectra were measured with an acquisition time of 0.17413 s in ^{1}H and in 0.1925 s ^{15}N for MRAP; and with an acquisition time of 0.1069056 s in ^{1}H and in ^{15}N 0.0663385 s for RAMP1tm (Webb et al. 2008; Kay et al. 1989). The {^{1}H}-^{15}N heteronuclear NOEs, which are sensitive to the mobility of individual N_H-bonds, were determined from the ratio of peak intensities with and without the saturation of the amide protons, I_{on}/I_{off}.

Sample	Environment	Relaxation times
MRAP (2-67)	In 100 mM DHPC	T_1: 1200 ms, 20 ms, 1800 ms
		T_2: 100ms, 10ms, 160 ms
	In 50 mM SDS	T_1: 800 ms, 10 ms, 1200 ms
		T_2: 170 ms, 10 ms, 100 ms
	mixed micelles	T_1: 120 ms, 20 ms, 1800 ms,
		T_2: 120 ms, 10 ms, 200 ms
RAMP1tm (116-148)	In 40 mM SDS	T_1: 10 ms, 400 ms, 600 ms
		T_2: 5 ms, 48 ms, 72 ms
RAMP1tm (101-148)	In 40 mM SDS	T_1: 540 ms, 360 ms, 10 ms
		T_2: 5ms, 52 ms, 78 ms

Table 3.2: Relaxation delays for experiments to obtain T_1 and T_2 values

^{15}N longitudinal (T_1) and transverse (T_2) relaxation experiments were recorded using a previously published approach (Farrow et al. 1994). T_2 values were

acquired using a spin-echo sequence with a CPMG delay (Meiboom & Gill 1958). ^{15}N T_1 and T_2 relaxation rates were measured by collecting spectra at different relaxation delays chosen according to Cramer-Rao theory (Jones et al. 1996)(Table 3.2). Acquisition times of 0.1069056 s (^{1}H) and 0.0663385 s (^{15}N) were used in all T_1 and T_2 experiments for RAMP1tm. 0.1072146 s (^{1}H) and 0.0694387 s (^{15}N) were used for measurements of MRAP, respectively. Each set of T_1 and T_2 relaxation experiments consisted of a series of 9 spectra (each delay was recorded three times) with increasing ^{15}N relaxation time delays chosen to sample the entire decay. The acquired relaxation data were analysed for all residues with visible and resolved peaks.

3.4.7 Site-specific paramagnetic relaxation enhancement (PRE) experiments for MRAP(2-67)

To obtain structural insights into potential dimerisation of MRAP in mixed micelles, PRE experiments were recorded on site-specifically spin-labelled MRAP(2-67). Intensity measurements of ^{1}H-^{15}N crosspeaks in HMQCs of samples containing a mixture of differently labelled peptides were used to measure the effect of paramagnetic broadening. Interactions with electron spin increase spectral linewidths, which can be quantified by measuring the relative intensities of spectra with and without the presence of the electron spin (Fanucci 2006). A single cysteine was introduced at position 65 (MRAP-S65C) using site-directed mutagenesis, in order to attach the nitroxide paramagnetic spin label S-(2,2,5,5-tetramethyl-2,5-dihydro-1H-pyrrol-3-yl)methyl-methanesulfonothioate (MTSL).

Equimolar amounts of spin-labelled MRAP-S65C (natural abundance isotope) were mixed with ^{15}N-labelled MRAP(2-67) after HPLC purification and before lyophilisation. After lyophilisation the mixed sample was taken up in 400 µl of 50 mM sodium phosphate buffer, 8 M urea, 10 mM tris(2-carboxyethyl)phosphine (TCEP), 100 mM Fos-Choline-10, 20 mM DMPC and 5 mM DMPG. MTSL was freshly dissolved in dimethylsulfoxide (DMSO) and added to the solution to a final concentration of 1 mM. Since MTSL is light sensitive it was important that all steps were performed in the dark.

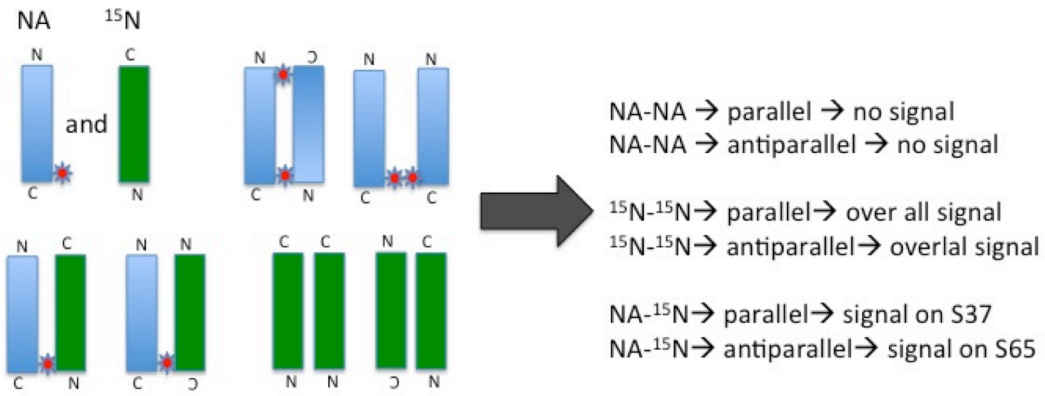

Figure 3.2: Schematic model of PRE measurements: Unlabelled and ^{15}N-labeled protein was mixed to same amounts to allow specific labelling

The PRE solution with peptide was incubated at room temperature for two hours and then dialysed against 50 mM sodium phosphate buffer (pH 6.5) overnight. The complete incorporation of MTSL was confirmed by MS. ^{1}H-^{15}N-SOFAST-HMQC (Schanda et al. 2005) experiments on the oxidised sample were acquired at 303 K at 600 MHz. Total experimental times were ~6 hours. Addition of a 3 to 4 molar excess of ascorbic acid from a 200 mM stock solution was used to reduce the nitroxide and the NMR experiments were repeated. To ensure complete reduction of the spin label the sample was placed in the spectrometer at 303 K for

at least one hour before the experiment was started. In a second experiment, ^{15}N labelled MRAP-S65C by itself was labelled with MTSL using the above-described method and PREs were measured. The spectra were processed with NMRPipe and the ratios of crosspeak intensities (I_0/I) were quantified in NMRDraw (Delaglio et al. 1995).

3.4.8 Water-soluble paramagnetic broadening enhancement

The depth of insertion of peptides in a lipid bilayer or a micelle can be determined using water-soluble paramagnetic metal complexes. Water-soluble chelates of paramagnetic Mn^{2+} ions will selectively increase the R_2 relaxation rates of nuclear spins that are exposed to water and thus affect the linewidth and signal intensity (Altenbach et al. 1994; Lau et al. 2008). 4 mM of $Mn^{2+}EDDA^{2-}$ was added to the protein sample to achieve line-broadening and to probe for water accessibility. ^{15}N-edited HSQCs were recorded before and after addition of a three-fold molar excess of Mn^{2+} EDDA. N_H protection from $Mn^{2+}EDDA^{2-}$ was expressed quantitatively as the ratio of N-H signal intensities in the presence (I) and absence (I_o) of the paramagnetic agent, I/I_o. This allowed identification of residues that are embedded in the water-excluded hydrophobic micelle or mixed micelle core.

3.4.9 Hydrogen-deuterium exchange measurements in RAMP1tm

The hydrogen deuterium exchange (H-D-exchange) reaction was conducted on a sample containing 270 µM ^{15}N-labeled RAMP1tm(102-148) protein. The lyophilised protein was split in half and solubilised in either 40 mM SDS, 50 mM sodium phosphate buffer (pH 6.5) in 350 µl 99.9% D_2O or in 350 µl 95% H_2O and 5% D_2O. SOFAST-HMQCs (Schanda et al. 2005) at 600 MHz were recorded to monitor hydrogen exchange of the protein amides with D_2O. 64 scans for each direct increment and 128 for each increment in the indirect dimension were collected. The intensities of ^{1}H-^{15}N crosspeaks in the SOFAST-HMQC spectra were estimated from the volumes of the peaks and corrected for variations of protein concentration in each sample using the intensities of three non-exchangeable up-field methyl resonances in the proton 1D NMR spectra.

3.4.10 Hydrodynamic radius determination by pulse gradient field experiments

Pulsed field gradient (PFG) NMR methods were used to determine the effective hydrodynamic radii and radii of gyration of the protein and micelle complexes (Wilkins et al. 1999). The radius of gyration is the root-mean-squared distance of all atoms in the molecule from the protein centre of mass, while the hydrodynamic radius describes the radius of a sphere that has the same diffusion coefficient as the protein molecule. Thus, the results of such data can provide experimental evidence for the oligomeric state of proteins, similar to scattering

methods such as small angle scattering (Glatter & Kratky 1982) or dynamic light scattering (DLS) methods (Pecora 1985). In theory, PFG NMR techniques allow for a more sensitive measure of hydrodynamic properties. For the PFG experiments, a large excess of 1,4-dioxane was added to the protein sample to act as a viscosity probe and an internal reference. (Wilkins et al. 1999). All NMR experiments were recorded on a 500 MHz home-built spectrometer with a triple-resonance pulsed-field-gradient probe at 303 K using the PG-SLED (pulse gradient stimulated echo longitudinal encode-decode) approach (Jones et al. 1997). In PG-SLED, strong magnetic field gradient echos are used with variable diffusion delays to obtain decay profiles proportional to the molecular diffusion rates. The decay in the signal from the experiment was fitted to a Gaussian function as well as to a decay function that could be observed by NMR. This led to an additional signal loss that was accounted for by multiplying the Gaussian function used to fit the diffusion coefficient by a linear decay term. For large aggregates, such as proteins buried within micelles, the decay in intensity is very small over the range of gradient strengths used to monitor the monomeric states. This analysis was done using the program Felix 2.3 (http://www.felixnmr.com/).

3.5 BIOCHEMICAL METHODS

3.5.1 Chemical crosslinking with DSP and glutaraldehyde

Chemical crosslinking is the process of covalently linking two or more molecules via a protein-reactive compound. Primarily there are three functional groups that are useful targets for crosslinking reactions: Primary amines (-NH_3) found at the peptide N-terminus and the side chains of lysines; carboxyls (-COOH) found at peptide C-termini and in the side chains of aspartates and glutamates; and the sulfhydryls (-SH) of cysteines. Two commonly used crosslinking reagents are the homobifunctional compounds glutaraldehyde and dithiobis[succinimdyl propionate] (DSP; MW = 404.4 Da). The crosslinker glutaraldehyde is a commonly used crosslinking reagent that is both self-reactive and reactive with the following amino acids (Migneault et al. 2004): lysine (Bowes & Cater 1968); tyrosine, tryptophan, and phenylalanine (Hopwood et al. 1970); histidine, cysteine, proline, serine, glycine and arginine (Schwieters et al. 2003; Kuszewski et al. 1997).

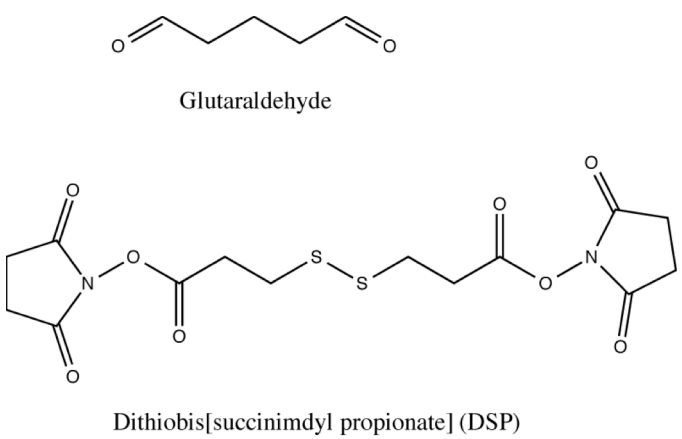

Figure 3.3: Chemical structures of Glutaraldehyde and DSP. These crosslinkers were chosen according to their reactivity and their targeting functional groups.

The imidoester DSP is a more specific acylating reagent and only reacts with amine groups, such as the side chains of lysines and peptide N-termini (http://www.piercenet.com/). Hydrolyses of the N-hydroxysuccinimide (NHS) esters are a major competing reaction of the NHS-ester acylation reaction (Mattson et al. 1993).

Crosslinking by glutaraldehyde and DSP were used to investigate the oligomeric states of MRAP(2-67) and RAMP1tm constructs. Each sample was incubated with between 2 and 7 mM DSP or 1.6 mM glutaraldehyde for 5 to 15 minutes and the reactions terminated by the addition of 50 mM Tris-HCl (pH 8). The reactions were analysed by SDS-PAGE.

3.5.2 Studies of MRAP dimerisation via disulphide bonds formation

To study the dimeric state of MRAP in lipid vesicles an analytical assay was adapted that has been previously described (Suk et al. 2012). Single cysteines were introduced at positions His36 (MRAP-H36C) and Ser65 (MRAP-S65C) to allow formation of intermolecular disulphide bonds. The first experiment included three different samples of MRAP(2-67): MRAP-H36C, MRAP-S65C, and a mixture of MRAP-H36C and MRAP-S65C. MRAP-H36C and MRAP-S65C by themselves were used as controls for parallel dimerisation. Mixing equimolar amounts of MRAP-H36C and MRAP-S65C directly after HPLC purification produced a mixed sample of MRAP-H36C/MRAP-S65C. Experiments were conducted according to the following protocol. Membranes were formed using

Yeast Polar Lipids and Brain Total Lipid Extract. 2 mg of lipids were dissolved in 50 % chloroform and 50 % TFE. TCEP was added to a final concentration of 5 mM to prevent spontaneous formation of disulphide bonds. Thin films of the lipid solution were formed on the wall of a glass vial by rotating the vials under a weak nitrogen stream. This process was repeated twice. Residual traces of organic solvents were removed by lyophilising the sample of interest. The dried thin film was dissolved in 300 µl of TFE and 60 µg of the target peptide was added. Formation of the thin film and subsequent lyophilisation were repeated to fully solubilise the peptide in the lipid mixture. The thin films were rehydrated in 100 µl of 50 mM sodium phosphate buffer (pH 6.5) and split in two. One half was set aside as a negative control. To accelerate disulphide formation the hydrophobic oxidant Cu^{2+}·[phenanthroline]$_2$ was added to a final concentration of 0.25 mM to half of the sample. The Cu^{2+}·[phenanthroline]$_2$ was prepared fresh by mixing equal volumes of 200 mM $Cu^{2+}SO_4$ in water and 400 mM 1,10-phenanthroline in N,N- dimethylformamide (Suk et al. 2012). The crosslinking reaction was allowed to proceed for one hour at room temperature so that disulphide-linked dimers could accumulate. To stop the reaction and to block any remaining free cysteines 10 mM EDTA and 2 mM N-ethylmaleimide (NEM) were added. To remove any traces of solvent the sample was lyophilised overnight before resuspension in 50 mM sodium phosphate buffer (pH 6.5) and 8 M urea. Resulting samples were run on SDS-PAGE to evaluate disulphide

formation, and the program ImageJ was used to quantify the gel band intensities (Rasband 2012).

3.5.3 Circular dichroism

Circular dichroism (CD) measurements were recorded in a 1 mm path length cuvette on a Jasco J-720 circular dichroism spectropolarimeter in the Biophysical Facilities of the New Biochemistry Department of the University of Oxford using the following parameters: wavelength of λ = 340 nm to 190 nm with a speed of 50 nm/min, sensitivity of 50 ndeg, and a resolution of 0.5. An average of five spectra was taken and baseline corrected through background subtraction.

Freshly purified aliquots of peptides were diluted to a final concentration between 10 and 40 μM in 50 mM Tris-HCl buffer (pH 6.5) with addition of detergent mixtures. Additionally, CD was performed on peptides in liposomes. Liposomes were produced by thin films (as described previously) prior to adding the protein. The procedure of making thin films was repeated four times before a final lyophilisation step. The sample was rehydrated in sodium phosphate buffer (pH 6.5). To minimise dispersion, the size of the liposomes of each sample was decreased by high power (70 W) sonication 15 times for 10 seconds each.

By convention, CD data are presented as either ellipticity θ or differential absorbance ΔA. For far UV CD proteins the Mean Residue Weight (MRW) for a peptide bond is calculated by

$$MRW = \frac{M}{N-1} \qquad \text{(Eq. 10)}$$

where *M* is the molecular mass of the peptide chain (in Da) and N the number of amino acids, where *N-1* gives the number of peptide bonds.

The mean residue ellipticity at wavelength λ$[\theta]_{mrw_\lambda}$ is given by

$$[\theta]_{mrw\lambda} = \frac{MRW * \theta_\lambda}{10 * d * c} \quad \text{(Eq. 11)}$$

where θ_λ describes the observed ellipticity [º] at a wavelength λ, d the path length [cm] and c the peptide concentration [g/mL]. The units for the mean residue ellipticity is deg cm^2 $dmol^{-1}$ (Kelly et al. 2005). The protein concentration in all cases was determined by A_{280} absorption

3.5.4 Dynamic light scattering

To determine the size of MRAP(2-67) complexed with different detergent mixtures, several samples of varying detergent and peptide concentrations were studied by dynamic light scattering using a Malvern Protein Solutions particle size detector model 801 in the Biophysical Facilities of the New Biochemistry Department (University of Oxford). Laser light with a wavelength of 827.6 nm was used, and intensities were measured at an angle of 90°. Data were collected at 293 K.

MRAP(2-67) solubilised in 50 mM SDS or 100 mM Fos-Choline-10 + 20 mM DMPC + 5mM DMPG were tested. For comparison, samples containing 50 mM SDS, or 100 mM Fos-Choline-10 , or 100 mM Fos-Choline-10 + 20 mM DMPC, or 100 mM Fos-Choline-10 + 20 mM DMPC + 5mM DMPG in the absence of MRAP(2-67) were tested. All samples contained 50 mM sodium phosphate buffer (pH 6.5). Each sample was prepared with filtered water and large particles were

spun down before usage. 15μl samples were loaded into a quartz cuvette. The refractive index and viscosity of the samples were taken into account within the instrument software manager. All data were analysed using Malvern OmniSIZE 3.0.

3.5.5 Analytical ultracentrifugation (AUC)

Sedimentation equilibrium AUC measurements were carried out using a Beckman Optima XL-I, with integrated absorbance and interference optics, in the Biophysical Facilities of the New Biochemistry Department of the University of Oxford. The peptide samples were prepared in 50 mM sodium phosphate buffer (pH 6.5), containing either 100 mM DHPC or 50 mM SDS in 100 % D_2O (Cambridge Isotope Laboratories, Andover, MA, US) to match the buoyant density of the detergent. "Density matching" was entirely done according to Tanford *et al*. (Tanford et al. 1974; Tanford & Reynolds 1976). All data were collected using a double-sector centrepiece with absorbance optics set at 280 nm. Data for MRAP(2-67) were collected at a peptide concentration of 60 μM and at 25,000 rpm, 30,000 rpm, 35,000 rpm and 40,000 rpm at 303 K. A total equilibration time of 12 h was used for each step with scans taken at 12 and 14 h to ensure that the equilibrium has been reached. The moving boundary was monitored by repetitive radial scanning at a constant step size of 0.005 cm at 280 nm using UV-absorption optical system.

Fitting of the obtained profiles was achieved using SEDFIT and SEDPHAT (Schuck 2000). In these programs the sedimentation coefficient distribution

function was obtained from a direct fit to the data (Dam & Schuck 2004) and subsequently converted to a molecular mass distribution using a monomeric mass of 7559.7 Da and a dimeric mass of 15119.4 Da for MRAP(2-67). Buffer density values were achieved by calculating the expected density, based on experimental data from Tanford *et al.* (Tanford et al. 1974). Buffer densities of 1.1 g/cm^3 and 1.15 g/cm^3 were used for 100 mM DHPC and 50 mM SDS, respectively.

3.6 COMPUTATIONAL STUDIES OF MRAP

3.6.1 Theoretical background

Molecular dynamic (MD) simulations were conducted to explore the dimerisation state of MRAP(2-67). Molecular dynamic and molecular mechanic simulations can be used to mimic the positions of atoms in time according to well-defined interaction potentials (Karplus & Kuriyan 2005; Deng & Roux 2009). Both methods allow evaluation of structure-function relationships of biomolecules, prediction of protein mutation effects, protein folding landscapes, and quantification of entropic effects and free energies on an atomic level (Adcock & McCammon 2006; Leach 2001). No assumptions are made on the mechanism of functional processes when setting up the experiment, which permits generation of testable hypotheses.

In classical MD simulations, atoms are treated as van der Waals spheres with point charges at the centre of each sphere. Quantum mechanical molecular mechanic (QM-MM) methods is typically used as the basis of MD simulations, by modelling small parts of a protein at the QM level and the rest of the protein at the molecular mechanics (MM) level (Senn & Thiel 2007). However, since QM-MM calculations are computationally very demanding, they cannot be used for larger, biologically relevant units like proteins. For full protein studies the level of detail must be lowered. Therefore, the so-called classical MD simulations rely on simplified, empirical force field models that are imposed on atom distances,

angles and dihedral geometries in covalent bonding, van-der-Waals interactions and charge distribution (Leach 2001; Sansom & Biggin 2010).

3.6.1.1 The force field

An MD force field describes the potential energy of the simulated particles as a function V of its atomic coordinates. The force F_i on a particle i can be calculated through $F_i = -\frac{\partial V(r)}{\partial r_i}$ (Eq. 12)

where V(r) describes the potential energy function of the position r of a particle i. The individual contributions to a force field can be grouped into bonded and non-bonded interactions. Bonded interactions act only between covalently bound particles. Non-bonded ones act between all atoms and include electrostatics, dispersion and Pauli exclusion (Guvench & MacKerell 2008; Van Der Spoel et al. 2005). Force field parameters are usually designed to reproduce experimental and quantum chemical data. There are several widely used biomolecular force fields, including Amber, CHARMM, GROMOS and OPLS-AA.

3.6.1.2 Coarse-grained simulations

A significant limitation of MD of macromolecules is the system size (number of atoms) and/or the time-scale that can be simulated. Especially, simulations of membrane proteins within lipid bilayers require a large number of atoms to be simulated. One way to overcome this problem is by replacing groups of atoms with simplified representations, which sacrifices atomic level detail for improvements in computational efficiency. The advantages of that simplification, called coarse-graining, are the increase of time and length scale by up to 100

times. Coarse-grain (CG) method is based on statistical coarse graining prescription (Rudd & Broughton 1998). In such models, 'pseudo-atoms' are used to represent or are mapped to groups of atoms instead of explicitly representing every single atom. Such models enable simulation of macromolecular systems on the order of a micron. A commonly used force field for coarse-grain MD simulations in bilayers is MARTINI (Marrink et al. 2007) and its variant BOND (Bond & Sansom 2006; Bond et al. 2007).

In the CG simulations in this thesis, MARTINI version 2.2 force field and the variant BOND (Bond et al. 2007) were used for all described CG-MD simulations in Chapter 5.

3.6.1.3 CG-model: MARTINI

MARTINI is a CG-MD force field providing parameters for amino acids that have been developed specifically for proteins in lipid bilayers. The main features of MARTINI are an inclusion of interaction energy levels and particle types, and a correlation between calculated and experimental partitioning free energies. For the latter, MARTINI is based on the reproduction of partitioning free energies between polar and apolar phases of a large number of chemical compounds (Marrink et al. 2004; Marrink et al. 2007). This provides an empirically supported basis for protein and membrane interactions. MARTINI uses a four-to-one mapping, which means that four heavy atoms such as carbons and oxygens are represented by one interaction centre. Four main CG particle types of interaction sites are defined in MARTINI: polar (P), non-polar (N), apolar (I) and charged (Q). Polar particles represent water-soluble neutral groups, non-polar represent a

mixed (polar/apolar) group of atoms, apolar (I) represent a hydrophobic group of atoms, and charged represent an overall net charged group of atoms (Marrink et al. 2007) (Figure 3.4).

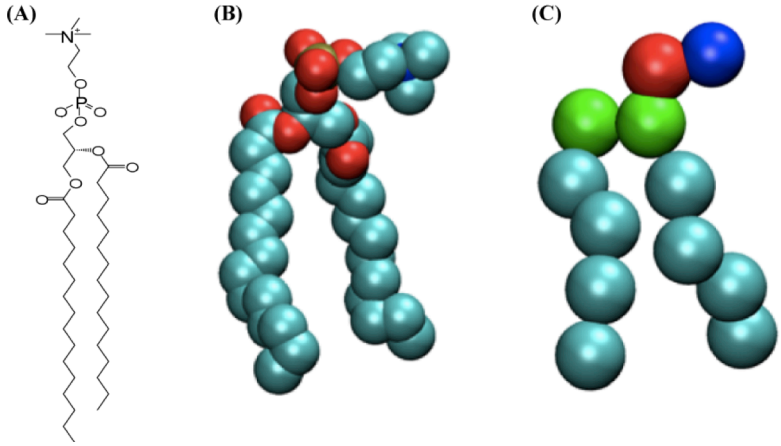

Figure 3.4: Atomistic (AT) vs. coarse-grained (CG) representations of DPPC
(A) The chemical structure of DPPC.
(B) Atomistic representation of DPPC.
(C) Coarse-grain representation of DPPC in MARTINI.
In the AT models oxygen atoms are displayed in red and carbons in cyan. In the CG-model the particles are coloured according to the following scheme: green - nonpolar particle; cyan - apolar particle; red or blue – negative or positive charged particle (Adapted from Bond et al. 2007)

A general scheme of MARTINI is implemented in the GROMACS software package (Van Der Spoel et al. 2005) to develop models: non-bonded interactions are cut off at a distance of 1.2 nm with smooth switching of the interactions and forces from 0.0 to 1.2 nm for the Coulomb potential and 0.9 to 1.2 nm for the Lennard-Jones (LJ) potential. The pair-list update frequency is set to once per 10 steps (de Jong et al. 2013).

3.6.1.3.1 BOND

BOND force field was developed on the basis of MARTINI for Glycophorin A by Bond and Samson (Bond & Sansom 2006; Bond et al. 2007). In this force field, protein folding driven by atomic-detail interactions preserves additional constraints for the secondary and tertiary protein structure. Therefore, in theory,

one should be able to get a more dynamic model of proteins in detergent micelles and lipid bilayers.

3.7 MD SOFTWARE AND PRACTICAL CHOICES

All MD simulations were performed using the GROMACS open-software package (Van Der Spoel et al. 2005). GROMACS (GROningen Machine for Chemical Simulation) is a versatile and efficient MD program developed for the simulation of biomolecules (Van Der Spoel et al. 2005). It contains size, shape, number and types of molecules, as well as the coordinates and velocities of all atoms that define the system. The system is usually described as a rectangular box with periodic boundary conditions. GROMACS does not have a general force field for intramolecular interactions, but it has an organisation of force and energy evaluations, e.g. MARTINI2.2 or BOND. The lipid force fields (DPPC, POPC) were established in the group of Professor Mark Sansom in the New Biochemistry Department, University of Oxford (Sansom & Biggin 2010). Three environments were chosen to study MRAP with MD: DPPC, POPC and DPPC:DPPG (75:25).

3.7.1 Establishing the conditions for MD simulations

In order to study MRAP's dimerisation, the sequences between residues Ser13 and Gln67 were employed. Since the lipid force fields for DPPC and POPC were already established, micelles were formed using self-assembly with the protein being present. For creating the bilayer containing DPPC:DPPG (75:25) a script written by Heidi Koldsoe was used that randomly exchanges PC-lipids with

DPPG-lipids. The two helices were inserted into the system and positioned at a distance of ~60 Å from each other (either in parallel or anti-parallel conformation). Crucially, this distance between helices was larger than the cut-off distance for electrostatic and Van-der- Waals interactions in the force field to exclude inter-helical interactions at the beginning of the simulations and hence did not artificially favour dimer formation. In an initial simulation, the lipids were allowed to freely self-assemble into a lipid bilayer around the fixed helices. All performed simulations were run for one μs and are listed in table 3.3. Re-sampling of simulations increases the confidence of the obtained results.

3.7.2 Atomistic MD simulations

Atomistic simulations were used to check the stability of dimer structures, as well as to refine a possible dimeric interface. For MRAP(13-67) in DPPC the five most representative CG-calculated structures of parallel or anti-parallel conformations and either left-handed or right-handed orientations were selected and converted to AT representations using the fragment-based approach, CG2AT written by Dr. Phillip Stansfeld (Stansfeld & Sansom 2011). After equilibration of the system, 50 ns atomistic simulations were run.

3.7.3 Simulation Analysis

Simulations were analysed using a script written by Amanda Buyan, which evaluates the proposed dimeric interface of each simulation, looking at the crossing angle of two helices, the minimum distance as well as z-displacement. To obtain greater confidence in coarse-grain simulations, re-sampling was

applied, with most simulations in BOND and MARTINI2.2 repeated between 15 and 20 times.

Simulation	Force Field	Environment	Duration (ns)
CG-MRAP(13-67) anti-parallel	BOND	DPPC	~15 x 1000
CG-MRAP(13-67) parallel	BOND	DPPC	~15 x 1000
CG-MRAP(13-67) S61D anti-parallel	BOND	DPPC	~ 5 x1000
CG-MRAP(13-67) S61D parallel	BOND	DPPC	~ 5 x1000
CG-MRAP(13-67) S61E anti-parallel	BOND	DPPC	~ 5 x1000
CG-MRAP(13-67) S61E parallel	BOND	DPPC	~ 5 x1000
CG-MRAP(13-67) anti-parallel	MARTINI2.2	DPPC	~20 x 1000
CG-MRAP(13-67) parallel	MARTINI2.2	DPPC	~20 x 1000
CG-MRAP(13-67) anti-parallel	MARTINI2.2	POPC	~20 x 1000
CG-MRAP(13-67) parallel	MARTINI2.2	POPC	~20 x 1000
CG-MRAP(13-67) anti-parallel	MARTINI2.2	DPPC:DPPG (75:25)	~20 x 1000
CG-MRAP(13-67) parallel	MARTINI2.2	DPPC:DPPG (75:25)	~20 x 1000
AT-RH- MRAP(13-67) anti-parallel		DPPC	2 x 50
AT-RH- MRAP(13-67) parallel		DPPC	1 x 50
AT-LH- MRAP(13-67) anti-parallel		DPPC	1 x 50
AT-LH- MRAP(13-67) parallel		DPPC	1 x 50

CHAPTER 4

STRUCTURAL AND BIOPHYSICAL CHARACTERISATION OF MONOMERIC MRAP

"Man soll den ehrlichen Menschen achten, auch wenn der andere Meinungen hat und vertritt als man selbst."

(Albert Einstein)

4.1 INTRODUCTION

4.1.1 Melanocortin system and the Melanocortin Receptors

Melanocortin receptors (MCR) belong to the rhodopsin-like class A family of GCPRs (Fredriksson et al. 2003; Cooray & Clark 2011) and have diverse physiological roles (Abdel-Malek 2001). The number of melanocortin receptors varies from species to species. In zebrafish for example, six melanocortin receptors are known whereas in pufferfish only four are known (Västermark & Schiöth 2011). In mammals five melanocortin receptors (1 to 5) are known, where the following physiological roles have been described (Table 4.1):

- MC1R: pigmentation (Västermark & Schiöth 2011; Cooray & Clark 2011; Chhajlani & Wikberg 1992) (also known as the melanocyte-stimulating hormone receptor)
- MC2R: adrenal corticosteroid synthesis and steroidogenesis (Abdel-Malek 2001; Chida et al. 2007; Cone 2006; Västermark & Schiöth 2011; Hirsch et al. 2011) (also known as the adenocorticotropic hormone (ACTH) receptor)
- MC3R: energy homeostasis and adipose tissue deposition (Chen et al. 2000; Getting et al. 2008; Sutton et al. 2008; Grieco et al. 2002; Vaisse et al. 1998)
- MC4R: energy homeostasis, appetite regulation, adipose tissue deposition (Cone 2006; Getting et al. 2008; Västermark & Schiöth 2011; Sutton et al. 2008; Hirsch et al. 2011; Grieco et al. 2002; Abdel-Malek 2001; Vaisse et al. 1998; Chida et al. 2007; Farooqi et al. 2003; Chen et al. 2000)
- MC5R: exocrine gland secretion and immune regulation (Chen et al. 1997; Abdel-Malek 2001; Taylor & Namba 2001; Reinick et al. 2012).

MCRs respond with different affinities to the four peptide agonists ACTH, α-melanocyte-stimulating hormone (MSH), β-MSH, and γ-MSH, all of which are derived from the proopiomelanocortin precursor (POMC) protein. In addition, MCRs interact with two inverse agonists, agouti signalling protein (ASP) and agouti-related proteins (AGRP) (Lu et al. 1994; Hadley et al. 1996; Naville et al. 1997; Cone 2006). ASP antagonises MC1R, MC2R and MC4R, whereas AGRP antagonises MC3R, MC4R and MC5R (Yang et al. 1999).

In general, ligand binding of all MCRs leads to activation of $G\alpha_s$ that initiates the cAMP/PKA pathway, which is a common signalling cascade essential for cell communication (Alberts 2008). Activation of $G\alpha_s$ first leads to activation of adenylate cyclase causing production of cyclic adenosine monophosphate (cAMP), which then activates several intracellular enzymes, including protein kinase A (PKA) (Cone 2006; Alberts 2008).

Receptor	Peptide agonist	Main sites of expression	Physiological function	Disease phenotype	OMIM
MC1R	α-MSH, ACTH	Melanocytes, macrophages	Pigmentation, inflammation	Increased risk of skin cancer	155555
MC2R	ACTH	Adrenal cortex	Adrenal steroidogenesis	Familial glucocorticoid deficiency	202200
MC3R	α-, β-, γ-MSH, ACTH	Central nervous system, gastrointenstinal tract, kidney	Energy homeostasis, inflammation	Obesity	155540
MC4R	α-, β-, γ-MSH, ACTH	Central nervous system, spinal cord	Energy homeostasis, appetit regulation, erectile function	Obesity	15541
MC5R	α-MSH, (β-MSH, ACTH)	Lymphocytes, exocrine cells	Exocrine function, regulation of sebeceaous glands	Decreased procution of sebaceous lipids	600042

Table 4.1: The members of the melanocortin receptor family, peptide agonist, expression, action, phenotype with mutations

MCRs are small members of the GPCR superfamily with short N- and C-terminal

domains. They share 39 – 61 % sequence homology on amino acid level among each other (Figure 4.1). The MCRs exhibit the general GPCR family characteristics, including seven α-helical transmembrane domains connected by three alternating extra- and intracellular loops (Abdel-Malek 2001). As with many other GPCRs, melanocortin receptors have predicted N-glycosylation sites in the N-terminal domains, phosphorylation recognition sites for PKA and protein kinase C (PKC) and conserved cysteines in their C-terminal ends (Abdel-Malek 2001; Cone 2006; Lu et al. 1994; Hadley et al. 1996; Yang et al. 1999; Rana 2003).

```
tr|Q1JUM3|MC1R_HUMAN        -MAVQGSQRRLLGSLNSTP-----TAIPQLGLAANQTGARCLEVSISDGL 44
sp|Q01718|MC2R_HUMAN        ----MKHIINSYENINNTA-----RNNSD-----------CPRVVLPEEI 30
sp|P41968|MC3R_HUMAN        -MNASCCLPSVQPTLPNGS-----EHLQAPFFSNQSSSAFCEQVFIKPEV 44
tr|A0N0W9|MC4R _HUMAN       MVNSTHRGMHTSLHLWNRSSYRLHSNASESLGKGYSDGGCYEQLFVSPEV 50
sp|P33032|MC5R_HUMAN        -MNSSFHLHFLDLNLNATE-----GNLSGPNVKNKSSP--CEDMGIAVEV 42
                                       :                          : :   :

tr|Q1JUM3|MC1R_HUMAN        FLSLGLVSLVENALVVATIAKNRNLHSPMYCFICCLALSDLLVSGSNVLE 94
sp|Q01718|MC2R_HUMAN        FFTISIVGVLENLIVLLAVFKNKNLQAPMYFFICSLAISDMLGSLYKILE 80
sp|P41968|MC3R_HUMAN        FLSLGIVSLLENILVILAVVRNGNLHSPMYFFLCSLAVADMLVSVSNALE 94
tr|A0N0W9|MC4R_HUMAN        FVTLGVISLLENILVIVAIAKNKNLHSPMYFFICSLAVADMLVSVSNGSE 100
sp|P33032|MC5R_HUMAN        FLTLGVISLLENILVIGAIVKNKNLHSPMYFFVCSLAVADMLVSMSSAWE 92
                            *.::.::.::** :*: :: :* **::*** *:*.**::*:* *  .  *

tr|Q1JUM3|MC1R_HUMAN        TAVILLLEAGALVARAAVLQQLDNVTDVITCSSMLSSLCFLGAIAVDRYI 144
sp|Q01718|MC2R_HUMAN        NILIILRNMGYLKPRGSFETTADDIIDSLFVLSLLGSIFSLSVIAADRYI 130
sp|P41968|MC3R_HUMAN        TIMIAIVHSDYLTFEDQFIQHMDNIFDSMICISLVASICNLLAIAVDRYV 144
tr|A0N0W9|MC4R_HUMAN        TIVITLLNSTD-TDAQSFTVNIDNVIDSVICSSLLASICSLLSIAVDRYF 149
sp|P33032|MC5R_HUMAN        TITIYLLNNKHLVIADAFVRHIDNVFDSMICISVVASMCSLLAIAVDRYV 142
                            .  * : .         .    *:: * :   *::.*:  *  **.***.

tr|Q1JUM3|MC1R_HUMAN        SIFYALRYHSIVTLTRARRAVAAIWVASVVFSTLFIAYYDHVAVLLCLVV 194
sp|Q01718|MC2R_HUMAN        TIFHALRYHSIVTMRRTVVVLTVIWTFCTGTGITMVIFSHHVPTVITFTS 180
sp|P41968|MC3R_HUMAN        TIFYALRYHSIMTVRKALTLIVAIWVCCGVCGVVFIVYSESKMVIVCLIT 194
tr|A0N0W9|MC4R_HUMAN        TIFYALQYHNIMTVKRVGIIISCIWAACTVSGILFIIYSDSSAVIICLIT 199
sp|P33032|MC5R_HUMAN        TIFYALRYHHIMTARRSGAIIAGIWAFCTGCGIVFILYSESTYVILCLIS 192
                            :**:**:** *:*  :    :  **. .   .  :: : .   .:: :
```

Figure 4.1: Sequence alignment of human melanocortin receptors, using CLUSTAL 2.1

```
tr|Q1JUM3|MC1R_HUMAN        FFLAMLVLMAVLYVHMLARACQHAQGIARLHKRQR-PVHQGFGLKGAVTL 243
sp|Q01718|MC2R_HUMAN        LFPLMLVFILCLYVHMFLLARSHTRKISTLPRAN---------MKGAITL 221
sp|P41968|MC3R_HUMAN        MFFAMMLLMGTLYVHMFLFARLHVKRIAALPPADGVAPQQHSCMKGAVTI 244
tr|A0N0W9|MC4R_HUMAN        MFFTMLALMASLYVHMFLMARLHIKRIAVLPGTG--AIRQGANMKGAITL 247
sp|P33032|MC5R_HUMAN        MFFAMLFLLVSLYIHMFLLARTHVKRIAALPGAS--SARQRTSMQGAVTV 240
                            :*  *: ::  **:**:  *  * : *: *            ::**:*:

tr|Q1JUM3|MC1R_HUMAN        TILLGIFFLCWGPFFLHLTLIVLCPEHPTCGCIFKNFNLFLALIICNAII 293
sp|Q01718|MC2R_HUMAN        TILLGVFIFCWAPFVLHVLLMTFCPSNPYCACYMSLFQVNGMLIMCNAVI 271
sp|P41968|MC3R_HUMAN        TILLGVFIFCWAPFFLHLVLIITCPTNPYCICYTAHFNTYLVLIMCNSVI 294
tr|A0N0W9|MC4R_HUMAN        TILIGVFVVCWAPFFLHLIFYISCPQNPYCVCFMSHFNLYLILIMCNSII 297
sp|P33032|MC5R_HUMAN        TMLLGVFTVCWAPFFLHLTLMLSCPQNLYCSRFMSHFNMYLILIMCNSVM 290
                            *:*:*:* .**.**.**: :   ** :  *      *:    **:**:::

tr|Q1JUM3|MC1R_HUMAN        DPLIYAFHSQELRRTLKEVLT-CSW---------- 317
sp|Q01718|MC2R_HUMAN        DPFIYAFRSPELRDAFKKMIF-CSRYW--------- 297
sp|P41968|MC3R_HUMAN        DPLIYAFRSLELRNTFREILCGCNGMNLG------- 323
tr|A0N0W9|MC4R_HUMAN        DPLIYALRSQELKKTFKEIIC-CYPLGGLCDLSSRY 332
sp|P33032|MC5R_HUMAN        DPLIYAFRSQEMRKTFKEIIC-CRGFRIACSFPRRD 325
                            **:***::* *:: ::::::  *
```

Figure 4.1 (continued): Sequence alignment of human melanocortin receptors, using CLUSTAL 2.1

4.1.1.1 MC2R - the corticotropin (ACTH) receptor

MC2R activation stimulates the production of cortisol in response to many types of stress. Mutations in MC2R are responsible for 25 % of all known cases of familial glucocorticoid deficiency (FGD) (familial Addison's disease), an autosomal recessive ACTH insensitivity syndrome, which was reported for the first time in 1959 by Shepard *et al*. (Shepard et al. 1959). FGD results in unresponsiveness to ACTH on the adrenal cortex (in the zona fasciculata) and leads to isolated adrenal glucocorticoid deficiency with normal mineralocorticoid secretion and abnormally high peripheral blood levels of ACTH (Clark et al. 2005). Symptoms involve adrenal insufficiency, hyperpigmentation, tall stature, hypoglycaemic seizures, transient hepatitis and recurrent infections as well as feeding problems in infancy, failure to thrive, hypoglycaemic attacks, convulsions, collapse, and coma (Abdel-Malek 2001; Metherell et al. 2006; Metherell et al. 2005). FGD

type I (OMIM 202200) is caused by mutations in MC2R (Metherell et al. 2006; Chung et al. 2008), whereas mutations of an accessory protein (see below) cause FGD type II (OMIM no. 607398) (Figure 4.2) (Metherell et al. 2005; Webb et al. 2008; Chan et al. 2008; Clark et al. 2005).

The MC2R gene is located on chromosome 18p11.2. MC2R is the smallest member of the class A rhodopsin-like GPCR family with 297 amino acids (33kDa) (Cone et al. 1993; Naville et al. 1997). This receptor is primarily expressed in the adrenal cortex (Cone et al. 1993), however, studies have shown that it is also expressed at lower levels in adipose tissue (Boston & Cone 1996), the pituitary gland (Morris et al. 2003), skin (Slominski et al. 1996) and sympathetic ganglia (Nankova et al. 2003).

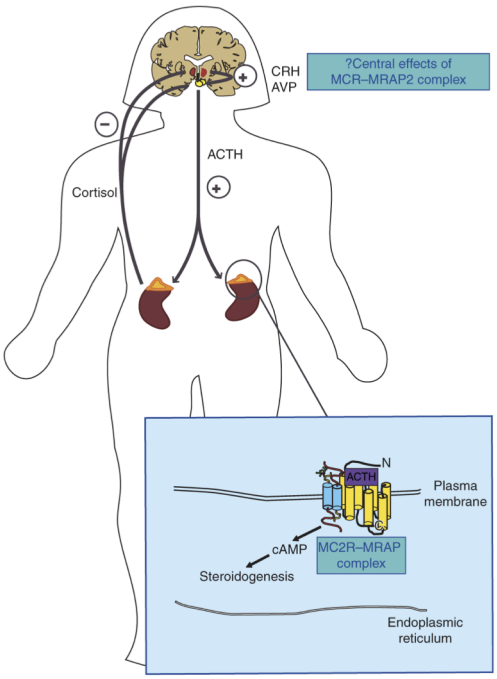

Figure 4.2: Schematic overview of interaction between MRAP and MC2R
MRAP and MC2R act predominantly in the adrenal cortex. Activated MC2R binds to ACTH and consequently stimulates cortisol production. Unresponsiveness to ACTH leads to the disease familial glucocorticoid deficiency (FGD).
Further FGD types relate to mutations in the steroidogenic acute regulatory gene (StAR) region (FGD type III - OMIM 5609197) (Metherell et al. 2009), the NNT encoding nicotinamide nucleotide transhydrogenase gene (FGD type IV) (Metherell et al. 2006; Meimaridou et al. 2012) and mutations in the genes encoding minichromosome maintenance-deficient 4 and POMC (OMIM602638)(Gineau et al. 2012). (Figure taken from Novoselova et al. 2013).

MC2R possesses two N-glycosylation sites on the extracellular domain (Asn12-Asn13-Thr14 and Asn17-Asn18-Ser19) and is known to homodimerise in the ER (Cooray et al. 2011). Both glycosylation sites are essential for MC2R cell-surface expression, however, not for cAMP production (Roy et al. 2010). Roy *et al*. (Roy et al. 2012) established that on

position 143 of MC2R a negatively charged amino acid or one containing a hydroxyl group is essential for plasma membrane expression and normal function of MC2R. Furthermore, the receptor has the canonical E/DRY (Asp127-Arg128-Tyr129) motif at the cytoplasmic end of the third transmembrane domain (Yang et al. 2007). This motif is conserved across the entire class A GPCR superfamily. MC2R contains four conserved asparagines at the top of TM3, which are critical for binding to ACTH (Chen et al. 2007). In addition, it is known that the two highly conserved HFRW and KKRRP motifs of ACTH are required (Slominski et al. 1996; Dores 2009; Dores & Baron 2011).

Activation of MC2R in the adrenal gland by the pituitary hormone ACTH promotes glucocorticoid biosynthesis (Gantz & Fong 2003; Cerdá-Reverter et al. 2013). There MC2R responds to the presence of picomolar concentrations of the ligand ACTH (K_D ~132 pM) but not to any other MSH (Gantz & Fong 2003; Chan et al. 2011). ACTH binding induces a rapid conformational change and subsequently relaxes the complex (Cooray & Clark 2011), followed by an acute decrease in MC2R concentration at the cell surface (Mountjoy et al. 1994; Clark et al. 2003; Kilianova et al. 2006). During this signalling cascade cAMP production and PKA activation (Kilianova et al. 2006) are stimulated. PKA then down-regulates the receptor by phosphorylation (Cooray & Clark 2011). PKC also enhances MC2R desensitisation (Kilianova et al. 2006). Moreover, intracellular cAMP activates protein kinase C (PKC) that subsequently positively affects the mitochondrial cholesterol import and gene expression of steroidogenic enzymes, resulting in steroidogenesis (Chan et al. 2011). Ultimately, MC2R internalises to endocytic vesicles through a clathrin-dependent pathway, which is followed by scission of the vesicles from the plasma membrane (Kilianova et al. 2006).

4.1.2 Melanocortin Receptor Accessory Proteins

MC2R can be efficiently expressed alone in non-adrenal cells, but remains non-functional, unless a second protein, the Melanocortin Receptor Accessory Protein (MRAP) is co-expressed (Metherell et al. 2005) (Figure 4.2). MRAP was discovered in 2002 as a putative membrane protein expressed during adipose conversion in 3T3-L1 preadipocytes and adipocytes and referred to as FALP (FAt-tissues specific Low molecular weight Protein) (Xu et al. 2002). Mutations on MRAP cause FGD type II (OMIM no. 607398) (Webb et al. 2008) and are responsible for about 20–25 % of all FGD patients (Metherell et al. 2005; Webb et al. 2008; Chan et al. 2008; Clark et al. 2005). Patients with FGD type II have a severe phenotype due to an absent or severely truncated MRAP (Chung et al. 2010; Modan-Moses et al. 2006). In addition, two missense mutations described in MRAP lead to a mild phenotype later in life. These mutations are V26A, located in the N-terminal domain, and Y59D, at the end of the transmembrane domain. Y59D mutant MRAP shows significant cAMP response reduction, whereas that of V26A was smaller but still significant (Hughes et al. 2010). After the relationship of MRAP to MC2R and FGD was established, the small protein was renamed to MRAP (Metherell et al. 2005). MRAP's origin can be traced back ~530 million years to the P. marinus, a jawless vertebrate (Valsalan et al. 2013). Interestingly, the protein's origin coincides with the origin of the MC2R gene (Västermark & Schiöth 2011).

The primary role of MRAP is thought to be the result of its interactions with MC2R. At the early stages of MC2R production, MRAP promotes glycosylation of MC2R in the endoplasmic reticulum (ER) and the subsequent trafficking of the receptor to the plasma membrane (Figure 4.3) (Hinkle et al. 2011). In the absence of MRAP most MC2R

molecules are trapped in the ER in non-adrenal cell types and eventually get degraded there (Gineau et al. 2012; Gardiner et al. 2002; Chan et al. 2009; Sebag & Hinkle 2007). Little is known about MC2R dimerisation, however it is interesting, that MC2R homodimerisation is not dependent on MRAP (Cooray & Clark 2011).

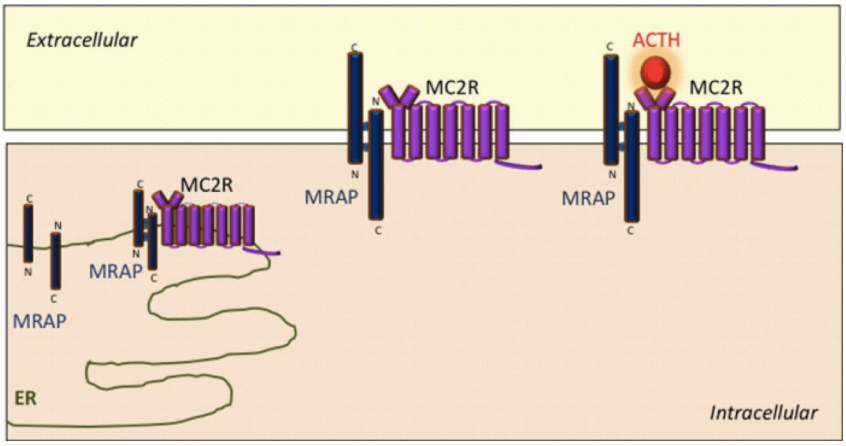

Figure 4.3: Hypothetical model of the interaction between MRAP and MC2R
MRAP monomers forms antiparallel homodimeric complexes within the ER, which interact with MC2R and assist its traffic to the cell surface, where it is capable of recognising and responding to the ACTH peptide. (Figure taken from Ramachandrappa et al. 2013)

MRAP is also necessary for ACTH signalling. MRAP constrains MC2R to strict ACTH specificity (Cone 2006) and is required to mediate ACTH–dependent MC2R signalling at the cell surface (Sebag & Hinkle 2007; Webb & Clark 2010; Metherell et al. 2005). Adrenal MRAP and MC2R levels correlate with high ACTH and cortisol production (Webb et al. 2008). In the presence of a hexameric complex, formed by one MC2R homodimer and at least two dimeric MRAP molecules (Cooray & Clark 2011), ACTH strongly stimulates phosphorylation of extracellular signal-regulated kinases 1 and 2 (ERK1 and ERK2) (Roy et al. 2011; Sebag & Hinkle 2010). This characteristic has been shown in *Danio rerio* (zebrafish) (Agulleiro et al. 2010), *Oncorhynchus mykiss* (rainbow trout) (Aluru & Vijayan 2008)- and in *Xenopus tropicalis* (Western clawed frog) (Liang et al. 2011) .

In addition to its involvement with the melanocortin system, MRAP induces the activation of the hormone-sensitive lipase, which hydrolyses a variety of esters in murine

adipocytes (Kim et al. 2013). It has been suggested that the activation induced by ACTH-mediated MRAP of the lipase is ultimately regulated by the peroxisome proliferator-activated receptor γ (PPARγ). This receptor is a critical transcription factor in regulation of adipocyte differentiation, lipid metabolism and insulin sensitivity. It activates target genes by binding to promoter regions after forming complex with retinoid X receptor a (RXRa) (Tontonoz et al. 1994).

4.1.2.1 Genetics of MRAP

In total, MRAP is found in four isoforms arising from alternative splicing. In humans, MRAP is encoded by a gene located on chromosome 21q22.1 and contains six exons. Exons 1 to 5 encode MRAP isoform α, which consists of 172 amino acids (19 kDa). Exon 1 to 4 and exon 6 get alternatively spliced and produce the 102 amino acid long MRAP isoform β (14.1 kDa) (Metherell et al. 2005; Cooray & Clark 2011). The single transmembrane helix is encoded by exon 4 (Sebag & Hinkle 2007). MRAP isoform α is preferentially found in intracellular structures, like endosomes, and around the nuclear envelope, whereas MRAP isoform β is mainly localised at the plasma membrane and partially associated with rapid recycling endosomes (Roy et al. 2012). The N-terminus and transmembrane domain of MRAP are highly conserved, whereas the C-terminus is highly variable across different eukaryotes (see Figure 4.8, 4.9) (Larkin et al. 2007).

Recently, Kim *et al*. (Kim et al. 2013) showed that in murine adipocytes MRAP mRNA expression is regulated by PPARγ. In the presence of MC2R, MRAP is expressed in the adrenal cortex, lymph nodes, brain, testis, breast, thyroid and adipose tissue (Gantz & Fong 2003; Metherell et al. 2005; Cerdá-Reverter et al. 2013; Sebag & Hinkle 2009b; Chan et al. 2009). MRAP isoform α is preferentially found in intracellular structures, like

endosomes, and around the nuclear envelope, whereas MRAP isoform β is mainly localised at the plasma membrane and partially associated with rapid recycling endosomes (Roy et al. 2012).

4.1.2.2 Structure of MRAP

MRAP has one N-linked glycosylation site (Asn-X-Ser/Thr) at position Asn3 (Figure 4.4), however glycosylation is not required for functionality or membrane topology (Hinkle & Sebag 2009). Residues EYY (Glu15-Tyr16-Tyr17), also in the N-terminal domain, are highly conserved and suggested to be important for controlling MC2R trafficking (Agulleiro et al. 2010). Furthermore, Sebag and Hinkle (Sebag & Hinkle 2009) identified an N-terminal LDY(I/L)-motif (residues Leu18 to Leu21) that is required for ACTH binding to MC2R and signal transduction but not for trafficking MC2R to the plasma membrane. It is hypothesised that this motif might be involved in stabilisation of the MRAP/MC2R complex or otherwise could interact with another regulatory protein (Webb et al. 2008). Deletion of the N-terminal region residues Met1 to Lys30 results in MC2R localising to the plasma membrane, but lacking ACTH-induced cAMP production (Hinkle & Sebag 2009).

Several studies indicate that MRAP adopts a dual topology in the membrane and homodimerises in an antiparallel orientation (Webb et al. 2008). Residues Leu31 to Ser37 (LKAHKHS), which are located N-terminally to the transmembrane domain, and form a positively-charged "KH-rich" region has been shown to be important for this dual topology as well as MC2R activation (Hinkle & Sebag 2009). MRAP's dual membrane topology is discussed in detail in Chapter 5 of thesis.

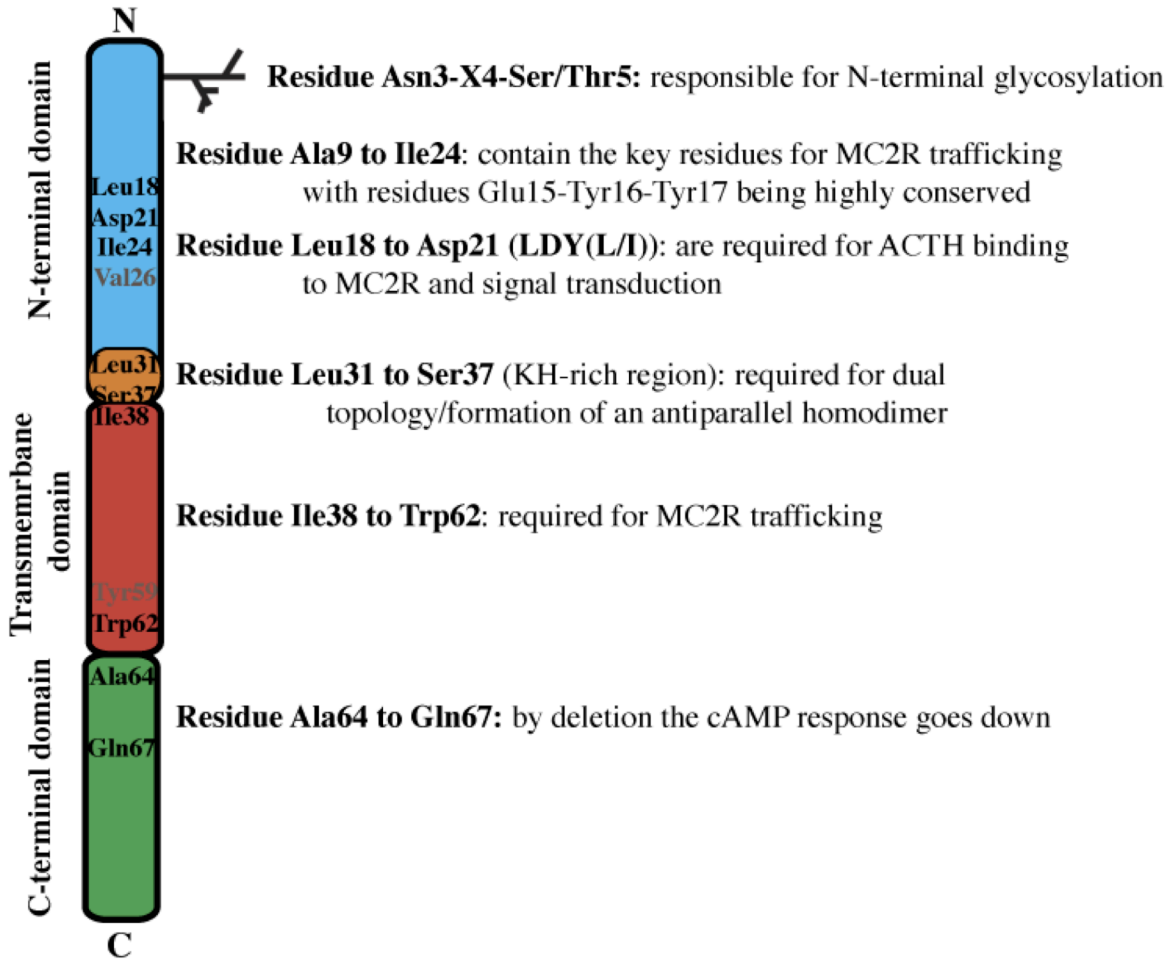

Figure 4.4: Schematic representation of essential MRAP regions highlighting regions of functional significance in MRAP dimerisation and interaction with MC2R (Sebag and Hinkle 2009; Webb et al. 2009).

The ability to promote trafficking of MC2R requires the 23 amino acid long predicted transmembrane domain as well as portions of the N-terminal region, though it is not sufficient to promote cell surface expression (Sebag & Hinkle 2009b; Hinkle & Sebag 2009). MRAP interacts through its transmembrane domain with one or more MC2R transmembrane domains via hydrophobic interactions (Webb & Clark 2010). Studies of MC2R and MC4R chimeric constructs led Fridmanis *et al*. (Fridmanis et al. 2010) to propose that MRAP interacts with TM4 and TM5 of the MC2R. This finding however is controversial, since Hinkle *et al.* (Hinkle et al. 2011) did not find that substitution of TM4 and TM5 of the MC2R with the MC4R have a negative effect on MRAP dependency.

Deletion of the four highly conserved C-terminal residues Ala64-Ser65-Pro66-Gln67

appeared to decrease the cAMP response by about half, suggesting that at least some of the functional importance of the C-terminus is attributable to these residues (Hinkle & Sebag 2009).

4.1.2.2.1 MRAP2 is a second Melanocortin Receptor Accessory Protein

By sequence analysis Metherell *et al*. (Metherell et al. 2005) identified a putative protein encoded on chromosome 6q14.3 that was similar in sequence to MRAP and named it MRAP2 (Chan et al. 2009). Like MRAP, MRAP2 (23.5 kDa, 205 amino acids) is a single-pass transmembrane protein, and is conserved in all eukaryotes (Valsalan et al. 2013). MRAP2 is expressed primarily in the adrenal gland and brain tissue (Webb & Clark 2010).

MRAP2 is 36 % identical and 52 % similar to the first 67 amino acid residues of MRAP. In addition, MRAP2 can heterodimerise with MRAP (Figure 4.5). However, MRAP2 appears to antagonise MRAP and MC2R activity when overexpressed, resulting in decreased ACTH affinity (~10^{-6} M) (Roy et al. 2010; Sebag & Hinkle 2010; Gorrigan et al. 2011; Metherell et al. 2005; Chan et al. 2009). MRAP has been shown to stabilise ACTH binding to MC2R by 1000-fold more than MRAP2 (Chan et al. 2009).

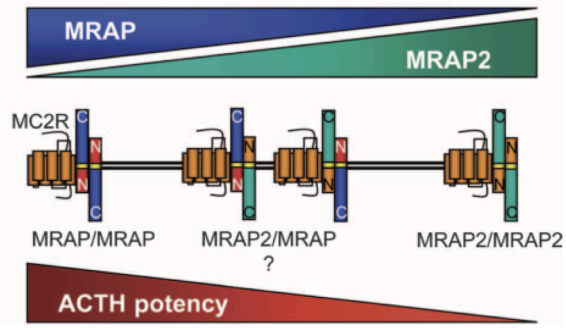

Figure 4.5: Schematic representation of possible dimeric MRAP and MRAP2 conformation
MRAP and MRAP2 can form individual homodimers, however they can also heterodimerise with each other. MRAP2 acts as a natural dominant-negative form of MRAP and MC2R activity and hence decreases ACTH affinity. The effects of the MRAP-MRAP2 heterodimers on MC2R signalling are hypothetical. (Figure taken from Sebag et al. 2010)

4.1.2.2.2 Complex regulation of melanocortin receptors by MRAP and MRAP2

Until recently, it was believed that the sole functions of MRAP and MRAP2 were to inhibit the activity of MC1R, MC3R, MC4R and MC5R (Chan et al. 2009). However, it was shown that MRAP and MRAP2 have more specific effects on the activities of melanocortin receptors and hence may be more important in regulating the melanocortin system than originally anticipated (Metherell et al. 2005; Chung et al. 2010; Kay et al. 2013a; Modan-Moses et al. 2006; Hinkle et al. 2011; Valsalan et al. 2013; Asai et al. 2013; Västermark & Schiöth 2011; Sebag et al. 2013).

MC1R and MC3R co-localise with MRAP and MRAP2 in the perinuclear region, in the cytoplasm and at the cell surface of HEK293 cells (Cone 2006; Gantz et al. 1993). In both cases the interaction leads to an increase of functional coupling to adenylyl cyclase (Kay et al. 2013a). Interestingly, in Chinese hamster ovary (CHO)-cells MRAP alters exclusively MC4R and MC5R functional expression (Chan et al. 2011; Chan 2009). It remains to be tested whether these experimental discrepancies arise from the use of different agonists and different cell lines.

Modulation of MC4R by accessory proteins is of great interest since mutations in this receptor are the largest monogenic cause of obesity (Vaisse et al. 1998; Yeo et al. 2003; Tao 2010; Farooqi et al. 2003). Despite not co-localising with the receptor, MRAP increases the apparent mass and constitutive activity of MC4R in HEK293 cells (Kay et at. 2013a). The three N-linked glycosylation sites Asn3, Asn17 and Asn26 of the receptor are closely linked to obesity, and the alteration in mass is likely due to increased glycosylation mediated by MRAP (Kay, Botha, Montgomery & Mountjoy 2013b). Unlike

MRAP, MRAP2 is co-expressed with MC4R (Chan et al. 2009) in the brain. MRAP2 has two isoforms that can either inhibit (isoform α) or stimulate (isoform β) the ligand-mediated receptor activation (Sebag et al. 2013). Until now the role of both isoforms is not established. Mutations or inactivation of MRAP2 are associated with early-onset, severe obesity (Webb et al. 2008; Asai et al. 2013; Sebag et al. 2013).

Furthermore, both MRAP and MRAP2 affect the ubiquitous receptor MC5R, which is proposed to be the ancestral MC2R receptor (Baron et al. 2009). MRAP modifies MC5R activity through preventing dimerisation, which leads to MC5R being retained within the intracellular compartments of the ER and the Golgi apparatus (Aluru & Vijayan 2008; Chan et al. 2009; Grieco et al. 2002). MRAP's N-terminal region has been implicated in restraining MC5R trafficking and function, however, MRAP does not prevent the MC5R post-translational glycosylation (Tontonoz et al. 1994; Liang et al. 2011; Sebag & Hinkle 2009a).

The physiological function of MRAP2 remains poorly understood compared to that of MRAP. However, recent findings (Kay et al. 2013a; Kay et al. 2013b; Sebag et al. 2013; Asai et al. 2013) suggest that MRAP and MRAP2 are more crucial for cellar regulation than previously thought.

4.1.3 Aims of studying MRAP on a molecular level

MRAP and MRAP2 modulate most, if not all, melanocortin receptors either positively or negatively (Chan et al. 2009; Chan 2009; Sebag et al. 2013). The role of MRAP in MC2R expression and activity, as well as its unusual dual membrane topology (Sebag & Hinkle 2007), have been the most well studied. Nonetheless, there are currently no molecular details known for MRAP, nor for its dimerisation, and MRAP and MRAP2 do not share

sequence homology with any other known protein

Due to its small size, MRAP is amenable to high-resolution studies by solution NMR. As a first step toward understanding the molecular basis of MRAP function and assembly, I have characterised the structural and biophysical properties of monomeric MRAP. These studies are the first atomic-level studies of the membrane-integral region of any GPCR transmembrane accessory protein.

4.2 RESULTS

4.2.1 Secondary structure prediction and transmembrane insertion prediction

The TMHMM (Krogh et al. 2001; Sonnhammer et al. 1998) and (SP)Octopus server (Viklund et al. 2008; Viklund & Elofsson 2008) were used to predict MRAP membrane topology and the residues in the transmembrane domain. Both tools use hydrophobicity, charge bias, helix lengths, and geometrical constraints to generate a single model based on hidden Markov model statistics. Both predicted one single transmembrane domain from amino acids Val39 to Tyr59 for MRAP. TMHMM (Figure 4.6.(A)) predicted a C_{in}-N_{out} and N_{in}-C_{out} orientation with equal probability. However (SP)Octopus (Figure 4.6.(B)) suggested that MRAP is a type II integral membrane protein, with a low preference for the N_{in}-C_{out} orientation (Sebag & Hinkle 2007; Hinkle & Sebag 2009).

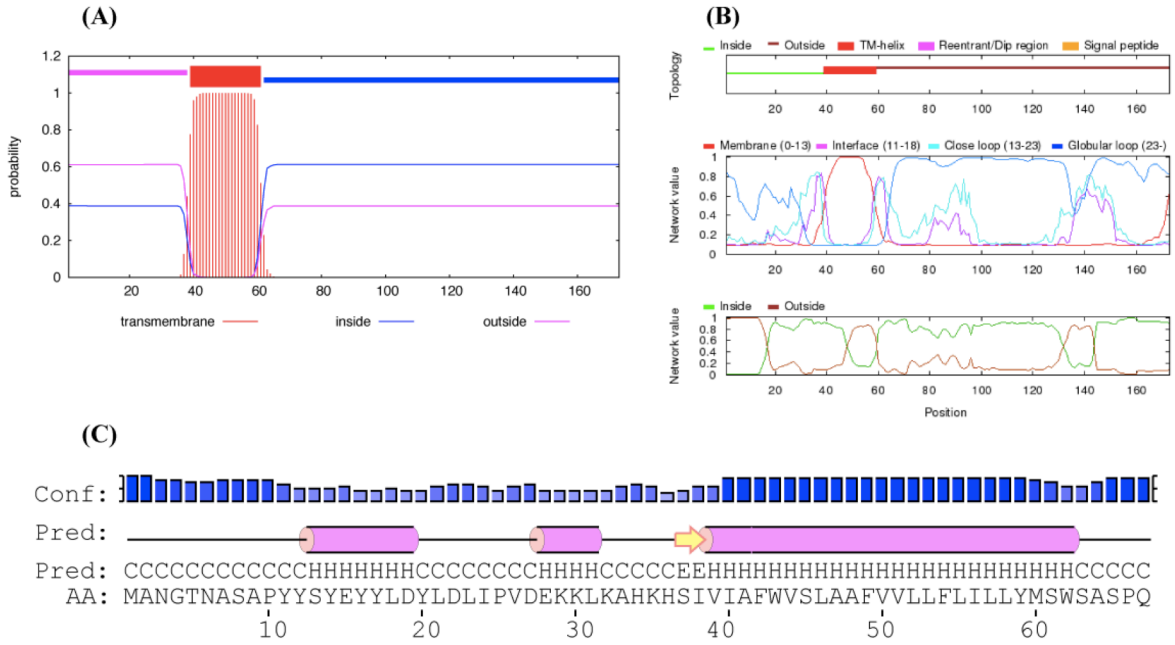

Figure 4.6: Secondary structure predication of MRAP
Predication of transmembrane domain topology of MRAP with (A) TMHMM-Server and (B) OCTOPUS-Server, both are based on a hidden Markov model and artificial neural networks. (C) Secondary structure prediction of the N-terminal domain and the transmembrane domain of MRAP with PSI-PRED-Server.

Secondary structure features of the conserved N-terminal and transmembrane domains of MRAP were further explored using PSI-PRED (Buchan et al. 2010; Jones 1999). The analysis predicted two α-helical regions in addition to the transmembrane helix (Figure 4.6.(C)). Residues Tyr11 to Tyr19 and Gln28 to Leu31 in the N-terminal domain proposed to form short α -helices, however, the prediction confidence for residues Gln28 to Leu31 was very low. The α-helical transmembrane domain was suggested to be between residues Val39 and Trp62, which is slightly longer than that predicted by TMHMM and (SP)Octopus.

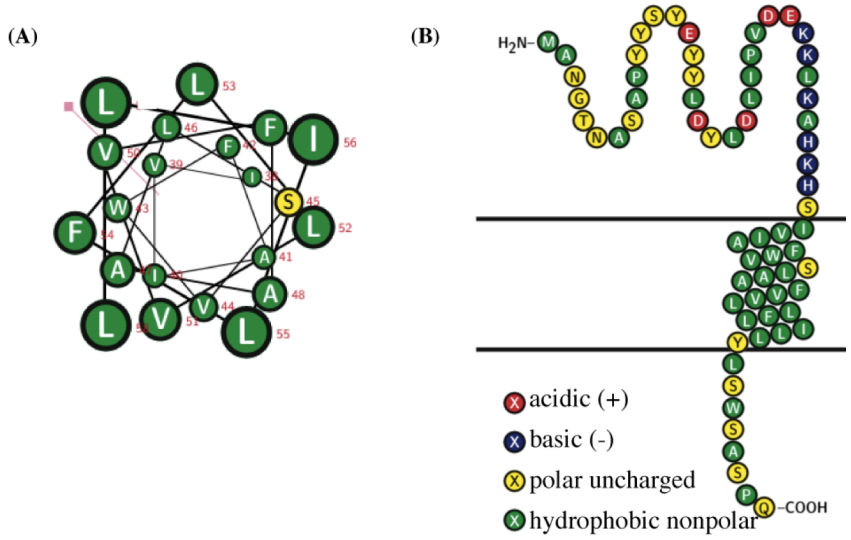

Figure 4.7: MRAP(2-67) sequence analysis
(A) Helical wheel representation of MRAP(2-67) viewed from the C-terminal side showing the mainly hydrophobic transmembrane helix

In general, residues Met1 to Glu28 within the N-terminal region are highly acidic (theoretical pI = 3.30) and contain a high percentage of tyrosines (~21 %). By contrast the following eight residues (Lys29 to Ser37) are highly basic (theoretical pI = 10.48) (Figure 4.7. (C)). This positively charged "KH-rich" region (residues Lys29 to Ser37; sequence "KKLKAHKH") adjoins to the transmembrane domain and was shown to be crucial for MRAP's dual topology, and MC2R trafficking and activity (Hinkle & Sebag 2009). This stretch contains 40 % small hydrophobic amino acids, with a slightly acidic isoelectric

point is (pI = 5.52). In addition to the previous described glycosylation site on Asn3, no further post-translational modifications were predicted by two on-line bioinformatic severs www.cbs.dtu.dk/services and www.expasy.org/proteomics/posttranslational_ modification.

4.2.2 Construct design rationale

Hinkle *et al*. have investigated MRAP function in cultured mammalian cells and established that the smallest functional unit of MRAP contains the first 63 amino acids of the full-length protein (Sebag & Hinkle 2007; Hinkle & Sebag 2009).

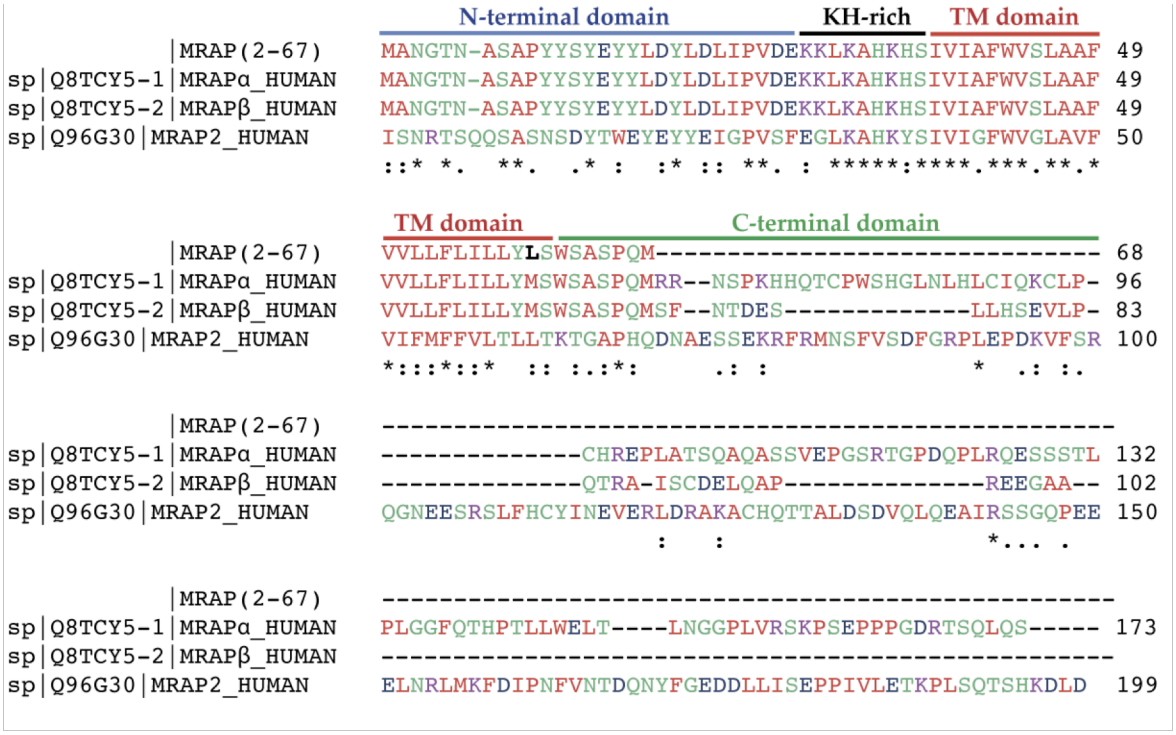

Figure 4.8: Alignment of human MRAP. CLUSTAL 2.1 was used to generate alignment

However, residues Ala64 to Gln67 are proposed to have some importance for cAMP response (Hinkle & Sebag 2009; Roy et al. 2012). Additionally, this region shows high sequence homology and conservation across different eukaryotic species (Figure 4.8) as well as between MRAP and MRAP2 (Figure 4.9).

To facilitate structural and biophysical studies, I investigated a construct containing residues 2-67 of human MRAP, comprising the N-terminal and transmembrane domains and eight C-terminal residues. Since the construct was intended to be expressed with an insoluble, N-terminal fusion protein and cleaved with cyanogen bromide at Met1, the substitution Met60Leu was made. The Met60Leu variant has been shown to be competent for reconstituting MC2R activity in cells (P. Hinkle, personal communication). This construct is referred to as MRAP(2-67) throughout this thesis.

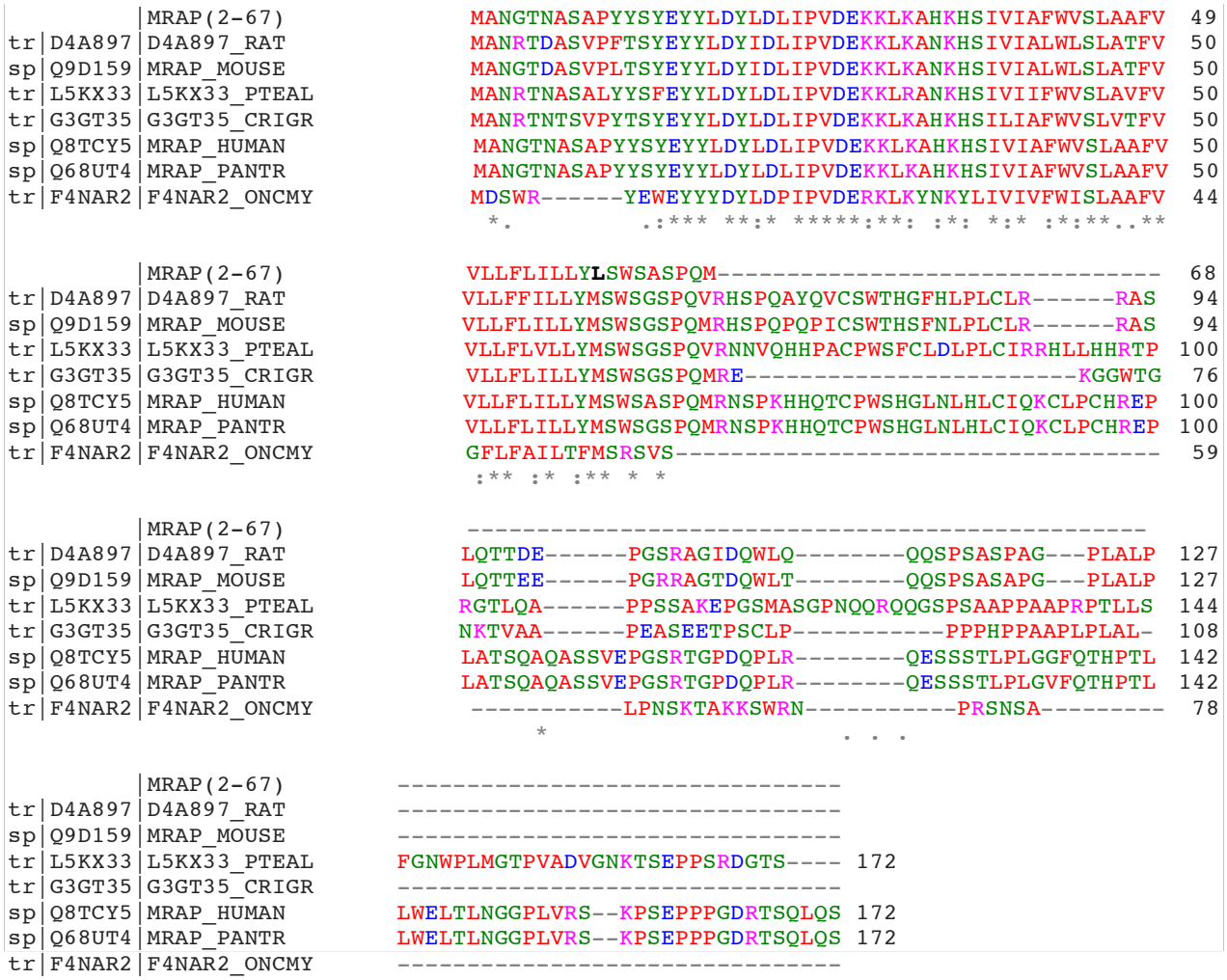

Figure 4.9: Alignment of MRAP in different species.

4.2.3 Expression and purification of MRAP(2-67)

The ability to produce milligram quantities of pure protein is required for resonance assignment and structural characterisation by solution NMR.

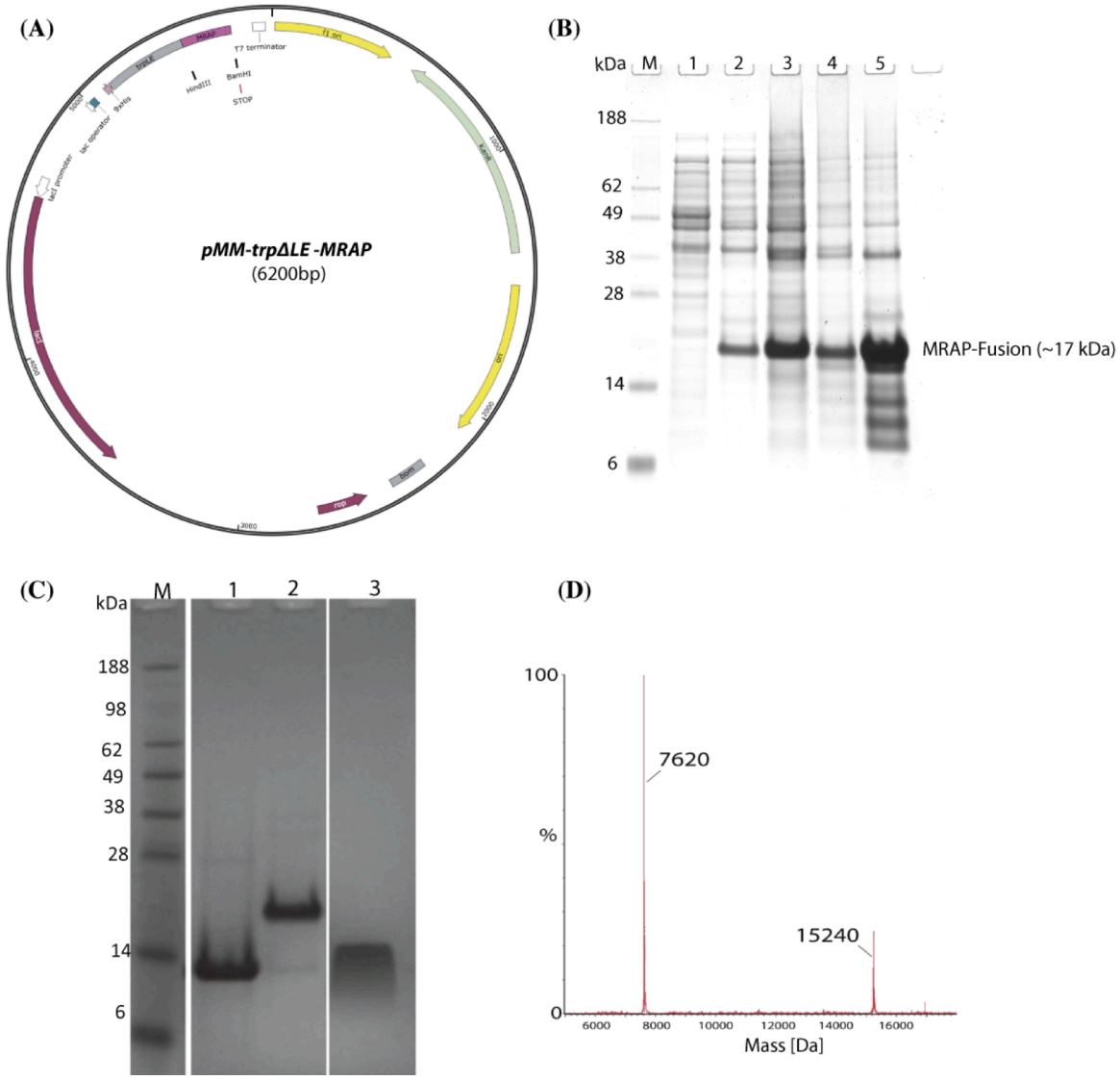

Figure 4.10: Expression and Purification of MRAP(2-67)
(A) Schematic representation of MRAP(2-67) construct in trpΔLE-vector.
(B) Expression of MRAP (2-67): 1: no expression, 2-5: Expression after 1 h, 2 h, 6 h and 12 h of induction with 1mM IPTG.
(C) HPLC-purified components of MRAP(2-67)-trpLE construct: 1: trpLE; 2: fusion, 3: MRAP(2-67)
(D) Analysis of MRAP(2-67) by Mass-Spectroscopy after purification.

To achieve adequate quantities of pure and natively folded protein, the gene for the construct MRAP(2-67) was cloned into the pMM-LR6 vector as a fusion to the *trpΔLE* gene, which produces a protein that is strongly directed into inclusion bodies, allowing

non-toxic expression of the target protein. *TrpΔLE* comprises the leader sequence of the trp operon of *E.coli* fused to a 97 amino acid sequence, which is derived from the C-terminus of the anthranilate synthase gene (North & Blacklow 1999) (Figure 4.10 (A)). High level expression of MRAP(2-67) was obtained in *E.coli* strain BL21(DE3) pLysS cells, with about 70 % of protein being expressed within the first three hours after induction with 1 mM IPTG (Figure 4.10 (B)). Following expression and cell lysis, MRAP(2-67) was located primarily in inclusion bodies. Inclusion bodies were purified and solubilised by 6 M guanidine buffer and afterwards separated from the crude lysate by a Ni^{2+}-NTA column. This step was followed by two hours of cyanogen bromide cleavage (0.2 g/mL) in 70 % formic acid under a low-pressure stream of nitrogen gas, to separate MRAP(2-67) from its fusion partner. To remove most of the cyanogen bromide the sample was dialysed against H_2O (pH 7) for one hour using 3.5 kDa MWCO dialysis cassettes. In preparation for reverse-phase high-pressure liquid chromatography (HPLC) the sample was lyophilised and then solubilised in 50 % 2,2,2-triflouroethanol (TFE) and 25 % formic acid. This solution was loaded onto a C4 column (Grace-Vydac) (Figure 4.10 (C)). Fragments were separated on a gradient of buffer A (5 % acetonitrile, 95 % H_2O, 0.1 % TFA) and buffer B (40 % acetonitrile, 60 % isopropanol, 0.1 % TFA). The overall yield of homogeneous protein from one litre of Luria Broth media was approximately 6 mg. Using condensation methods, as described in Methods and Materials, for isotope labelling gave yields of approximately 4 mg of pure protein per litre of M9 minimal media. Mass spectrometry was used to confirm the molecular weight of the sample (Figure 4.10 (D)).

4.2.4 Establishing suitable conditions for MRAP(2-67)

4.2.4.1 Screening detergent/lipid mixtures

In order to determine a high-resolution structure of MRAP(2-67) by solution NMR different membrane-mimicking detergents had to be tested for their ability to enable collection of high quality NMR spectra indicative of a pure, monodisperse sample. Therefore, MRAP(2-67) was reconstituted into micelles by the addition of detergent solutions to lyophilised peptide. To ensure complete and homogenous solubilisation the sample was freeze-thawed at least seven times. For several detergents, slower refolding experiments were carried out either by dialysis from 6 M guanidine, or reconstitution from thin films. In most cases, the results were similar, and thus the simpler reconstitution from lyophilised powder was performed. Complete protocols for refolding and reconstitution methods are described in Chapter 3.1.3.

Two-dimensional $^{1}H-^{15}N$ HSQC or $^{1}H-^{15}N$ SOFAST-HMQC NMR (Schanda et al. 2005) experiments were used to screen MRAP(2-67) in different detergent solutions. The quality of these spectra was evaluated based on the resonance line widths and the chemical shift dispersion. Tested detergents included Fos-Choline-10, Fos-Choline-12, Fos-Choline-14, DHPC, diC7PC, LMPG, LPPG, CHAPS, SDS, DDM, $C_{12}E_8$ and sodium perflourooctanoate (97 %). In addition, a number of mixtures of detergents and lipids tested included the following lipids: DMPC, DPPC, POPC, DMPG, DPPG. Table 4.2 displays all tested detergent mixtures. Most of the tested compounds were not compatible with MRAP(2-67) as assessed by ^{1}H-^{15}N correlation spectra. Detergents resulting in low solubility (as assessed by visual inspection), few or no detectable crosspeaks in 2D HSQCs or HMQCs, or poorly resolved crosspeaks were excluded.

Detergent	Reconstitution method	Detergent	Reconstitution method
25mM SDS	M	25mM Fos10	M
50mM SDS	M	50mM Fos10	M
100mM SDS	M + TF	100mM Fos10	M + TF
50mM NLS	M + TF	100mM Fos10 20mM DMPC	M
100mM NLS	M	100mM Fos10 30mM DMPC	M
25mM LMPG	M + TF	100mM Fos10 20mM DPPC	M + TF
50mM LMPG	M	100mM Fos10 40mM DPPC	M
50mM DHPC	M + TF	100mM Fos10 10mM DMPG	M
100mM DHPC	M + TF	100mM Fos10 30mM DMPG	M
100mM DHPC 5mM SDS	M	100mM Fos10 20mM DMPC 5mM DMPG	M
100mM DHPC 20mM SDS	M + TF	100mM Fos10 20mM DMPC 10mM DMPG	M
100mM DHPC 50mM SDS	M + TF	100mM Fos10 20mM DMPC 20mM DMPG	M + TF
70mM DHPC 20mM DPPG	M + TF	100mM Fos10 20mM DPPC 10mM DPPG	M
70mM DHPC 30mM DPPG	M + TF	100mM Fos10 20mM DPPC 20mM DPPG	M + TF
100mM DHPC 30mM NLS	M + TF	30mM Fos12	M
100mM DHPC 50mM POPC	M + TF	40mM Fos12	M
100mM DHPC 30mM DMPC	M	50mM Fos12	M
100mM DHPC 20mM SDS	M + TF	100mM Fos12	M
100mM DHPC 40mM SDS	M	100mM Fos12 25mM SDS	M + TF
100mM DHPC 60mM SDS	TF	100mM Fos12 50mM DHPC	M + TF
50mM DDM	M	100mM Fos12 20mM DMPC	M + TF
50mM DDM 5mM SDS	M + TF	100mM Fos12 40mM DMPC	M
50mM DDM 25mM POPC	M + TF	100mM Fos12 30mM DMPG	M
50mM EDDA	M	100mM Fos12 30mM DPPG	M
100mM EDDA	M+TF	100mM Fos12 20mM DMPC 10mM DPPG	M + TF
50mM CHAPS	M	100mM Fos12 20mM DMPC 30mM DPPG	M + TF
100mM CHAPS	M	100mM Fos12 20mM DMPC 15mM DMPG	M + TF
50mM CHAPS 10mM DMPC	M + TF	100mM Fos12 20mM DMPC 30mM DMPG	M + TF
50mM CHAPS 25mM DMPC	M	30mM Fos14	M
50mM CHAPS 50mM DMPC	M	40mM Fos14	M
50mM LPPG	M	50mM Fos14	M + TF
100mM LPPG	M+TF	100mM Fos14	M
50mM diC7	M	100mM Fos14 5mM SDS	M
100mM diC7	M+TF	100mM Fos14 25mM SDS	M
25mM $C_{12}E_8$	M	100mM Fos14 30mM DPPC	M + TF
50mM $C_{12}E_8$	M	100mM Fos14 30mM DPPC 15mM DPPG	M + TF
50mM sodium perflouro-octanoate (97 %)	M	100mM Fos14 30mM DPPG	M
100mM sodium perflouro-octanoate (97 %)	M	100mM Fos14 30mM LPPG	M

Table 4.2: Screened detergent and lipid mixtures for establishing the best environment for MRAP(2-67) Reconstituted by mixing (M) or by making a thin film (TF)

4.2.4.2 Establishing the best environments of MRAP(2-67)

After much effort two detergents and one detergent/lipid mixture were selected for further characterisation of MRAP(2-67) (Figure 4.11): 100 mM DHPC, 50 mM SDS, and a mixture of 100 mM Fos-Choline-10, 20 mM DMPC, and 5 mM DMPG. The detergent concentration in all conditions was identified from the lowest amount required to fully solubilise MRAP(2-67). In all cases the best method to reconstitute MRAP(2-67) was to first solubilise the detergent in 50 mM sodium phosphate buffer (pH 6.5), then add the solution to lyophilised protein. All three of these detergent environments provided excellent spectral homogeneity, resulting in NMR linewidths that were consistent with monodisperse MRAP(2-67) and detergent or detergent/lipid complexes.

DHPC has a lipid-like headgroup, but because of its short acyl-chain DHPC forms micelles, rather than bilayers, it is suitable for solution NMR studies (Hauser 2000). SDS is an anionic and strongly denaturing detergent, which is routinely used for determining protein molecular weights in gel electrophoresis. However, helical transmembrane domains in SDS micelles have been shown to retain highly similar secondary structures to that in crystal structures or other detergents (Micelli et al. 2004; Tulumello & Deber 2012). MRAP in mixed micelles (Fos-Choline-10, DMPC and DMPG) was also studied, since the inclusion of lipids is expected to serve as a better mimic for lipid bilayers but small enough to tumble in the nanosecond timescale (Luchette et al. 2001; Andersson & Mäler 2005).

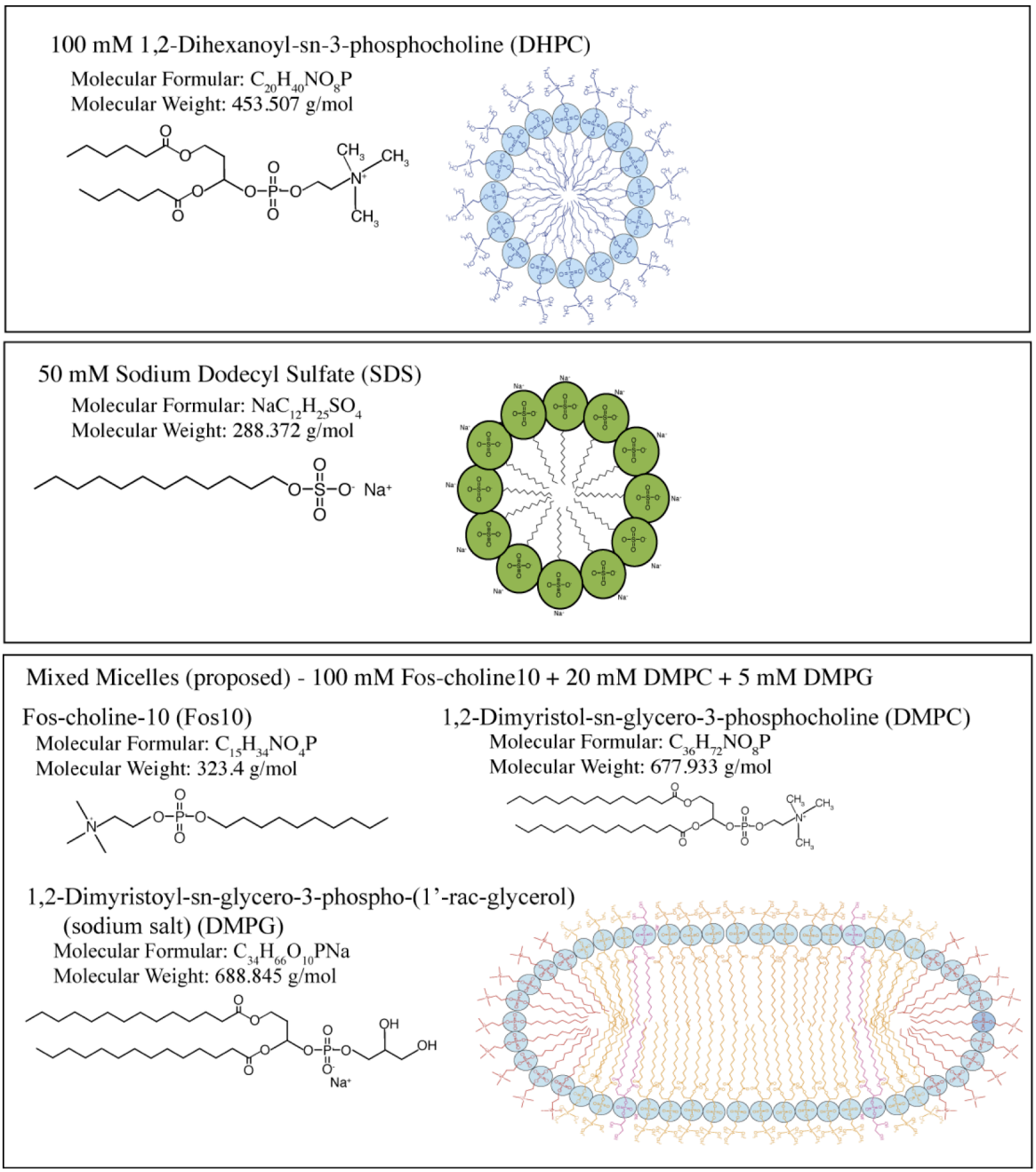

Figure 4.11: Properties of the detergents providing the best environment to study MRAP(2-67) by NMR at 303 K. A schematic is shown of a bicelle-like structure that may form in the detergent and lipid mixture.

Figure 4.12(A) displays the ^{1}H-^{15}N correlation spectra for MRAP(2-67) in all three detergent systems. Figure 4.12(D) shows MRAP(2-67) electrophoretic mobility in presence of detergent on a SDS-PAGE and on a urea-gel. No large differences arising from the contribution of detergents in the gel mobility were detected.

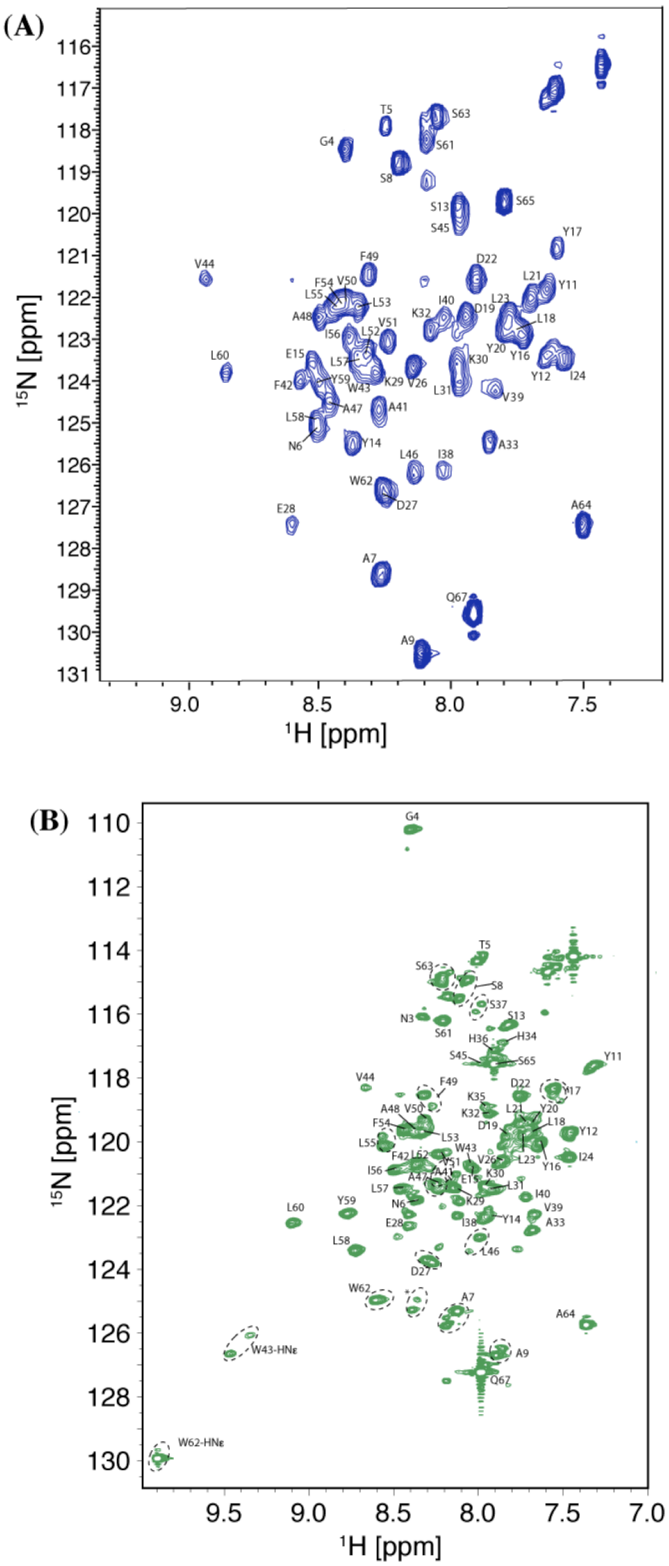

Figure 4.12: MRAP(2-67) characterisation
^{1}H-^{15}N HSQC of MRAP(2-67) in 50 mM sodium phosphate buffer (pH 6.5) and
(A) 100 mM DHPC
(B) 50 mM SDS

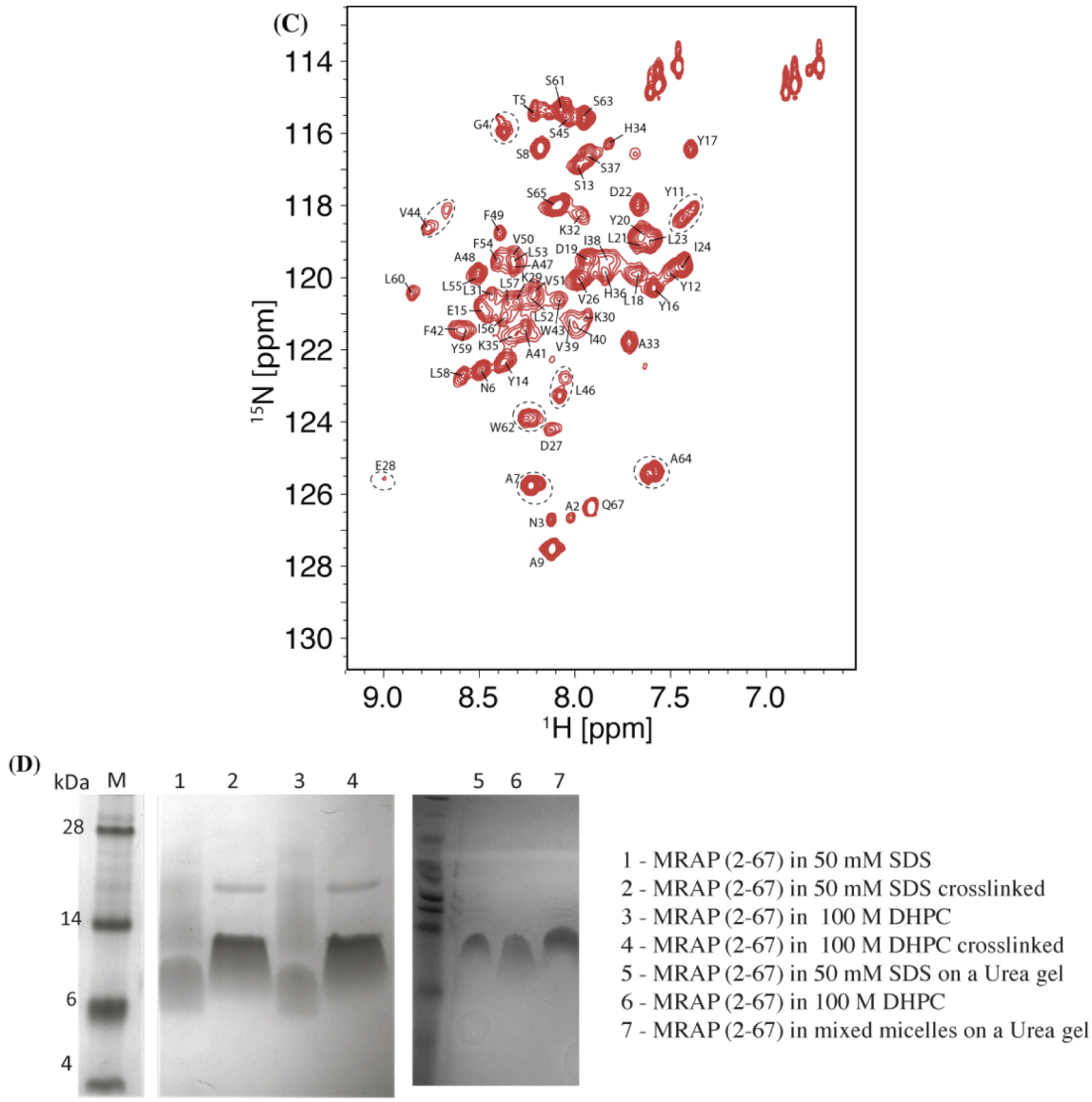

Figure 4.12: MRAP(2-67) characterisation
^{1}H-^{15}N HSQC of MRAP(2-67) in 50 mM sodium phosphate buffer (pH 6.5) and
(C) Mixed micelles containing 100 mM Fos-Choline-10, 20 mM DMPC, and 5 mM DMPG.
(D) MRAP(2-67) characterisation on SDS-PAGE and UREA gel

MRAP(2-67) was soluble in Fos-Choline-10 alone by visual inspection, but only resonances arising from C-terminal residues could be observed by NMR (Figure 4.13(A)).

The addition of 20 mM DMPC to the sample resulted in peaks from the transmembrane domain becoming detectable as well as most of those arising from the N-terminal domain. To examine the impact of negatively charged lipid headgroups, which are present in native membranes, several ^{1}H-^{15}N HSQC spectra were recorded with and

without DMPG (Figure 4.13). The homogeneity of crosspeak lineshape was improved by incorporation of DMPG to the detergent mixture.

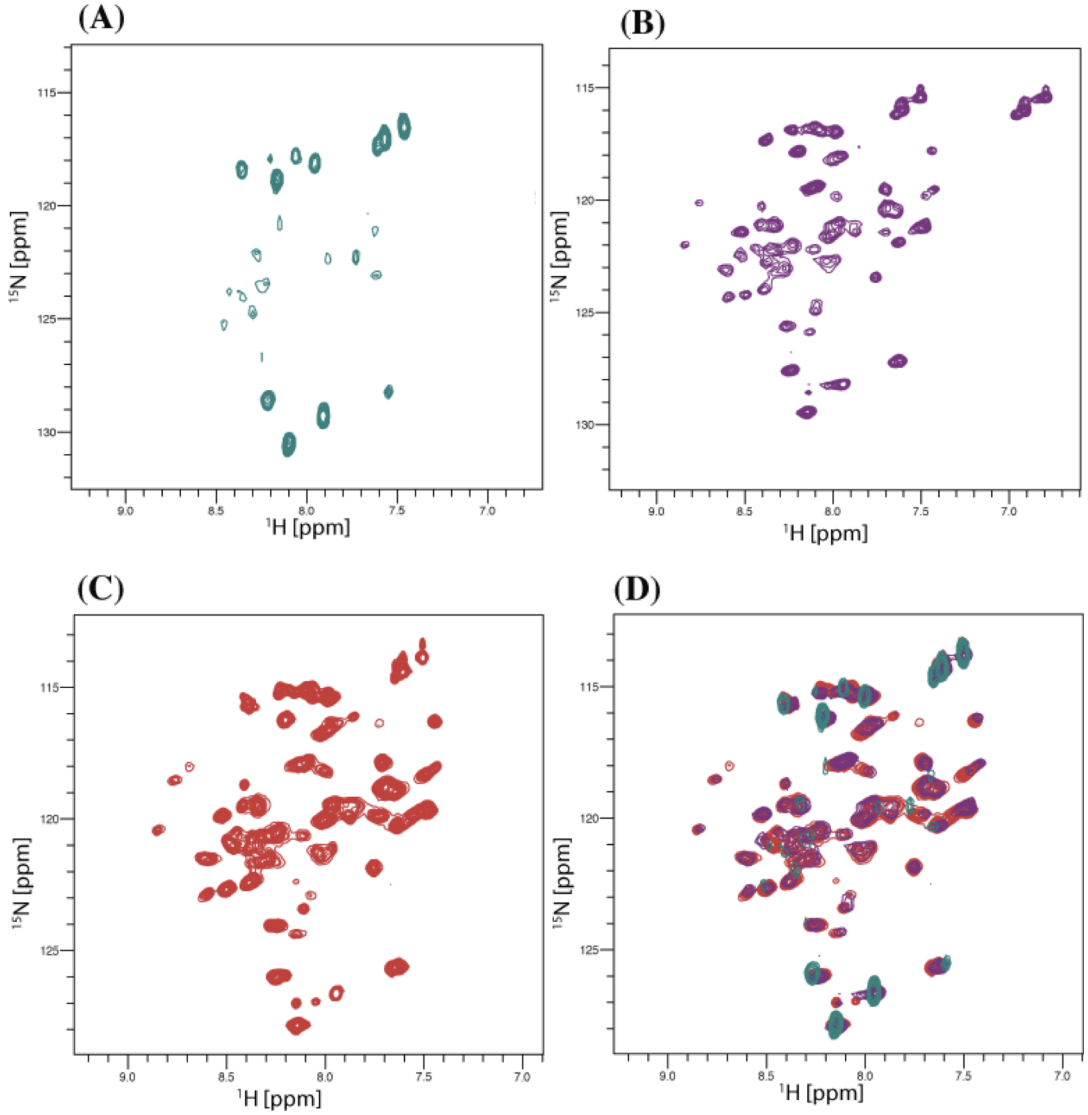

Figure 4.13: The impact of DMPG on MRAP(2-67)
(A) MRAP(2-67) in 100 mM Fos-Choline-10
(B) MRAP(2-67) in 100 mM Fos-Choline-10 + 20 mM DMPC
(C) MRAP(2-67) in 100 mM Fos-Choline-10 + 20 mM DMPC + 5 mM DMPG
(D) Overlay of all three detergent mixtures

4.2.4.3 Establishing a temperature

MRAP(2-67) was tested in all three established conditions at different temperatures (323 K, 315 K, 310 K, 303 K, 298 K, and 291 K) to identify the most advantageous one (Figure 4.14). Although a small number of resonances were sensitive to temperature, all peaks

remained visible at all tested temperature conditions. 303 K MRAP(2-67) gave narrow line shapes at a physiological relevant temperature. Therefore, all further NMR experiments were carried out at 303 K, unless otherwise stated.

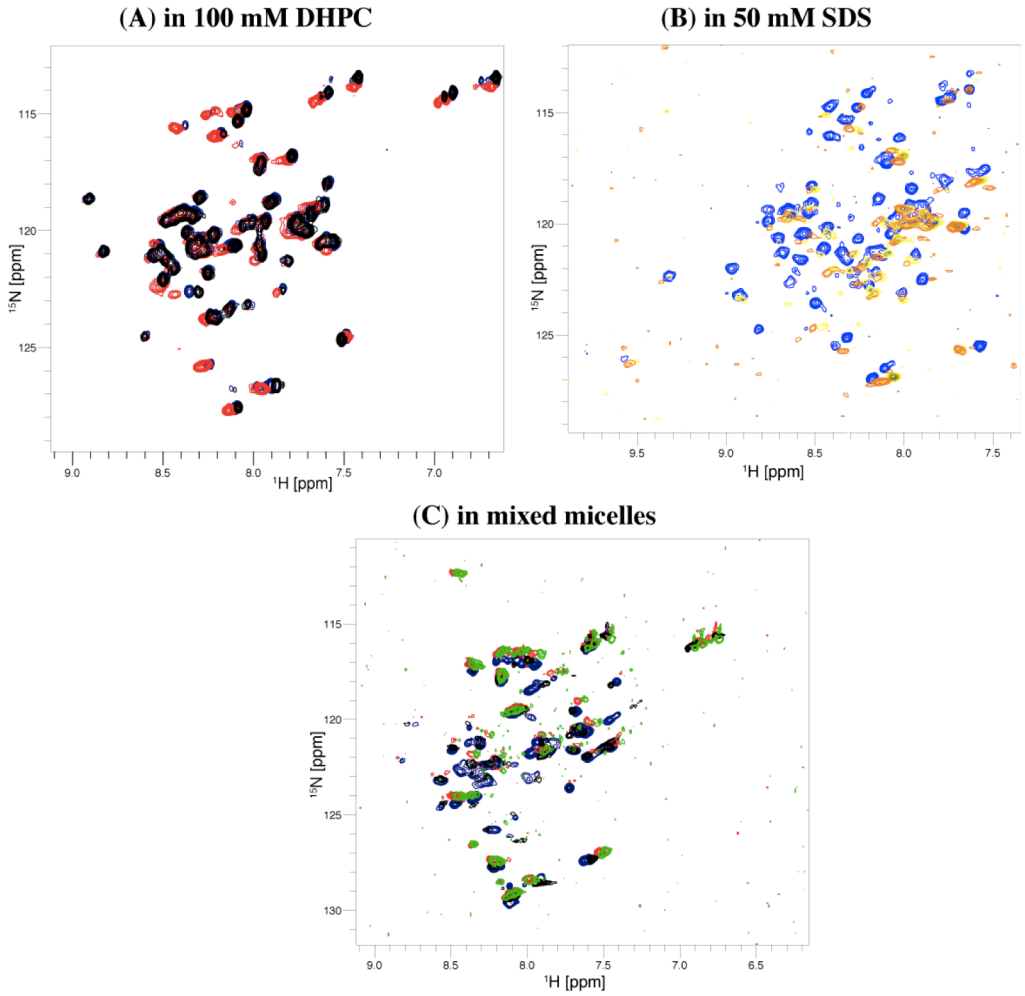

Figure 4.14: Temperature dependence of MRAP(2-67) in 50 mM sodium phosphate buffer (pH 6.5) and (A) 100 mM DHPC, (B) 50 mM SDS, (C) mixed micelles (100 mM Fos-Choline-10, 20mM DHPC, 5mM DMPG),
Colouring: yellow - 323 K, orange - 315 K, black - 310 K, blue - 303 K, red - 298 K, green - 291 K

4.2.5 Circular Dichroism of MRAP(2-67)

MRAP(2-67) was examined by circular dichroism (CD) spectroscopy to gain insights into folding and secondary structure in 100 mM DHPC, 50 mM SDS, mixed micelles and liposomes. The spectra obtained in DHPC, SDS and mixed micelles revealed two negative maxima at ~220 nm and ~210 nm indicating a high α-helical content (Figure 4.15).

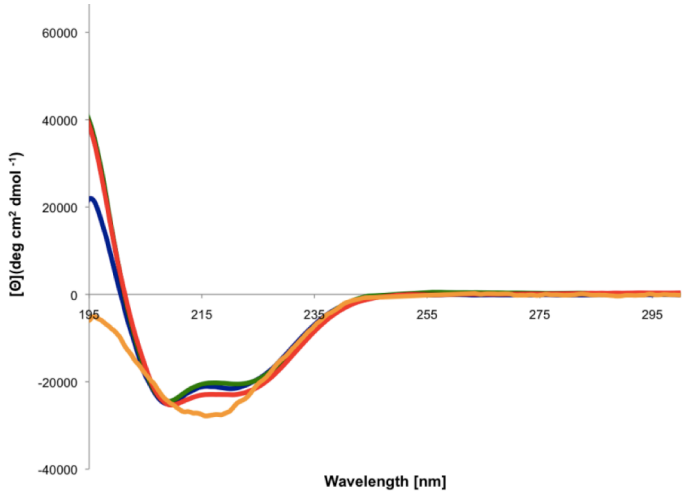

Figure 4.15: Circular dichroism spectra of MRAP(2-67) in different detergents and liposomes
Colouring: blue - in 100 mM DHPC, green - in 50 mM SDS, red - in mixed micelles;
orange - in DMPC Liposomes

To assess the degree of α-helicity the ratio $\theta_{222}/\theta_{208}$ was calculated (Libich et al. 2009) for MRAP(2-67) in each tested environment (Table 4.2). The CD spectrum in DMPC liposomes provided no clear results, which was attributed to the difficulty in creating a protein-free liposome sample that is identical in all aspects (e.g., concentration and liposome size) for reliable background subtraction.

Detergent	$\theta_{222}/\theta_{208}$	Conclusion
100 mM DHPC	0.859	α-helical
50 mM SDS	0.849	α-helical
Mixed micelles	0.935	α-helical
Liposomes	Not applicable	

Table 4.3: Examination of the α-helical ratio of MRAP(2-67).
Well-defined coiled coil structures display a ratio $\theta_{222}/\theta_{208} > 1$ (Libich et al. 2009)

In all micelle mixtures MRAP(2-67) appeared to behave similarly. In SDS and mixed micelles the ratio between the positive maxima and the negative ones was 2:1, which is an expected value for well-defined α-helical proteins. MRAP(2-67) adapted the highest α-helical propensity in SDS with a $\theta_{222}/\theta_{208}$ ratio of 0.86. This was not surprising since SDS is known to stabilise α-helices (Wu & Yang 1978; Micelli et al. 2004). However, obtaining a CD spectrum in DMPC liposomes proved to be more challenging. Under these experimental conditions MRAP(2-67) seemed to adopt a α-helical and β-sheet conformations without a positive maximum at 192 nm.

4.2.6 Spectroscopic characterisation and structure determination

4.2.6.1 Assignment of MRAP(2-67) backbone amide resonances in different conditions

Resonance assignment is a prerequisite for atomic resolution studies of proteins by NMR. However, it can be challenging for helical membrane proteins, which are high in aliphatic amino acids, exhibit poor dispersion, and have broad line widths due to the additional mass of the micelles or bicelles. Sequential backbone amide assignments in all three environments were obtained using 3D ^{1}H-^{15}N NOESY-HSQC (Kumar et al. 1981) and ^{1}H-^{15}N HSQC-TOCSY (Davis & Bax 1985) (Figure 4.12). All spectral parameters, including mixing times are listed in Methods and Materials – Table 3.1. Besides the first two residues in the construct (Ala2, Asn3) all backbone amide resonances (excluding prolines) were assigned in two out of three detergent/lipid mixtures. In DHPC, resonances corresponding to residues 34 to 37 in the positively charged KH-rich region were too weak to be observed or assigned in DHPC.

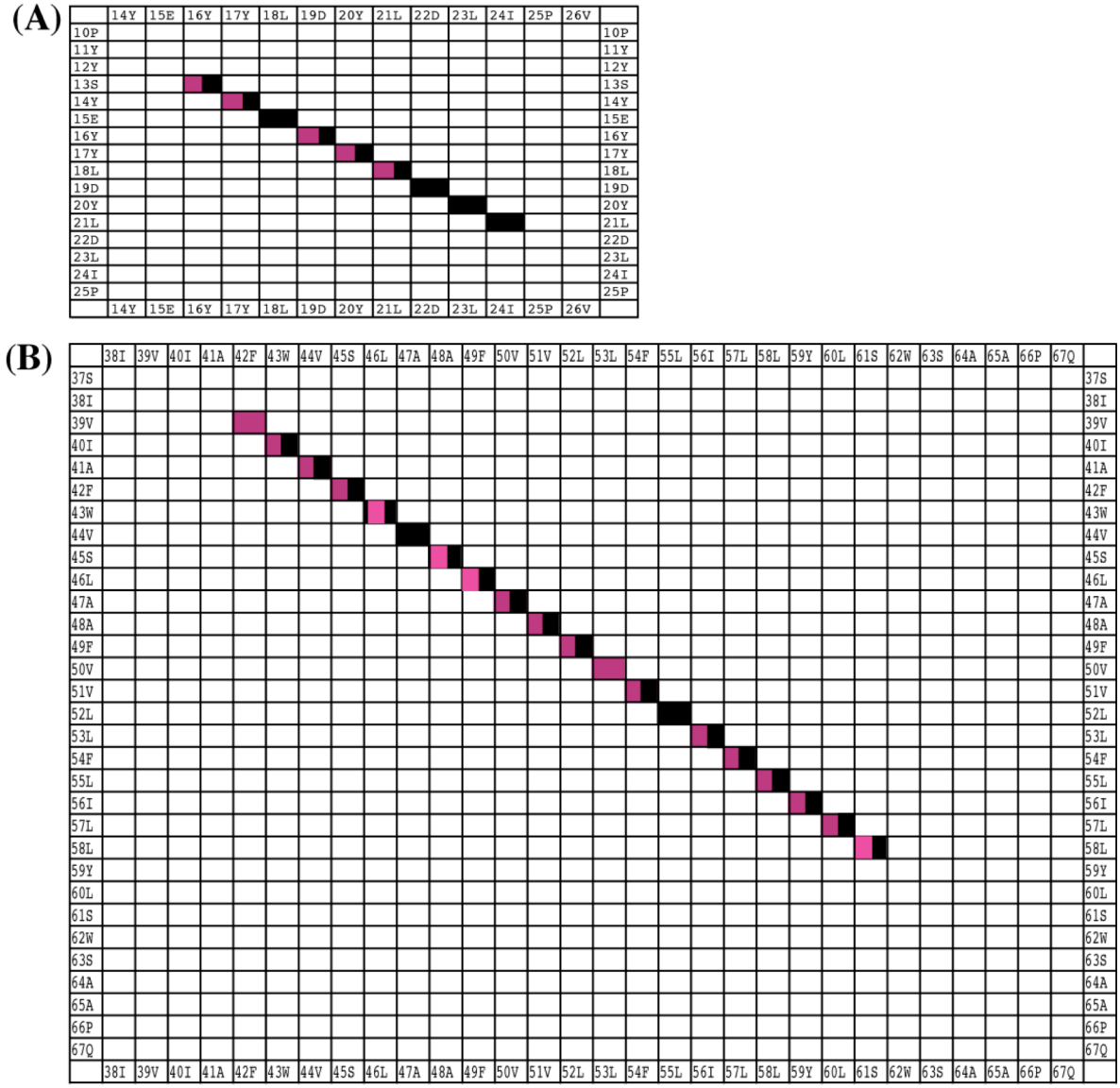

Figure 4.16: Intramolecular NOEs of MRAP(2-67) in 100 mM DHPC and mixed micelles
Investigation of the consistency of {i}Hα-{i-3} {i}HN-{i-3} NOEs in MRAP(2-67) across the N-terminal helical region (A) and the transmembrane domain (B), with back indicating all found intramolecular NOEs in DHPC and pink indicating the ones found in mixed micelles
Similar intramolecular NOEs were obtained in SDS, though not used for structure calculation.

Medium-range H_N-{i-3} connectivities indicative of α-helical structure were observed in a 3D ^{1}H-^{15}N NOESY-HSQC for the entire transmembrane domain (residues Ile38 to Trp62) as well as for a small N-terminal helix (residues Tyr16 to Asp22) in all three detergent/lipid mixtures. These findings suggested secondary structure elements for both regions in all detergent environments (Figure 4.16). Additionally, triple-resonance experiments HNCA, HNCO, and CBCACONH in all three environments were used to

obtain the chemical shifts for Cα and/or Cβ resonances and to verify backbone amide assignments (Methods and Materials Table 3.1).

4.2.6.2 Methyl-based and aromatic resonance assignments of MRAP(2-67) in 100 mM DHPC and 50 mM SDS

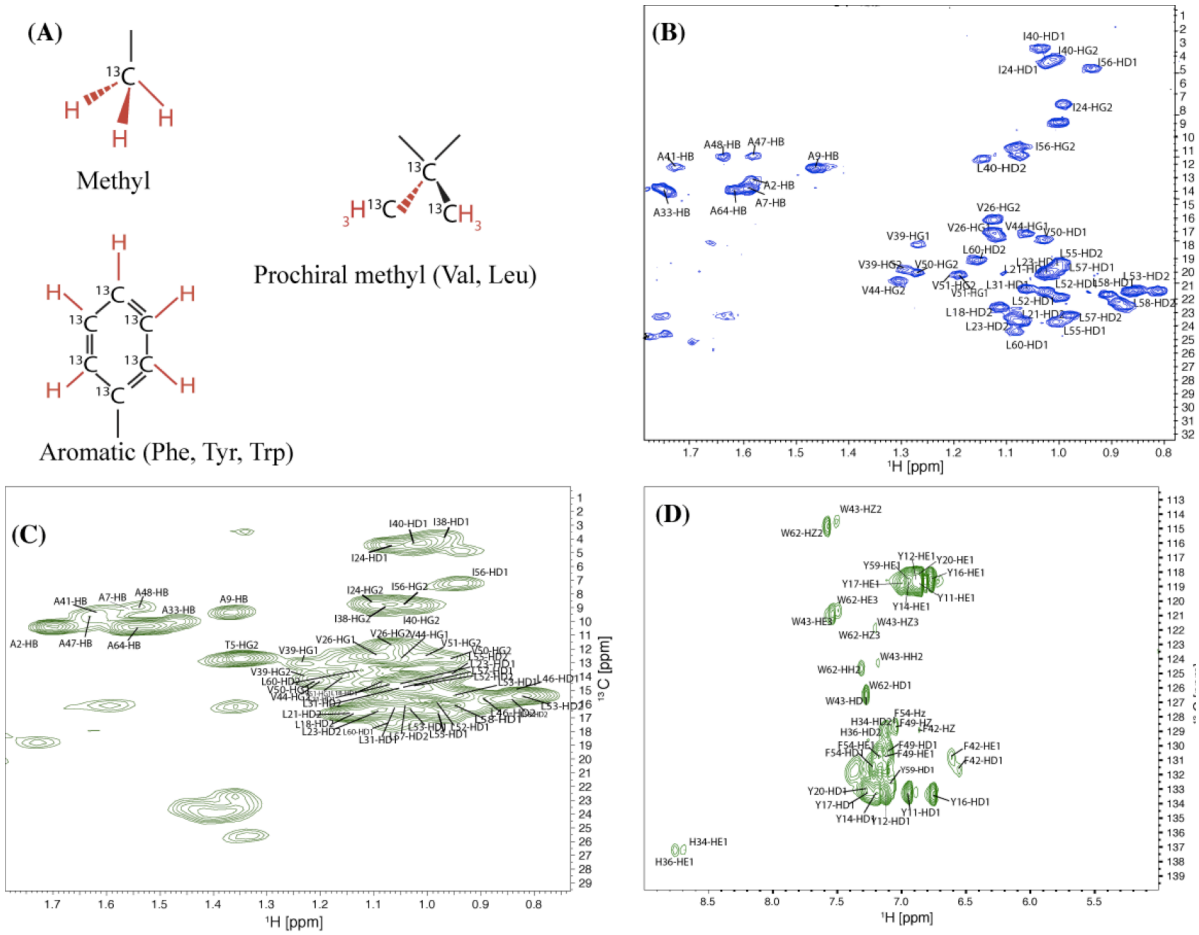

Figure 4.17: Sidechain assignment of MRAP(2-67) in 100 mM DHPC [blue] and 50 mM SDS [green]
(A) Methyl groups of amino acids
(B) ^{1}H-^{13}C assignment of methyl protonated valines, leucines, isoleucines in 100 mM dDHPC
(C) Assignment of Hδ and Hγ of aromatic amino acids in 50 mM dSDS
(D) ^{1}H-^{13}C assignment of methyl protonated valines, leucines, isoleucines in 50 mM dSDS

^{1}H and ^{13}C resonance assignments of valine and threonine γ-methyls, alanine β-methyls, and the δ-methyls of leucine and isoleucine were obtained in ^{1}H-^{15}N-NOESY-HSQCs (in deuterated DHPC a mixing time of 160 ms and in deuterated SDS mixing times of 160 ms and 250 ms were used). Stereospecific assignment of the valine γ-methyls and the leucine δ-methyls was achieved by using a 10 % ^{13}C-labelled sample (Szyperski et al.

1992). Partial assignments for aromatic ring resonances of tyrosines, tryptophans and phenylalanines were obtained using an aromatic 3D ^{1}H-^{13}C-NOESY-HSQC (mixing time 200 ms). Due to signal overlap and dynamic range limitations, deuterated detergent was required for the 3D ^{1}H-^{13}C- NOESY-HSQCs. While deuterated DHPC or SDS was commercially available, deuterated Fos-Choline-10 is not. As a result, sidechain methyl assignments were only obtained for the DHPC and SDS samples. For MRAP(2-67) a total of 140 distance restraints in deuterated DHPC were collected. In deuterated SDS, 246 distance restraints were observed.

4.2.6.3 Collection of residual dipolar couplings in 100 mM DHPC and 50 mM SDS

Residual dipolar couplings (RDCs) provide long-range orientational restraints to improve the resolution of protein structures and to validate NOE-based structures (Skrynnikov et al. 2000). RDCs can be especially useful for membrane proteins in micelles since long-range distance constraints from NOEs are often sparse or absent (Opella & Marassi 2004; Lipsitz & Tjandra 2004). Stretched polyacrylamide gels can be used to generate partial protein alignment, independent of the magnetic field direction (Chou et al. 2001). Protein alignment arises from collisions with the polyacrylamide gel (Prestegard et al. 2004). Optimising the anisotropic sample conditions was not a trivial process since soaking of MRAP(2-67) in DHPC micelles into the gels was inefficient at high acrylamide concentrations and led to fragile gels that were subject to rupturing at low acrylamide concentrations, resulting in either low signal-to-noise spectra or heterogeneous spectra. The extreme pH and the reactivity of TEMED excluded the possibility of polymerising acrylamide in presence of the protein in micelles (D. H. Jones

& Opella 2004). RDCs were not obtained for MRAP(2-67) in mixed micelles, as the size of the mixed micelle prevented incorporation of sufficient protein into the gel under all tested conditions. For MRAP(2-67) in DHPC and SDS the one-bond ^{1}H-^{15}N coupling constants were measured first with a combination of ^{1}H-^{15}N HSQC and ^{1}H-^{15}N TROSY experiments. After soaking the protein sample into a 4.2 % polyacrylamide gel that was subsequently stretched radially, the couplings were measured again, which were a sum of the coupling constant and the RDC. The RDC for each residue was then obtained by subtracting the coupling constant measured in the isotropic sample from that measured on the anisotropic sample.

A total of 29 RDCs in DHPC were experimentally measured for structured regions of MRAP(2-67). Dipolar wave analysis was performed, by fitting the experimental data to a simple sinusoid with a periodicity of 3.6 (Figure 4.18 (A)) - red lines) (Mesleh et al. 2002; Mascioni & Veglia 2003; Lee et al. 2003). The helical regions detected by dipolar wave analysis matched reasonably well with the helical regions determined from NOEs in MRAP(2-67). A decreasing sinusoid was best fit to the small helix in the N-terminal region (residues Tyr16 to Leu22) indicating a gradual change in the RDC amplitude. This can indicate helix curvature (Opella & Marassi 2004). The observed curvature was ascribed to the interaction with the micelle surface. The low deviations of the dipolar waves from the experimental data and consistent amplitude suggested an ideal straight α-helix for the transmembrane domain (residues Ile38 until Trp62).

A second RDC set was collected in SDS and RDCs and data for 23 residues was obtained. An initial dipolar wave analysis was performed. This examination indicated also a curved helical region from residue Tyr17 to Leu21, consistent with the results in DHPC.

For the transmembrane domain an α-helix with a kink at Phe49 was observed (Figure 4.18 (B)).

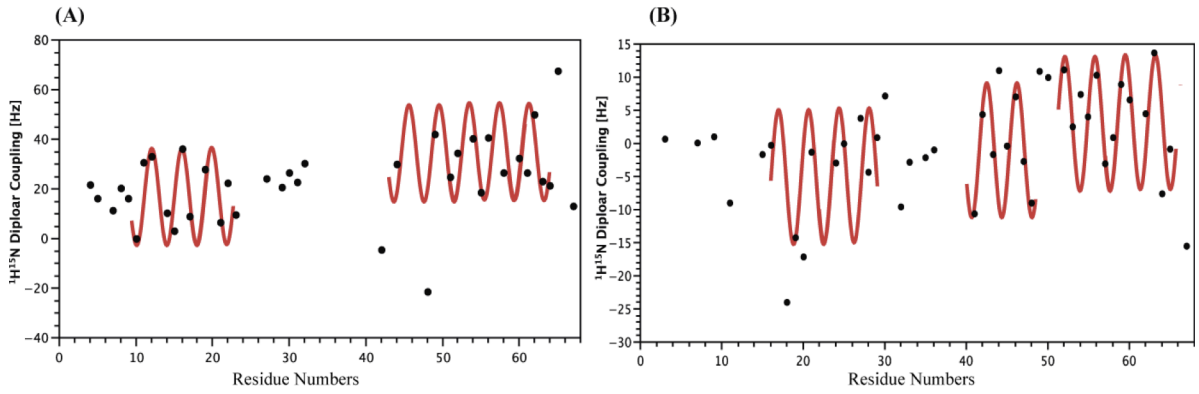

Figure 4.18: Dipolar wave analysis of experimental ^{15}N-^1H_N Residual dipolar coupling data sets of MRAP(2-67)
(A) in 100 mM DHPC
(B) in 50 mM SDS

The information obtained from these two RDC sets in different detergents suggested a similar secondary structure of MRAP(2-67). However, the different average magnitudes determined by dipolar wave analysis suggested that the molecular alignment tensors were not "degenerate". The unique orientations were likely generated by distinctive interactions between the detergent micelles and the alignment media.

4.2.6.4 Structure calculation of MRAP(2-67)

XPLOR-NIH 2.21 (Schwieters et al. 2003) was used for structure calculations of MRAP(2-67) in DHPC and mixed micelles. The complete protocol comprised an initial high-temperature annealing step (1000 K) to enable conformational sampling, followed by a transition to a lower temperature (300 K) and finally a refinement step at 300 K against all restraints including RDCs. For structure calculations in DHPC a total of 359 intramolecular distance restraints and 51 hydrogen bond restraints were used. In mixed micelles 642 distance-restraints, and 51 hydrogen bond restraints were used. In addition, secondary structure motifs and torsion angle restraints were determined from backbone

chemical shifts by TALOS+ (Shen et al. 2009). A total of 90 ϕ and ψ backbone torsion angles were predicted for MRAP(2-67) in DHPC. 66 ϕ and ψ backbone torsion angles were computed for MRAP(2-67) in mixed mixed micelles. TALOS+ predication was consistent with the hydrogen bonds. 29 residual dipolar coupling restraints were determined in DHPC and used for further refinement. These restraints were implemented into structure calculations. A complete list of NMR distances and dihedral constraints used for structure calculations is shown in Table 4.3.

NMR distance and dihedral constraints		
Distance constraints	**100 mM DHPC**	**Mixed micelles**
Total NOE	359	642
Sequential (*i, i-1*)	141	257
Medium-range (*i-3*)	214	371
Long-range (*i-4*)	4	14
Backbone H_N RDC constraints	29	0
Hydrogen bonds	51	51
Total dihedral angle restraints		
ϕ	45	33
ψ	45	33

Table 4.4: NMR statistics for MRAP(2-67) in two different detergents

The average root-mean square deviation (RMSD) in DHPC for Cα backbone residues over the structured regions of MRAP(2-67) was 0.29 ± 0.13 Å. For the structures in DHPC, the RMSD for the Cα backbone residues of the N-terminal domain (residue Tyr16 – Leu21) and the transmembrane domain (residue Ile38 – Leu60) was 0.18 ± 0.08 Å and 0.30 ± 0.16 Å, respectively. In mixed micelles, the RMSD was 0.19 ± 0.06 Å for all structured Cα backbone residues, and 0.04 ± 0.01 Å and 0.22 ± 0.06 Å for the Cα backbone residues for N-terminal domain (residue Tyr16 – Leu21) and the transmembrane domain (residue Ile38 – Trp62), respectively. The complete statistical evaluation is presented in Table 4.4. Overall RMSD values for MRAP(2-67) in both

detergent mixtures were very good and hence proposed a high accuracy between ensembles of calculated structures. However, calculated RMSD values were lower for MRAP(2-67) in mixed micelles were lower than for the one in DHPC.

Structure statistics		
Violations (mean ± s.d.)	**100 mM DHPC**	**Mixed micelles**
Distance constraints (Å)	0.060	0.072
Dihedral angle constraints (º)	0.442	0.491
RDCs, rms in Hz	1.408	-
Deviations from idealised geometry		
Bond length (Å)	0.003	0.004
Bond angle (º)	0.001	0.000
Impropers (º)	0.211	0.362
ϕ/ψ in most favoured or allowed regions, %	100	100
Average pairwise r.m.s.deviation (Å)		
RMSD (Å)	100 mM DHPC	Mixed micelles
Backbone (all structured regions)	0.29 ± 0.13	0.19 ± 0.06
Backbone (N-terminal helix)	0.18 ± 0.08	0.04 ± 0.01
Backbone (TM)	0.30 ± 0.16	0.22 ± 0.06
Heavy (all structured regions)	0.69 ± 0.18	0.44 ± 0.06
Heavy (N-terminal helix)	0.73 ± 0.30	0.22 ± 0.17
Heavy (TM)	0.65 ± 0.22	0.48 ± 0.08

Table 4.5: NMR refinement statistics for MRAP(2-67) structure in 100 mM DHPC and mixed micelles

Figure 4.19 depicts an ensemble of the ten best calculated structures of MRAP(2-67) in DHPC and mixed micelles, derived from experimentally obtained NOEs. These ensembles were used to evaluate the quality of calculated structures. The ensembles indicated that the structures were well defined for the helical regions. The N-terminal helix from Tyr16 to Leu22 was consistent in both detergents. The transmembrane domain helices are formed by residues Ile38 to Leu60 in DHPC micelles and Ile38 to Trp62 in mixed micelles (Figure 4.19).

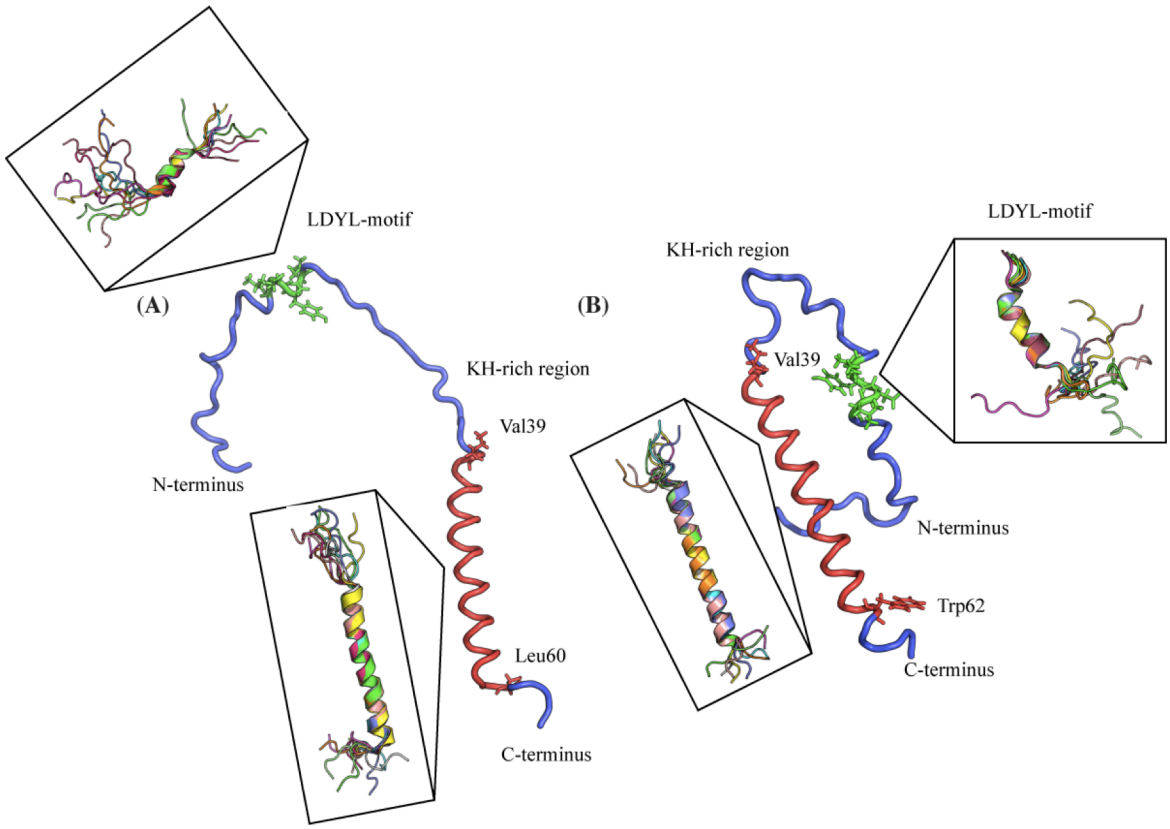

Figure 4.19: Investigation of the structure of MRAP(2-67)
Ensembles of ten structures were refined and an overall average was calculated. However, the disordered regions in between the helical domains made an overlay of the entire structure impossible. The helical regions were well defined across detergents.
(A) MRAP(2-67) in 100 mM DHPC
(B) MRAP(2-67) in mixed micelles
Colouring: green indicating the helical LDYL-motif, red the transmembrane domain and blue the flexible regions

4.2.6.5 Evaluation of structure quality

iCing (Doreleijers et al. 2012), an integrated residue-based structure validation program for NMR data, was used to compared experimental data with the NMR-derived structural models. Ramachandran plots gave additional quality assessment. Ensembles in both detergents exhibited excellent Ramachandran statistics for the structured parts (Figure 4.20. (A)) while fulfilling the experimental data. MRAP(2-67) in DHPC showed slightly better values than in mixed micelles by 3.2 % (Figure 4.20. ((B)). In DHPC all residues were located in the most favoured regions, whereas in mixed micelles 8 outliers in the N-terminal domain were found to be in the additionally allowed regions.

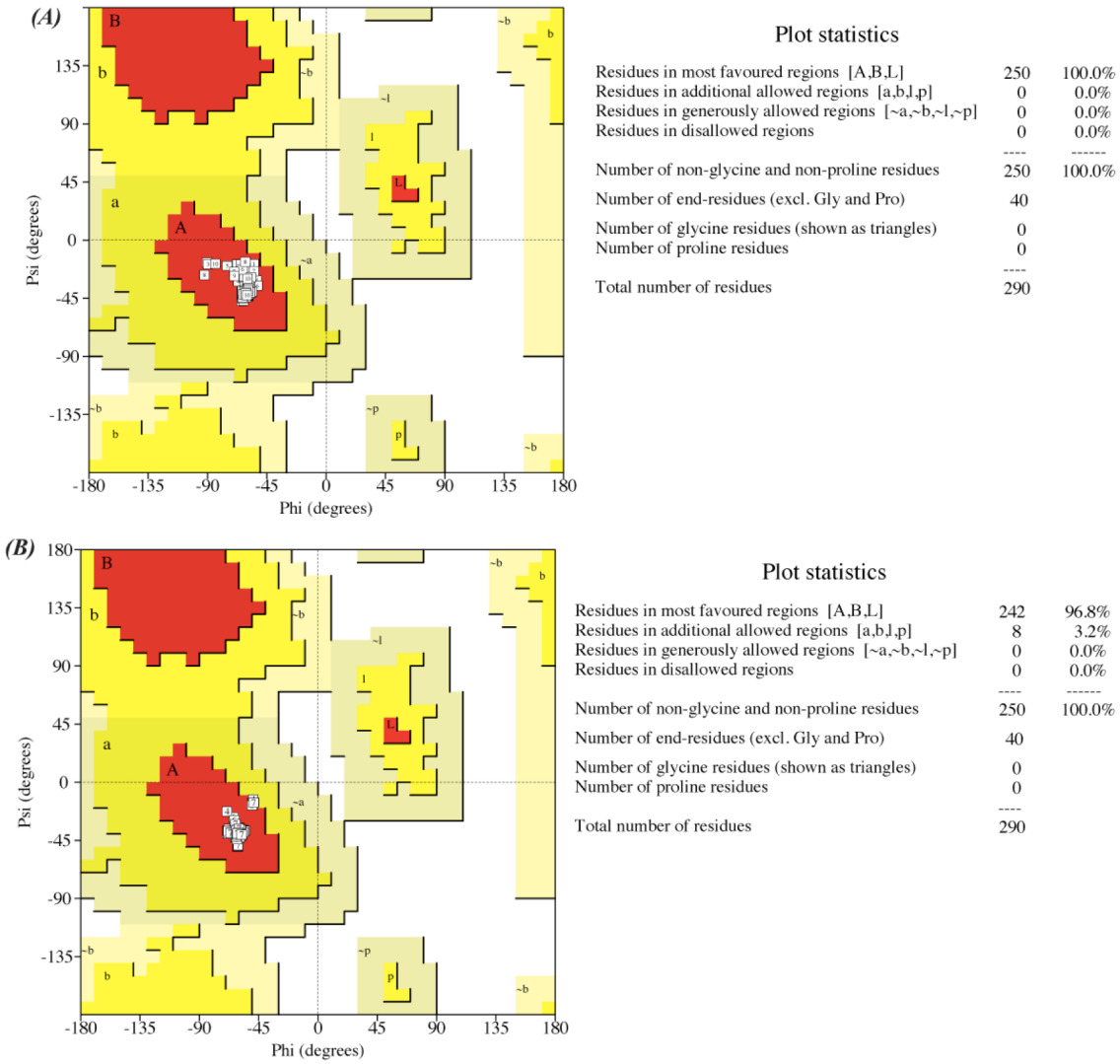

Figure 4.20: Ramachandran plot of MRAP(2-67) [Procheck]
(A) Ramachandran plot of MRAP(2-67) in 100 mM DHPC
(B) Ramachandran plot of MRAP(2-67) in mixed micelles

4.2.6.5.1 Residual dipolar coupling in 100 mM DHPC for evaluation

50 structures of MRAP(2-67) in DHPC were calculated using XPLOR-NIH 2.21 (Schwieters et al. 2003), including the experimentally obtained RDC restraints. RMSDs over the ten best structures illustrated good convergence (Table 4.5). In general, RMSD values over the structured region as well as across the transmembrane domain increased after the refinement with the measured RDCs.

RMSD (Å)	without RDCs	with RDCs
Backbone (all structured regions)	0.29 ± 0.13	0.22 ± 0.06
Backbone (N-terminal helix)	0.18 ± 0.08	0.33 ± 0.16
Backbone (TM)	0.30 ± 0.16	0.16 ± 0.06
Heavy (all structured regions)	0.69 ± 0.18	0.72 ± 0.11
Heavy (N-terminal helix)	0.73 ± 0.30	0.86 ± 0.31
Heavy (TM)	0.65 ± 0.22	0.66 ± 0.10

Table 4.6: RMSD assessment for structures calculated with and without RDC restraints in 100 mM DHPC

Ramachandran plot analysis was used for further evaluation of obtained structures. iCing provided confident RMSD-values as well as Ramachandran plots (Doreleijers et al. 2012). The Ramachandran statistics for the structured regions (Table 4.6) without RDCs showed slightly better values than the one including RDCs. All residues appearing in the additional allowed region are located in the N-terminal domain, which might have been a consequence of choosing too tight RDC-dependent distance bounds within the structure calculation.

Region assessment (%)	without RDCs	with RDCs
Most favoured regions	100.0 %	99.6 %
Additional allowed regions	0.0 %	0.4 %
Generously allowed regions	0.0 %	0.0 %
Disallowed regions	0.0 %	0.0 %

Table 4.7: Ramachandran plot assessment for structures calculated without and with RDC restraints in 100 mM DHPC

Overall, the extensive agreement between structure ensembles calculated by XPLOR-NIH2.2 and obtained after refinement with RDCs is not surprising, since the calculated structures (using XPLOR-NIH) were already well refined with an overall low RMSD of 0.29 ± 0.13 Å (Table 4.6).

For further evaluation RDCs constraints were fitted onto the NOE-derived structure in MODULE (Dosset et al. 2001). Fitting of RDCs to the helical regions in the N-terminal domain and the transmembrane domain required the use of two different alignment

tensors (Figure 4.21 (A)). The requirement for two alignment tensors might result from the interaction (steric and/or electrostatic) between the protein-micelle complex and the polyacrylamide gel matrix or that the structural elements do not adopt a fixed orientation relative to each other. Since no significant shift changes were observed between isotropic and anisotropic samples it is unlikely that the protein-micelle complexes interact with the gel matrix. Using two independent alignment tensors for residues Tyr14 to Asp22 and Ile38 to Leu60 resulted in a good correlation between the experimental and back-calculated RDC values (Figure 4.21 (A)). The central residues of the N-terminal helix exhibited only small differences between the experimental and back-calculated RDCs, however residues toward the ends of the helix displayed relatively large differences (Figure 4.21 (B)). The correlation coefficient R^2 after refinement of the structure with RDCs was 0.93, as shown in Figure 4.21 (D+E). The increased fit and the excellent agreement between the experimental data and the calculated values Figure 4.21 (C) demonstrated that the calculated MRAP(2-67) structure satisfied the RDC data.

Further examination of experimental RDCs was done by analysis of domain dependent parameters, which are listed in Table 4.7. A_a and A_r are the axial and rhombic components obtained from the alignment tensor. The χ^2_{Exp} value for the fit of the RDC data was acquired for each module. All variables were calculated using MODULE. The Euler rotation *R* defines the transformation from the alignment tensor frame to the local frame. Its parameters are α, β, γ, which represent different orientations for each axis, depending on the mean orientation of the axis with respect to the alignment tensor (Blackledge 2005).

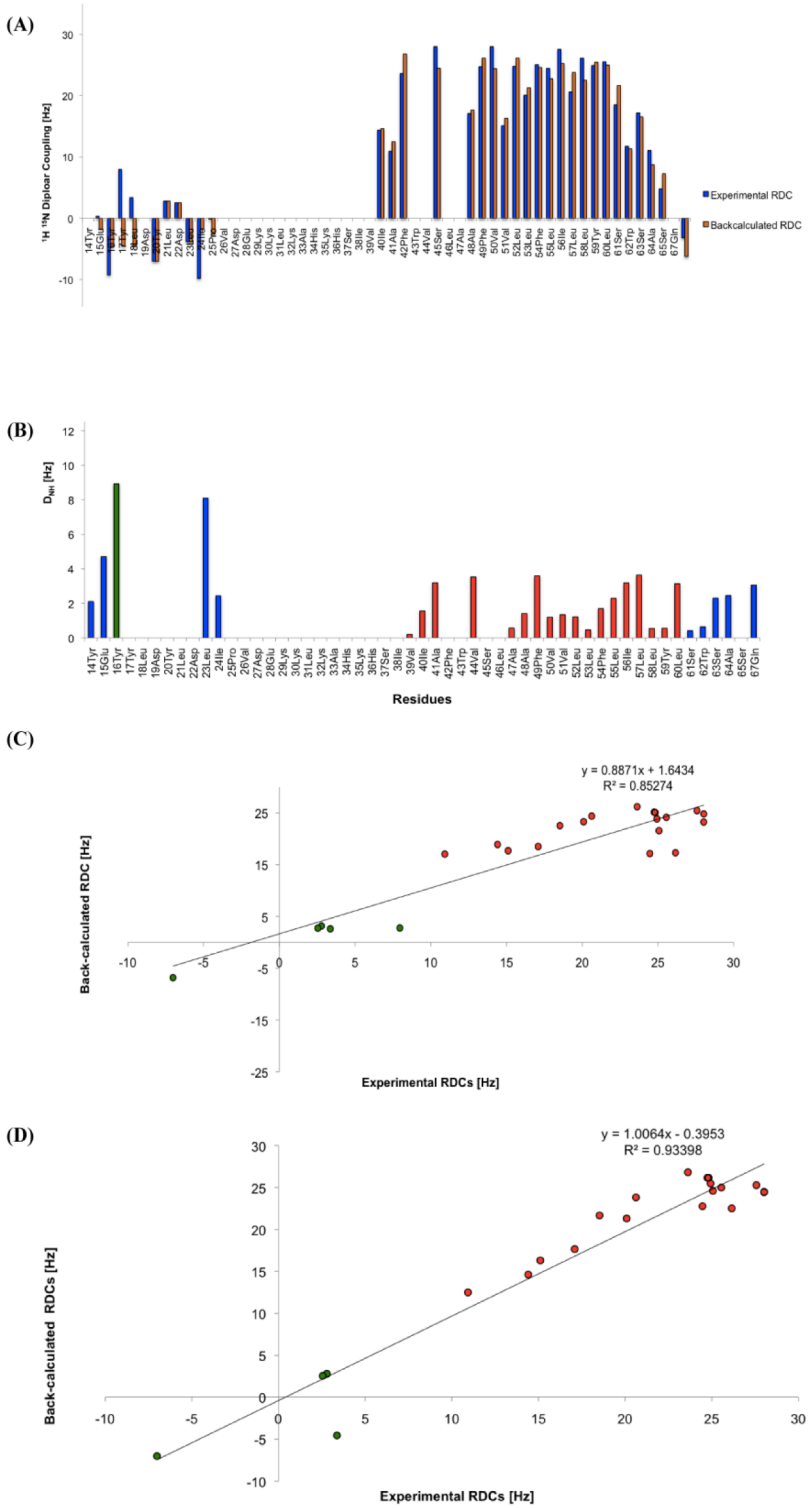

Figure 4.21: Correlation plots of experimental ^{15}N-$^{1}H_N$ RDC data sets of MRAP(2-67) in 100 mM DHPC calculated with two alignment tensors
Two separate alignment tensors were set while back-calculating the RDCs: The first alignment tensor was defined at the LDYL motif helix and the second one at the transmembrane domain.
(A) Experimental and back-calculated ^{15}N-$^{1}H_N$ RDCs with two alignment tensor after refining against MRAP(2-67) structure
(B) Difference between experimental and back-calculated ^{15}N-$^{1}H_N$ RDCs after refining against MRAP(2-67) structure
Correlation plots for the structure calculated using the information from RDCs of experimental and back-calculated ^{15}N-$^{1}H_N$ (C) before refining (D) after refined against MRAP(2-67) structure
Colouring: blue - unstructured regions; green - N-terminal α-helix, with embedded LYDL motif;
red - α-helical transmembrane domain

	Alignment tensor on residues Glu15 - Ile24	Alignment tensors on residues Ile38 - 64Ala
A_a ($1e^{-4}$)	-25.35	-19.27
A_r ($1e^{-4}$)	-16.11	-11.96
α	112.48	153.84
β	65.58	70.10
γ	-169.38	129.30
χ^2_{Exp}	3.359e-29	8.79

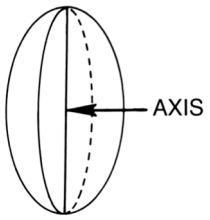

Table 4.8: Alignment tensors for MRAP(2-67) in 100 mM DHPC

Assuming that the shape of the micelle dominates the tumbling of the protein-micelle complex, the ratio between A_r and A_a gives an estimation of the spheroid form the detergent micelles occupy. Generally, $A_a > A_r$ indicates a prolate spheroid, whereas $A_a < A_r$ describes an oblate spheroid. A_a / A_r obtained from DHPC was calculated to be 1.6 suggesting DHPC micelles to adopt a prolate spheroid. In conclusion, collected RDCs in DHPC were consistent with the finding that MRAP(2-67) comprises two α-helices (residues Glu15 to Leu22 and Ile38 to Leu60) linked by the highly flexible KH-rich region.

4.2.6.5.2 RDC-based evaluation of detergent-dependent MRAP(2-67) structure

To ascertain whether the calculated structures of MRAP(2-67) in DHPC and mixed micelles were similar, RDC values obtained in SDS were first back-calculated on the NOE-based structure of MRAP(2-67) in DHPC (Figure 4.22). A reasonably good correlation of 0.67 was calculated for the experimental and back-calculated RDCs of the transmembrane domain. By contrast, RDCs measured for the N-terminal helix in SDS were more poorly correlated with the structure determined in DHPC indicating structural divergence and the conclusion that this region was more influenced by local micelle environment.

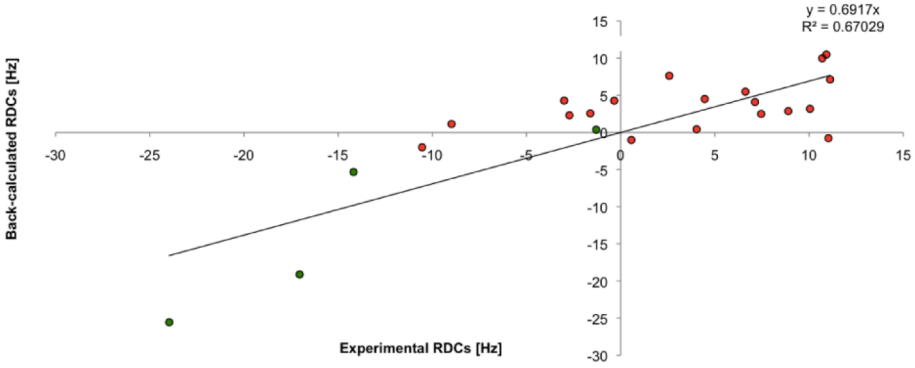

Figure 4.22: Correlation plots of experimental ^{15}N-$^{1}H_N$ RDC data sets of MRAP(2-67) in 50 mM SDS and 100 mM DHPC
The alignment tensors were defined across the LYDL-motif and the transmembrane domain separately (2 tensors)

Secondly, the RDC sets obtained in DHPC and SDS were applied to the NOE-based MRAP(2-67) structure in mixed micelles to differences in MRAP(2-67) structure upon addition of lipids and/or introduction of Fos-Choline-10 detergent.

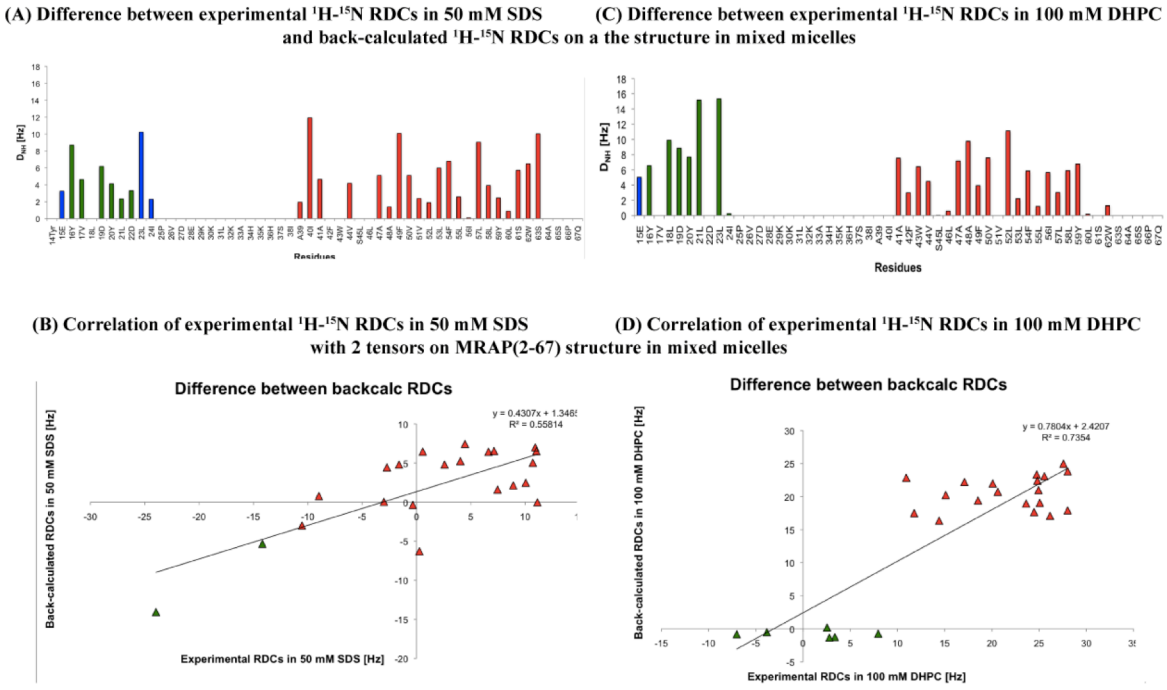

Figure 4.23: Correlation plots of experimental ^{15}N-$^{1}H_N$ RDC data sets of MRAP(2-67) in 50 mM SDS and 100 mM DHPC with its structure in mixed micelles
The alignment tensor were defined across the LDYL-motif and the transmembrane domain separately (2 tensors).
(A-B) ^{15}N-$^{1}H_N$ RDC of MRAP(2-67) in 50 mM SDS in comparison to MRAP (2-67) in mixed micelles.
(C-D) ^{15}N-$^{1}H_N$ RDC of MRAP(2-67) in 100 mM DHPC in comparison to MRAP (2-67) in mixed micelles.

Both RDC sets could be fitted reasonably well to the structure, with RDCs obtained in DHPC achieving a slightly better fit. Regression values were 0.78 and 0.56 for the RDCs measured in DHPC and SDS, respectively. Thus, the structures determined in DHPC and mixed micelles were relatively similar, whereas in SDS differed from both the DHPC and the mixed micelle structures (Figure 4.23).

4.2.6.6 Dynamics of MRAP(2-67) in different environments

The structure and dynamics of proteins are interconnected and both are crucial for understanding the protein's function. For MRAP(2-67) the relaxation parameters ^{15}N R_1, ^{15}N R_2 and $\{^1H\}$-^{15}N heteronuclear NOEs were measured at 500 MHz (303 K) in all three established sample conditions. $\{^1H\}$-^{15}N heteronuclear NOEs were determined from the ratio of peak intensities with and without the saturation of the amide protons, I_{on}/I_{off}. ^{15}N longitudinal (R_1) and transverse (R_2) relaxation experiments were obtained from a series of 2D experiments according to Farrow *et al.* (Farrow et al. 1994). For determining R_1 and R_2 values, the delay times were chosen according to the Cramer-Rao theory (Jones et al. 1996) . Relaxation parameters were calculated from the experimental data, using the program NMRPipe (Delaglio et al. 1995). A detailed description of all used parameters is described in Methods and Materials – Table 3.2.

4.2.6.6.1 $\{^1H\}$-$\{^{15}N\}$-Heteronuclear NOEs of MRAP(2-67)

$\{^1H\}$-^{15}N heteronuclear NOEs were determined for all three detergent mixtures, where values > 0.50 indicated ordered regions.

The lack of assignments in the KH-rich region in DHPC hindered the collection of dynamic data for residues His34 to Ser37 in DHPC. However, $\{^1H\}$-^{15}N heteronuclear NOE values > 0.50 were observed in residues Tyr11 to Ser63 (Figure 4.24 (A)). $\{^1H\}$-^{15}N

heteronuclear NOE values decreased at the N- and C-termini of MRAP(2-67) implying comparative disorder.

In SDS, stable regions were determined between residues Tyr11 and Ser63. Residue Ser37 exhibited a very low NOE value, (~0.01), hence flexibility was apparent in the positively charged KH-rich region (Figure 4.24 (B)). In the N- and C-termini, residues Asn3 – Ala9 and residues Ala64 – Gln67, experienced values below 0.09.

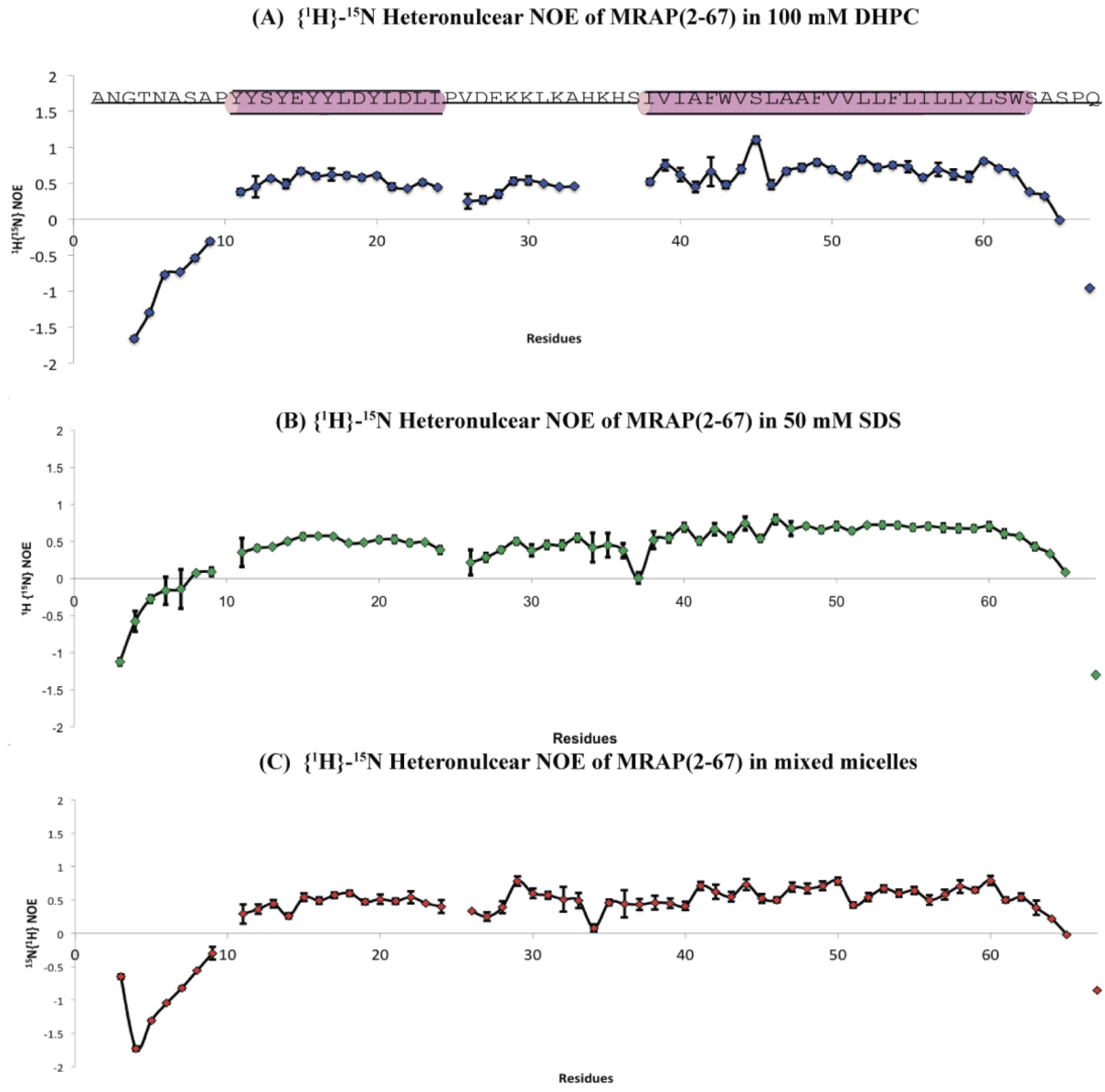

Figure 4.24: {¹H}-¹⁵N Heteronuclear NOE of MRAP(2-67) in all three detergents

Both data - sets were also confirmed in mixed micelles, where results towards a highly flexible N-terminus up to residue Tyr11, a flexible C-terminus showing fast timescale exchange from residue Trp62 onwards, and a fairly stable region between residues Tyr11 and Ser63 with a dramatic decrease in NOE at residue Ser37 (0.08).

4.2.6.6.2 R_1 and R_2 of MRAP(2-67)

In all three detergent environments the R_2 values in the N-terminal domain increased gradually up to residue Ile38, the start of the transmembrane helix, which exhibited the highest R_2 values, consistent with it being embedded in detergent (Figure 4.25 (A, B, C)). By contrast, R_1 values were relatively constant from residue Tyr11 onwards (Figure 4.26 (A, B,C)).

In DHPC micelles, Leu58 exhibited a significantly higher R_2 value than any other residues in the transmembrane domain, possibly indicating motion that is comparable to the NMR time scale (microsecond-millisecond). By contrast, the lower R_2 values in Ile40, Ser45 and Val51 represented relatively fast motions in these residues (Figure 4.26 (A)). Interestingly, in SDS Lys35 showed a lower R_1 of 0.40 s^{-1}, whereas Ser37 experienced the relatively high value (R_1 = 0.72 ± 0.03 s^{-1}) (Figure 4.26(B)). In mixed micelles residues Ala64, Ser65, and Gln67 had R_1 values higher than 0.50 s^{-1}. R_1 error bars are higher than in any other detergent, which was attributable to a lower quality of spectrum (Figure 4.25 (C)). Interestingly, the KH-rich region and the transmembrane domain (residue Lys32 – Leu60) showed a larger variation in R_2 with large error bars. Specifically, residues His34 (R_2 = 6.36 ± 1.25 s^{-1}) and Ser61 (R_2 = 5.36 ± 1.08 s^{-1}) showed an increase of transverse magnetisation, while surrounding residues had comparatively high values (R_2 = 21.66 ± 2.34 s^{-1}; R_2 = 21.47 ± 2.60 s^{-1} for those residues around His34 and Ser61, respectively).

Values for mean and standard deviation of R_1 and R_2 are displayed in Table 4.9.

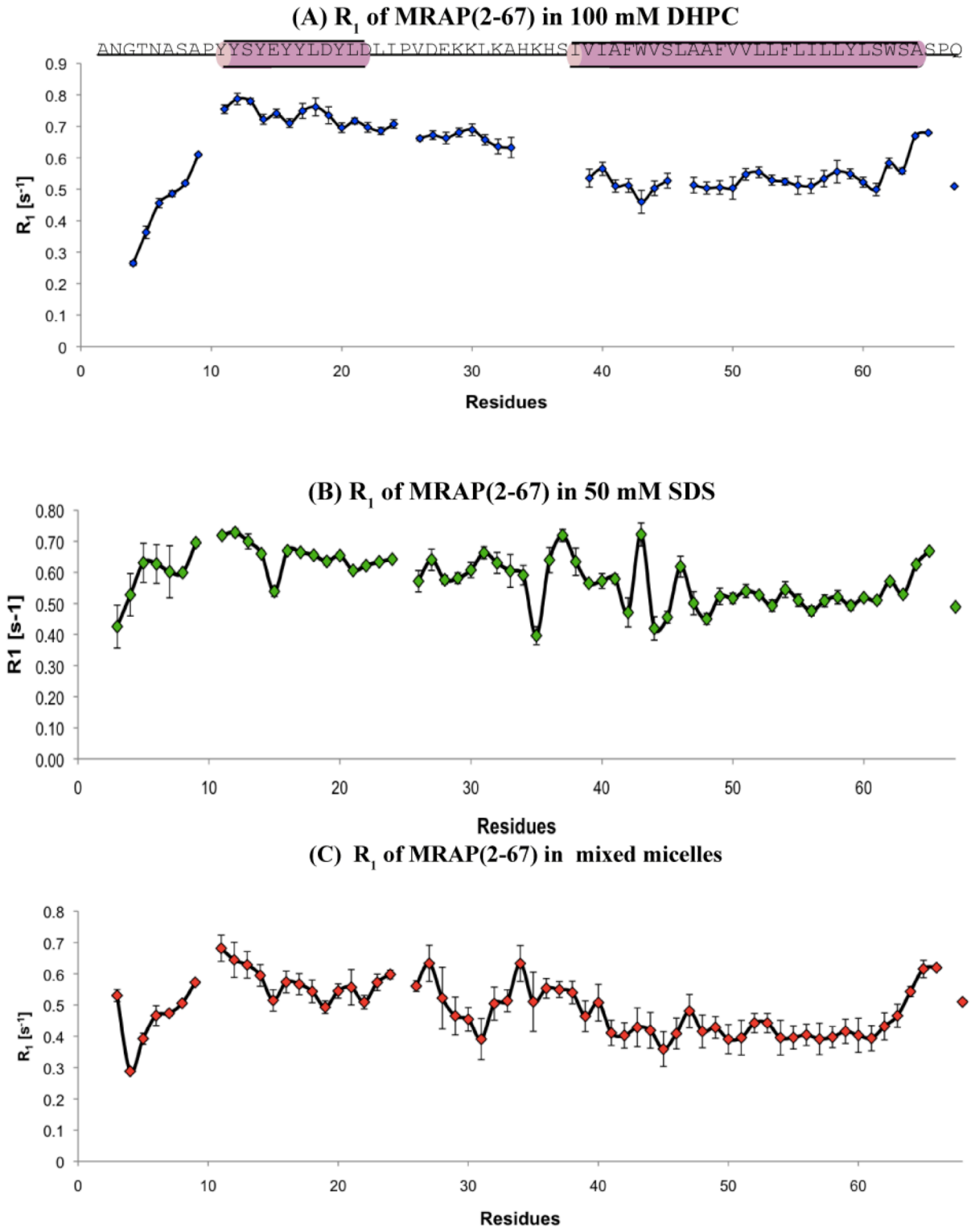

Figure 4.25: R_1 of MRAP(2-67) in different detergents

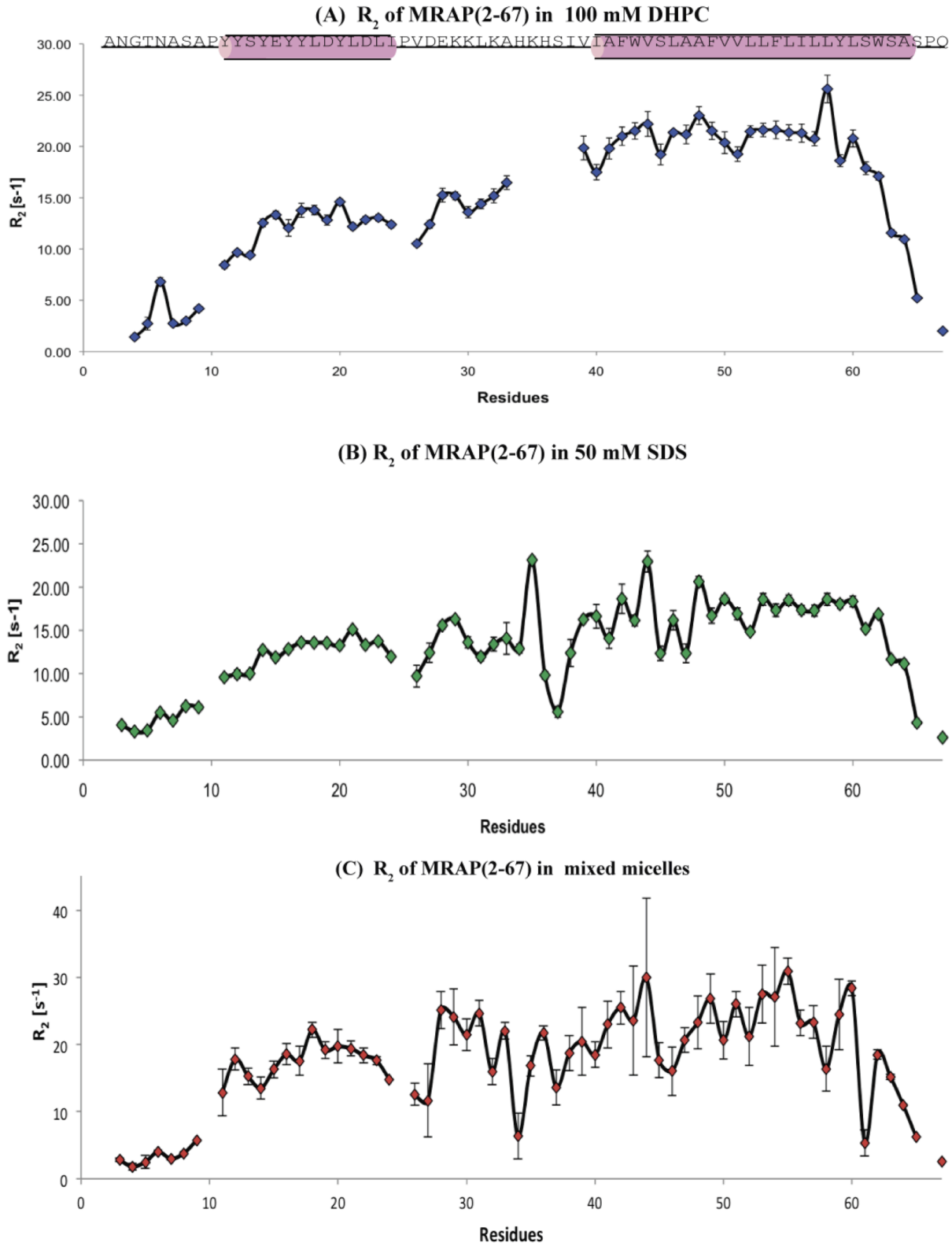

Figure 4.26: R_2 of MRAP(2-67) in different detergents

4.2.6.6.3 Further analysis of R_1 and R_2 relaxation data of MRAP(2-67)

The ratio R_2/R_1 and R_1*R_2 for each residue was calculated and provided initial estimations for structured regions of MRAP(2-67) and those that undergo chemical shift exchange on the microsecond to millisecond timescale. R_2/R_1 identified residues that undergo chemical exchange and estimated a global correlation time. R_1*R_2 was used to further distinguish between motional anisotropy and chemical exchange (Kneller et al. 2002). R_1*R_2 provides an indication of exchange motion of each residue as taking the product R_1*R_2 rather than R_2/R_1 removes the contribution of motional anisotropy. Moreover, separate investigation of the motional anisotropy and chemical exchange was performed by display of R_1*R_2 versus R_1/R_2 (Kneller et al. 2002). Anisotropic variations largely cancelled in R_1*R_2, therefore R_1/R_2 indicated variations of the rotational anisotropy when plotted against each other. The distribution of ^{15}N relaxation rates suggested a strong bias in the orientation of the H_N bond vectors and a motionally anisotropic transmembrane region.

The R_2/R_1 ratio for residues Glu15 to residue Ile24 in DHPC indicated a comparatively unstructured N-terminus with similar values of R_2/R_1 (~18.11) (Figure 4.27 (A)). R_2/R_1 values from Val26 to Ala33 increased to approximately 21.41. High R_2/R_1 values for residues Ile38 to Leu60, which delimited the transmembrane domain, were consistent with embedding of these residues within the detergent micelle. The average R_2/R_1 ratio over the whole protein was 25.78 ± 1.95. Initial visual estimation for structured regions suggested residues Trp43, Ala48 and Leu58 to experience the least flexibility across the transmembrane domain. R_1*R_2 showed low values for the N- and C-terminus region with similar values for Tyr11 to Leu60 displaying an average R_1*R_2 ratio of 10.79 ± 0.62.

(Figure 4.27 (B)). Residues Val44 and Leu58 experienced the fastest exchange motion across the construct. Separate investigation of the motional anisotropy and chemical exchange exhibited an N-terminal helix close to the trimmed mean (Figure 4.27(C)-indicated in green), whereas the lower values for the unstructured N-terminal and C-terminal region suggested fast timescale exchange (Figure 4.27(C)-indicated in blue).

In SDS, the R_2/R_1 ratio suggested as well comparatively unstructured, mobile, N-terminal domain and a transmembrane region with lower mobility. Fluctuations were displayed between residues Lys35 and Ala47. Especially Lys35 appeared to be highly inflexible. This was likely due to interactions between negatively charged detergent and the surrounding positively charged amino acids. Apparent dynamics in the vicinity of residues Trp43 and Phe49 may have arisen from ring-flips or other small conformational changes within the transmembrane region. Especially, residues Phe42, Val44 and Val48 are affected by these events (Figure 4.28 (A)). The mean R_2/R_1 ratio for MRAP(2-67) in SDS was calculated to be 21.56 ± 2.04 , in comparison to the higher value of 25.78 ± 1.95 obtained in DHPC. This suggested a lower overall tumbling time for MRAP(2-67) in SDS than in DHPC, perhaps due to changes in micelle size or the fraction of detergent molecules that were tightly bound to MRAP(2-67). R_1*R_2 showed low values for the N-terminal residues Asn3 to Ala9 and the C-terminus region Ala65 to Gln67. However, R_1*R_2 values in the region Ser37 to Ala47 were heterogeneous, with, for example, relatively fast motions in residues Ser37, Ser45 and Ala47 (Figure 4.28 (B)). The observed "clustering" close to the trimmed mean, which was observed when separately investigating R_1/R_2 and R_1*R_2' could be a result of further stabilisation of the N-terminal helical region by SDS. The positively charged amino acid Lys29 experienced slower

motional exchange than other residues in the N-terminal domain. Additionally, residue Lys35 seemed to be a dramatic outlier. This residue appeared to be in highly slow motion, which might be due to an interaction of the positively charged amino acid with the negatively charged detergent. (Figure 4.28 (C)).

The R_2/R_1 values of MRAP(2-67) in mixed micelles showed an unstructured N-terminal region. Residues Asn3 to Ala9 as well as residue Ser65 and Gln67 displayed a R_2/R_1 ratio below 10. The N-terminal helix between residue Glu15 and Asp22 exhibited values around $R_2/R_1 = 33.75 \pm 4.53$. The unstructured KH-rich region and transmembrane region showed fluctuations in R_2/R_1, with His34 having the lowest value ($R_2/R_1 = 10.04 \pm 2.90$) and Leu55 the highest ($R_2/R_1 = 76.57 \pm 25.22$) in this region (Figure 4.29 (A)). This heterogeneity in R_2/R_1 may be due to variable interactions with the detergent. This comparably high value also reflects the larger size of the mixed micelle, and hence slower tumbling time, compared to the DHPC and SDS micelles. As in R_2/R_1, the R_1*R_2-ratio of MRAP(2-67) showed variation in motion across the whole construct. Similar as observed in DHPC and SDS, investigation of the motional anisotropy and chemical exchange indicated that the N-terminal domain was relatively flexible, whereas the transmembrane underwent little internal motion. Residues Lys30 and Ala33 experienced comparatively fast motion, which can be seen in R_2/R_1 and R_1*R_2 as well. Residues Ser45, Leu46 and Leu58 might interact with the detergent, which would explain the fluctuation that was already established by investigation of R_2/R_1 and R_1*R_2 (Figure 4.29 (C)).

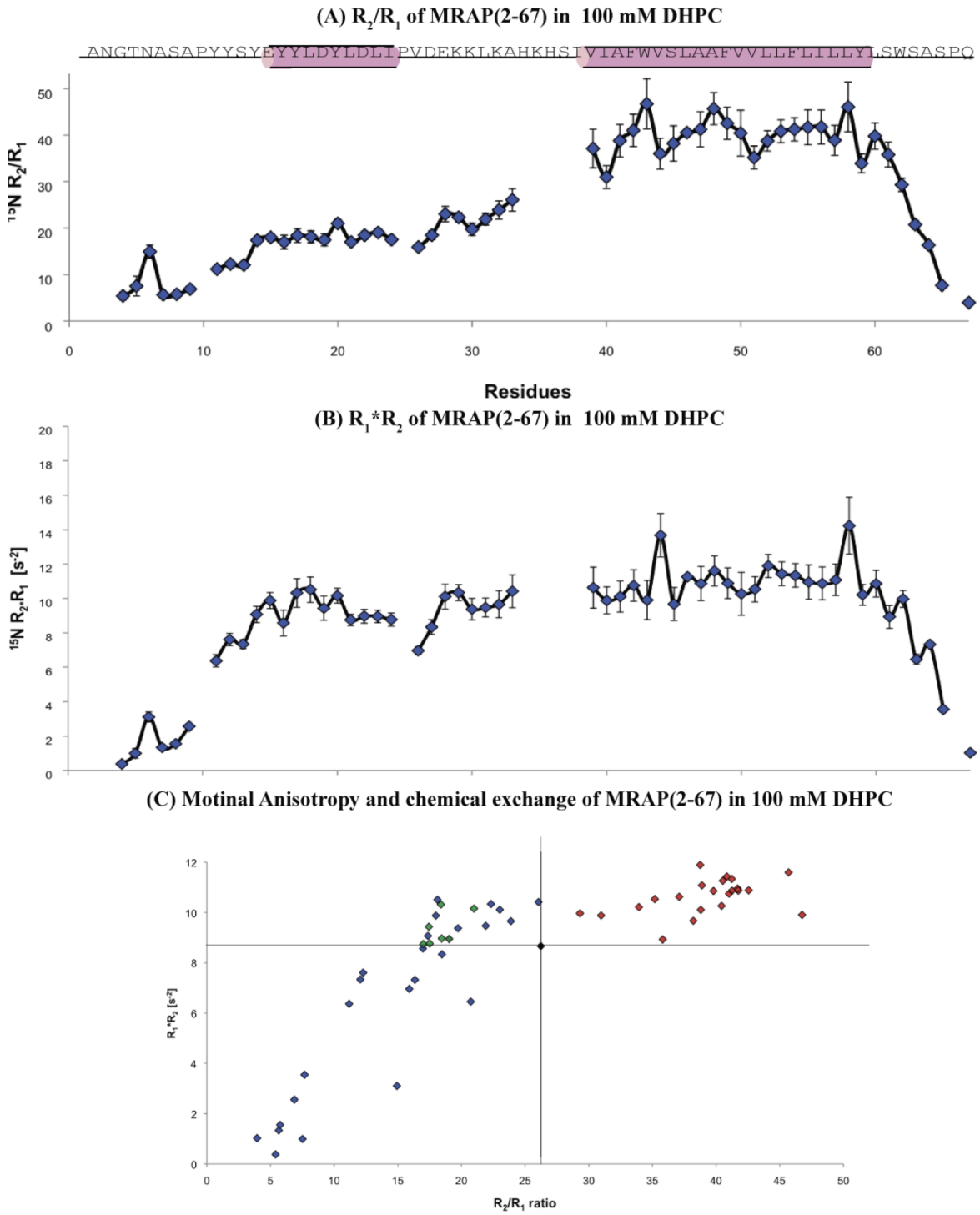

Figure 4.27: Dynamics of MRAP(2-67) in 100 mM DHPC
*(A) R_1*R_2, (B) R_1/R_2, (C) Motional Anisotropy of MRAP(2-67) in 100 mM DHPC*
Colouring: blue- N-terminal unstructured region, green - N-terminal helix, red – transmembrane domain

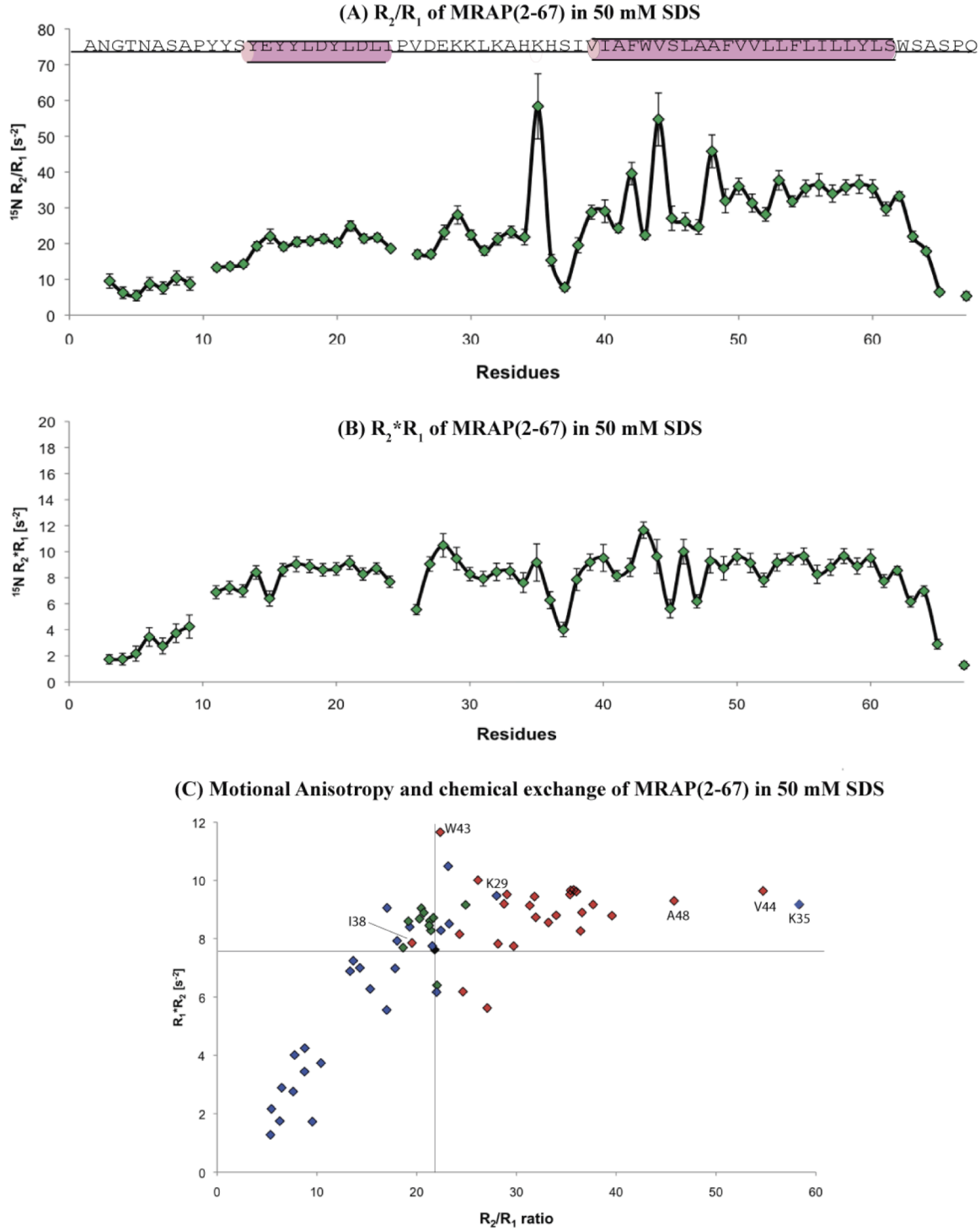

Figure 4.28: Dynamics of MRAP(2-67) in 50 mM SDS
*(A) R_1*R_2; (B) R_1/R_2; (C) Motional Anisotropy of MRAP(2-67) in 50 SDS*
Colouring: blue- N-terminal unstructured region, green - N-terminal helix, red - transmembrane domain

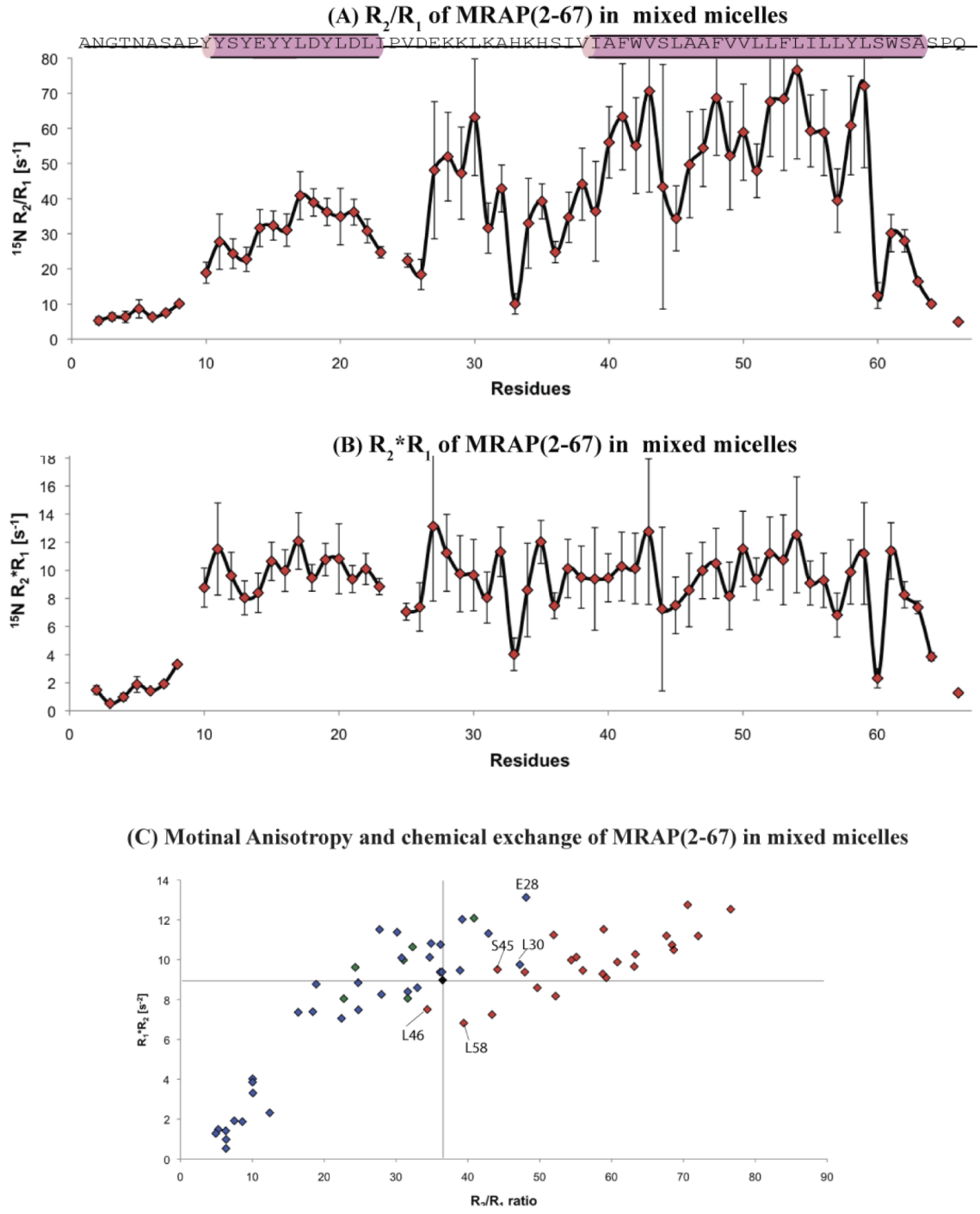

Figure 4.29: Dynamics of MRAP(2-67) in mixed micelles
(A) R_1/R_2 ,(B) R_1*R_2, (C) Motional Anisotropy of MRAP(2-67) in mixed micelles
Colouring: blue- N-terminal unstructured region, green - N-terminal helix, red - transmembrane domain

In 100 mM DHPC

	R_1	R_2	R_2/R_1
Trimmed mean	0.60 ± 0.02 s^{-1}	15.00 ± 0.34 s^{-1}	24.00 ± 1.83
Standard deviation	0.11	6.17	

In 50 mM SDS

	R_1	R_2	R_2/R_1
Trimmed mean	0.58 ± 0.02 s^{-1}	13.20 ± 0.54 s^{-1}	21.56 ± 2.04
Standard deviation	0.08	4.85	

In mixed micelles

	R_1	R_2	R_2/R_1
Trimmed mean	0.49 ± 0.04 s^{-1}	17.35 ± 2.37 s^{-1}	36.92 ± 8.77
Standard deviation	0.09	7.67	

Table 4.9: R_2/R_1 ratio values for MRAP(2-67) in different conditions

Detailed investigation of R_2/R_1 ratios and R_2*R_1 ratio of a structure provide a useful initial estimate for the overall rotational correlation time, τ_c, which can be calculated as followed:

$\tau_C \approx \frac{1}{4\pi\nu_N}\sqrt{6\frac{T_1}{T_2 - 7}}$, with ν_N describing the ^{15}N resonance frequency (in Hz).

τ_c-values for different MRAP(2-67) regions in different environments are stated in Tables 4.9.

	100 mM DHPC	**50 mM SDS**	**Mixed micelles**
τ_c of MRAP(2-67)	18 ns	18 ns	24 ns
τ_c of the transmembrane region	22 ns	21 ns	28 ns
τ_c of the N-terminal helix	16 ns	17 ns	20 ns

Table 4.10: Rotational correlation time τ_c of MRAP(2-67)

A comparison of the τ_c values between detergent/micelle mixtures indicated that the transmembrane domain exhibited consistently slower tumbling time than the N-terminal domain. Comparison of τ_c values across the whole construct showed an increase of τ_c in a detergent-dependent manner, with the following order: SDS < DHPC < mixed micelles. Thus, MRAP(2-67) in mixed micelles had the highest τ_c value, as expected due to the

large mass of the mixed micelle, which may be forming a membrane-like lipid bilayer (see below). For the transmembrane helix, the τ_c values were ordered identically to that of the overall tumbling rates. Interestingly, however, the tumbling times of the N-terminal helix were in the order of DHPC < SDS < mixed micelles. This observation would suggest that the more water-soluble N-terminal domain is either more ordered or has greater interactions with the micelle in SDS micelles.

Summarising, R_1 and R_2 values in all three environments suggested a limited degree of detergent-dependent dynamics. In all conditions, the N-terminal helix (residues Tyr16 to Leu22) and transmembrane (residues Ile38 to Leu60/Trp62) helix were most well ordered, with increased flexibility at the termini and around the KH-rich region. Additional comparison of the mean R_2/R_1 ratio across detergents suggested a relatively small micelle size for SDS, but possibly with greater interactions of the N-terminal helix with the SDS surface. The largest micelle was that of the mixed micelles containing lipids.

4.2.6.7 Investigation of MRAP(2-67)'s interaction with detergent

Interactions of MRAP(2-67) with the more natural lipid-like DHPC and mixed micelles containing lipids were investigated further by detecting NOEs between the backbone amides and surfactants. No NOEs between SDS and MRAP(2-67) were observed, since all experiments in SDS were collected in deuterated SDS. In DHPC, NOEs from detergent to MRAP(2-67) were observed in N-terminal residues Tyr20 and Ala33 (Figure 4.30 (A)). Interestingly, both residues experienced rather high R_1*R_2 and R_2/R_1 ratios of 10.15 and 10.45 for R_1*R_2 and 20.98 and 26.05 for R_2/R_1. Surprisingly, no clear NOEs to DHPC could be detected in the transmembrane domain, which is possibly due to the

dynamic nature of the detergent molecules (S. Rouse, PhD Thesis, 2012). By contrast, in mixed micelles MRAP(2-67) exhibited a large number of NOE crosspeaks corresponding to lipid acyl chains throughout the construct (Figure 4.30 (B)). Residues involved in interaction with the detergent or lipid were Tyr14, Glu15, Tyr16, Tyr17, Leu18, Asp19, Tyr20, Leu21 and Leu23 in the N-terminal domain as well as Ala41, Phe42, Trp43, Val44, Leu52, Leu53, Phe54 and Ser65 within the transmembrane domain and the C-terminus. The contact within the N-terminal domain appeared to be limited to the structured regions. Interaction of the transmembrane domain with the detergent or lipid might be caused by either inhomogeneous micelles or by a "tilted" insertion of MRAP(2-67) into the mixed micelles. Both regions experienced dynamic fluctuations in R_1*R_2 and R_2/R_1. Interestingly, the interaction with detergent is clustered in two regions around aromatic residues (Figure 4.30 (B)) Studies to further characterise this observation still need to be done. Ser65 is at the edge of the transmembrane domain and hence interaction with the micellar environment, is very likely.

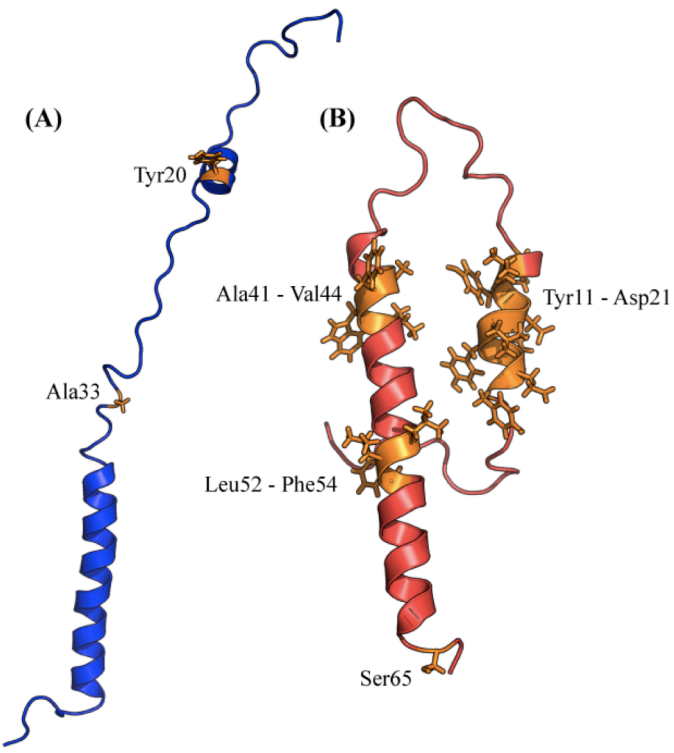

Figure 4.30: Interaction of MRAP(2-67) with the detergent in
(A) 100 mM DHPC
(B) mixed micelles
Colouring: orange - residues interacting with the detergent

An explanation for the observed different behaviour of MRAP(2-67) can be given by the nature of the used

detergents. The positive charges of zwitterionic DHPC are likely to bind the KH-rich region less tightly thereby allowing further flexibility and motion. On the contrary, SDS and mixed micelles are anionic and are expected to stabilise the positively charged region when entering the micelle environment. The overall flexibility in all three environments of the KH-rich region is responsible for motional freedom of the N-terminal domain.

4.2.6.8 Comparison of chemical shift perturbation of MRAP(2-67) in three different local environments

Further insights into the effect of detergents on MRAP(2-67) were gained by examining the chemical shift perturbations (CSP) between the detergent/lipid mixtures. ^{1}H-^{15}N HSQC-experiments were recorded of 250 μM MRAP(2-67) in DHPC, SDS and the mixed micelles. To remove possible non-detergent dependent CSP parameters, the buffer, pH, temperature, sample concentration and spectrometer were identical. Comparison of ^{1}H-^{15}N backbone resonances between MRAP(2-67) in DHPC and mixed micelles, showed an increase of CSP across the N-terminal domain (residues Gly4 to Ser37), consistent with some interaction of this region with at least the micelle surface (Figure 4.31 (A)). The positively charged KH-rich region (residue Glu28 to Ser37) experienced the largest shift changes ($\Delta\delta > 0.20$) within the construct, consistent with its positioning close to the transmembrane domain. Ile38, the first residue in the transmembrane domain, encountered the most substantial CSP of $\Delta\delta = 0.83$. However, due to lack of assignments between residues His34 and Ser37 in DHPC only little information was available for CSP in the KH-rich region (residue Asp28 to Ser37). Additionally, residues Val39 until

residue Ala47 perceived a change in environment. In contrast, the amino acids Ala48 to Ala64 did not show any significant perturbations.

Figure 4.31: Chemical shift perturbation difference of MRAP(2-67) in the main environments were observed within the KH-rich region with a detergents at 600 MHz
(A) 100 mM DHPC versus mixed micelles
(B) 100 mM DHPC versus 50 mM SDS
(C) 50 mM SDS versus mixed micelles

CSPs between DHPC and SDS were found throughout the construct, with Trp62 exhibiting the largest change (Δδ = 0.48 ppm) (Figure 4.31 (B)). The transmembrane domain between residues Ser45 and Ile56 perceived the least shift changes, consistent with their positioning in the chemically similar acyl chain region of the micelle.

Finally, MRAP(2-67) chemical shifts were compared between SDS and mixed micelles. Glu28 in the N-terminal domain exhibited one of the largest CSPs (Δδ = 0.92 ppm), probably as a result of electrostatic interactions with the higher charge density of the SDS micelle surface (Figure 4.31 (B)). As observed between DHPC and SDS, the transmembrane domain between residues Ala47 and Leu60 exhibited the least detergent-dependent CSP.

Summarising, an alteration of any detergent affected mostly the N-terminal edge of the transmembrane domain. In particular, the KH-rich region (residues Glu28 to Ser37) revealed a likely interaction with the detergent.

4.2.6.9 Investigation of the depth of insertion of MRAP(2-67) in different conditions

The paramagnetic relaxation agent $Mn^{2+}EDDA^{2-}$, which is water-soluble, was used to determine the residues that are protected, and therefore buried within the detergent/lipid micelles (Lau et al. 2008). MRAP(2-67) in presence of the paramagnetic relaxation agent was examined in DHPC, SDS and in mixed micelles.

For MRAP(2-67) in DHPC, a clear increase in I/I_0 defined the region of protection for residues Ile38 to Ser61. The N-terminal domain was, in general, strongly affected by the presence of the paramagnetic spin label indicating water accessibility. However, the regions spanning residues Ala9 to Tyr17 ($I/I_0 > 0.27$) and Lys29 to Ala33 ($I/I_0 > 0.47$)

exhibited relative increases in protection, suggesting they may have some limited interaction with the micelle. Since residues His34 to Ser37 were not assigned, no information was obtained from this part of the protein.

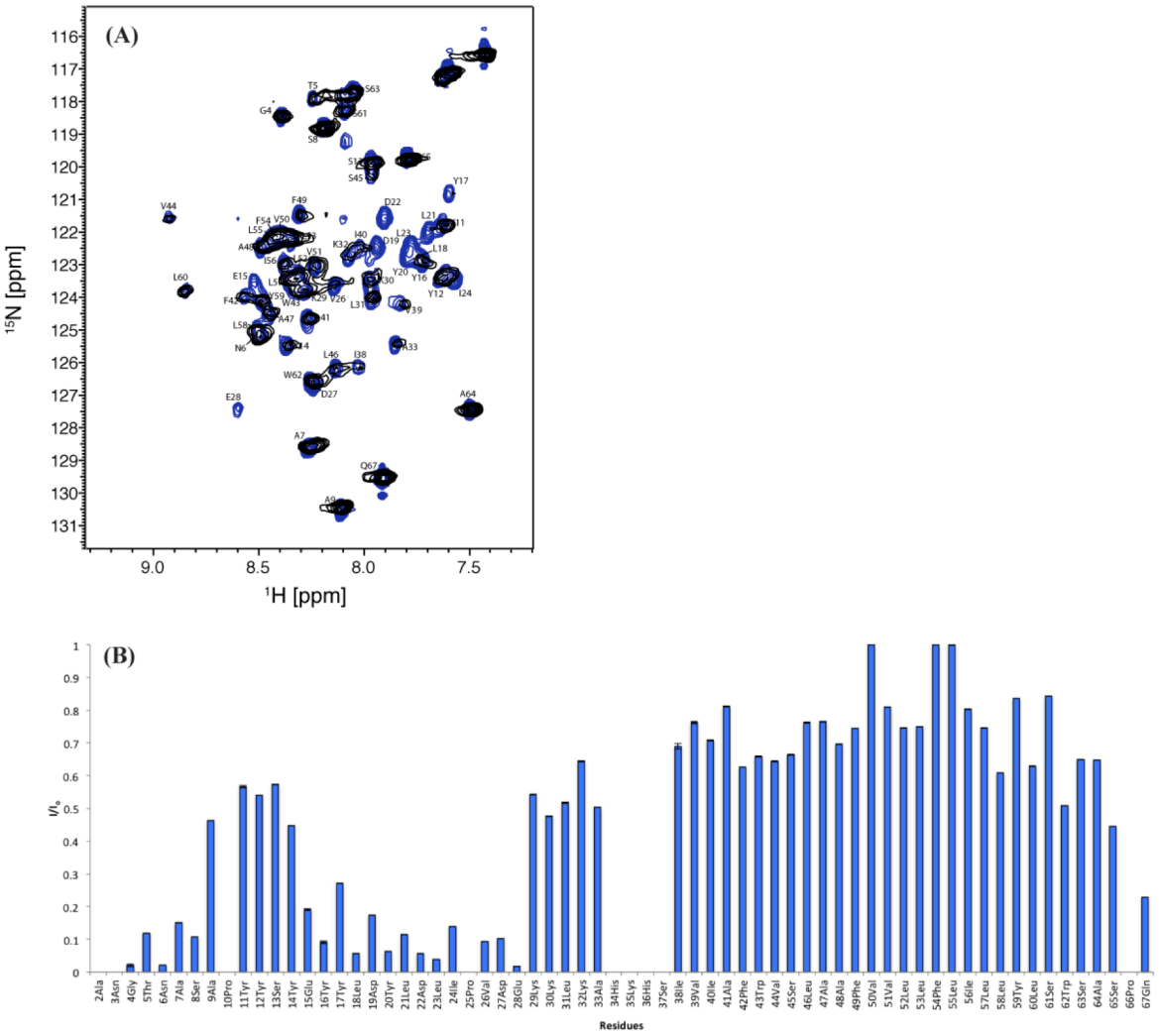

Figure 4.32: Water-soluble paramagnetic broadening enhancement of the backbone ^{1}H-^{15}N groups of MRAP(2-67) in 100 mM DHPC
(A) Signal broadening is due to paramagnetic relaxation enhancement arising from the presence of Mn^{2+} $EDDA^{2-}$. The normalised ratio of ^{1}H-^{15}N HSQC signal intensities in the presence (black) and absence (blue) of 1 mM of Mn^{2+} $EDDA^{2-}$.
(B) Exchange rate of backbone N_H with water. I/Io is used to quantify signal broadening for each residue.

In SDS, the N-terminal domain and the C-terminus were as well heavily broadened by the water-soluble $Mn^{2+}EDDA^{2-}$, whereas the transmembrane domain (residues Ile38 to Leu59) appeared to be deeply buried within the micelle (Figure 4.33). The shorter protected transmembrane region was consistent with the smaller micelle size suggested

by the dynamic data. A τ_c-value of 18.2 ns was recorded for this domain of MRAP(2-67) in SDS, which was 0.2 ns faster than the one obtained in DHPC.

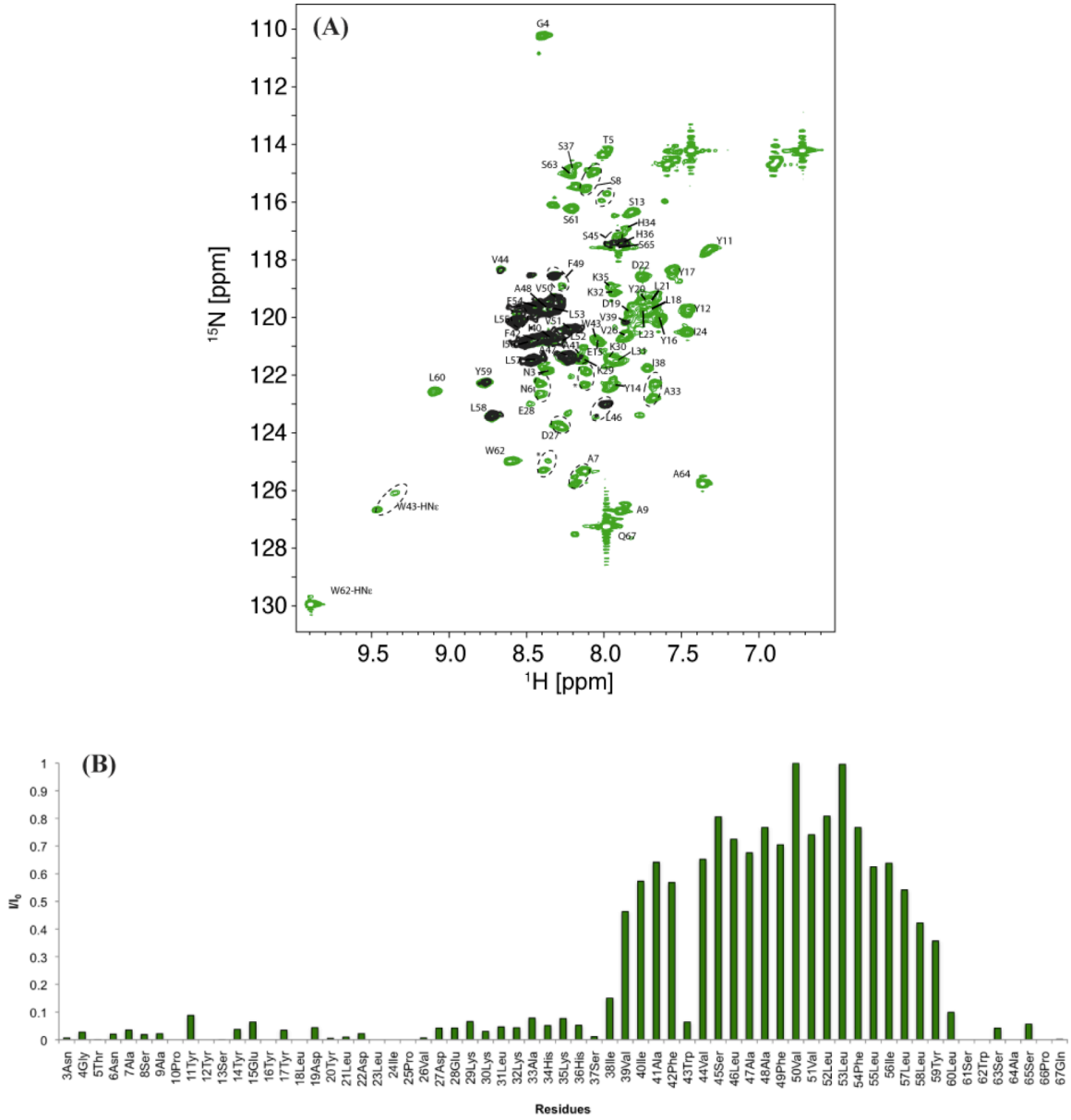

Figure 4.33: Water-soluble paramagnetic broadening enhancement of the backbone ^{1}H-^{15}N groups of MRAP(2-67) in 50 mM SDS
(A) Signal broadening due to the presence of $Mn^{2+}EDDA^{2-}$. The normalised ratio of ^{1}H-^{15}N HSQC signal intensities in the presence (black) and absence (green) of 1 mM Mn^{2+} $EDDA^{2-}$
(B) Exchange rate of backbone N_H with water

In mixed micelles, the steepest rises in I/I_0 values indicated a micelle-buried region in residues Ile38 to Trp62. This result corresponded well with the predicted transmembrane domain from PSI-PRED, TMHMM and (SP)Octopus. As seen in DHPC, residues Gly4 - Glu15 ($I/I_0 > 0.09$) appeared to have some interaction with the micelle, as indicated by the

relatively increased protection. Interestingly, resonances of the N-terminal helical region (Tyr16 to Val24) were broadened (Figure 4.34).

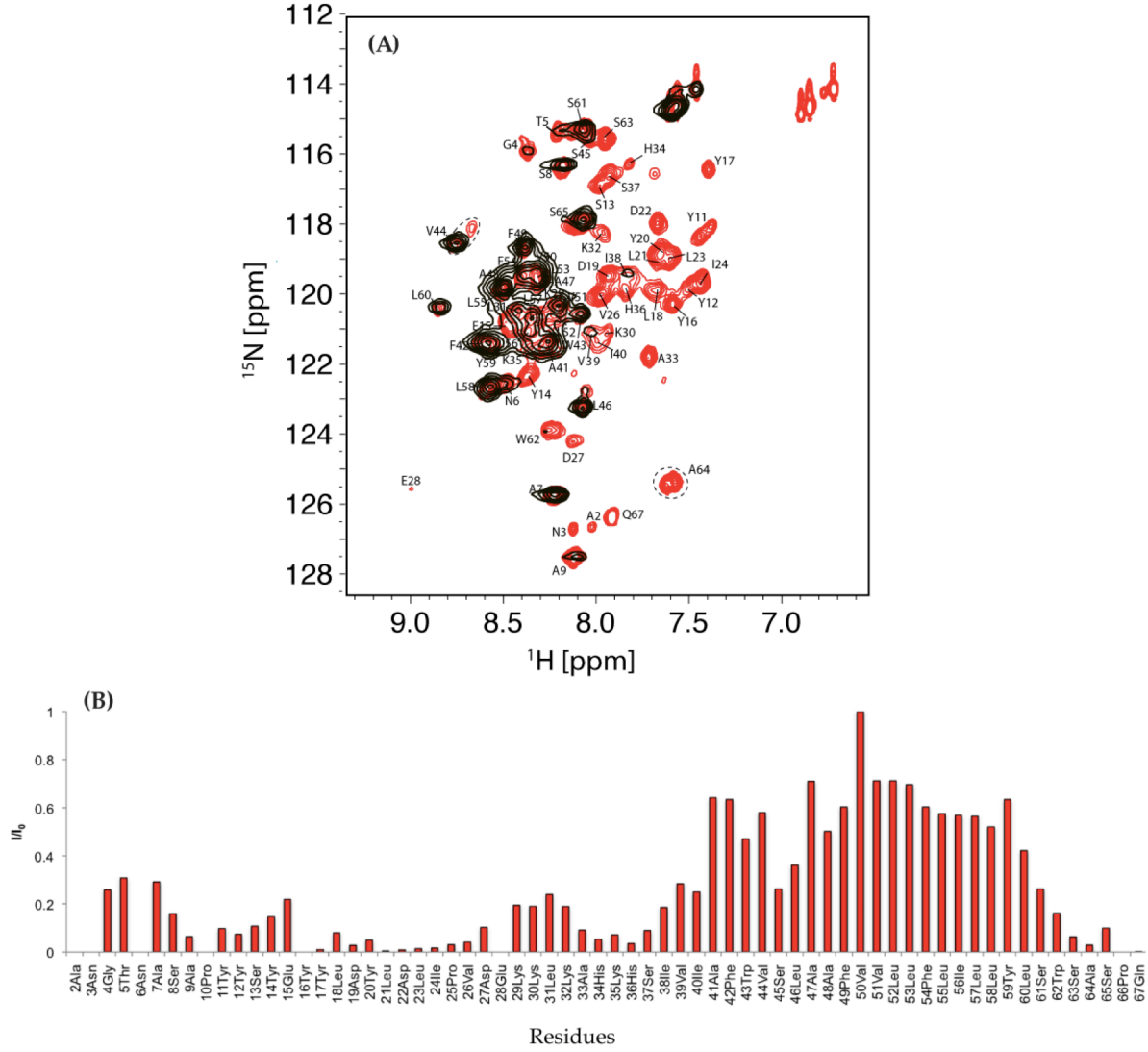

Figure 4.34: Water-soluble paramagnetic broadening enhancement of the backbone ^{1}H-^{15}N groups of MRAP(2-67) in mixed micelles
(A) Signal broadening arising from the presence of $Mn^{2+}EDDA^{2=}$. The normalised ratio of ^{1}H-^{15}N groups signal intensities in the presence (black) and absence (red) of 1 mM $Mn^{2+}EDDA^{2=}$.
(B) Exchange rate of backbone N_H with water.

To summarise, Ile38 was the first residue in the transmembrane domain to be protected regardless of micelle composition. The C-terminal boundary, however, varied slightly between micelles, with Trp62 protected in mixed micelles, but only out to residue Leu59 was protected in SDS micelles.

4.2.6.10 Investigation of the N-terminal helical region's stability

The N-terminal helix (residue Tyr16 to Ile24) is rich in tyrosines, which are known to interact with lipid headgroups, and may be stabilising the helical conformation. To test this hypothesis, residue Tyr17 was mutated to an alanine (Y17A) using QuikChange. The construct was expressed and purified as described for MRAP(2-67). Y17A on SDS-PAGE behaved similar to the wild-type (~15 kDa). A ^{1}H-^{15}N HSQC of Y17A solubilised in mixed micelles indicated that the resonances corresponding to Tyr11, Tyr12, Glu15, Tyr16, Tyr17 and Leu18 were undetectable, suggesting an introduced flexibility within that region. Interestingly, this finding is fairly consistent with residues interacting with the detergent. As described in Subchatper 4.2.6.7, residues Tyr14, Glu15, Tyr16, Tyr17, Leu18, Asp19, Tyr20, Leu21 and Leu23 within this region strongly associate with the lipids in the mixed micelle environment (Figure 4.30). The high percentage of aromatic amino acids, such as tyrosines, allows for exchange and interaction with the detergent. The substitution of this residue removed the interaction and introduced additional flexibility. However, the amino acids composition of this region shows that this region is not amphipathic (Figure 4.35).

When comparing the obtained structures of MRAP in DHPC and in mixed micelles it is obvious that the KH-rich region experiences less motional freedom in mixed micelles, which may result in a possible interaction of the N-terminal domain with mixed micelles. This hypothesis is supported by the investigation of the twenty best-calculated structures in mixed micelles, for which the N-terminal domain is in a parallel orientation to the transmembrane domain. However, this analysis is based on observed interaction

peaks with the detergent, since no membrane potential was included in the structure calculation.

Therefore, the final conclusion is that the flexible KH-rich region acts as "linker", allowing free movement and interaction of the N-terminal helix with its mixed micelle environment.

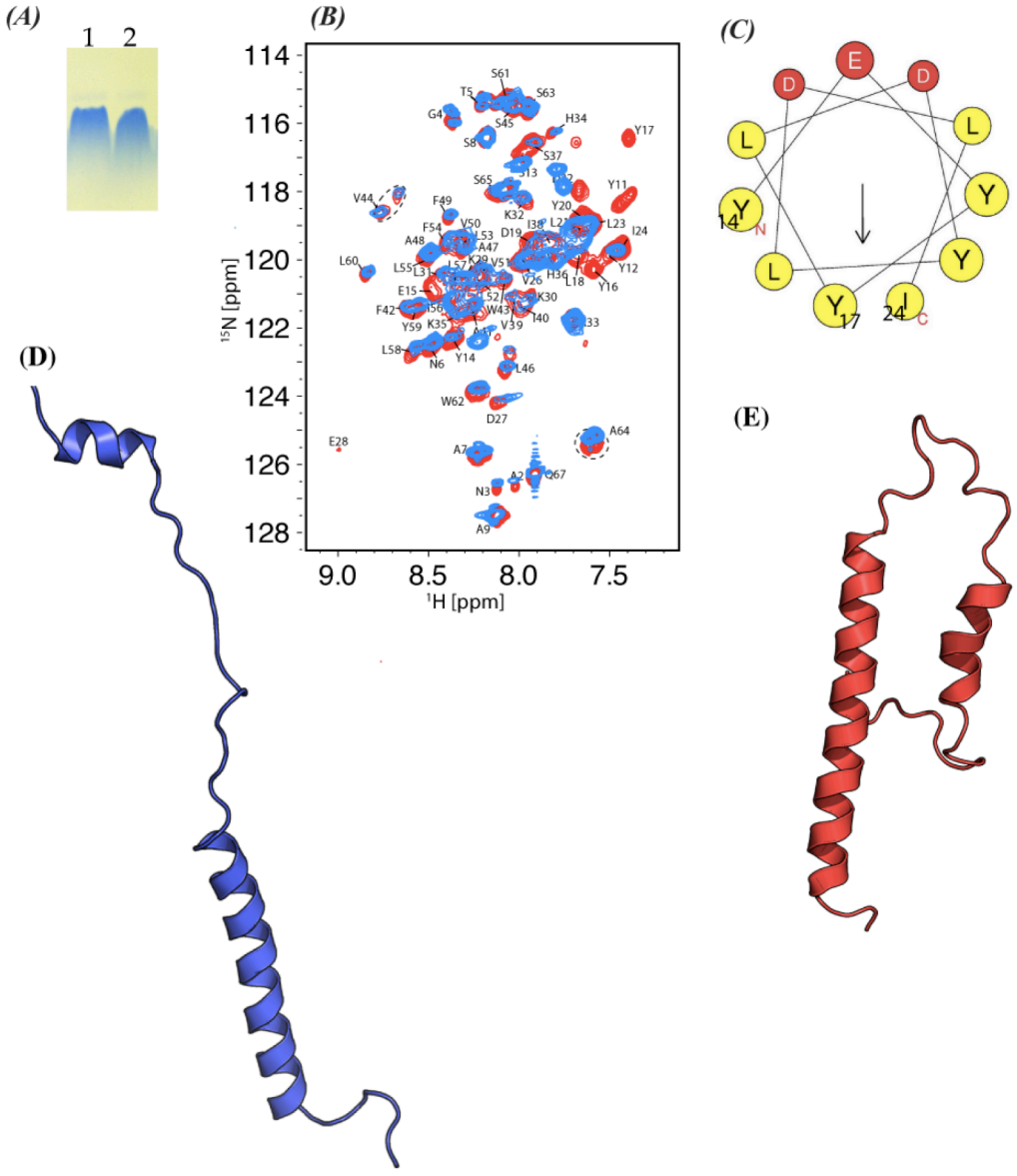

Figure 4.35: Further investigation of the N-terminal domain
(A) MRAP(2-67)Y17A in 50 mM SDS on a SDS-PAGE (1 – WT, 2 – Y17A)
(B) Investigation of the mutant MRAP(2-67)Y17A in mixed micelles by NMR
(C) Amino acids composition of the N-terminal helical structure
(D) DHPC - the structure is extended and did not interact with the detergent
(E) Mixed micelles - the structure was bend and the N-terminal domain interacted strongly with the detergent environment

4.2.7 The structure of MRAP is robust and detergent-independent

I investigated the biochemical and biophysical properties of the MRAP in three different environments (DHPC, SDS micelles and in mixed micelles) to verify whether the obtained structure is robust and not affected by its environment. Like all integral membrane proteins, MRAP is surrounded by a lipid membrane, which is crucial for its biological activity. The protein is anchored by an apolar transmembrane segments and polar flanking regions in the membrane (von Heijne 2006). The clustering of apolar and polar residues on the surface complement the transmembrane profile of partial charge density in their native environment (Nagle et al. 1996). This leads to an exposure of a belt of hydrophobic residues to the apolar bilayer core, and expose hydrophilic apical surfaces to zwitterionic/ionic lipid headgroups and aqueous solution (Sebag & Hinkle 2007; Hinkle & Sebag 2009; Sipos & von Heijne 1993; Higy et al. 2004; Neale et al. 2013). To evaluate the resulting electrostatic interaction, one can use Coulomb's law, which calculates the electrostatic interaction energy of the system consisting of N point charges immersed in the homogenous medium:

$$\Delta G_{el} = \frac{332 kcal/mol}{\varepsilon_r} \sum_{i=1}^{N} \sum_{j=1, i<j}^{N} \frac{q_i q_j}{r_{ij}},$$

where ΔG_{el} represents the electrostatic interaction energy (kcal/mol at room temperature) relative to the energy between charges positioned at infinite separation. q_i and q_j are point charges given in units of electron charge and divided by the distance r_{ij} (Å). ε_r represents the relative dielectric constant of the system and is expressed by the value relative to that of a vacuum (Warshel et al. 2006; Kukić & Nielsen 2010). The

heterogeneous dielectric properties of MRAP are shown in Figure 4.36. Unsurprisingly, MRAP displays a highly negative electrostatic potential for the N-terminal domains, and residues with an electrostatic positive potential flank the electrostatic neutral transmembrane domain.

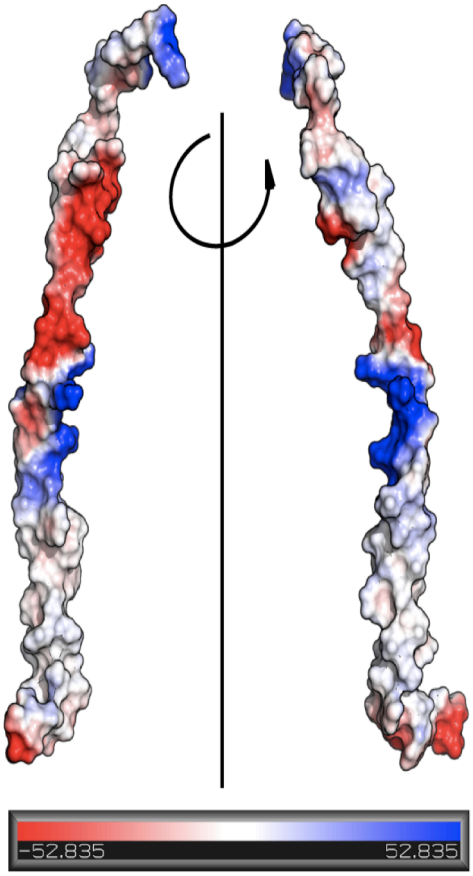

Figure 4.36: Electrostatic potential for MRAP(2-67)
Showing an electrostatic negative potential (red) for one side of the N-terminal, tyrosine rich region, a relatively electrostatic neutral potential for the transmembrane region and an electrostatic positive (blue) KH-rich region as well as C-terminus of MRAP's surface.

Furthermore, the boundaries of MRAP's N- and C-terminal edges of the transmembrane domain are detergent dependent. Investigation of detergent dependent CSP resulted in alteration in the KH-rich region and the C-terminus. Additionally, solvent accessibility studies suggested that the N-terminal residue Val39 is detergent-independent and defines the first structured residue of the transmembrane region, whereas the C-terminus is detergent-dependent and relies on the characteristics given by the local environment.

A possible explanation might be given by the chemical properties of the KH-rich region, which identify the boundary for the transmembrane domain at the N-terminal site. Whereas the C-terminal properties are rather polar uncharged and hydrophobic nonpolar and therefore the boundary there might depend on the micelle size. Local changes as a consequence of the detergent environment at the edges of the

transmembrane domain are expected. However, the overall structure of MRAP appears to be robust because it is consistent between detergent and detergent/lipid environments. Obtained RDC and dynamic results confirm this observation. RDCs in two different detergents and R_1, R_2 and $\{^1H\}$-^{15}N heteronuclear NOE values suggest detergent-independent mobility and chemical exchange, resulting in a detergent-insensitive conformation as well as a similar secondary structure for MRAP(2-67). Thus, it was concluded that the monomeric structure of MRAP(2-67) was a useful starting point for the understanding MRAP dimerisation and receptor interactions. The former will be discussed in the following Chapter 5.

CHAPTER 5

INVESTIGATIONS INTO MRAP DIMERISATION

"Somewhere, something incredible is waiting to be known."

(Carl Sagan)

5.1 INTRODUCTION

The melanocortin-2 receptor accessory protein (MRAP) is necessary for melanocortin-2 receptor (MC2R) maturation, intracellular trafficking and ACTH-dependent signalling (Metherell et al. 2005; Sebag & Hinkle 2007; Webb & Clark 2010; Kay et al. 2013a; Kay et al. 2013b), and likely modulates other melanocortin receptors (Chan et al. 2009; Chan 2009). Besides MRAP's remarkable functional properties, it is suggested to have an unusual structure: This single-pass transmembrane protein is proposed to adopt a dual membrane topology and to form antiparallel homodimers mediated by the transmembrane domain (Sebag & Hinkle 2007; Webb et al. 2008; Cerdá-Reverter et al. 2013).

5.1.1 What governs membrane topology?

The 'charge-difference' rule was first developed to explain the correlation between the net charge difference and the orientation of transmembrane segments, and is a good predictor for the orientation of most N-terminal transmembrane segments (Hartmann et al. 1989). More recently, Gunnar von Heijne developed a 'positive-inside' rule for defining the topology of transmembrane domains. This rule was developed based on the typically observed characteristics of transmembrane helices in which the hydrophobic transmembrane domains are flanked by positively charged amino acids or tryptophans that are located predominantly on the cytoplasmic side of the membrane (Huschilt et al. 1989; von Heijne & Gavel 1988; von Heijne 1986; von Heijne 2006; von Heijne 1992). Dual topology describes the situation in which a membrane protein is able to insert into the membrane in both orientations with an approximately 1:1 stoichiometry. Few proteins are known to adopt this unusual characteristic, presumably due to requirements for

directional membrane activity or to place extramembrane domains in the cellular compartments appropriate for their function. The most prominent examples for dual topology include the prokaryotic proteins camphor-resistance protein (CrcB) (Rapp et al. 2006) and the two small multidrug resistance (SMR) proteins EmrE (Butler et al. 2004; Schuldiner 2009) and SugE (Paulsen et al. 1996). Additionally, the eukaryotic V-type ATPase ductin, a protein with four transmembrane helices is known to adopt dual topology (Finbow & Pitts 1998; Dunlop et al. 1995). All investigated prokaryotic dual topology proteins can have the topology shifted towards either the N_{in}–C_{in} or the N_{out}–C_{out} orientation by introducing or removing a single positively charged residue in the loop regions connecting the transmembrane helices (von Heijne 2006; Seppälä et al. 2010). The most likely evolutionary scenario is that a single dual-topological protein undergoes gene duplication, followed by two resulting proteins becoming fixed in opposite orientations and finally fusing into one single polypeptide (Rapp et al. 2006).

The homodimeric EmrE protein is so far the best-studied membrane protein that can adopt dual topology (Korkhov 2009; Seppälä et al. 2010). EmrE can be engineered into a functional heterodimer composed of two oppositely oriented monomers, EmrE(N_{in}) and EmrE(N_{out}) through suitable positioning of positively charged residues (Rapp et al. 2007; Seppälä et al. 2010). While EmrE functions as a dual topology protein, several classes of transporter proteins have pseudo-twofold symmetry in the plane of the membrane, which might have evolved from gene duplication and divergence of single dual-topology proteins. They then evolve into opposite single-topology proteins that ultimately undergo gene fusion (Rapp et al. 2006). Thus, studying the structural features

of dual topology proteins may aid in understanding the evolution of more complex membrane proteins.

For human MRAP, membrane topology prediction by TMHMM (Sonnhammer et al. 1998) predicts a ~1:1 stoichiometry for C_{in}-N_{out} and N_{in}-C_{out} orientation (Sebag & Hinkle 2007). That MRAP exhibits dual topology has been confirmed experimentally using a variety of methods (Sebag & Hinkle 2007; Webb et al. 2008; Cooray et al. 2008). In addition, the positively charged N-terminal juxtamembrane region (residues Leu31 to Ser37) has been shown to be critical for dictating the final orientation of MRAP. Therefore, it is possible that MRAP membrane insertion follows the 'positive inside' (von Heijne 1986) and 'charge difference' (Hartmann et al. 1989) rules and that the N-terminal juxtamembrane region is responsible for balancing charges in the wild-type protein.

5.1.2 Evidence for dual topology and antiparallel homodimerisation

Sebag *et al*. (Sebag & Hinkle 2007) first described MRAP's antiparallel homodimeric conformation. Since then multiple research groups have published additional evidence, from epitope-tagging, co-immunoprecipitation and BRET/FRET assays, supporting the original finding (Sebag & Hinkle 2007; Webb et al. 2008; Cooray et al. 2008; Sebag & Hinkle 2009; Cooray et al. 2011).

In the original investigation, Sebag *et al.* (Sebag & Hinkle 2007) observed that differentially labelled N- and C-terminal epitope tags were accessible on the extracellular face of CHO cells at comparable levels. Upon insertion into both orientations, MRAP is then proposed to homodimerise in an antiparallel orientation. Antiparallel dimerisation was suspected based on co-immunoprecipitation of MRAP-V5 and MRAP-Flag after

their co-expression (Sebag & Hinkle 2007). To further distinguish between antiparallel dimerisation and the presence of parallel but oppositely oriented dimers, CHO cells were transfected with MRAP-V5 and an additional anti-V5 antibody. This allowed only MRAP-V5 with the V5-epitope facing outward (N_{cyt}/C_{exo}) to immunoprecipitate. Immunoprecipitates of N_{cyt}/C_{exo} MRAP-V5 contained both glycosylated and non-glycosylated MRAP, showing that non-glycosylated N_{cyt}/C_{exo} MRAP was tightly bound to glycosylated N_{cyt}/C_{exo} MRAP (Sebag & Hinkle 2007). In addition, monitoring glycosylation of MRAP variants provided further support for the dual topology: Wild-type mouse MRAP (N-terminal glycosylation) and its variant MRAP-Asn3Gln/Gln96Asn (C-terminal glycosylation) were both glycosylated (Sebag & Hinkle 2007). Since glycosylation happens only in the ER lumen, for a single topology protein only the wild-type or the variant would be glycosylated but not both constructs. These results provided compelling evidence for the presence of both N_{exo}/C_{cyt} and N_{cyt}/C_{exo} orientations of MRAP.

In 2009 Sebag *et al.* (Sebag & Hinkle 2009) confirmed using split-YFP tagged human MRAP that the unique antiparallel homodimeric structure must be achieved in the ER during or soon after MRAP synthesis. Furthermore, they demonstrated that the positively charged region (residues Leu31 to Ser37) proximal to the transmembrane domain is required for the dual topology of MRAP. Additionally, they observed a reduction of MC2R expression and activity when deleting this region.

Subsequently, another lab used bioluminescence resonance energy transfer (BRET) assays as well as co-immunoprecipitation to confirm the antiparallel homodimeric conformation of human MRAP in HEK293 cells (Cooray et al. 2011). They engineered

MRAP constructs with luciferase onto either the N- or C-terminus of MRAP and co-expressed a second construct of MRAP with EYFP at the N-terminus. They showed that all constructs were functional and that only expression of MRAP with C-terminal luciferase in place of the N terminally tagged variant together with N-terminal EYFP-MRAP produced a significant BRET response. RAMP1 was used as a negative control and confirmed the specificity of the MRAP dimer, since no BRET signal was generated between MRAP and RAMP1. They additionally demonstrated that the receptor forms homodimers in the ER and complexes with at least two antiparallel MRAP homodimer molecules. Importantly, Sebag *et al*. (Sebag & Hinkle 2009) also showed with surface epitope immunoprecipitation (YFP) that mouse MRAP forms antiparallel homodimers in the absence of MC2R.

5.1.3 Aim of studying the MRAP antiparallel dimer

Although numerous cell-based assays have confirmed the formation of an antiparallel MRAP dimer, there has been no published characterisation of the structural properties of the MRAP interface. Therefore, we chose to explore the ability of human MRAP(2-67) to form antiparallel dimers *in vitro*. Different approaches were taken to address this question:

- Gel mobility
- Chemical crosslinking in detergent
- Intermolecular disulphide bond formation in membranes
- Intermolecular NOEs
- Concentration dependence and peak doubling in different detergent-mixtures

- Investigation of a transmembrane domain construct
- Mutational studies
- Hydrodynamic properties (including dynamic light scattering and analytical ultracentrifugation)

As described in this chapter, although a wide range of biochemical and biophysical methods were used, no clear evidence of MRAP(2-67) antiparallel dimerisation *in vitro* was found. As a final attempt to understand MRAP dimerisation, a series of molecular dynamics studies were carried out using coarse-grain and atomistic simulations.

5.2 RESULTS

5.2.1 Anomalous gel mobility of MRAP(2-67) in SDS

I have sought to characterise the intrinsic potential for dimerisation of purified MRAP protein *in vitro*. Since the MRAP homodimer extracted from cells was shown to be highly resistant to dissociation by SDS (Cooray et al. 2008), the oligomeric state of MRAP(2-67) was initially characterised using SDS polyacrylamide gel electrophoresis (SDS-PAGE) on 4-12 % Bis-Tris gels. MRAP(2-67) migrated on SDS-PAGE with an apparent molecular weight of ~15 kDa, which would be consistent with a homodimer ($MW_{monomeric}$ = 7.3 kDa) (Figure 5.1). However, the absence of a clear monomer band, and the finding that membrane proteins frequently exhibit anomalous gel mobility (Rath et al. 2009), made interpretation of the oligomeric state of MRAP(2-67) on SDS-PAGE ambiguous.

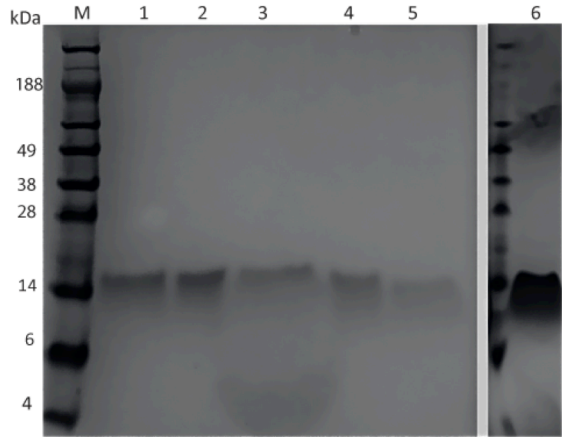

Figure 5.1: MRAP(2-67) anomalous gel mobility on SDS-PAGE
1 - MRAP (2-67) in 100 mM SDS
2 - MRAP (2-67) in 100 mM LPPG
3 - MRAP (2-67) in 100 mM DH(6)PC
4 - MRAP (2-67) in 100 mM Fos-Choline-14
5 - MRAP (2-67) in 100 mM Fos-Choline-12 (DPC)
6 - MRAP (2-67) in 100 mM Fos-Choline 10 + 20 mM DMPC + 5 mM DMPG

Although the direct effects on gel mobility can be difficult to establish (Rath & Deber 2013), strong interactions of the positively charged KH-rich region of MRAP with the anionic SDS, in addition to the hydrophobic transmembrane domain, may have altered the gel mobility (Otzen 2002; Wang et al. 1996; Yonath et al. 1978). As shown in Figure 5.1 the anomalous gel mobility was largely independent of the sample detergent.

5.2.2 Chemical crosslinking of MRAP(2-67)

Chemical crosslinking is an established method for examining protein-protein interactions (Kluger & Alagic 2004). This technique was applied to probe for MRAP(2-67) oligomerisation. The underlying mechanism of chemical crosslinking involves the formation of covalent bonds between two or more molecules by bifunctional reagents. The specific and reversible crosslinking reagent N-hydroxysuccinimide ester dithiobis[succinimdyl propionate] (DSP) was used (Migneault et al. 2004). Crosslinking of MRAP(2-67) was tried first. Rather surprisingly, crosslinked MRAP(2-67) experienced an increase in gel mobility by SDS-PAGE, and hence ran closer to the expected molecular weight of a monomer. Since DSP reacts with the primary amines of lysines, this result was consistent with the hypothesis that the KH-rich region binds an unusually large amount of SDS per residue since lysine derivatisation is likely to alter their SDS binding properties. However, it remained possible that derivatisation of the lysines also disrupts an antiparallel dimer that is not crosslinked due to the lack of DSP-reactive groups at the C-terminus of MRAP(2-67). To test this hypothesis, two lysines were introduced at positions Pro66 and Gln67 (P66K/Q67K) C-terminal to the transmembrane domain via site-directed mutagenesis. ^{1}H-^{15}N HSQC indicated only small chemical shift changes upon introduction of the two lysines. Hence it was concluded that these substitutions caused only small, local changes in structure (Figure 5.2). The construct P66K/Q67P was crosslinked in mixed micelles (Figure 5.2), in SDS and Fos-Choline-14 (Figure 5.2). DSP at a concentration of 2 mM and an incubation time of 10 minutes was used to gain more insights into MRAP(2-67)'s properties. In all tested conditions P66K/Q67K ran higher than expected and gave multiple high molecular bands, indicating multimeric states of

the protein or aggregation. Although the presence of oligomers suggested some intermolecular interactions, the lack of a distinctly enriched dimer band suggested that the crosslinked species was not specific. Therefore no conclusive evidence for specific dimerisation of MRAP was revealed.

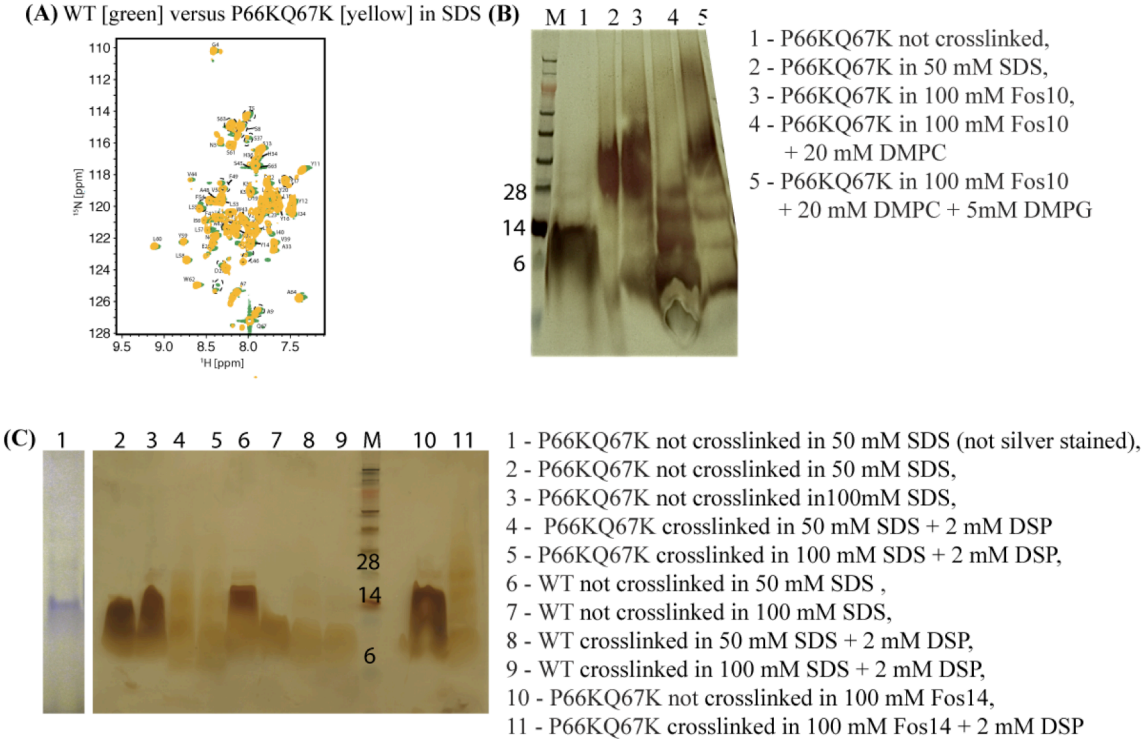

Figure 5.2: Crosslinking of MRAP(2-67)P66KQ67K
(A) Verification of the construct via NMR studies
(B) Crosslinking of MRAP in mixed micelles
(C) Crosslinking of MRAP in SDS and DPC

5.2.3 Biochemical analysis of the dimeric interface of MRAP(2-67) via disulphide bonds in membranes

To investigate whether MRAP(2-67) dimerises in lipid bilayers an analytical assay based on disulphide bond formation was adapted from that of Suk *et al*. (Suk et al. 2012). A detailed protocol outline can be found in Chapter 3 (Methods and Materials). Yeast Polar Lipids (YPL) and Brain Total Lipids (BTL) were used to mimic the membrane. Introduction of a single cysteine residue within the protein of interest was necessary to

allow specific formation of disulphide bridges. Thus, several single cysteine MRAP(2-67) variants (residues His36, Ser37, Ser61, Ser63, Ser65) were tested. The main criteria for choosing the substitution sites were proximity to the transmembrane domain and relative lack of structure, which may facilitate crosslinking. The substitutions H36C and S65C (Figure 5.3) were chosen based on minimal chemical shift perturbations in ^{1}H-^{15}N HSQCs (shown in Appendix). Next, MRAP(2-67) and DTT or TCEP solubility in different organic solvents were tested (Figure 5.3). MRAP(2-67) was not soluble in chloroform, and ran with multiple bands and as smears (Figure 5.3 B) after being solubilised separately in 1,1,1,3,3,3-hexafluoro-2-propanol (HFIP) or showed the wrong molecular weight in methanol. By contrast, 2,2,2-trifluoroethanol (TFE) showed no artefacts on SDS-PAGE and hence was chosen for further studies of MRAP(2-67) in membranes. The choice of reducing reagent did not impact behaviour nor gel mobility of MRAP(2-67) (Figure 5.3).

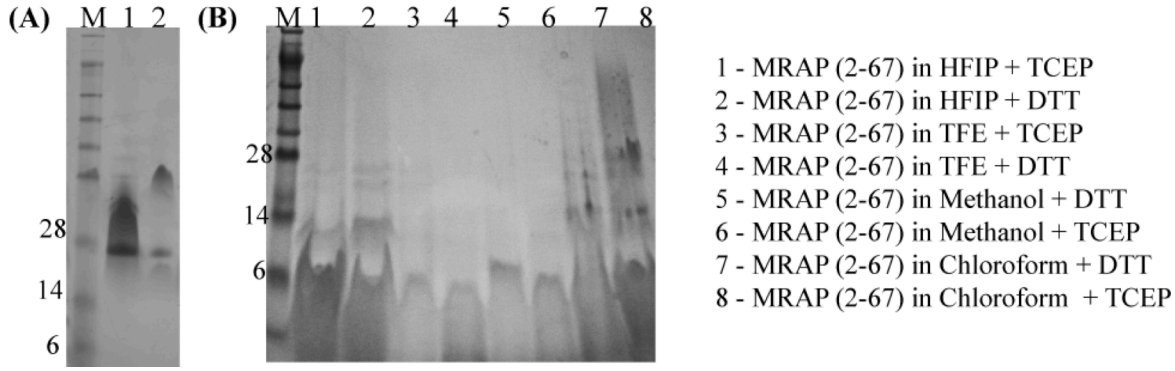

Figure 5.3: Monomerising of MRAP(2-67) and solubility in solvents
(A) H36C: 1- reduced H36C with DTT; 2 - oxidised H36C
(B) MRAP(2-67)'s solubility in different solvents with DTT and TCEP

To prevent oxidation of the cysteines in H36C and S65C β-mercaptoethanol was added to all solutions during purification. SDS-PAGE with additional DTT was used to distinguish between reduced and oxidised states of the proteins (Figure 5.4). For testing for antiparallel dimerisation, H36C and S65C were mixed in 1:1 ratios after HPLC

purification. Thin films were formed out of lipids in TFE:chloroform (50:50) with DTT. The peptide of interest solubilised in TFE was then added to the thin films, and protein and lipid thin films were reformed using a low-pressure stream of nitrogen gas. Each sample was rehydrated in 50 mM sodium phosphate buffer (pH 6.5) and the hydrophobic oxidant Cu^{2+}·[phenanthroline]$_2$ (final concentration 0.25 mM) was added to catalyse disulphide formation. The reaction was allowed to proceed for one hour before running on a 4 - 12 % Bis-Tris SDS-PAGE and the band intensities were quantified using ImageJ (Rasband 2012; Abràmoff et al. 2004). Samples containing only H36C or S65C in lipids were used as negative controls, confirming that they were monomeric (Figure 5.4 lanes 1d-3f). The results indicated that H36C in presence of the oxidant did not form parallel dimers, but rather remained monomeric. In contrast, S65C formed a subpopulation of disulphide-linked dimers, indicative of at least some parallel dimerisation. The H36C/S65C mixed sample showed both monomeric and dimeric bands. All mutants behaved similarly in the different lipid mixtures.

Band intensity quantification with ImageJ (Rasband 2012) revealed further information on the ratio of monomeric and dimeric species in YPE and BTL. In both lipid mixtures the intensity ratio between the 'monomeric' bands (at ~12 kDa) of the combined sample H36C/S65C (Figure 5.4(A/B) lane 3c) and H36C (Figure 5.4(A/B) lane 1a) was estimated to be ~0.75. The intensity difference between the monomeric band of H36C/S65C (Figure 5.4(A/B) lane 3c) and S65C (Figure 5.4(A/B) lane 2b) was ~0.22. These results suggested that the ~12 kDa monomeric band in the H36C/S65C consisted to of ~75 % of monomeric H36C and ~25 % of S65C. Interestingly, intensity ratios for the dimeric band of

H36C/S65C suggested a solely 100% component of S65C. The negative control without crosslinking reagent (Figure 5.4(A/B) lanes 1d, 2e, 3f) displayed only monomeric MRAP.

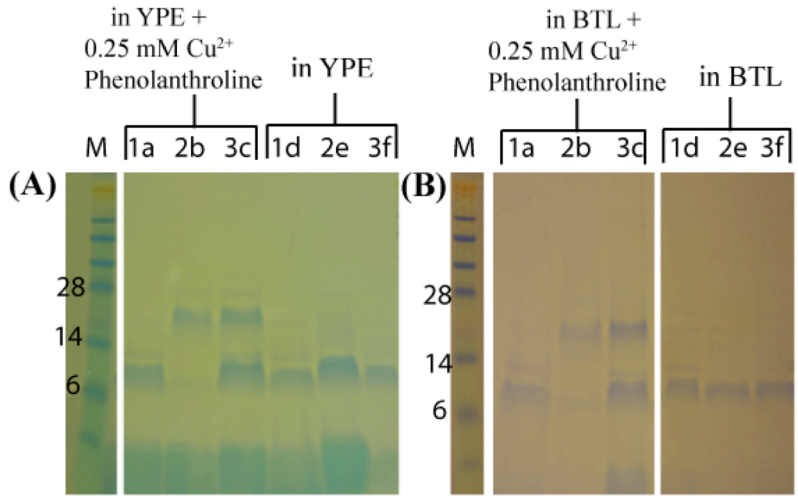

Figure 5.4: Membrane assay of MRAP(2-67) in
(A) Yeast Polar Lipids (YPE)
(B) Brain Total Lipids (BTL)
Samples: 1 - MRAP(2-67)-H36C, 2 - MRAP(2-67)-S65C, 3 - MRAP(2-67)-H36C + MRAP(2-67)-S65C

These findings were similar in YPL and BTL and showed that a mixture of H36C and S65C did not significantly enhance disulphide bond formation, suggesting that an antiparallel dimer was not formed in lipid membranes. However, an increase in disulphide formation for the S65C variant indicated that parallel dimerisation might be occurring.

5.2.4 Attempts to acquire intermolecular NOEs for a dimeric MRAP(2-67)

Since oligomerisation was observed in crosslinking studies of the P66K/Q67K construct, and disulphide formation of the S65C construct suggested the possibility at the least of parallel dimerisation, attempts were made to observe intermolecular contacts by NMR. Although no intermolecular NOEs were apparent in the previously acquired 3D NOESYs, spectral crowding from intramolecular NOEs can prevent their detection.

Thus, unlabelled (fully protonated) MRAP(2-67) peptide was mixed in equal parts with $^{2}H^{15}N$-labelled one and solubilised into SDS micelles. A 3D ^{1}H-^{15}N-NOESY-HSQC was recorded at 750 MHz (^{1}H frequency) with a mixing time of 170 ms. Although NOEs from the detergent were observed, no clear intermolecular NOEs between MRAP(2-67) monomers were detected.

5.2.5 Concentration dependence and peak doubling of MRAP(2-67) in different detergent-mixtures

Since protein-protein interactions are concentration dependent, the impact of the peptide to detergent ratio on the spectra of MRAP(2-67) was investigated. During the detergent screening process, it was observed that apparent peak doubling occasionally occurred, which can arise from oligomerisation. To gain insights into the source of the peak doubling and to establish whether the doubling was a consequence of oligomerisation, sample variation, or due to conformational changes, spectra of MRAP(2-67) in 100 mM DHPC, 50 mM SDS or mixed micelles (100 mM Fos-Choline10 + 20 mM DMPC + 5 mM DMPG) were collected while varying either protein or surfactant concentration.

Firstly, the impact of DHPC on MRAP(2-67) was investigated. Due to a high cmc (~15 mM), DHPC can be efficiently removed while maintaining the peptide concentration by dialysis across a membrane with a suitable molecular weight cut-off (MWCO). The zwitterionic detergent DHPC was added to the peptide with a starting concentration of 110 mM and diluted by dialysis against 50 mM sodium phosphate buffer (pH 6.5) using a 3.5 kDa MWCO filter. NMR spectra were recorded after dialysing the sample for two, three and ten hours. The exact protein and micelle concentrations were not able to get determined. No significant change in the spectral properties of MRAP(2-67) were

observed, suggesting that DHPC concentration did not affect MRAP(2-67)'s conformation and that the construct was stable at even very low detergent concentration (Figure 5.5). Additionally, different MRAP(2-67) concentrations (200 μM, 400 μM and 600 μM) were tested at a fixed DHPC concentration of 100 mM. Neither shift perturbations nor resonance doublings were detected.

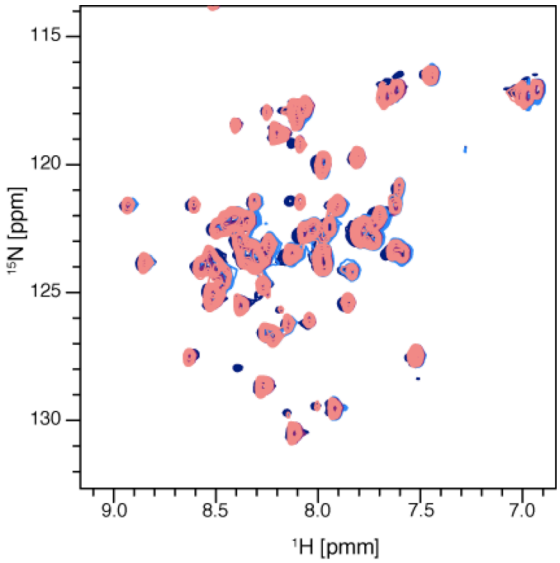

Figure 5.5: Concentration dependence of MRAP (2-67) in DHPC
Colouring: dark-blue - 110 mM DHPC; light blue - 2h dialysis; red - 3h dialysis, pink - 10h dialysis

This examination was followed by investigation of MRAP(2-67) in 50 mM SDS and mixed micelles, in which some of the largest sample variation in peak doubling of MRAP(2-67) had been observed previously during the structural studies. To test whether the peak doubling was dependent on peptide concentration, the measured crosspeak intensities were normalised to the peak intensity of Leu55, a resonance that was not affected by peak doubling. Figure 5.6 (A) illustrates that a concentration increase of SDS detergent had no obvious effect on MRAP(2-67)'s peak doubling. Increasing the peptide concentration to 600 μM (Figure 5.6 (B, D)) however, showed an intensification of peak resonances contingent on concentration. Peak doubling occurred already at lower peptide concentration (200 μM peptide) and became more visible according to a

concentration increase. This phenomenon was mainly observed at the very N-terminal residues Ala7, Ser8 and Ala9 as well as at residues Asp27 and Ser37 in the KH-rich region. However, no clear patterns of intensity increase for the second peaks when compared with the main peaks were observed. All doublets of resonances increase at approximately the same level. This observation excludes the possibility of dimerisation dependent peak doubling. Thus, peak doubling seemed to occur as a consequence of either an internal flexibility or the interaction with the surrounding detergent. One possible explanation for N-terminal resonance doubling might be a local change in environment and additional SDS binding to MRAP(2-67). Interestingly, resonance doubling also occurred within the transmembrane domain at residues TrpHe43, Leu46 and Phe49. Peak doubling in this region may be attributable to multiple conformations of the aromatic rings of Trp43 and Phe49. Figure 5.6(C) illustrates the consequences of a ring flip and how a flip of the tryptophan benzene ring can affect its local environment leading to peak doubling. Aromatic benzene rings are known to have the ability to adapt several conformations, usually with unequal populations (Preininger et al. 2013). The increases in protein concentration and resulting magnification in the signal to noise ratio perhaps allowed observation of minor aromatic ring conformations, and their impact on surrounding amino acids. Because of the lack of change in the intensity ratios for the main and doubled peaks, oligomerisation could be ruled out as the cause of peak doubling. Similar, but stronger results were obtained in mixed micelles (Figure 5.7(A)). Each peak doublet increased to similar amounts according to an increase in concentration.

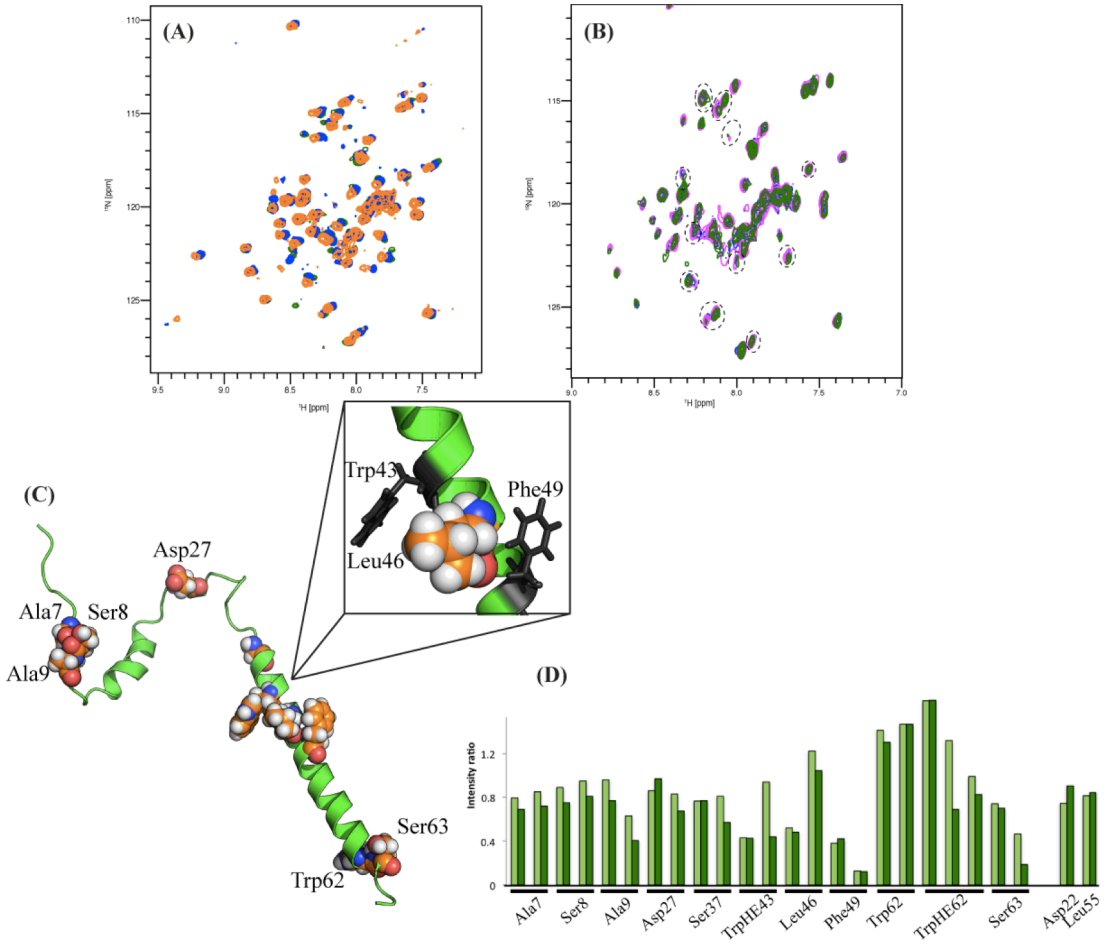

Figure 5.6: Concentration dependence of MRAP (2-67) in 50 mM SDS
(A) SDS-concentration dependency of MRAP(2-67)
Colouring: green - 50 mM SDS, blue - 100 mM SDS, orange - 500 mM SDS
(B) Peptide concentration-dependency of MRAP(2-67) in presence of 50 mM SDS
Colouring: green - 200 M MRAP (2-67), blue - 400 µM MRAP(2-67), pink - 600 µM MRAP(2-67)
(C) Schematic figure of residues that experience peak doubling, highlighting a possible ring-flip in the transmembrane domain
(D) Comparison of peptide concentration: difference in intensity between 200 µM and 400 µM of MRAP(2-67) [light green] in comparison to 200uM and 600 µM of MRAP(2-67) [dark green]

No significant change in the peak ratios however, which might result from dimerisation, was observed. As in SDS, local environment and interactions with the negatively charged headgroup of the detergent DMPG may have affected the very N-terminal residues. This interaction may also account for the observed peak doubling of residues Tyr11 and Glu28. In addition, Glu28 is in close proximity to Pro25, and thus proline peptide bond isomerisation is another possible cause for the peak doubling (Figure 5.7(B)). Resonances from Trp43 (sidechain indole) and Leu46 were also influenced by

resonance doubling - similar to that observed in SDS. In addition, amino acid Val44 showed peak doubling. Closely located aromatic side chains, such as from Trp43, could result in an observable and direct effect of Val44, Leu46 and the TrpHe43.

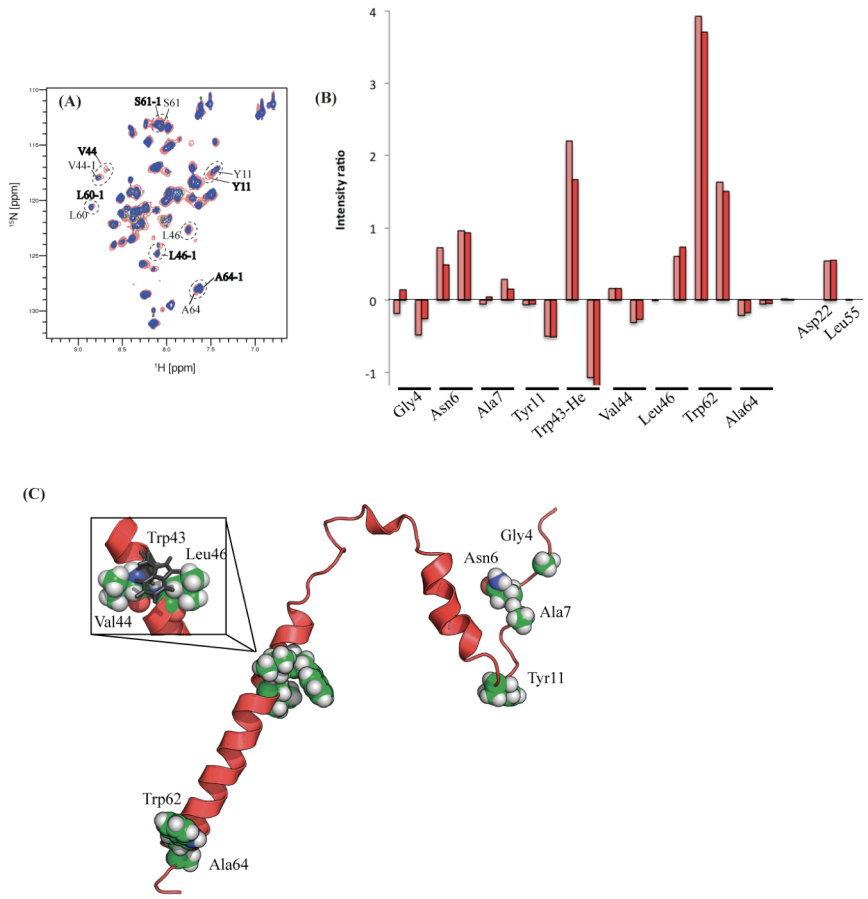

Figure 5.7: Concentration dependence of MRAP(2-67) in mixed micelles
(A) Peptide concentration-dependency of MRAP(2-67) in mixed micelles.
Colouring: blue - 200 µM MRAP (2-67), green - 400 µM MRAP (2-67), pink - 600 µM MRAP(2-67)
(B) Comparison of peptide concentration: difference in intensity between 200 µM and 400 µM of MRAP(2-67) [light red] in comparison to 200 µM and 600 µM of MRAP (2-67) [dark red]
(C) Schematic figure of residues that experience peak doubling, highlighting a possible ring-flip in the transmembrane domain

Summarising, all residues that showed resonance doublets across the entire construct in two of the detergent environments did not show a trend as a function of the peptide to detergent ratio, and other factors could be identified, which may lead to peak doubling. Therefore, the observed finding did not suggest dimerisation of MRAP(2-67).

5.2.6 Investigation of the transmembrane domain of MRAP

Sebag *et al*. (Sebag & Hinkle 2009) showed that residues Leu31 to Ser37 are involved in dual topology and hence dimerisation of MRAP(2-67). They demonstrated by using YFP fusion tags that by deletion of this region, MRAP adopts a single orientation. Additionally, it was shown using RAMP1 that dimerisation occurs more efficiently in vitro without the extended transmembrane domain (Chapter 6). Therefore, the construct MRAPtm(28-67), including residues Glu28 to Gln67, was investigated to determine whether a shorter construct containing only the KH-rich region and the transmembrane domain could permit dimerisation.

MRAPtm(28-67) was expressed and purified according to MRAP(2-67) as a fusion to the trpLE protein. Fortunately, MRAPtm(28-67) was expressed at high levels within inclusion bodies, suggesting that the expression and purification protocol for the wild-type could be applied to the shorter construct. However, it was not possible to properly separate the fusion from the pure protein by HPLC due to a more similar overall hydrophobicity of the two proteins (Figure 5.8 (A)). Nevertheless, the remaining fusion protein was insoluble in 100 mM DHPC and mixed micelles, and therefore, did not affect the final NMR sample purity. MRAPtm(28-67)'s properties were examined in 100 mM DHPC and in mixed micelles. Interestingly, MRAPtm(28-67), with a molecular weight of only 4.1 kDa migrated at an apparent molecular weight of ~12 kDa on SDS-PAGE. The increase of four times in molecular weight was unexpected, but was of a similar apparent molecular weight to that observed with MRAP(2-67) and may be a consequence of SDS binding to the KH-rich region. As discussed above for MRAP(2-67), these residues are likely to have a strong impact on the local environment and favour a

tight interaction with SDS molecules (Alvares et al. 2013). To establish the "real" size of the transmembrane domain construct, cross-linking experiments were performed. Despite testing several concentrations of DSP and different incubation times, only a ladder of bands was observed on an SDS-PAGE (Figure 5.8 (A)). Thus, while there was a greater propensity for MRAP(28-67) than MRAP(2-67) to self-associate, the results suggested that the interactions are not specific. 2D ^{1}H-^{15}N SOFAST-HMQC (Schanda et al. 2005) experiments in both detergents and 3D ^{1}H-^{15}N-HSQC-NOESY (110 ms and 200 ms mixing time) (Kumar et al. 1981) in mixed micelles were performed to compare MRAPtm(28-67) to the wild-type MRAP(2-67). An increase of protein concentration had no effect on peak doubling or chemical shift perturbations (CSP). CSP were observed only at the N-terminus near the site of truncation. Residues Glu28 to Val39, were either not visible in the studied environments or experienced large shift changes (Figure 5.8 (D)). These changes were likely due to local interaction with detergent and the high flexibility of this region. The transmembrane domain itself experienced no significant changes in either detergent condition.

To summarise, no significant changes in the spectral properties were observed upon removing a large fraction of the N-terminal domain (residues Ala2 to Asp27). Interestingly, however, the transmembrane domain did not exhibit peak doubling in mixed micelles, suggesting that the N-terminal domain was able to modulate the conformational heterogeneity.

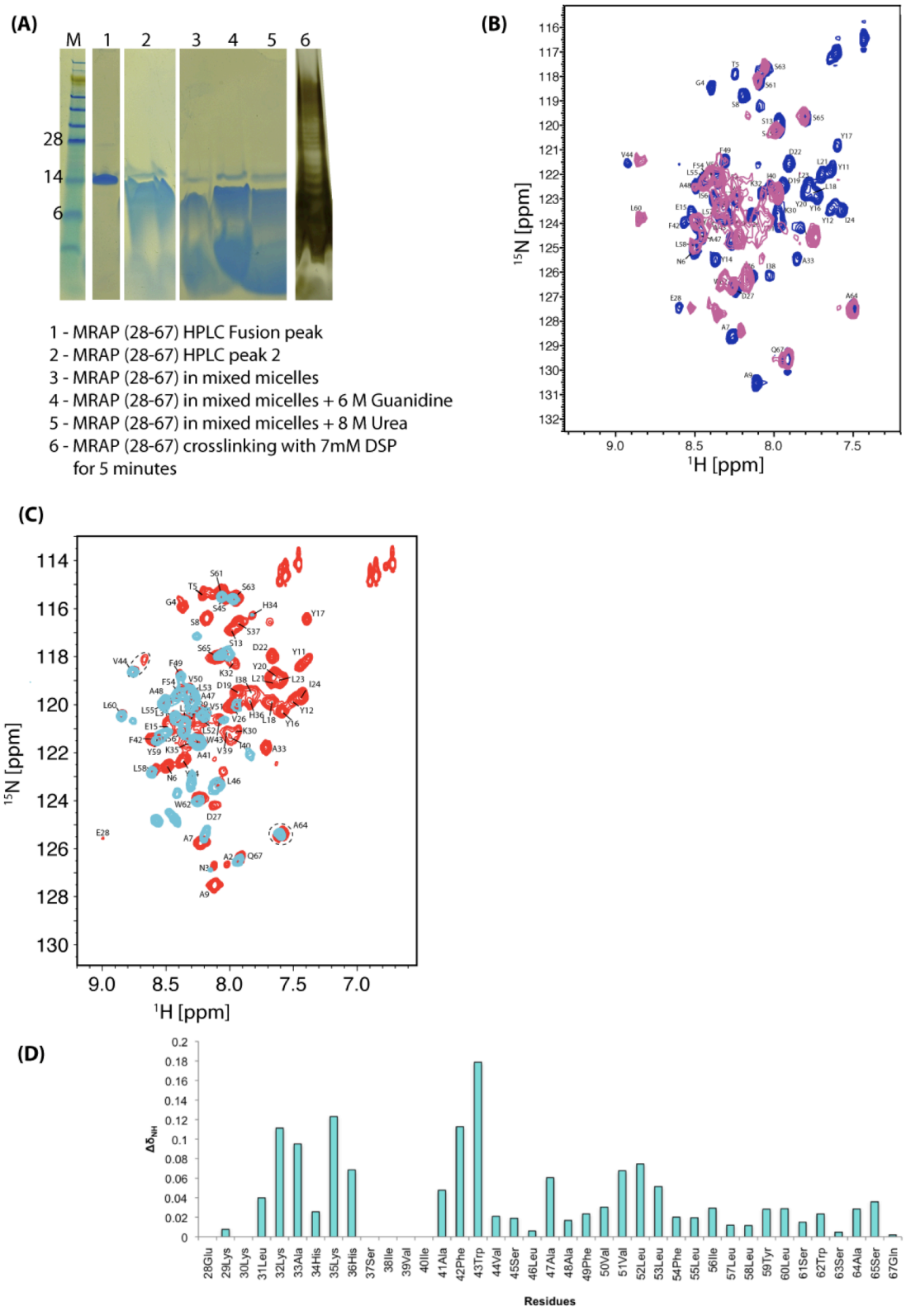

Figure 5.8: The transmembrane domain of MRAP(2-67) at 600 MHz
(A) MRAP (28-67) after HPLC, in mixed micelles and crosslinked
(B) MRAP (2-67) [blue] versus MRAP (28-67) [pink] in 100 mM DHPC
(C) MRAP (2-67) [red] versus MRAP (28-67) [cyan] in mixed micelles
(D) Chemical shift perturbation difference between MRAP (2-67) and solely its transmembrane domain

5.2.7 Investigation of the roles of post-translational modifications in MRAP(2-67)

Post-translational modifications increase a protein's functional diversity by covalent addition of functional groups. Possible modifications include phosphorylation, glycosylation, ubiqutination, nitrosylation, methylation, acetylation, lipidation and many more. These alterations are crucial for many aspects of cell biology and are involved in many common mechanisms of control and regulation of a protein's behaviour. So far, MRAP was described to have one N-linked glycosylation site (Asn-X-Ser/Thr) at position Asn3, although mutation of the site did not appear to have a functional consequence (Hinkle & Sebag 2009). To investigate further post-translational modifications and their influence dimerisation, the two on-line bioinformatic severs http://www.cbs.dtu.dk/services/ and http://www.expasy.org/proteomics/post-translational_modification were used extensively. Only phosphorylation at Ser61 was strongly predicted by the prediction site NetPhos2.0 (Blom et al. 2004), scoring a likelihood of 94% to be phosphorylated. In eukaryotes, phosphorylation mainly occurs at serines, threonines and tyrosines (Manning et al. 2002) and introduces a negative charge to the amino acid side chains. Due to the high physical similarity to phosphoserines, aspartate or glutamate substitutions are commonly used to mimic phosphorylation (Figure 5.9(B)), and can have similar functional consequences: a prominent example was observed in the GRK7 protein kinase (Pearlman et al. 2011). On account of the high likelihood of phosphorylation and the possibility that in a symmetric MRAP(2-67) dimer S61D would be located opposite the positively charged KH-rich region and therefore favour dimerisation, Ser61 was mutated to an aspartate (S61D).

NMR studies of MRAP(2-67)-S61D in mixed micelles and 100 mM DHPC by solution-state NMR indicated only local chemical shift changes (Figure 5.9(C)). Although resonances for residues Leu58, Leu60, Trp62 and Ser63 moved, there appeared to be no other impacts on other parts of the protein. Therefore, it was surmised that a possible phosphorylation is not relevant for the proposed dimerisation of MRAP, at least *in vitro*.

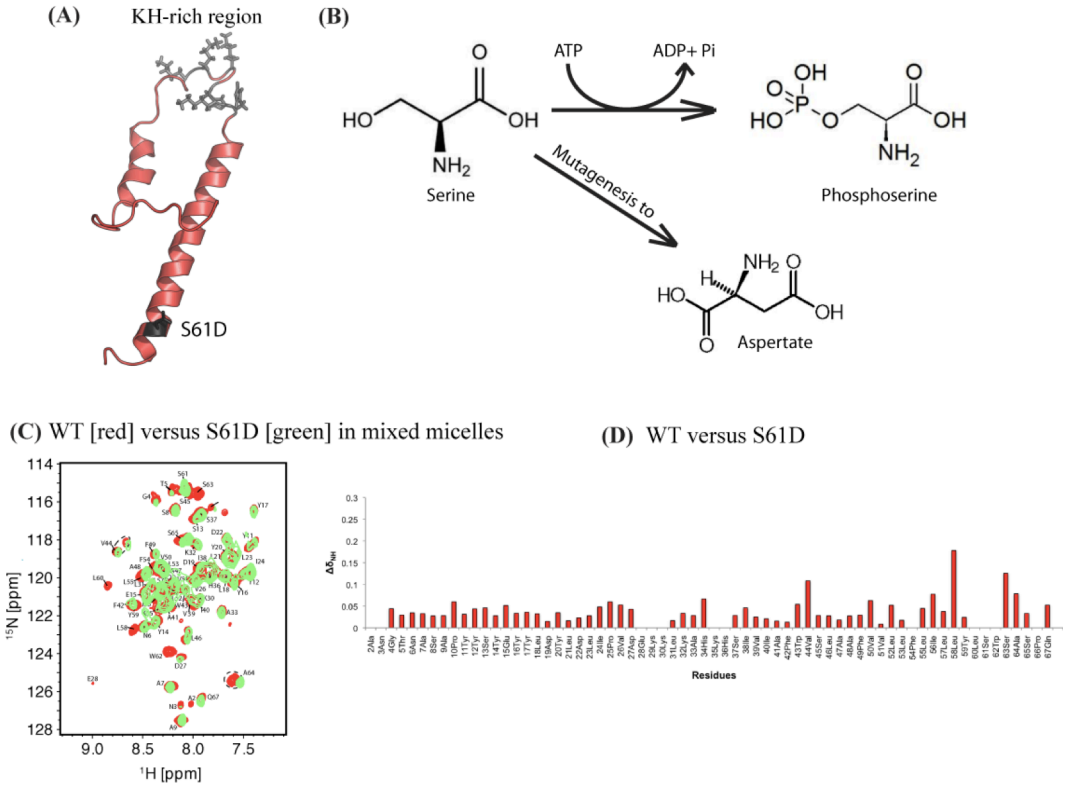

Figure 5.9: Mimicking of phosphorylation of MRAP (2-67)
(A) Position of S61D shown on MRAP (2-67) structure
(B) Chemical reaction of phosphorylation and similarity of phosphoserine and aspartate
(C) ^{1}H-^{15}N HSQC spectrum of S61D
(D) Chemical shift perturbation of S61D versus WT

5.2.8 Biophysical investigation of MRAP(2-67)

5.2.8.1 Diffusion of MRAP in detergent micelles and mixed lipid/detergent micelles

Dynamic light scattering (DLS) was performed to establish the hydrodynamic radii and the impact of detergent on the apparent size of the protein in SDS and in mixed micelles. All measurements were executed at 293.15 K. In 50 mM SDS and sodium phosphate buffer (pH 6.5) an approximate radius of 17 Å was determined. Addition of 250 μM MRAP(2-67) increased the hydrodynamic radius by ~3 Å, which is roughly equivalent to a diameter of one helix – the transmembrane domain. In mixed micelles multiple spectra were acquired after incorporation of each component and a final addition of the 250 μM peptide (Figure 5.10). The result showed that the size of the hydrodynamic radius was gradually enlarged according to incorporation of detergent and lipids to form the mixed micelles. The final hydrodynamic radius size of mixed micelles was 5 Å larger than the radius achieved in SDS.

That difference in size may be attributable to the different sensitivities to particle shape, since DLS calculates an average radius, but does not account for different shapes of detergent spheres. More importantly, the approximate radius of one helix of MRAP(2-67) was 3 Å. This led to the conclusion that the obtained experiments were consistent with a monomeric insertion of MRAP(2-67) into SDS micelles and into mixed micelles.

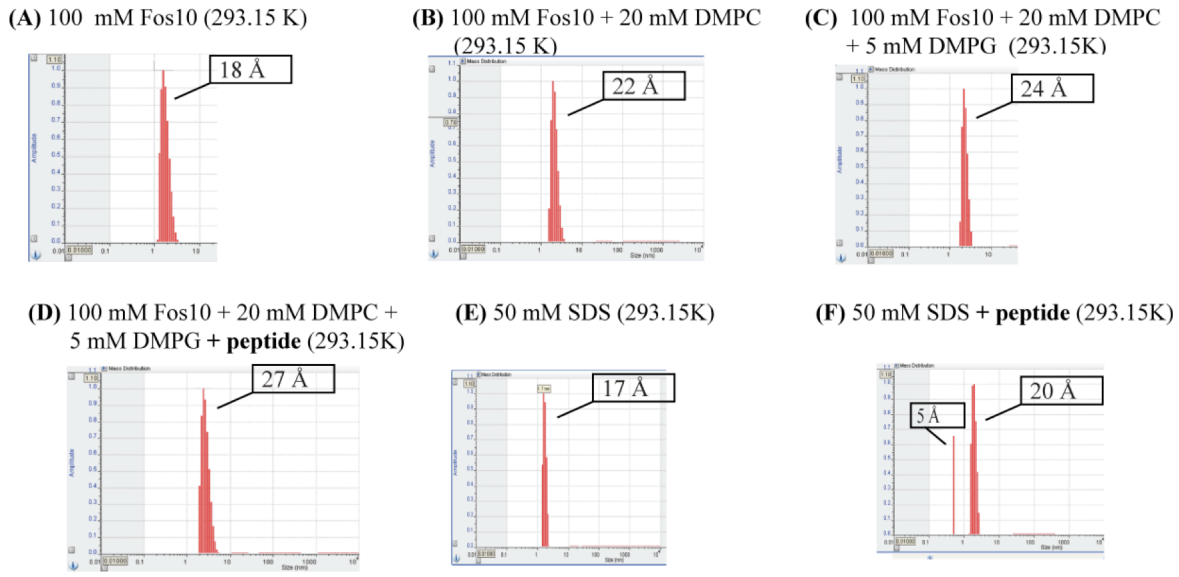

Figure 5.10: Dynamic light scattering of MRAP (2-67)
(A) of 100 mM Fos10 - main found mass 18 Å
(B) of 100 mM Fos10 + 20 mM DMPC - main found mass 22 Å
(C) of 100 mM Fos10 + 20 mM DMPC + 5 mM DMPG - main found mass 24 Å
(D) of 100 mM Fos10 + 20 mM DMPC + 5 mM DMPG + peptide - main found mass 27 Å
(E) of 50 mM SDS - main found radius 17 Å
(F) of 50 mM SDS + peptide - main found mass 20 Å

5.2.8.2 Determination of the effective hydrodynamic radius by pulse field gradient NMR

A further method to calculate the effective size of SDS micelles with incorporated protein is by pulse field gradient NMR (Wilkins et al. 1999). There, 1D pulse gradient stimulated echo longitudinal encode-decode pulse sequences were recorded with different gradient strengths. The reference molecule 1,4-dioxane was included in the protein solution and diffusion rates were extracted from the spectra for both the protein (d_{prot}) and the reference molecule (d_{ref}). The hydrodynamic radius was calculated according to:

$$R_h^{prot} = \frac{d_{ref}}{d_{prot}}(R_h^{ref}),$$

where R_h^{prot} is the protein hydrodynamic radius and R_h^{ref} is the radius of the reference molecule. In general, the radius of gyration (R_g) is the root-mean-squared distance of all

the atoms in the molecule from the protein center of mass, while the hydrodynamic radius (R_h) can be defined as the radius of a sphere that has the same diffusion coefficient as the protein molecule.

For SDS, a R_g of 17.4 Å was calculated. This corresponds well with the obtained result from DLS studies, which was calculated to be ~17 Å. For MRAP(2-67) a R_g of 20.7 Å and R_h of 26.8 Å were obtained. The difference between included and excluded target protein is approximately 3 Å, on the order of the diameter of an alpha helix. Thus, it can be concluded that PFG experiments were consistent with the obtained DLS results. The calculated effective radius of gyration gave further evidence of a monomeric insertion of MRAP(2-67) into SDS micelles.

5.2.8.3 Analytical Ultracentrifugation

The oligomeric state of MRAP(2-67) was further analysed by sedimentation equilibrium analytical centrifugation (AUC). Sedimentation equilibrium analysis represents a reliable method to study protein molecular masses. However, due to the large number of unknown parameters, setting up an experiment was not trivial. Sedimentation equilibrium measurements were carried out in 100 mM DHPC and 50 mM SDS. Mixed micelles turned out to not be suitable for that technique since appropriate density matching (the adjustment of the solvent density to that of the detergent by addition of D_2O) was not possible due to the large differences in buoyant masses between Fos-Choline-10, DMPC and DMPG. During ultra-centrifugation, the mixed micelle components would separate according to their individual densities – with Fos-Choline-10 “floating” and DMPC/DMPG “sinking” to the bottom of the tube.

Tanford *et al*. (Tanford et al. 1974; Tanford & Reynolds 1976) pioneered molecular characterisation of proteins in detergent solutions, which is important for density matching. Using the experimental data from Tanford *et al.* (Tanford et al. 1974) it was possible to calculate the expected density, to achieve sufficient "density matching" for DHPC and SDS. D_2O has a density of $\delta = 1.105$ g/cm^3 at 293.15 K. This value is very close to the calculated density of 100 mM SDS, being $\delta \sim 1.15$ g/cm^3 and closer yet to the density of 100 mM DHPC, being $\delta \sim 1.10$ g/cm^3. With that information density matching was achieved by using 100% D_2O. All experiments were recorded at 293.15 K.

In 100 mM DHPC a molecular weight for MRAP(2-67) of ~ 7.30 ± 0.25 kDa was determined. In 50 mM SDS a molecular weight of ~ 6.95 ± 0.5 kDa was calculated (Figure 5.11). In both cases the determination of a possible molecular weight resulted in the monomeric one (monomeric MRAP(2-67) = 7.56 kDa). No dimeric conformation of MRAP(2-67) could be verified.

Figure 5.11: Analytical Ultracentrifugation of MRAP(2-67) in

Detergent	*MRAP(2-67)*
100 mM DHPC	*7.30 ± 0.25 kDa*
50 mM SDS	*6.95 ± 0.5 kDa*

5.2.9 Molecular dynamic (MD) studies of MRAP inter-molecular interactions

In a final attempt to understand and establish a possible dimeric interface of MRAP molecular dynamics (MD) simulations in micelles and bilayers were explored. Coarse-grain simulations with two different force fields – BOND and MARTINI 2.2 – were used, followed by atomistic simulations (AT). MD theory and the coarse-grain force fields are further described in Methods and Materials.

5.2.9.1 Coarse-grained simulations

5.2.9.1.1 Establishing a coarse-grain system and choosing the construct

Lipid force fields of DPPC and POPC were established in the research group of Professor Mark Sansom in the New Biochemistry Department, University of Oxford (Sansom & Biggin 2010), and chosen for simulations of a dimeric MRAP. Additionally, a lipid bilayer environment of DPPC:DPPG (75:25) was generated by lipid exchange using a script developed by Dr. Heidi Koldsoe. Insertion into DPPC bilayers was tested with constructs of different length, since inclusion of the N-terminal domain of MRAP resulted in improper folding. Finally, a shortened construct, MRAP(13-67), was identified to be the most suitable to continue MD simulations. This construct comprised part of the distal N-terminal region (residues Ser13 to Glu28), the KH-rich region (Lys29 to Ser37), the transmembrane domain (Ile38 to Trp62) and the C-terminus (Ser63 to Gln67). In these simulations, two monomeric MRAP(13-67) constructs in two conformations – parallel and anti-parallel – were inserted into a single bilayer with a fixed distance of ~60 Å to each other. To establish the system and to form appropriate bilayers around the protein, one coarse-grain simulation was set up for the duration of one μs for each detergent and each conformation (Figure 5.12).

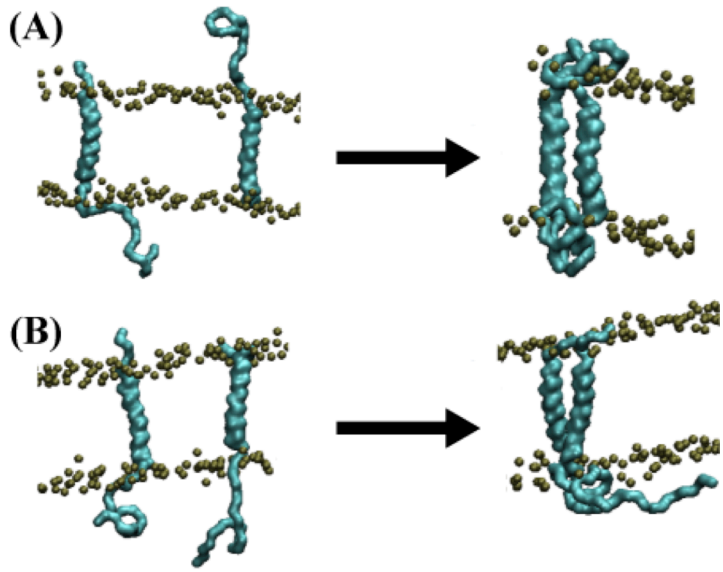

Figure 5.12: The initial set-up for CG-MD simulations
(A) For an anti-parallel conformation two monomers with opposite direction and 60 Å of fixed distance to each other were inserted into a single bilayer
(B) For a parallel conformation two monomers with the same direction and 60 Å of fixed distance to each other were inserted into a single bilayer

5.2.9.1.2 Investigation of MRAP(2-67)'s dimerisation in different coarse-grain force fields

To start with, all simulations were carried out using BOND force field, which is based on MARTINI (Marrink et al. 2004) and was established by Bond *et al*. (Bond et al. 2007; Bond & Sansom 2006). This general force field comprises additional constraints specifically for membrane proteins. BOND was mainly developed for studying the transmembrane protein glycophorin A (GpA), which forms a right-handed homodimer, and is a co-receptor for the influenza virus and Hepatitis A virus (Auffray et al. 2001; Sanchez et al. 2004). Each simulation was analysed on the bases of four main factors: (i) the minimum distance of Cα-atoms within two helices, (ii) the helix-helix crossing angle, (ii) the contact matrix, which gives indications of which residues were most likely to interact with each other in the simulation, and (iv) by visual inspection.

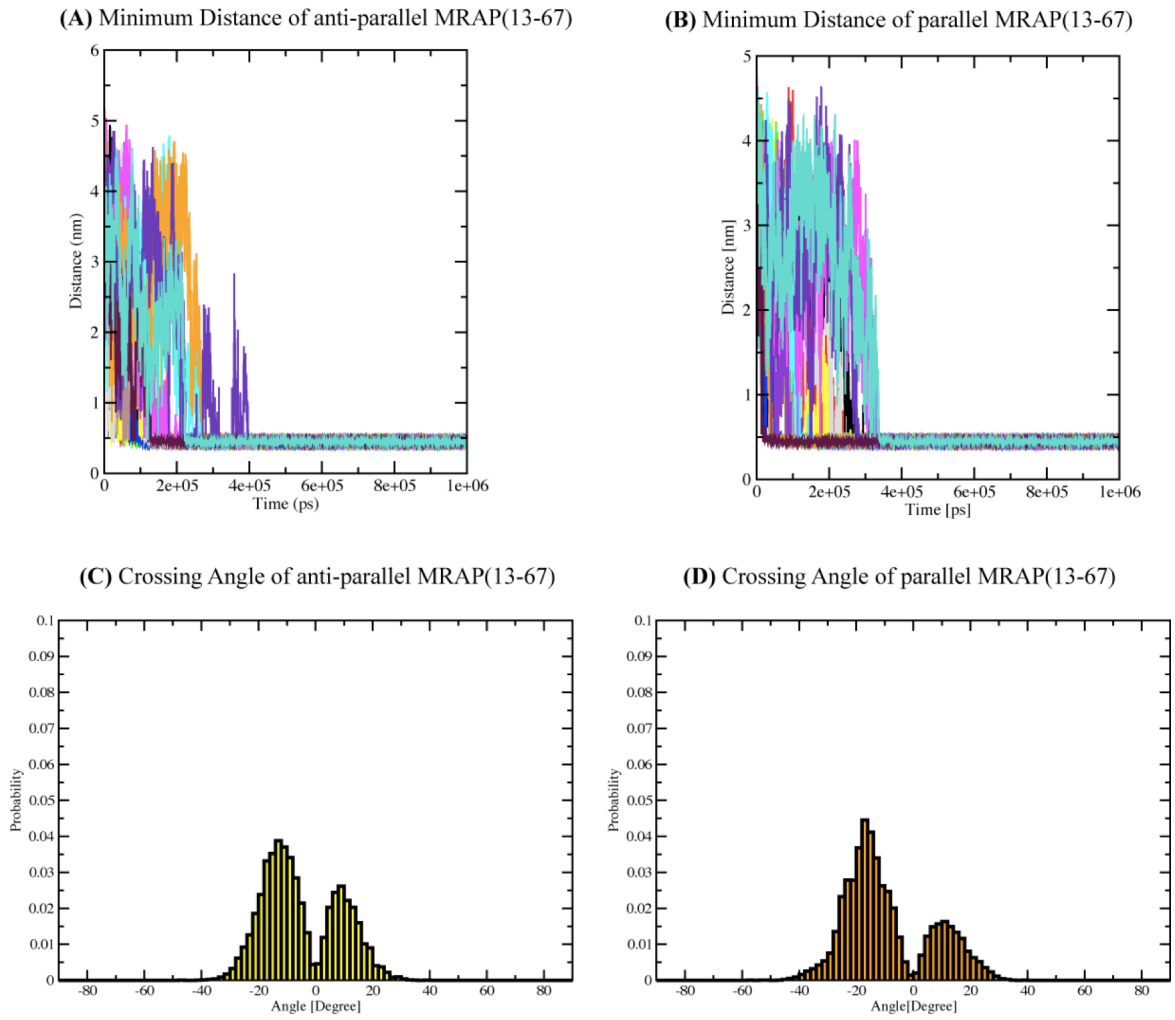

Figure 5.13: Coarse-grain simulation of MRAP(13-67) in BOND [15 simulations each]
(A) Minimum distance analysis over 15 simulations of an antiparallel MRAP(13-67) homodimer
(B) Minimum distance analysis over 15 simulations of a parallel MRAP(13-67) homodimer
(C) Average crossing angle over 15 simulations of an antiparallel MRAP(13-67) homodimer
(D) Average crossing angle over 15 simulations of a parallel MRAP(13-67) homodimer

A summary of all performed simulations can be found in Methods and Materials – Table 3.3. Visual inspection of the dimers revealed that all simulations, regardless of whether parallel or anti-parallel came together with the same probability. The crossing angle distribution revealed a bimodal distribution, with a slight majority corresponding to right-handed (RH) packing of the helices for both orientations (Figure 5.13(C+D)). The mean crossing angle in the right-handed packing mode for anti-parallel studies was approximately -16º, whereas for parallel dimer formation it was ~ -20º. In general, the

BOND force-field tends to be "sticky" (personal communication with Dr Phillip Stansfeld) and are biased toward RH crossing angles.

Therefore, the slight preferred RH-distribution for MRAP(2-67) was not surprising. All 15 simulations for each conformation showed a minimum distance between the two helices of ~5 Å. The crossing angle for an antiparallel conformation showed less bias for a right-handed packing than the parallel one. However, close inspection of all RH and left-handed (LH) structures displayed significant differences in the helix-helix interfaces. This was unexpected and hence further investigation in different force-fields were pursued.

MARTINI2.2 coarse-grain force-field (de Jong et al. 2013), a recently updated version of MARTINI (Marrink et al. 2004) with more flexible and suitable constraints for membrane proteins, was introduced to the study. Experiments of MRAP(13-67) were conducted in three lipid environments DPPC, POPC, and DPPC:DPPG(3:1). Since coarse-grain force fields tend to favour protein-protein association, it was expected that the two transmembrane helices would come together in all simulations, using coarse-grain force-field MARTINI2.2. This was the case, and therefore required greater analysis to assess the quality of the dimer interactions. Investigation of minimum distances between the two transmembrane domains showed that in each case the transmembrane domains dimerised and adapted a minimum distance of approximately ~5 Å to each other. Figure 5.14 shows a summary of minimum distances and average crossing angles of all simulations run in MARTINI2.2 force field. In all three environments, crossing angle analysis disclosed a bimodal distribution probability with no preferred packing orientation (Figure 5.14 (A)).

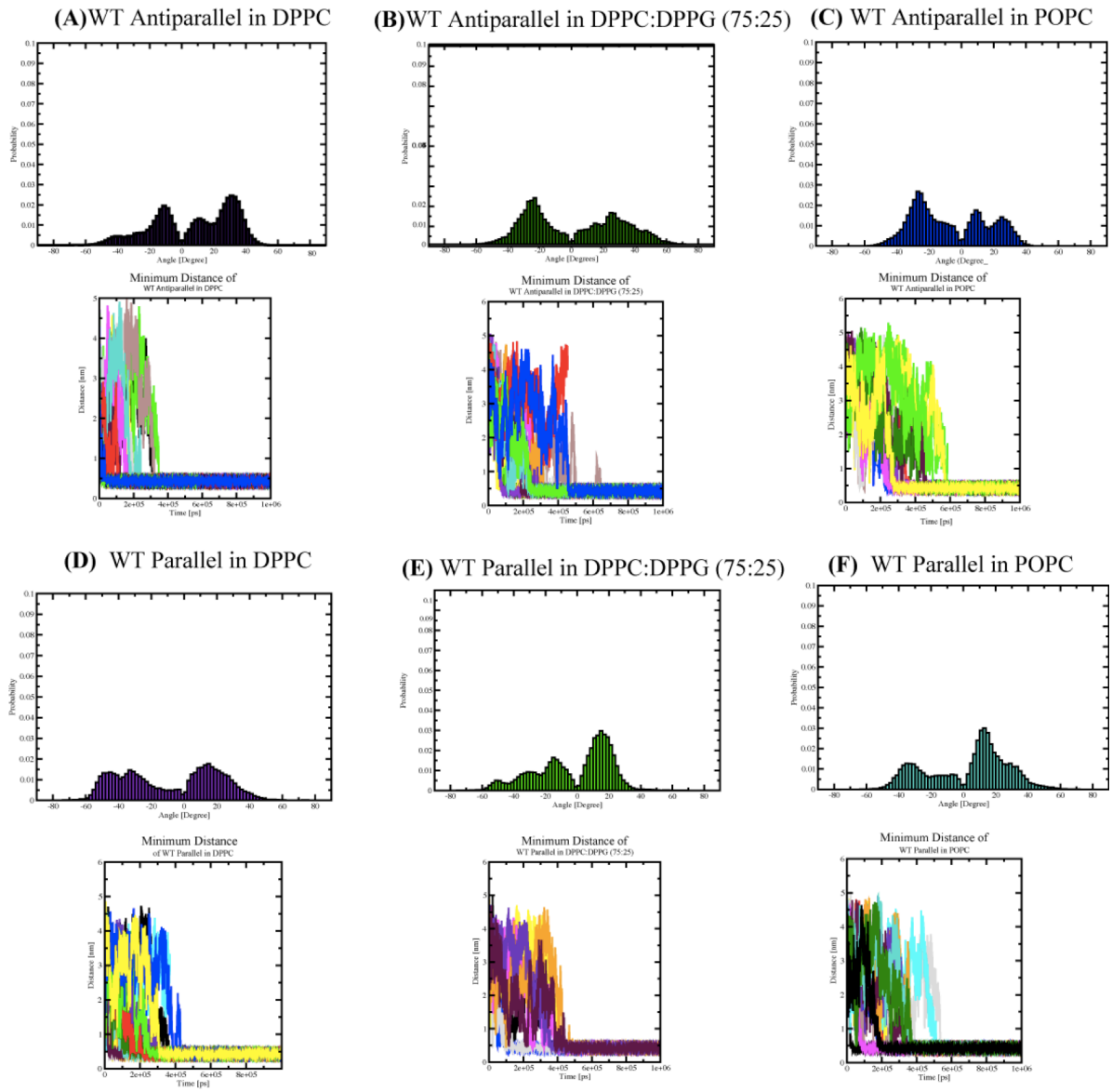

Figure 5.14: Coarse-grain simulation of MRAP (13-67) in MARTINI2.2 [each 20 simulations]
(A) Average crossing angle and minimum distance analysis over 15 simulations of an antiparallel MRAP(13-67) homodimer in DPPC
(B) Average crossing angle and minimum distance analysis over 15 simulations of an antiparallel MRAP(13-67) homodimer in DPPC:DPPG (75:25)
(C) Average crossing angle and minimum distance analysis over 15 simulations of an antiparallel MRAP(13-67) homodimer in POPC
(D) Average crossing angle and minimum distance analysis over 15 simulations of a parallel MRAP(13-67) homodimer in DPPC
(E) Average crossing angle and minimum distance analysis over 15 simulations of a parallel MRAP(13-67) homodimer in DPPC:DPPG (75:25)
(F) Average crossing angle and minimum distance analysis over 15 simulations of a parallel MRAP(13-67) homodimer in POPC

Additionally, energy potential for each performed simulation was calculated and contact matrix analysis was started from the point when both helices came tightly together

without experiencing large fluctuations. The potential energies were calculated to estimate the best time point where the transmembrane helices would be close in space to each other. Inspection of all structures revealed substantial differences in all helix-helix interfaces. Every single simulation had slightly different contacts within the two transmembrane helices. Consequently, it was concluded that the dimerisation interfaces that were observed were not robust, and suggestive of a non-specific association.

To provide a positive control for the simulations, findings of MRAP(13-67) were compared with coarse-grain simulations performed on GpA. GpA is one of the best-studied oligomeric transmembrane proteins and dimerises through a GxxxG-motif (Russ & Engelman 2000; Doura et al. 2004). Although the interactions of the GpA transmembrane helices are complex and modulated not only by the sequence context but also by the lipid and/or detergent environment (Doura et al. 2004; Doura & Fleming 2004), coarse grain simulations of GpA robustly converge to structures that are very similar to the experimentally determined homodimer conformation. Comparison of the MRAP(13-67) results with that of GpA (Figure 5.15) highlight the poor convergence of the MRAP(13-67) dimer.

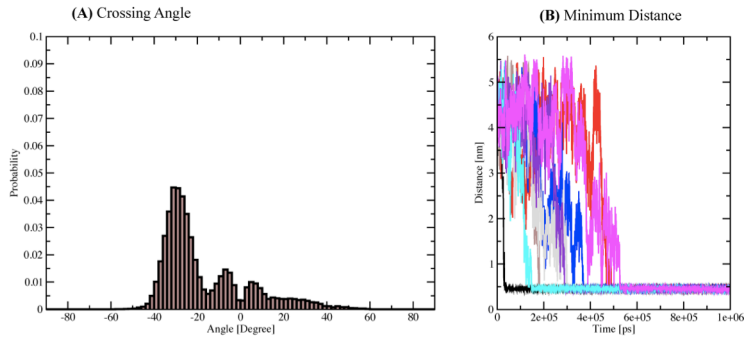

Figure 5.15: Coarse-grain simulation of Glycophorin A in MARTINI2.2
(A) Averaged crossing angle of Glycophorin A over 10 simulations
(B) Minimum distance of Glycophorin A over 10 simulations

Although GpA simulations resulted in a well-defined dimeric interface (across ten simulations), for MRAP(13-67) it was not possible to obtain even small "clusters" of similar structures.

DPPC appeared to be the most suitable environment to simulate MRAP(13-67) dimerisation, since overall the process of dimerisation was the fastest and the contact matrices appeared to be on average more symmetric than in other bilayers. Since the lack of a stable interface by coarse grain methods may be due to the approximations made for protein chemistry and the force field, atomistic simulations were performed to examine whether more accurate modelling methods could provide insights into a potential dimeric interfaces of MRAP.

5.2.9.2 Refinement and model assessment by atomistic molecular dynamic simulations

In order to refine and to further evaluate the dimeric models of anti-parallel and parallel conformations the five most representative models in DPPC were chosen, converted to atomistic detail using CG2AT (Stansfeld & Sansom 2011), and then simulated for 50 ns at 300 K. One anti-parallel RH, two anti-parallel LH, one parallel RH and one parallel LH coarse-grain simulations from MARTINI2.2 in a DPPC bilayer were selected. Criteria for choosing these particular simulations were defined by the most symmetric contact matrices and the best-defined crossing angles.

5.2.9.2.1 Antiparallel homodimerisation of MRAP(13-67) by atomistic simulations

Three antiparallel AT-MD simulations in DPPC bilayers were set up to more closely investigate a possible antiparallel homodimeric interface in more detail. The

conformational stability of each dimer was assessed during one simulation by its minimum distance between Cα of the two helices. All three simulations seemed stable, with the RH packing mode exhibiting better stabilisation. The antiparallel RH homodimeric conformation showed a crossing angle of approximately -30º with a constant minimum distance at ~10 Å.

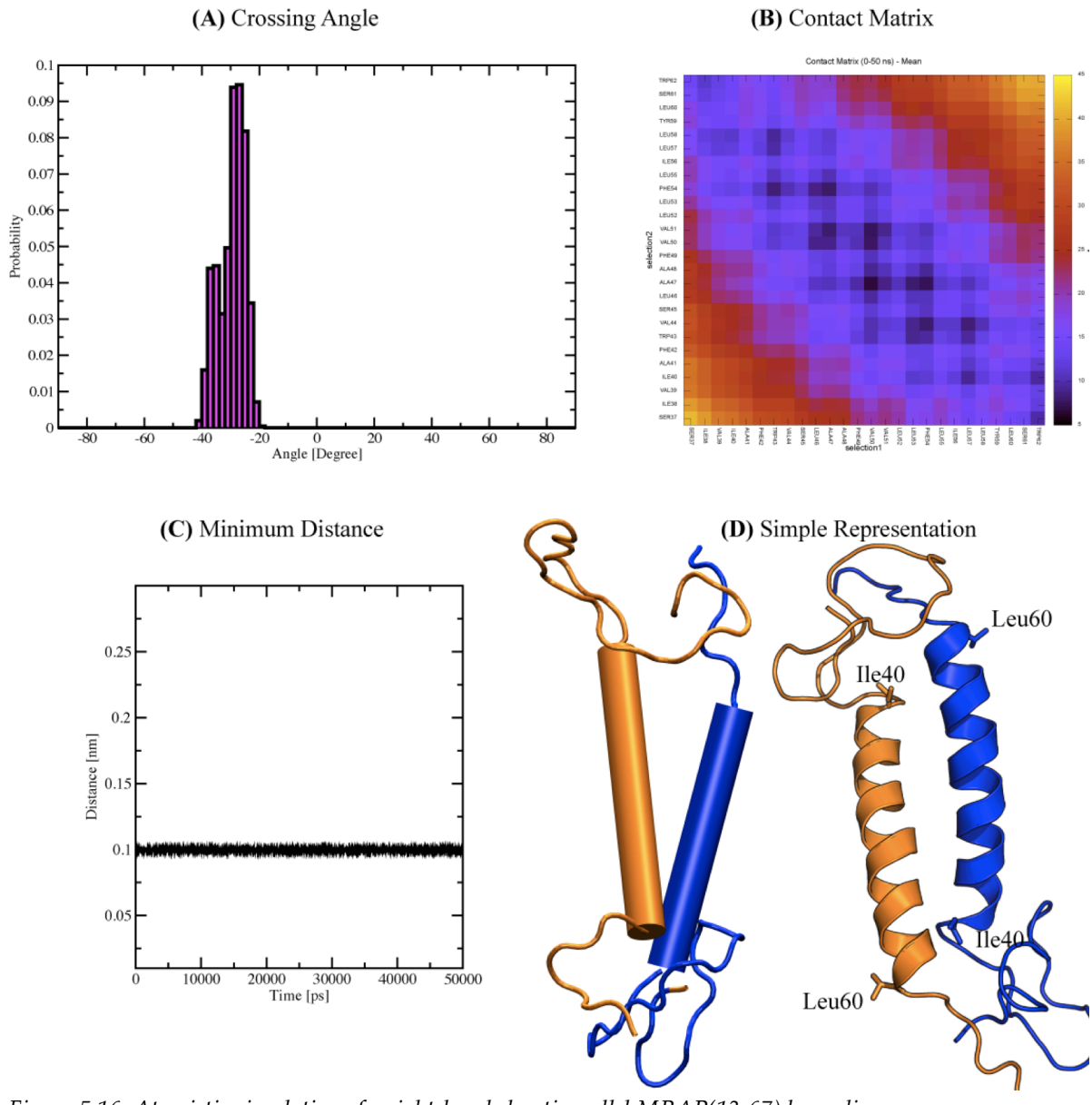

Figure 5.16: Atomistic simulation of a right-handed antiparallel MRAP(13-67) homodimer
(A) Crossing angle of an antiparallel right-handed atomistic simulation
(B) Contact Matrix of an antiparallel right-handed atomistic simulation
(C) Minimum distance during an atomistic, antiparallel right-handed simulation
(D) Ribbon and schematic representation of antiparallel right-handed atomistic simulation

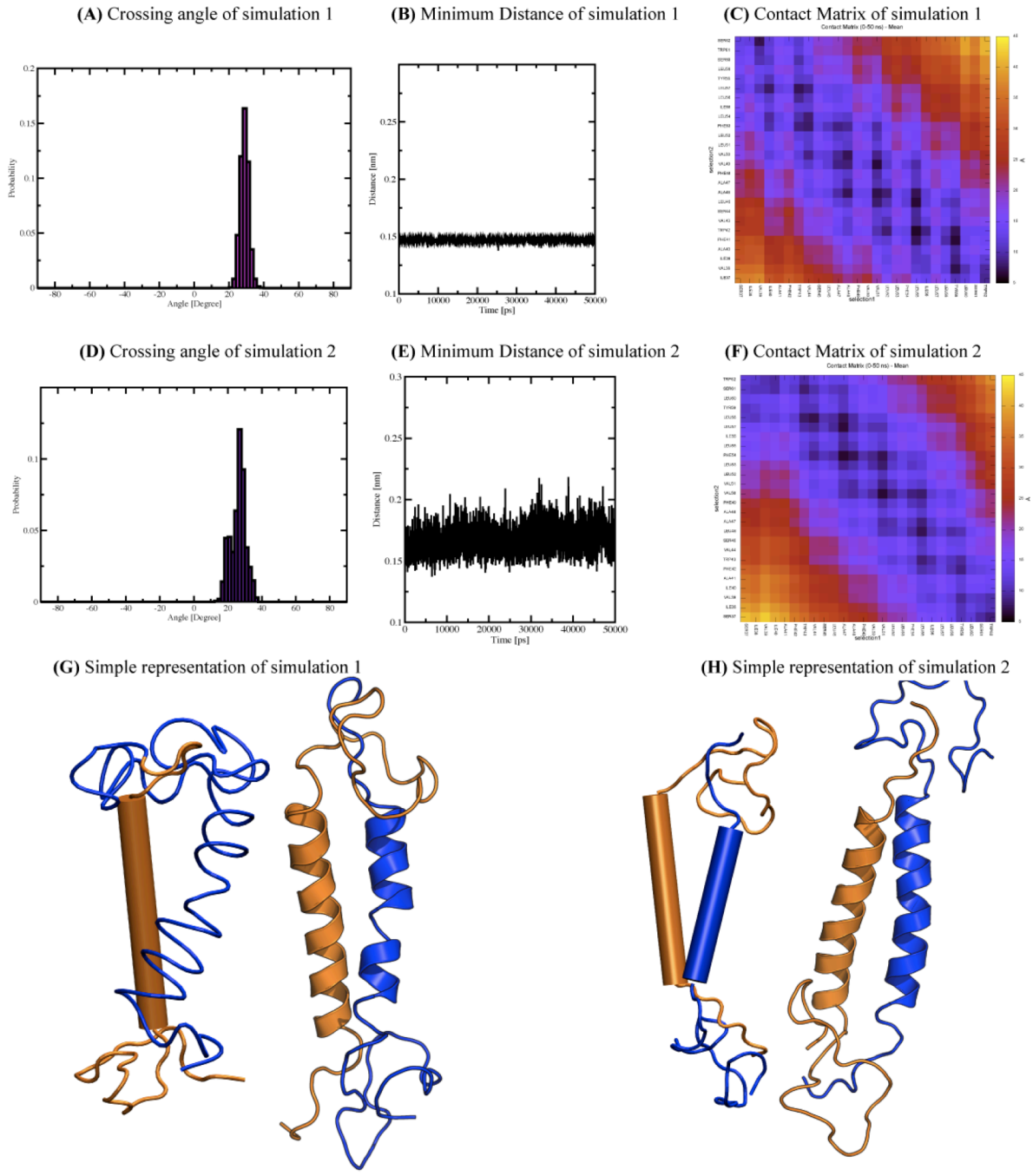

Figure 5.17: Atomistic simulation of a left-handed antiparallel MRAP(13-67) homodimer
(A) Crossing angle of an antiparallel left-handed simulation 1
(B) Minimum distance during an antiparallel, left-handed simulation 1
(C) Contact Matrix of antiparallel, left-handed simulation 1
(D) Crossing angle of an antiparallel left-handed atomistic simulation 2
(E) Minimum distance during an antiparallel, left-handed simulation 2
(F) Contact Matrix of atomistic, antiparallel, left-handed simulation 2
(G) Cartoon and schematic representation of antiparallel left-handed atomistic simulation 1
(H) Cartoon and schematic representation of antiparallel left-handed atomistic simulation 2

The edges of the structured transmembrane region within this simulation were located between Ile40 and Leu60. Examination of a potential contact matrix suggested close contacts at the helix core. However, visual examination of the simulation suggested a rather asymmetric packing of the two transmembrane domains (Figure 5.16 (D)).

In comparison, the two simulated LH antiparallel simulations showed a crossing angle at approximately 30º with minimum distances between ~15 Å and ~18 Å. Moreover, the increased minimum distance between two helices of both simulations (Figure 5.17 (E)) suggested "looser" packing in comparison to a possible RH antiparallel conformation, where the average minimum distance was calculated to be ~10 Å. Despite a similar crossing angle the contact matrices were different as could be seen by visual examination (Figure 5.17). The first simulation displayed a visible 'kink' between residues Ala48 and Val50 on one of the helices (Figure 5.17 (G)). In the second simulation a difference in helix length was noticed. The first was located between residues Ile40 and Leu60, whereas the second structured transmembrane segment was observed between residues Val39 and Leu60 (Figure 5.17 (H)).

As a further step of analysis between the simulated antiparallel left- and right-handed homodimer, the helix-helix interactions were tabulated (Table 5.1).

Right-handed homodimer of MRAP(13-67)	**Left-handed homodimer of MRAP(13-67)**
Ile39 Leu57	Leu57 Ile40 Phe42 Leu58
Trp43 Phe54	Leu53 Val44 Ala46 Phe54
Ala47 Val50	Val50 Ala48 Val50 Val51
Val50 Ala47	Ala46 Val51 Phe54 Ala47
Trp43 Phe54	Phe42 Leu55 Leu60 Ala47
Leu57 Ile39	

Table 5.1: Simulated dimeric interface of an antiparallel homodimeric MRAP

The interfaces of all three AT-MD simulation involved different residues and were not symmetric. However, it seemed likely that the right-handed interface might be slightly preferred over both left-handed ones. This is due to the symmetric interface and to lower values of the minimum distance in the right-handed interface, which would indicate more specific intermolecular contacts (Figure 5.18(A)).

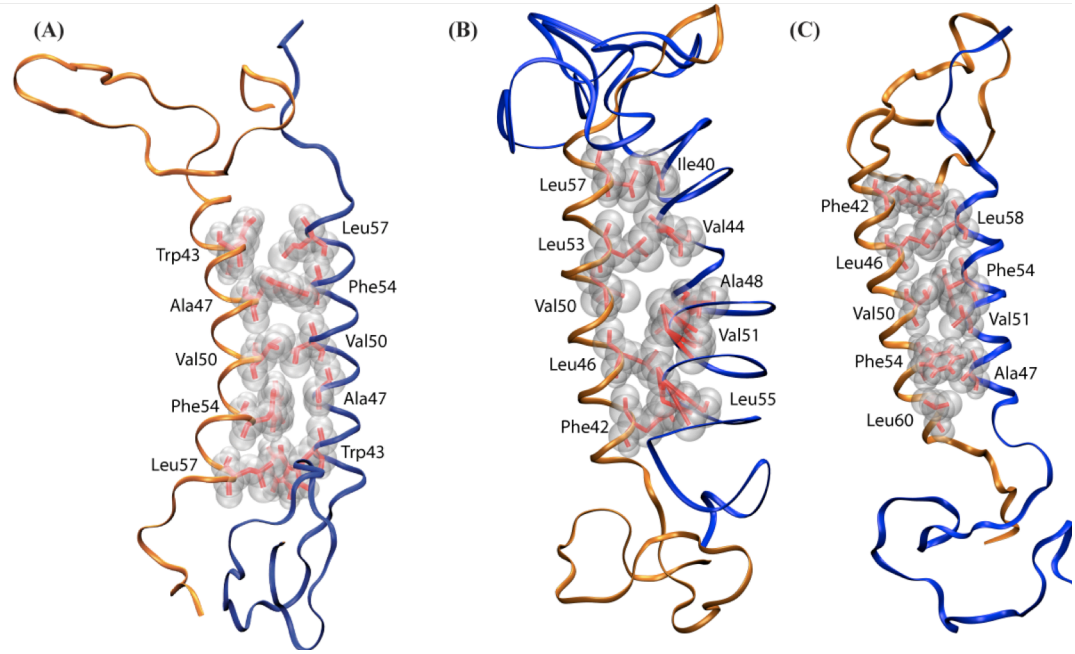

Figure 5.18: Interface of the atomistic simulations of an antiparallel MRAP (13-67) homodimer
(A) Dimeric interface of the right-handed antiparallel homodimer
(B) Dimeric interface of the left-handed antiparallel homodimer (1)
(C) Dimeric interface of the left-handed antiparallel homodimer (2)

However, the overall packing was not symmetric and showed an offset of one turn. Additionally, in the proposed interface the bulky sidechains of Trp43 and Phe54 are at the dimeric interface, which is an unusual finding for helix-helix interactions. Therefore, this result has to be taken under careful consideration.

5.2.9.2.2 Parallel homodimerisation of MRAP(13-67) by atomistic simulations

Two AT-MD simulations for a possible parallel homodimer were started from coarse-grain coordinates and analysed in DPPC bilayers. Both systems appeared to be

reasonably stable, with the RH dimer showing a more narrow distribution of crossing angles and more consistency across the transmembrane regions (Figure 5.19).

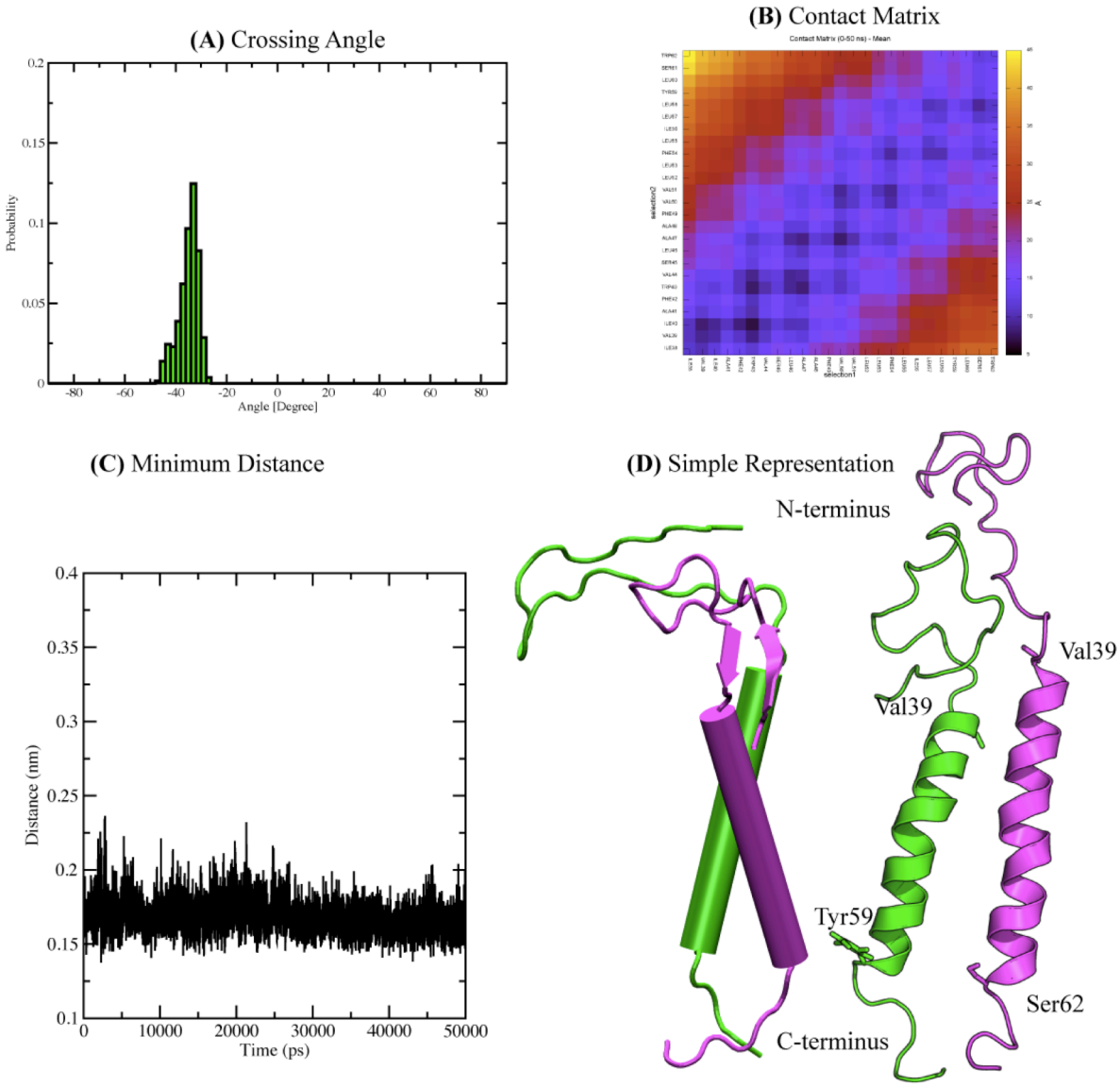

Figure 5.19: Atomistic simulation of a parallel right-handed MRAP(13-67) homodimer
(A) Crossing angle of a parallel right-handed atomistic simulation
(B) Contact Matrix of a parallel right-handed atomistic simulation
(C) Minimum distance during an atomistic, parallel right-handed simulation
(D) Ribbon and schematic presentation of a parallel right-handed atomistic simulation

The parallel simulation with RH packing showed a consistent minimum distance across the entire simulation of ~18 Å. Additionally, the crossing angle was calculated to be approximately -30º with a narrow distribution. Interestingly, the contact matrix indicated that the two helices interacted closely with each other (~8 Å) around residue Val50 as

well as in the KH-rich region (Figure 5.19 (B)). Residues Val39 and Ser62 on one helix and Val39 and Tyr59 on the second helix define the boundaries of the structured transmembrane region.

In comparison, the simulated LH parallel model experienced fluctuations in the average minimum distances between the two helices of about approximately ~15 Å to ~20 Å (Figure 5.20(C)).

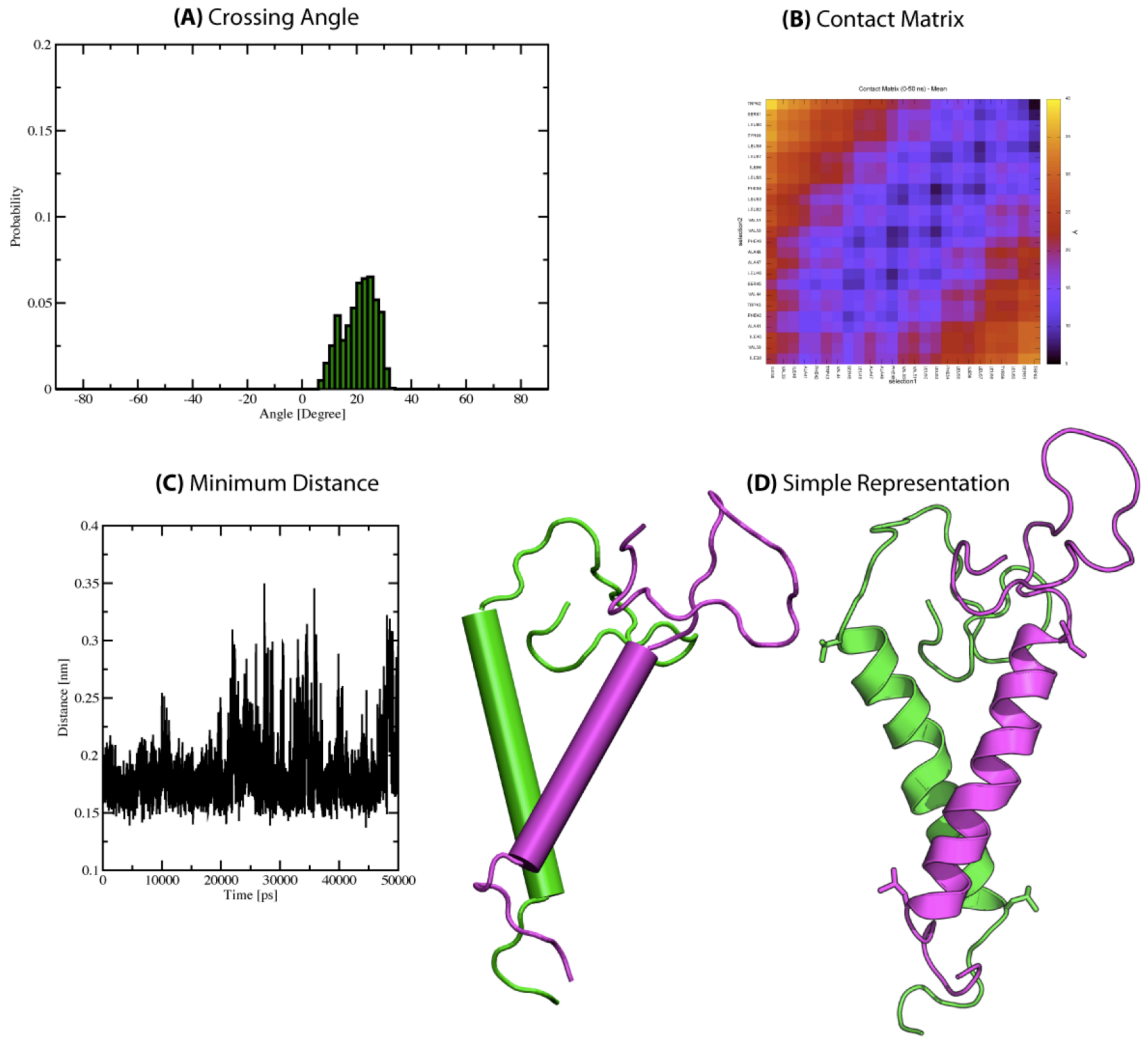

Figure 5.20: Atomistic simulation of a parallel MRAP (13-67) homodimer
(A) Crossing angle of a parallel left-handed atomistic simulation
(B) Contact Matrix of a parallel left-handed atomistic simulation
(C) Minimum distance during an atomistic, parallel left-handed simulation
(D) Ribbon and cartoon presentation of a parallel left-handed atomistic simulation

Moreover, its crossing angle distribution was considerably wider, ranging from ~5º to ~35º (Figure 5.20(C)). This suggested a looser packing of the two helices. However, visual inspection of the schematic representations and intensive analysis of the contact matrix of a dimerised parallel MRAP(13-67) showed that residues close to the C-terminus interacted more strongly with each other across the helix than those at the N-terminus, possibly due to electrostatic repulsion between the positively charged KH-rich regions at the N-termini.

As in the antiparallel case, inspection of helix-helix interactions of the simulated parallel left- and right-handed homodimers indicated different interfaces (Table 5.2).

Left-handed homodimer of MRAP(13-67)		**Right-handed homodimer of MRAP(13-67)**	
Leu46	Val50	Ala48	Phe49
Val51	*Leu53*	*Val51*	*Leu53*
Leu54	Leu53	Leu55	Leu57
Leu58	Leu58	Leu60	Leu57

Table 5.2: Simulated dimeric interface of a parallel homodimeric MRAP

Neither of the simulations was symmetric nor showed a preference for a likely interface. If a parallel homodimerisation of MRAP occurred, the left-handed parallel homodimeric conformation would be more likely, since it is in agreement with the positively charged residues avoiding each other. Interestingly, the interaction between Val51 and Leu53 occurred in both atomistic simulations.

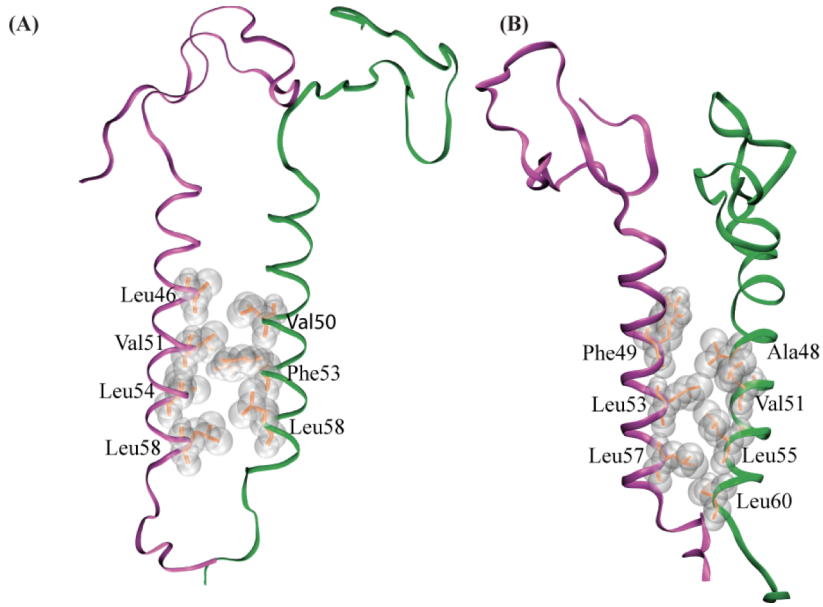

Figure 5.21: Atomistic simulation of a parallel MRAP(13-67) homodimer
(A) Dimeric interface of the right-handed parallel homodimer
(B) Dimeric interface of the left-handed parallel homodimer

Summarising, the right-handed anti-parallel conformation gave overall the most symmetric and stable dimeric interface. However, the proposed interface suggested that the tryptophan and phenylalanine head groups interacted on the dimeric interface. Due to the bulkiness of these sidechains, which prevents formation of an extensive interaction surface, this conformation is thought to be highly unlikely, though clearly further studies are needed. Left-handed anti-parallel as well as both parallel simulations showed asymmetric and non-convergent interaction between the two transmembrane regions, arising from probably nonspecific interactions. In conclusion, a clearly specific dimeric interface could not be determined by these simulation studies.

5.3 DISCUSSION

5.3.1 Investigation of the monomeric MRAP

Work presented in Chapter 4 demonstrated that MRAP adopts a highly conserved and robust monomeric structure in 3 different environments – DHPC micelles, SDS micelles and in mixed micelles containing lipids. Investigation of the biochemical and biophysical properties of MRAP revealed an α-helical transmembrane domain, and an α-helical N-terminal LDY(L/I)-motif. Furthermore, the KH-rich region was found to be highly flexible, suggesting that it acts as a "linker", allowing free movement and interaction of the N-terminal helix with its environment, at least in the absence of bound receptor. The obtained monomeric structure of MRAP(2-67) provided a starting point for the understanding of a possible dimerisation of MRAP.

5.3.2 What could drive dimerisation?

Sebag and Hinkle (Sebag & Hinkle 2007) first suggested that MRAP adopts a unique homodimeric structure with dual topological features in cell membranes. However, data presented in this chapter indicate that MRAP does not spontaneously dimerise *in vitro* under the conditions that were tested. In Chapter 5, I have shown that despite much effort using biophysical and computational approaches, it has not been possible to stabilise a specifically dimeric form of MRAP. Crosslinking, membrane assays and further biophysical methods were applied in an attempt to stabilise a possible dimeric conformation of MRAP. Additional experiments such as site-directed spin labelling and paramagnetic relaxation enhancement are ongoing (see Appendix). Moreover, extensive CG-MD simulations in combination with all-atom simulations (more than 120 simulations in total) failed to identify a conserved packing interface of the two

transmembrane domains in a membrane-like environment. The lack of convergence to a unique dimeric interface might be due to either approximations in the simulated environment or a more profound nature, such as an additional factor involved in dimerisation that is not yet discovered. Notably, it was shown that MRAP extracted from endogenously expressing tissue exists as a dimer that is insensitive to SDS and reducing agents, but that in transfected cells MRAP tends to migrate as a monomer (Cooray et al. 2008). Together, these results suggest that other endogenous factors present in cells that naturally express MRAP may be required to facilitate dimerisation.

In vivo a typical biological membrane is a complex structure, comprising an asymmetric bilayer of lipids, incorporated with proteins and small amounts of carbohydrates. The complexity and highly dynamic features of a membrane are difficult to mimic in a laboratory environment that is also suitable for biophysical studies. Especially, mimicking the asymmetric distribution of lipids across the membrane whilst enabling high quality structural characterisation is not yet feasible, but may be an important factor in MRAP dimerisation. The possibility that an additional cellular component, such as another protein or small molecule, is required will require additional *in vivo* experiments.

CHAPTER 6

TOWARDS A STRUCTURAL UNDERSTANDING OF THE TRANSMEMBRANE DOMAIN OF RECEPTOR ACTIVITY MODIFYING PROTEIN 1

"It is characteristic of science that the full explanations are often seized in their essence by the percipient scientist long in advance of any possible proof"

(John Desmond Bernal)

6.1 INTRODUCTION

The family of receptor activity–modifying proteins (RAMP) consist of type-1 single-span transmembrane proteins that regulate the function of several GPCRs. RAMP1 (located at 2q36 – 37.3) was originally discovered in 1998 by McLatchie *et al.* (McLatchie et al. 1998) as a chaperone allowing the GPCR class B Calcitonin-like receptor (CLR) to reach the cell surface. Subsequently, RAMP2 (located at 17q12 – 21.2) and RAMP3 (located at 7p13–12) were identified based on sequence homology (McLatchie et al. 1998; Derst et al. 2000; Foord & Marshall 1999). In humans, RAMP1 and RAMP3 contain 148 amino acids, whereas RAMP2 contains 175 amino acids. The three human proteins share between 23 % and 30 % sequence identity and ~56 % sequence similarity (Figure 6.1).

```
sp|O60894|RAMP1_HUMAN      -------------MARALCRLPRRGLWLLLAHH----------------L 21
sp|O60895|RAMP2_HUMAN      MASLRVERAGGPRLPRTRVGRPAALRLLLLLGAVLNPHEALAQPLPTTGT 50
sp|O60896|RAMP3_HUMAN      -------------METGALRRPQLLPLLLLLCG---------------GC 22
                                       :       *     ***

sp|O60894|RAMP1_HUMAN      FMTTACQEANYGALLRELCLTQFQVDMEAVGETLWCDWGRTIRSYRELAD 71
sp|O60895|RAMP2_HUMAN      PGSEGGTVKNYETAV-QFCWNHYKDQMDPIEK-DWCDWAMISRPYSTLRD 98
sp|O60896|RAMP3_HUMAN      PRAGGCNETGMLERL-PLCGKAFADMMGKVDVWKWCNLSEFIVYYESFTN 71
                             : .    .    :  :* . :   *  :    **: .     *  : :

sp|O60894|RAMP1_HUMAN      CTWHMAEKLGCFWPNAEVDRFFLAVHGRYFRSCPISGRAVRDPPGSILYP 121
sp|O60895|RAMP2_HUMAN      CLEHFAELFDLGFPNPLAERIIFETHQIHFANCSLVQPTFSDPPEDVLLA 148
sp|O60896|RAMP3_HUMAN      CTEMEANVVGCYWPNPLAQGFITGIHRQFFSNCTVDRVHLEDPPDEVLIP 121
                           *    *: ..  :**. .: ::   *  .* .*.:    . *** .:* .

sp|O60894|RAMP1_HUMAN      FIVVPITVTLLVTALVVWQSKRTEGIV 148
sp|O60895|RAMP2_HUMAN      MIIAPICLIPFLITLVVWRSKDSEAQA 175
sp|O60896|RAMP3_HUMAN      LIVIPVVLTVAMAGLVVWRSKRTDTLL 148
                           :*: *: :   :  ****:** ::
```

Figure 6.1: Sequence alignment of human RAMP family members

The focus of this thesis is on the transmembrane domain of RAMP1, which is required for its activity and proposed to be responsible for RAMP1 homo-dimerisation.

6.1.1 Function of RAMPs and their interaction with GPCRs

RAMP1 has been shown to interact with high affinity and a 1:1 stoichiometry to calcitonin-receptor-like receptors (CLR), which in turn yield the neuropeptide calcitonin gene-related peptide (CGRP is 37 amino acids) (McLatchie et al. 1998; Foord & Marshall 1999). In general, calcitonin receptor and CLR interact with several calcitonin family peptides including calcitonin, calcitonin gene related peptides (cGRP1 and cGRP2), amylin and adrenomedullin (AM). These peptides have overlapping though diverse physiological functions (Poyner et al. 2002; Kuwasako et al. 2004; Parameswaran & Spielman 2006). The CGRP exists in two isoforms (α-CGRP and β-CGRP). Both isoforms are potent vasodilators with important pathophysiological actions in chronic pain conditions, such as migraine and the postherpetic neuralgia. The CGRP peptides derive from separate genes and are differentially produced, with α-CGRP dominating in sensory neurons and CGRPβ in keratinocytes (Hou et al. 2011).

RAMP2 and 3 on association with CLR form two pharmacologically distinct receptor complexes for AM with similar potencies for cAMP activation (Christopoulos et al. 1999; Leuthäuser et al. 2000; Sexton et al. 2001; Hay et al. 2003; Pi et al. 2005). Interestingly, RAMP2/CLR has high affinity for AM and low affinity for CGRP, whereas RAMP3/CLR has a high affinity for AM however also modulates the affinity for CGRP (Figure 6.2) (Husmann et al. 2000; Oliver et al. 2001; Bouschet et al. 2005).

The pharmacological nature of AM receptors depends on host cell environment as a consequence of G-protein and endogenous CLR/RAMP complement (Christopoulos et al. 1999; Tilakaratne et al. 2000; Kuwasako et al. 2003). Similarly, individual RAMPs

interact with the related calcitonin receptor (CTR) to generate three subtypes of high-affinity amylin receptors (Christopoulos et al. 1999; Tilakaratne et al. 2000; Watkins et al. 2013).

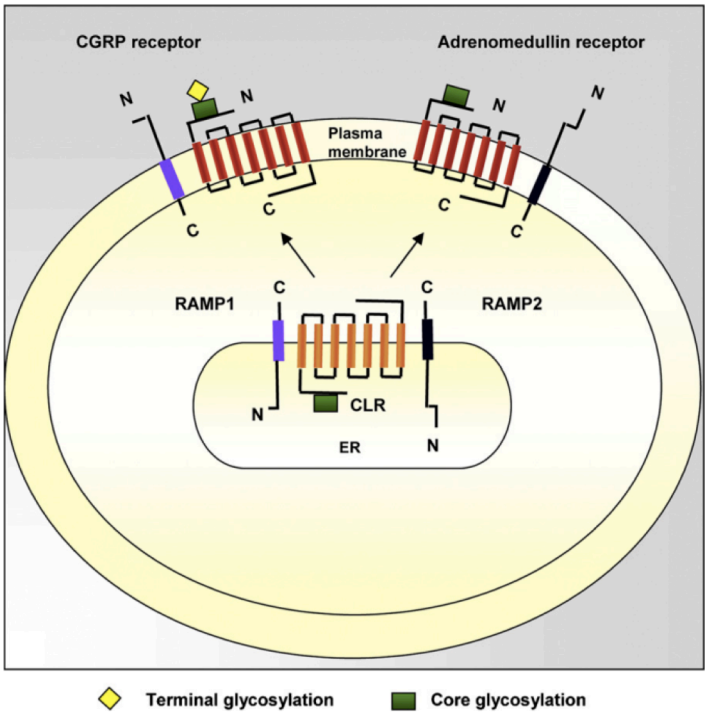

Figure 6.2: Heterodimerisaion of CLR and RAMPs.
Co-expression of CLR with RAMP1 leads to the ability of the receptor to bind to CGRP. Co-expression of RAMP2 (or RAMP3) with CLR results in the binding of Adrenomedullin. (Figure taken from Cooray et al. 2009)

All members of the RAMP family form complexes with multiple GPCRs. Examples for interaction partners with RAMPs are the class B GPCR parathyroid hormone receptor 1 and 2 (PTHR1 and PTHR2), the secretin receptor (SCTR) as well as the vasoactive intestinal polypeptide receptor 1. However, RAMPs can also modulate GPCRs that are not confined to class B GPCRs, such as the class C GPCR calcium^{2+}-sensing receptor (CaSR), which responds to changes in extracellular calcium concentration and plays a crucial role in calcium homeostasis. Therefore, as accessory proteins they act as chaperones and as modulators. There, RAMP1 and RAMP3 have been shown responsible for delivering CaSR to the cell surface in transfected HEK293 cells (Bouschet

et al. 2005). A complete list of known interactions of RAMPs with GPCRs can be found in table 6.1 (adapted from (Morfis et al. 2003)).

GPCR	RAMP	Consequence	Reference
CLR	RAMP 1, 2, 3	CLR+RAMP1= functional CGRP receptor CLR+RAMP2 = functional AM receptor 1 CLR+RAMP3 = functional AM receptor 2	(McLatchie et al. 1998) (Christopoulos et al. 2003)
CTR	RAMP 2, 3	Each RAMP isoform forms one distinct amylin receptor	(Hay et al. 2003) (Pi et al. 2005)
VPAC1	RAMP 1, 2, 3	VPAC1+RAMP2 show enhanced phosphoinositide hydrolysis	(Christopoulos et al. 2003)
PTH1R	RAMP 2	unknown	(Christopoulos et al. 2003)
PTH2R	RAMP 3	unknown	(Christopoulos et al. 2003)
GlucR	RAMP 2	unknown	(Christopoulos et al. 2003)
Secretin	RAMP 3	No change in signalling and internalisation of the receptor	(Harikumar et al. 2009)
CaSR	RAMP 1, 3	Essential for cell-surface trafficking of the receptor	(Bouschet et al. 2005)

Table 6.1: GPCR interacting partners of RAMPs

Like other small accessory proteins, RAMPs have to be co-expressed with the GPCR of interest to facilitate correct translocation to the cell surface, followed by expression and activation of the receptor (Kuwasako et al. 2000). The activated GPCRs in turn bind different ligands with varying affinities and potencies, indicating that RAMPs not only interact with distinct receptors, but also modulate their pharmacology and/or signalling capabilities (Christopoulos et al. 1999; Hay & Poyner 2006).

Considering the wide range of RAMP involvement in GPCR activation and the RAMP expression pattern in several tissues, it is highly likely that RAMPs have a much broader purpose than what is currently appreciated. Hay et al. (Hay & Poyner 2006) has reviewed the pharmacological function of RAMPs in detail.

6.1.2 Expression and disease relevance of RAMPs

RAMPs are widely distributed in the body with at least one RAMP being present in every tested tissue so far (Sexton et al. 2001). High expression levels of RAMP1 have been found in the heart, uterus, brain, bladder, pancreas, skeletal muscle and gastrointestinal system, whereas RAMP2 is mainly expressed in lung, heart, placenta, skeletal muscle and pancreas, and RAMP3 was found to be expressed widely across all tested tissues (Hay & Poyner 2006).

The expression levels of RAMPs are not static, with their mRNA levels differentially regulated in disease conditions such as heart failure, hypertension, kidney failure and diabetes (Doods et al. 2000). Moreover, RAMPs are changed during pregnancy (Thota et al. 2003; Gangula et al. 2003) and in patients who suffer from migraines (Doods et al. 2000). RAMP1 and RAMP3 can induce aortic stenosis and thus lead to cardiovascular disease (Cueille et al. 2002).

6.1.2.1 RAMP1 as drug target

As mentioned earlier, RAMPs enable the same GPCR to bind to multiple ligands. As a result, the GPCR-RAMP interface is exploited to develop drugs that confer a high level of specificity. Considering that more than 50 % of the drugs on the market target GPCRs, it is not surprising that the pharmaceutical industry has taken advantage of the drug-targetable GPCR-RAMP interface.

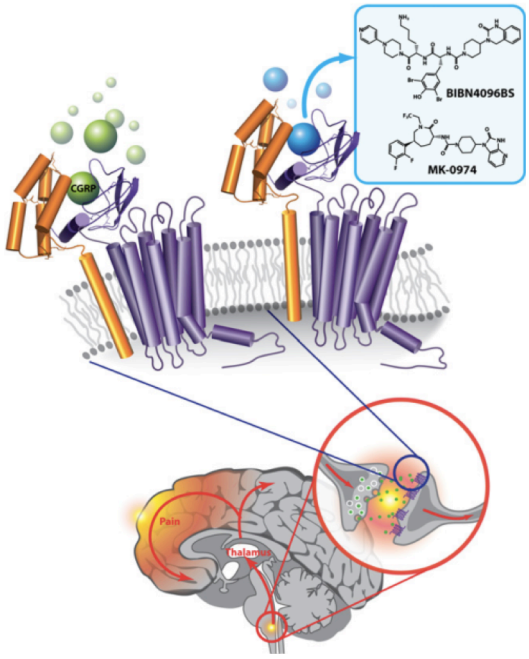

Figure 6.3: Physiological Function of CLR/RAMP1 heterodimer receptor and the role of two non-peptide antagonists
CLR/RAMP1 receptor complex triggers pain through high CGRP level in the brain during migraine attacks. The heterodimer of the extracellular domains of CLR and RAMP1 is responsible for recognising CGRP (green spheres). RAMP1 has potential to bind with high selectivity to the drugs olcegeplant, telcagepant (MK0974), MK-3207, and presumably BMS-694153 (Hay & Poyner 2006; Salvatore et al. 2006; Salvatore et al. 2008; Salvatore et al. 2010; Moore & Salvatore 2012). It is known that the two selective non peptide antagonists, olcegepant (BIBN4096BS) and telcagepant (MK0974) (as blue spheres), compete for the binding of CGRP to the CLR/RAMP1 receptor complex. These drugs are currently undergoing clinical trials. (Figure taken from Siu et al., 2010).

An example is given by migraine headaches, which are associated with the release of CGRP. Migraineurs have higher CGRP levels even between attacks, that triggers throbbing and pulsating pain. The drug prototype, BIBN4096BS (1-piperidinecarboxamide, N-[2-[[5amino-1-[[4- (4-pyridinyl)-1-piperazinyl]carbonyl]pentyl]amino]-1-[(3,5- dibromo-4-hydroxyphenyl)methyl]-2-oxoethyl]-4-(1,4-dihy- dro-2-oxo-3(2H)-quinazolinyl) (Doods et al. 2000), interacts with the N-terminal RAMP1 Trp74 residue and introduces strong selectivity for CGRP receptor (Mallee et al. 2002). This finding suggests that RAMP1 is the key predictor for the olcegeplant BIBN4096BS antagonism (Figure 6.3) (Salvatore et al. 2006). Novel molecules that target RAMP1 interfaces are being continually developed and tested (Benemei et al. 2007; Qi et al. 2011; Moore & Salvatore 2012).

6.1.3 The structure of RAMP1

All three RAMP family members exhibit a common domain structure, consisting of a large extracellular N-terminal domain, a single α-helical transmembrane domain, and a short intracellular C-terminal-domain (Figure 6.4). RAMP1 comprises a 27 amino acid long N-terminal signal sequence followed by a 90 residue long external N-terminal domain, a 22 amino acid long transmembrane domain and 9 C-terminal residues (Hay & Poyner 2006).

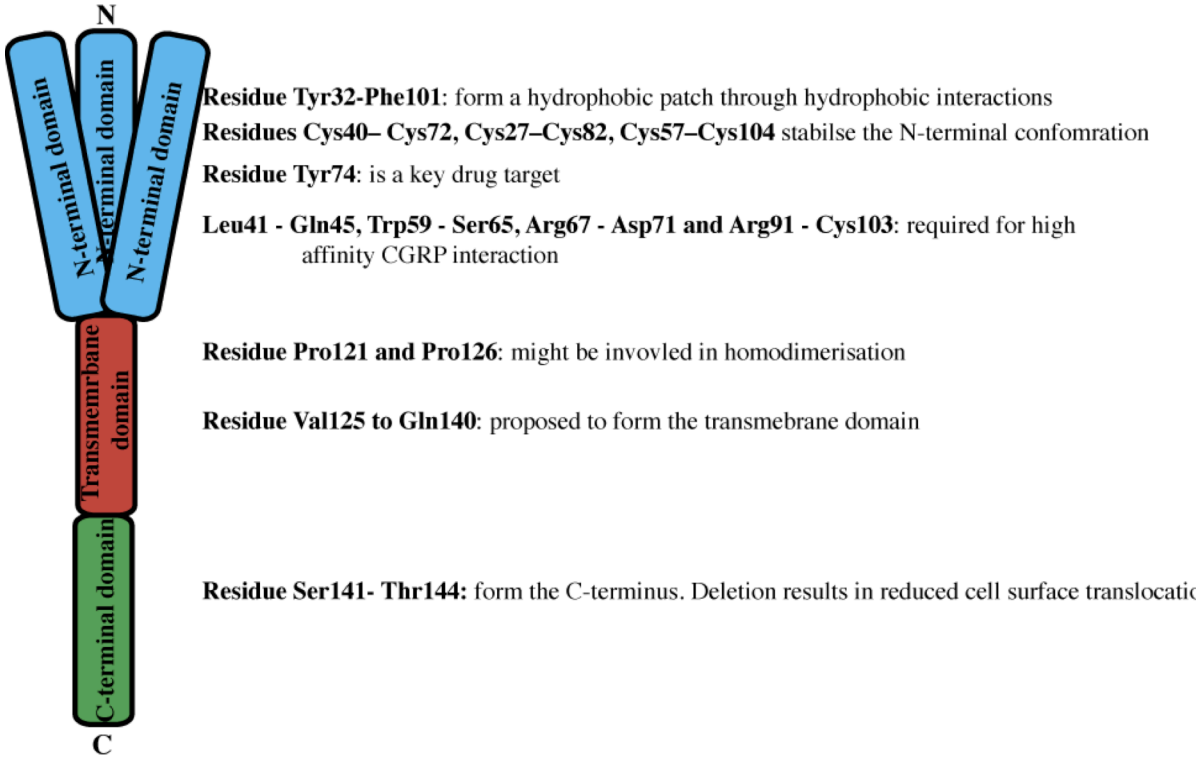

Figure 6.4: Schematic representation of essential RAMP1 regions
(Hilairet et al. 2001, Kuwasako et al. 2003, Udawela et al. 2004, Udawela et al. 2006, Kusano et al. 2008)

6.1.3.1 The N-terminal domain

The extracellular N-terminal domain of RAMP1 engenders specific ligand selectivity on CLR by modulating its glycosylation status from an immature to a mature glycosylated form (Fraser et al. 1999; Hilairet 2001; Fitzsimmons et al. 2003). In 2008 Kusano *et al.* (Kusano et al. 2008) determined the 2.4 Å X-ray structure of this domain in complex with

CLR (Figure 6.5). The overall N-terminal structure consists of a three-helix-bundle (α1 - α3), which is stabilised by three disulphide-bonds between Cys40 – Cys72 (between α1 and α2), Cys27 – Cys82 (between N-terminus to the α2 – α3 loop), Cys57 – Cys104 (between α1 – α2 loop to the C-terminus). RAMP1 heterodimers cluster to form a hydrophobic patch of the aromatic residues on the molecular surface, which is hypothesised to participate in the interaction with CLR and in the formation of the ligand-binding pocket (Kusano et al. 2008).

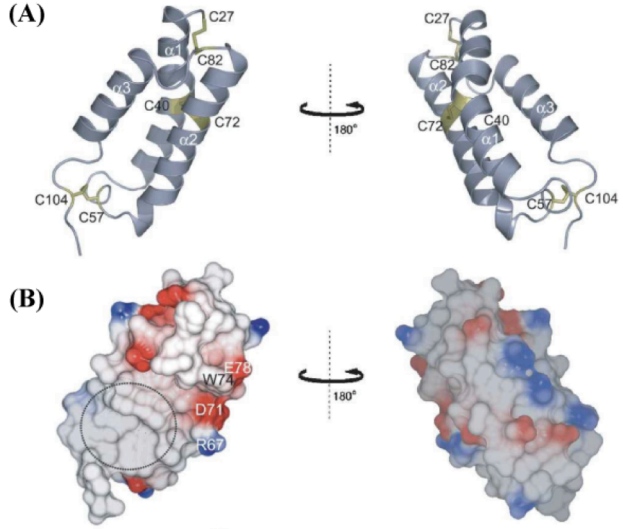

Figure 6.5: Structural features of the molecular surface of RAMP1
(A) Schematic representation of the N-terminal RAMP1 domain. The three disulphide-bonds are shown in yellow.
(B) Representation of the electrostatic potential. The circle indicates the location of the hydrophobic patch, which exists in the shallow concave area between a2 and a3.
(Figure taken from Kusano et al., 2008)

6.1.3.2 The C-terminal domain of RAMP1

The C-terminus of the RAMP1 is only 9 amino acids and exposed to the cytoplasm. Deletion analyses suggest that residues Ser141 to Thr144 form a retention sequence that leads to storage of RAMP1 in the ER in the absence of receptor co-expression (Steiner et al. 2002). Further analysis of the C-terminus revealed that deletion of the C-terminus

decreases the stability of RAMP1/CTR complex leading to reduced cell surface translocation (Udawela et al. 2006).

6.1.3.3 The transmembrane domain of RAMP1

In contrast to the N-terminal domain, little is known structurally about the transmembrane domain of RAMP1 due to the difficulties in working with membrane-embedded peptides. However, it has been shown that the transmembrane domain stabilises the interaction between RAMP1 and receptors and determines the maximal strength of binding (Udawela et al. 2004; Udawela, Christopoulos, Tilakaratne, et al. 2006b; Steiner et al. 2002). Additionally, it has been hypothesised that the transmembrane domain may be involved in RAMP1 dimerisation (see below).

6.1.4 A likely interaction pathway of RAMP1 with CLR

The interaction of RAMP1 with CLR is well studied and illustrates a possible model of RAMP1 in complex with any receptor. So far, it has been shown that CTR interacts with RAMP1 in a similar manner to CLR with a 1:1 stoichiometry. RAMP-CLR association promotes the formation of intramolecular disulphide bonds within RAMP1, which is however not necessary for its heterodimerisation with the receptor. Furthermore, the formation of a RAMP1/CLR complex is associated with a change in the electrophoretic mobility of the RAMP1 monomer (Figure 4.4). The RAMP1/CLR complex is able to continue through the Golgi apparatus, where it is terminally glycosylated, and forms the CGRP-receptor at the cell surface. The heterodimeric RAMP1/CLR complex is required for targeting to the plasma membrane. In the absence of RAMP1, CLR is restricted to the ER (Hilairet 2001). Additionally, when transported to the cell surface, RAMP1 can also interact directly with the immature and mature receptor (Figure 6.6). The following

activation mechanism is consistent with the classical GPCR mechanism (Ferguson et al. 1996; Aiyar et al. 2000).

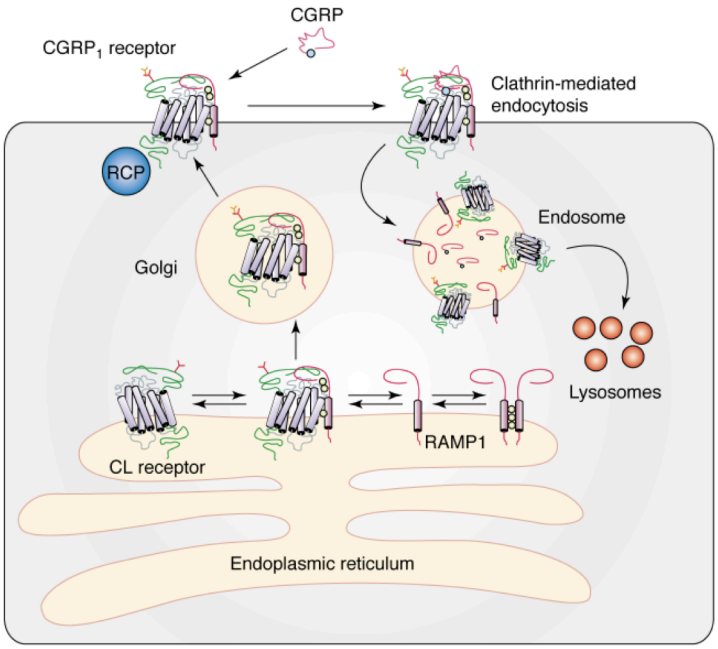

Figure 6.6: Schematic representation of a proposed cycle of RAMP1/CLR complex
In the absence of CLR co-expression, RAMP1 is retained in a parallel homodimeric conformation within the ER and the Golgi apparatus. When co-expressed, RAMP1 forms a heterodimer with the CLR with 1:1 stoichiometry. The CLR enables the complex to pass through the Golgi, where it is terminally glycosylated, and forms the calcitonin gene-related peptide (CGRP) receptor at the cell surface. Stimulation of the receptor by an agonist, such as CGRP, triggers G-protein-dependent intracellular signalling. The agonist–RAMP1–CLR complex is internalised, with the heterodimer remaining stable until lysosomal degradation. (Figure taken from Morfis et al. 2003)

RAMPs, however, remain unique in constituting a fundamental component of at least two GPCRs, CLR and calcitonin receptor. Thus, RAMPs might help us to understand how evolution enabled receptor selectivity through combinatorial mechanisms that generate maximum diversity from a relativly small gene pool (Hilairet 2001).

6.1.5 Current knowledge about dimerisation of RAMP1

Hilairet et al. (Hilairet 2001) discovered that RAMP1 can both heterodimerise with receptors as well as form homodimers. In the absence of the receptor, RAMP1 is retained within the ER and Golgi apparatus, and is able to form homodimers, as well as heterodimers with RAMP2 and RAMP3, which is proposed to regulate accessibility of

the RAMPs to receptors (Héroux et al. 2007; Udawela et al. 2004). Co-expression with CLR significantly increases the expression of RAMP1 and dramatically changes the dimer/monomer ratio such that the monomer becomes the major species. This indicates that the formation of RAMP1/CLR heterodimer is favoured over that of RAMP1 homodimers. A possible explanation for the occurrence of the homodimeric conformation could be a dynamic regulation of the amounts of RAMP1 available to particular receptors (Udawela et al. 2004) or an involvement in the protein synthesis quality control system (Hilairet 2001). Little is understood how RAMP1 homodimerisation occurs, though the extracellular domains of RAMP1 do not dimerise on their own, suggesting that the transmembrane domain may be responsible (Haar et al. 2010; Koth et al. 2010).

6.1.6 Aims of studying RAMP1 on a molecular level

The discovery of RAMPs has revolutionised our perspectives of how receptor diversity is implemented, and recent results support a broader role for RAMPs through interaction with more GPCRs than previously thought. Examination of RAMP1 properties outside of cultured cell systems is important in order to fully understand the molecular basis of RAMP1 function. Moreover, an understanding of what drives dimerisation could expand our view of small accessory proteins. Toward this goal, I have characterised the structural and biophysical properties of the human RAMP1 transmembrane domain and cytoplasmic tail in both monomeric and dimeric forms by solution-state NMR.

6.2 RESULTS

6.2.1 Construct design rationale and amino acid distribution

To facilitate structural and biophysical characterisation of human RAMP1 dimerisation two constructs were designed, which included the entire transmembrane domain and the C-terminal domain as well as some N-terminal residues. The first construct was 47 amino acids long and comprised residues Arg102 to Val148 of human RAMP1. This construct will be referred to as RAMP1tm(102-148). The second construct included solely the transmembrane domain and the C-terminus and included residues Gly116 to Val148. This construct will be described as RAMP1tm(116-148). Since both constructs were intended to be expressed with an insoluble, N-terminal fusion protein and cleaved with cyanogen bromide a methionine was introduced at the beginning of each construct.

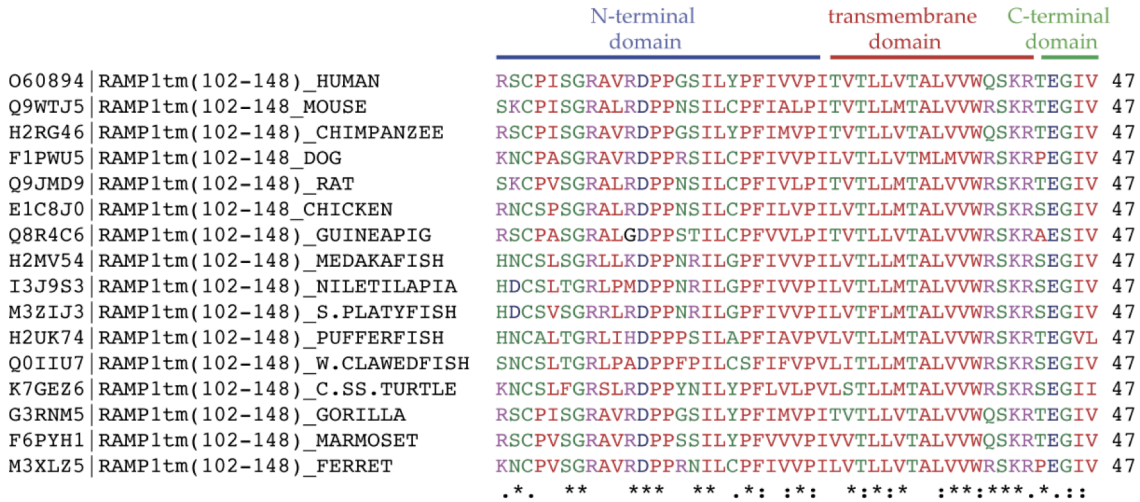

Figure 6.7: Alignment of RAMP1tm(102-148) in multiple organisms show similarity of over 72 % within each other. Alignment was done using the on-line server ClusterW2.

All available RAMP1tm(102-148) sequences indicate 72 % sequence identity (Figure 6.7). Interestingly, four transmembrane prolines at position 114, 115, 121 and 126 are highly conserved across all species, with 121 and 126 lying within the predicted transmembrane domain. Although prolines are not as uncommon in transmembrane α-helices as in

water soluble helices (where they normally break the helix (Heijne 1981)), they do introduce kinks in transmembrane α-helices. Thus prolines are disruptive in transmembrane helices, but they have been proposed to increase helix-packing diversity and specificity (Yohannan, Faham, et al. 2004a). Besides their conservations across species, the two transmembrane prolines in RAMP1 can be found in all three members of the RAMP family (Figure 6.9). The two prolines are at position 121 and 126 in RAMP1 and RAMP3, but are shifted towards the centre of RAMP2 such that the first proline (residue 153) is at the equivalent transmembrane position as Pro121 of RAMP1 and RAMP3, with the second proline (Pro158) four residues away. The RAMP1 region from Gly116 to Trp138 is acidic (theoretical pI = 5.52), whereas the N-terminal and the C-terminal juxtamembrane regions are basic (residues Arg102 to Pro115: theoretical pI = 10.26; residues Glu139 to Val148: theoretical pI = 8.75). Both constructs of interest, RAMP1tm(102-148) and RAMP1tm(116-148), are basic overall with theoretical pI values of 10.04 and 8.59, respectively.

6.2.2 Prediction of RAMP1tm secondary structure and possible dimerisation

The membrane topology and insertion of the transmembrane domain of RAMPs were predicted using TMHMM (Krogh et al. 2001) (Sonnhammer et al. 1998) and (SP)Octopus (Viklund et al. 2008; Viklund & Elofsson 2008). Both on-line prediction servers suggested a single transmembrane domain between amino acids Pro115 and Lys141 (26 amino acids) (Figure 6.8(A,B)). Both servers identified RAMP1tm as a type I integral membrane protein, oriented with an exoplasmic N-terminus (Viklund & Elofsson 2004), consistent with all functional data. RAMP2 and RAMP3 transmembrane regions were predicted to

be 22 amino acids long. RAMPtm's secondary structure features were explored further using PSI-PRED (Buchan et al. 2010; Jones 1999).

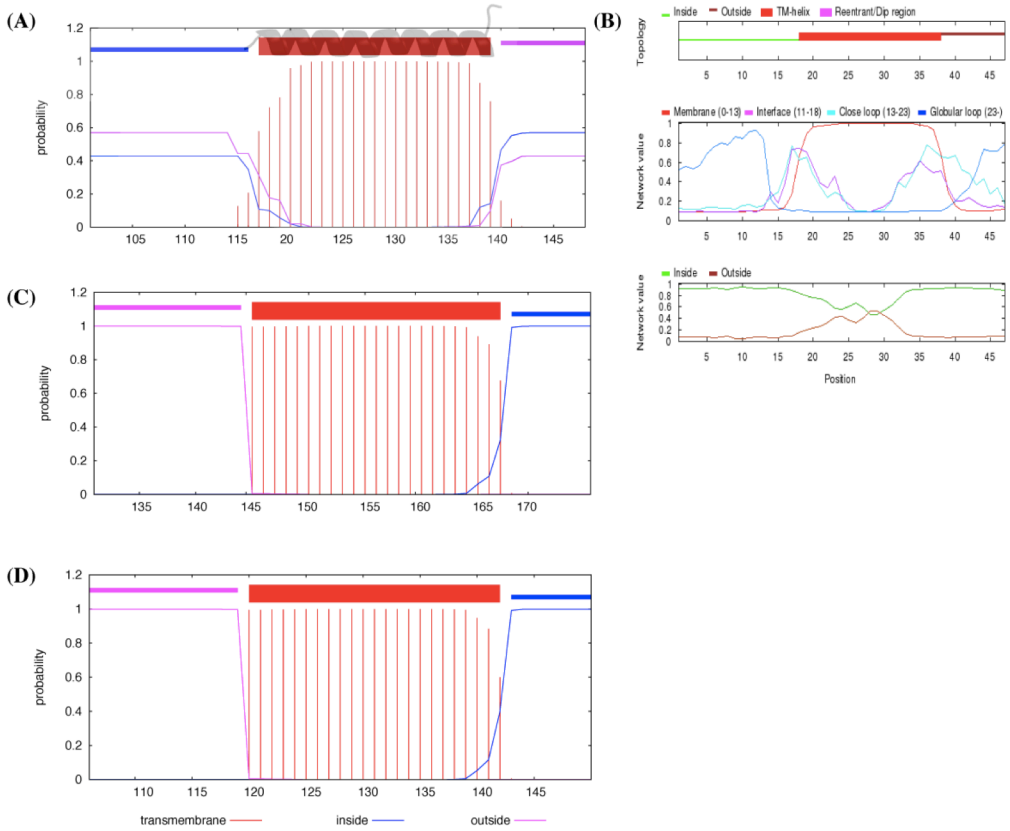

Figure 6.8: Predication of transmembrane domain topology of RAMPtm with
(A) Prediction of RAMP1tm(102-148) with TMHMM-Server and (B) OCTOPUS-Server. Both methods are based on a hidden Markov model and artificial neural networks.
(C) TMHMM-prediction of RAMP2(131-175)
(D) TMHMM-prediction of RAMP3(131-148)

For RAMP1tm, an α-helical region within the transmembrane domain was predicted between residues Val124 and Trp138 (Figure 6.9(B)). Additionally, a short β-sheet between Ser117 and Val123 was suggested, however the prediction confidence in this region was low. Moreover, this structural feature was not identified when predicting the secondary structure for the entire RAMP1 protein (Figure 6.9(A)).

Prediction for RAMP2 showed in PSI-PRED one single transmembrane helix between residues Pro141 and Trp166, with a buried PxxxxP-motif in the hydrophobic core of the domain (Figure 6.9(C)). Similar to RAMP1, RAMP3 was predicted to have a short α-

helical region between residues Ile123 and Gly135, flanked by two β-sheets (residues Glu117 to Val122 and Leu136 to Ser141) with low prediction confidence (Figure 6.9(D)). Investigation of the secondary structure of all three RAMPs suggested a similar secondary structure of RAMP1 and RAMP3. RAMP2 appeared to have an extended α-helical region, which is not affected by the PxxxxP-motif.

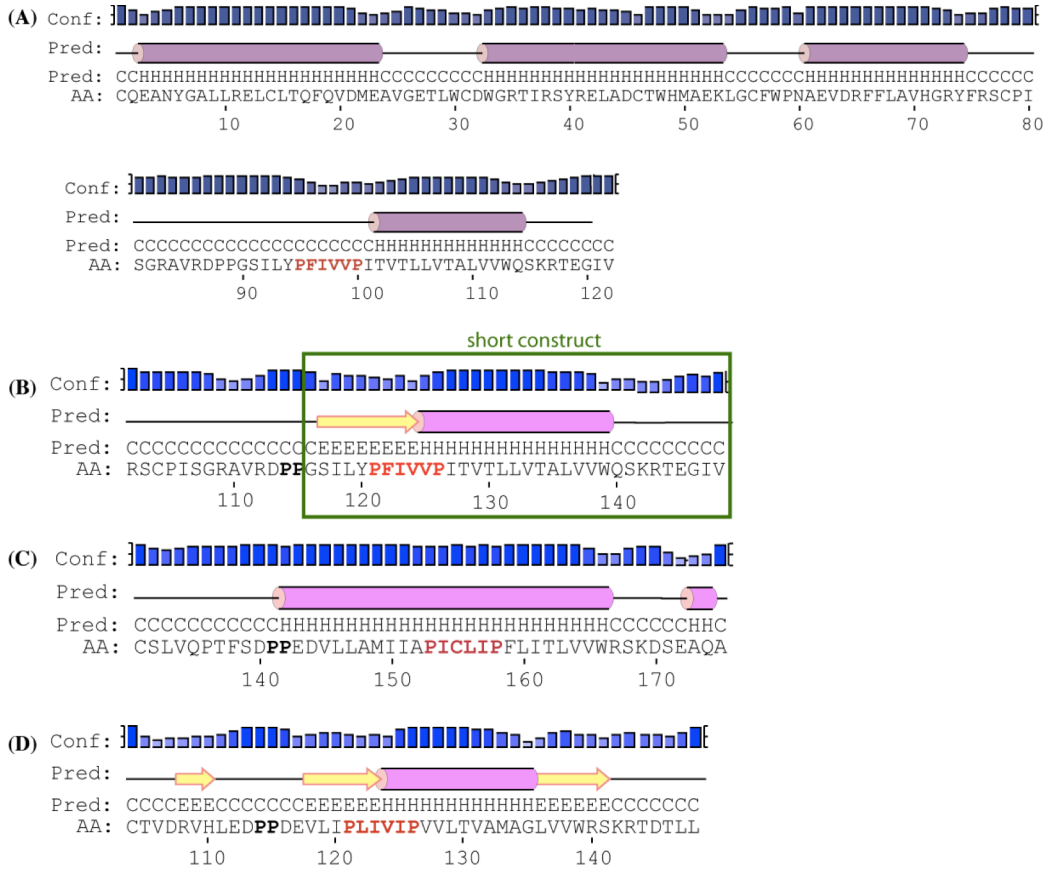

Figure 6.9: Secondary structure prediction of the transmembrane domain of all RAMP family members, using PSI-PRED server
(A) RAMP1
(B) RAMP1tm(102-148); the short construct comprising residues 116 to 148 is boxed.
(C) RAMP2tm(141-175)
(D) RAMP3tm(104-148)

6.2.3 Expression and purification of RAMP1tm constructs

Similar to MRAP constructs, RAMP1tm constructs were cloned into a pMM-LR6 vector as a fusion to the *trpΔLE* gene. RAMP1tm in inclusion-bodies was purified according to Claridge and Schnell (Claridge & Schnell 2011). A flowchart in Figure 6.10 displays the

purification method. The overall yield of homogeneous protein from one litre of Luria Broth media was approximately 6 mg/l. Condensation methods for isotope labelling gave yields of approximately 4 mg of pure protein per litre of M9 minimal media.

6.2.4 Establishing suitable reconstitution conditions for RAMP1tm constructs

Determination of a high-resolution structure of RAMP1tm by solution NMR is crucial to study RAMP's dimerisation and to understand the molecular basis of dimerisation motifs. Different membrane-mimicking detergents were tested for their ability to enable collection of high quality NMR spectra on RAMP1tm constructs. RAMP1tm(102-148) was used to screen suitable conditions and was reconstituted by several refolding methods. However, similar to MRAP(2-67), simple reconstitution into micelles from lyophilised powder gave similar results to more gentle reconstitution methods and thus was used for all subsequent samples. To ensure complete and homogenous solubilisation the sample was freeze-thawed at least five times. Two-dimensional $^{1}H–^{15}N$ HSQC or $^{1}H–^{15}N$ SOFAST-HMQC NMR (Schanda et al. 2005) experiments were routinely collected to evaluate sample properties in different detergent solutions judged by resolution of the spectrum, resonance linewidths together with chemical shift dispersion.

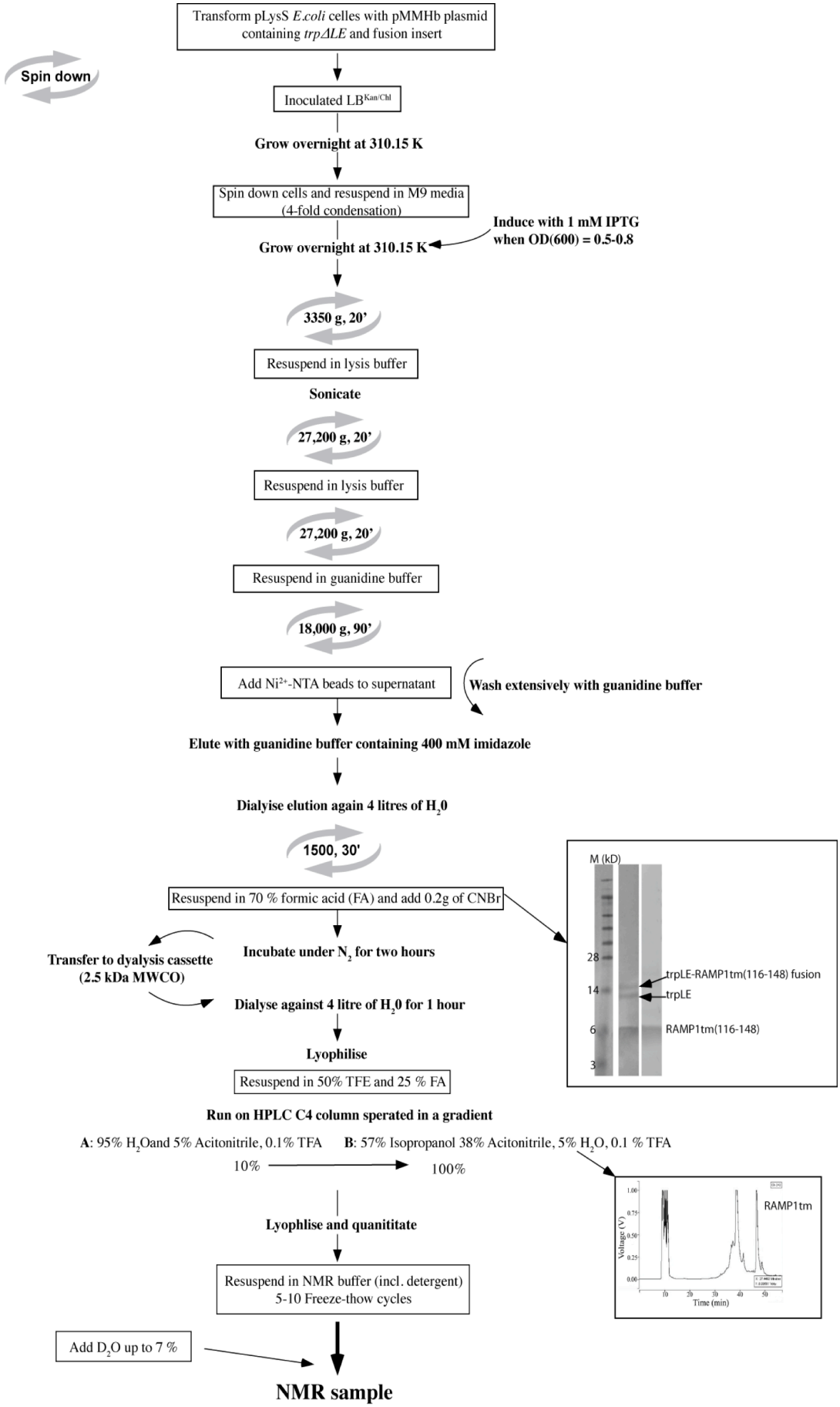

Figure 6.10: A generalised flowchart showing the production and purification of RAMP1tm constructs from trpΔLE fusion expressed in E.coli, with data from a representative RAMP1(116-148) purification shown (adapted from Claridge and Schnell 2011)

The protein concentration was fixed in all cases to 200 μM. Tested detergent included Fos-Choline-12, Fos-Choline-14, DHPC, SDS, LMPG, the lipids DMPG and DPPC as well as mixtures of detergents and lipids (Figure 6.11). Detergents resulting in low solubility (as assessed by visual inspection), yielding few or no detectable crosspeaks in 2D $^{1}H–^{15}N$ HSQCs or $^{1}H–^{15}N$ HMQCs, or poorly resolved crosspeaks in 2D $^{1}H–^{15}N$ HSQCs or $^{1}H–^{15}N$ HMQCs were excluded. Fos-Choline-14 and SDS were most compatible with RAMP1tm(102-148) as assessed by ^{1}H-^{15}N correlation spectra, thus a mixture of both was explored further (Figure 6.11).

Based on the linewidths, the number of observable peaks as well as chemical shift dispersion, 100 % SDS was selected as the most suitable solubilising detergent for further characterisation of RAMP1tm. The detergent concentration was kept at 40 mM, which was the lowest required for solubilisation.

Although highly denaturing for water soluble proteins, SDS micelles allow retention of highly similar secondary structures to that observed in crystal structures transmembrane regions (Micelli et al. 2004; Tulumello & Deber 2012). The molecular modality of SDS results from the anionic polar headgroup, which interacts very strongly with water to increase solubility, and the 12-carbon acyl chain that enwraps the hydrophobic part of the transmembrane peptides (Wu & J. T. Yang 1978; Tanford et al. 1974; Micelli et al. 2004) . As a result, SDS is a highly favourable detergent to study small helical transmembrane proteins, such as RAMP1tm. Notably, I have observed that MRAP(2-67) adopts a highly similar structure in SDS, DHPC or mixed micelles (Chapter 4). Moreover, recent studies have shown that SDS can preserve reasonably well the tertiary structure of membrane proteins with small extramembrane segments (Chill 2006; King et

al. 2011). All experiments were collected in 40 mM SDS (protonated or deuerated) and 50 mM sodium phosphate buffer (pH 6.5) at 310.15 K, unless otherwise stated.

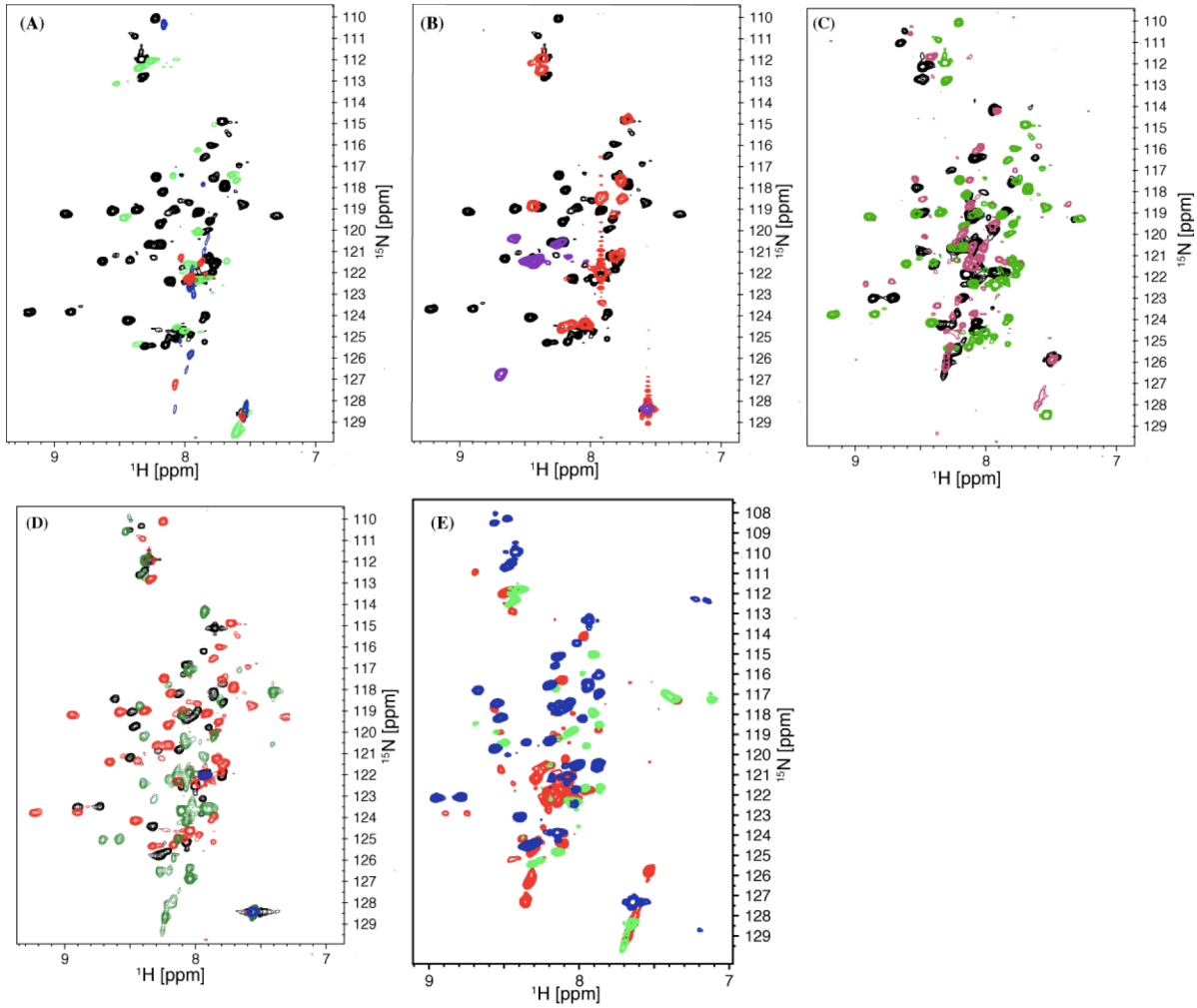

Figure 6.11: Detergent screening for RAMPtm1(102-148)
(A) black - 50 mM SDS; green - 50 mM LMPG; blue – Fos-Choline-14/DPPC (q = 0.4); red - 50 mM DPPC + 15 mM DHPC (q = 0.3); brown - 50 mM Fos-Choline-12
(B) black - 50 mM SDS; red - 44 mM Fos-Choline-14 + 35 mM SDS + 28 mM DMPC; pink - DPPC/DHPC (q = 0.3)
(C) black - 50 mM Fos-Choline-14; red- 50 mM Fos-Choline--12; green - 50 mM SDS
(D) black - 100 mM Fos-Choline-14 + 50mM SDS; red - 50 mM SDS; green - 50 mM Fos-Choline-14
(E) red - 100 mM Fos-Choline-14; green - 25 mM Fos-Choline-14 + 5 mM SDS; blue - 100 mM Fos-Choline-14 + 50 mM SDS

6.2.5 Circular dichroism of RAMP1tm constructs

Secondary structure and folding properties of RAMP1tm constructs were investigated by CD spectroscopy in 40 mM SDS. Additionally, CD of RAMP1tm(116-148) was tested in

DMPC liposomes. In SDS both constructs experienced two negative maxima at ~220 nm and ~210 nm indicating a high α-helical content (Figure 6.12).

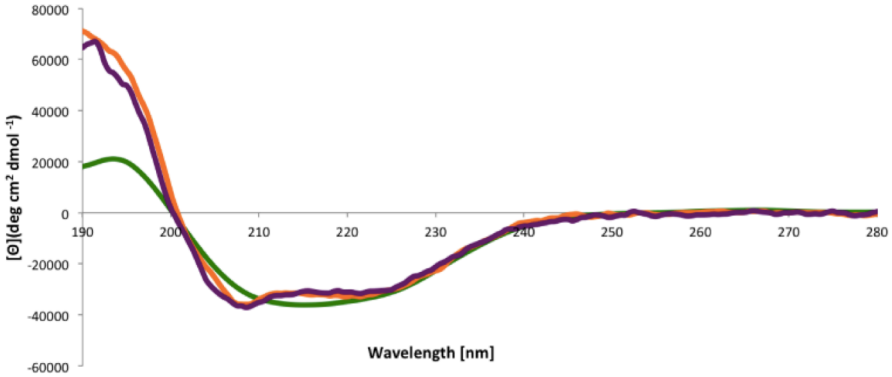

Figure 6.12: Circular dichroism spectra of RAMP1tm(116-148) in 40 mM SDS (orange) and DMPC liposomes (green); and of RAMP1tm(102-148) in 40 mM SDS (purple)

Detergent	**$\theta_{222}/\theta_{208}$**	**Conclusion**
RAMP1tm(102-148)	0.854	α-helical
RAMP1tm(116-148)	0.905	α-helical
Liposomes	Not applicable	

Table 6.2: Examination of the α-helical ratio of RAMP1tm constructs (Libich et al. 2009)

To assess the degree of α-helicity the ratio $\theta_{222}/\theta_{208}$ was calculated (Libich et al. 2009) for MRAP(2-67) in each environment (Table 6.2). RAMP1tm constructs were both found to be α-helical and adopted a highly similar CD spectrum in 40 mM SDS. The ratios between the positive maxima and the negative ones were 2:1, which was an expected value for well-defined α-helical proteins and similar to the one calculated in MRAP(2-67). The CD spectrum in DMPC liposomes provided no clear results, which was attributed to the difficulty in creating a protein-free liposome sample that is identical in all aspects (e.g., concentration and liposome size) for reliable background subtraction.

6.2.6 Spectroscopic characterisation and structure determination

6.2.6.1 Assignment of RAMP1tm(102-148) and RAMP1tm(116-148) in 40 mM SDS

Sequential assignments of RAMP(102-148) and RAMP(116-148) in 40 mM SDS was achieved by using 3D ^{1}H-^{15}N-NOESY-HSQCs (Kumar et al. 1981). For both constructs a mixing time of 110 ms was used. 3D ^{1}H-^{15}N-NOESY-HSQCs was the main experiment for obtaining high-resolution information, due to general signal overlap and low dispersion of peaks caused by the high content of aliphatic amino acids (34 % in RAMP1tm(102-148)). Helix-typical medium-range H_N-{i-3} connectivities were observed on a ^{15}N-separated NOESY throughout the entire transmembrane domain, between residues Pro121 and Thr144 (Figure 6.13).

Triple-resonance experiments HNCA, HNCO, and CBCACONH were collected on RAMP1tm(102-148) to obtain information on intramolecular and intermolecular Cα and Cβ resonances that can aid secondary structure assignment, and to verify the backbone amide assignments. Besides the first residue Arg102, all nonproline backbone amide resonances for RAMP1tm(102-148) were assigned (Figure 6.14). Amide resonances for all nonproline residues of RAMP1tm(116-148), excluding the first residue Gly116, were assigned.

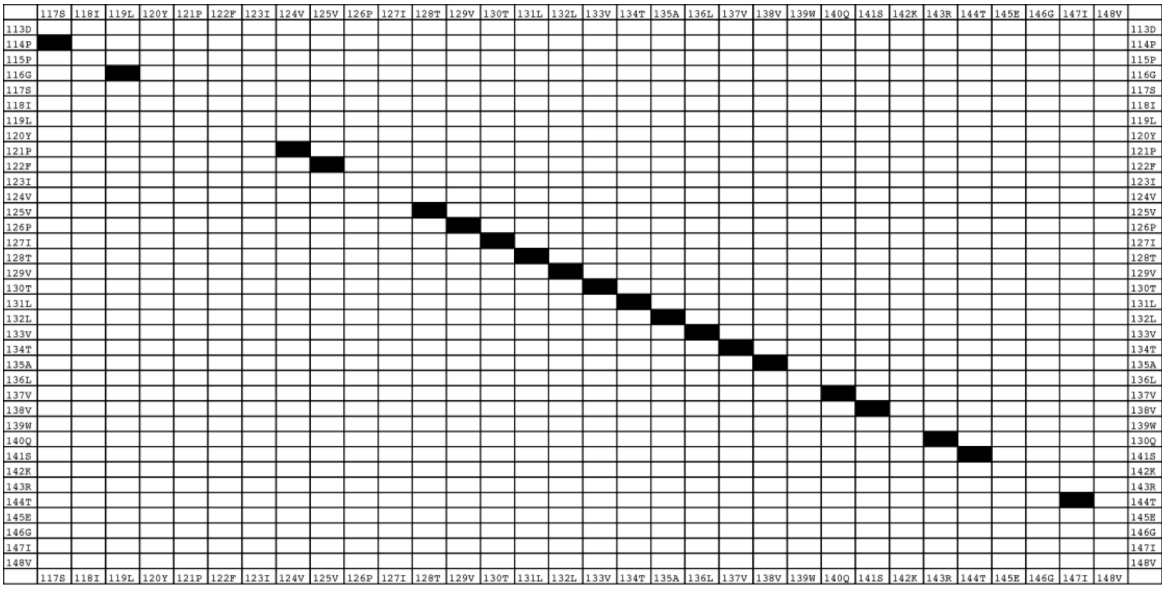

Figure 6.13: Intramolecular NOEs of RAMP(102-148) in 40 mM SDS
Investigation of the consistency of {i}Hα-{i-3} {i}HN-{i-3} NOEs in RAMP1tm(102-148) across the transmembrane domain in 40 mM SDS

Methyl proton and carbon assignments for valine γ-methyls, threonine γ-methyls, alanine β-methyls, and the δ-methyls of leucine and isoleucine in RAMP1tm(102-148) were obtained in a 3D ^{1}H-^{13}C-HSQC-NOESY (mixing time of 200 ms). Deuterated SDS was required to overcome signal overlap and dynamic range limitations. In total 197 resonances were observed. Besides proline residues and the first residue Arg102, all backbone amide resonances for RAMP1tm(102-148) were identified in a ^{15}N-^{1}H-HSQC-NOESY (Figure 6.14). Amide resonances for RAMP1tm(116-148), excluding prolines and the first residue Gly116, were entirely assigned based on ^{1}H-^{15}N-HSQC-NOESY.

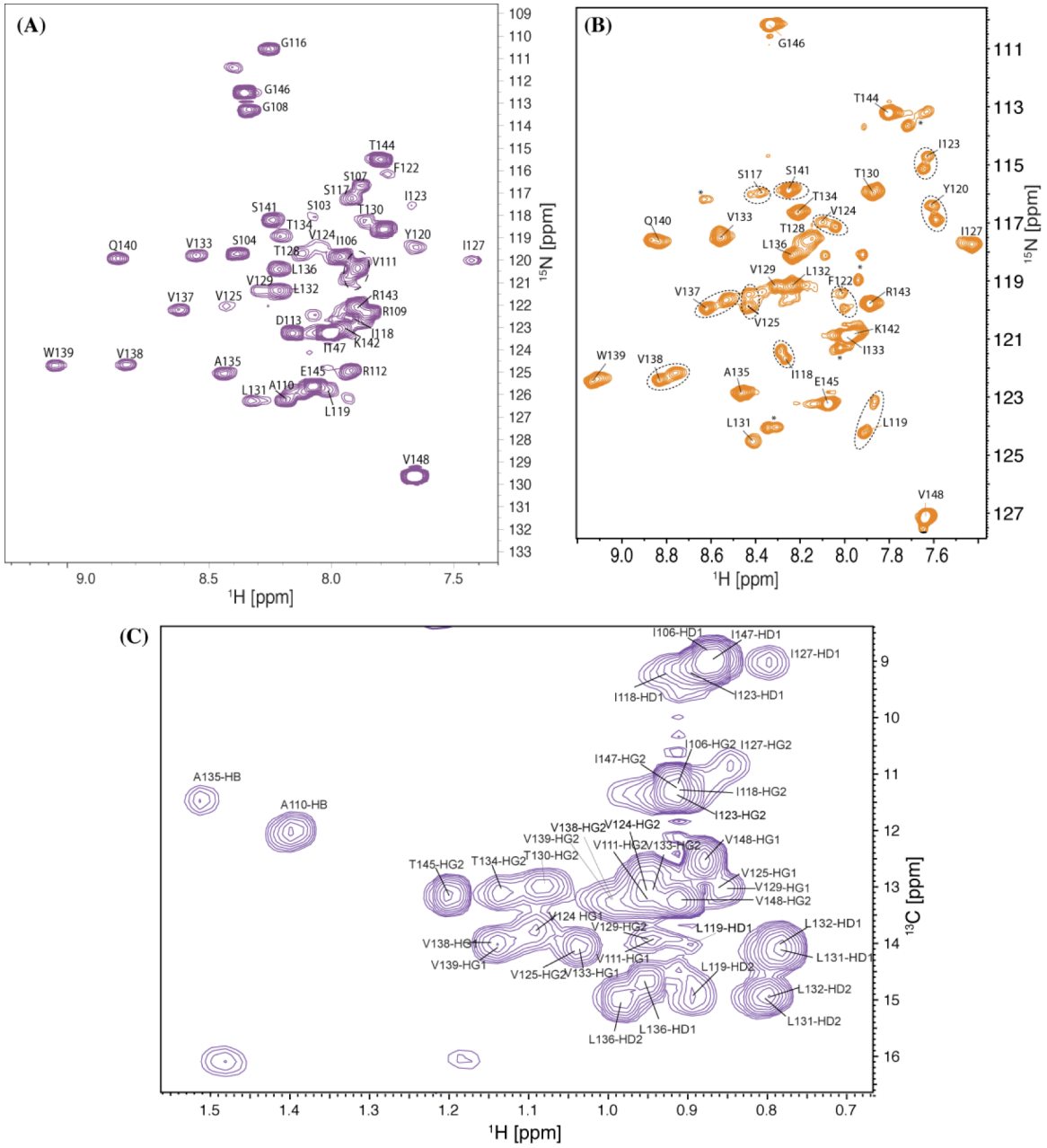

Figure 6.14: Characterisation of RAMP1tm(102-148) and RAMP1tm(116-148) in 40 mM SDS and 50 mM sodium phosphate buffer (pH 6.5)
(A) ^{15}N-^{1}H backbone assignment of RAMP1tm(102-148)
(B) ^{15}N-^{1}H backbone assignment of RAMP1tm(116-148)
(C) ^{13}C-^{1}H sidechain assignment of methyl protonated valines, leucines and isoleucines of RAMP1tm(102-148)

6.2.6.2 Collection of residual dipolar coupling in 40 mM SDS

Residual dipolar couplings (RDCs) were acquired to improve the resolution of RAMP1tm and to validate the NOE-based structures that were obtained (Opella & Marassi 2004; Lipsitz & Tjandra 2004). RDCs were only possible to obtain on the

construct RAMP1tm(102-148), which was attributed to the lack of alignability of the RAMP1tm(116-148)/micelle complex, which is expected to be approximately spherical. Similar to that described in Chapter 4 for MRAP(2-67) partial protein alignment was generated by an anisotropically stretched polyacrylamide gel with a concentration of 4.4 % (Chou et al. 2001). ^{1}H-^{15}N HSQC and ^{1}H-^{15}N TROSY experiments were collected on isotropic and anisotropic samples. The RDC for each residue was then acquired by subtracting the coupling constant measured in the isotropic sample from that measured on the anisotropic sample.

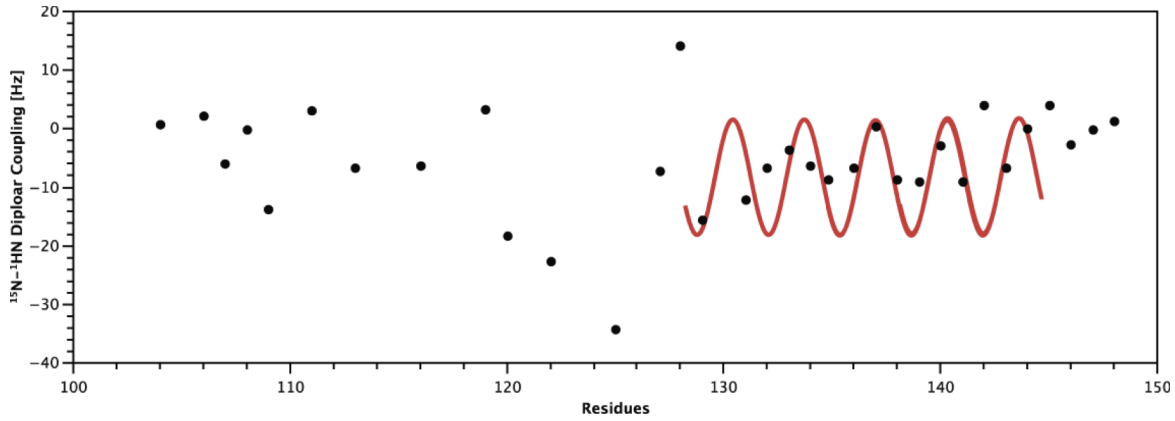

Figure 6.15: Dipolar wave analysis of experimental ^{15}N-$^{1}H_N$ Residual Dipolar Coupling data sets of RAMP1tm(102-148) in 40 mM SDS

A total of 23 RDCs were experimentally measured for structured regions of RAMP1tm(102-147). Dipolar wave analysis was performed, by fitting the experimental data to a simple sinusoid with a periodicity of 3.6 (Figure 6.15 - red lines) (Mesleh et al. 2002; Mascioni & Veglia 2003; Lee et al. 2003).

6.2.6.3 Structure calculation of monomeric RAMP1tm

Structure calculations of RAMP1tm were performed using XPLOR-NIH 2.21 (Schwieters et al. 2003). Both constructs, RAMP1tm(102-148) and RAMP1tm(116-148), were investigated separately. A python-based calculation protocol similar to the one applied

on MRAP(2-67) structure (see Chapter 4) was used. For structure calculations of RAMP1tm(102-148) a total of 360 distance restraints was obtained, for RAMP1tm(116-148) 295 distance restraints were measured. Additionally, secondary structure motifs and torsion angle restraints were determined from backbone chemical shifts by TALOS+ (Shen et al. 2009). A total of 74 ϕ and ψ backbone torsion angles were predicted for RAMP1tm(102-148) and 40 ϕ and ψ backbone torsion angles were computed for RAMP1tm(116-148). 31 residual dipolar coupling restraints were determined used for further refinement for the construct RAMP1tm(102-148). All experimentally obtained restraints were implemented into structure calculations. A complete list of NMR distances and dihedral constraints used for structure calculations is shown in Table 6.3.

NMR distance and dihedral constraints		
Distance constraints	**RAMP1tm(102-148)**	**RAMP1tm(116-148)**
Total NOE	360	295
Sequential (*i, i-1*)	127	102
Medium-range (*i-3*)	233	193
Long-range (*i-4*)	0	0
Backbone H_N RDC constraints	23	0
Hydrogen bonds	31	15
Total dihedral angle restraints		
ϕ	37	20
ψ	37	20

Table 6.3: NMR statistics for RAMP1tm constructs in 40 mM SDS

The average root-mean square deviation (RMSD) was calculated for only the structural regions of RAMP1tm constructs. For Cα backbone residues of RAMP1tm(102-148) the RMSD was 1.25 ± 0.32 Å, while that for RAMP1tm(116-148) was 1.52 ± 0.56 Å. The complete statistical evaluation is presented in Table 6.4. Overall RMSD values for RAMP1tm(102-148) were lower than for the one RAMP1tm(116-148).

Structure statistics		
Violations (mean ± s.d.)	**RAMP1tm(102-148)**	**RAMP1tm(116-148)**
Distance constraints (Å)	0.075	0.052
Dihedral angle constraints (º)	0.583	0.513
RDCs, rms in Hz	0.074	-
Deviations from idealised geometry		
Bond length (Å)	0.001	0.000
Bond angle (º)	0.037	0.026
Impropers (º)	0.476	0.368
ϕ/ψ in most favoured or allowed regions, %	98.7 %	97.8 %
Average pairwise r.m.s.deviation (Å)		
RMSD (Å)	RAMP1tm(102-148)	RAMP1tm(116-148)
Backbone (all structured regions)	1.25 ± 0.32 Å	1.52 ± 0.56 Å
Heavy (all structured regions)	1.86 ± 0.30 Å	2.37 ± 0.84 Å

Table 6.4: NMR refinement statistics for RAMP1tm constructs

Figure 6.16 depicts an ensemble of the ten best monomeric RAMP1tm structures in 40 mM SDS, derived from experimentally obtained NOEs. These ensembles were used to further evaluate the quality of calculated structures. The ensembles indicated that the structures were well defined for the helical regions. Both constructs displayed the same α-helical regions. The PxxxxP-motif was embedded in a short helix between residues Pro121 and Val125. Residues Val129 and Arg143 formed the transmembrane domain helix (Figure 6.16).

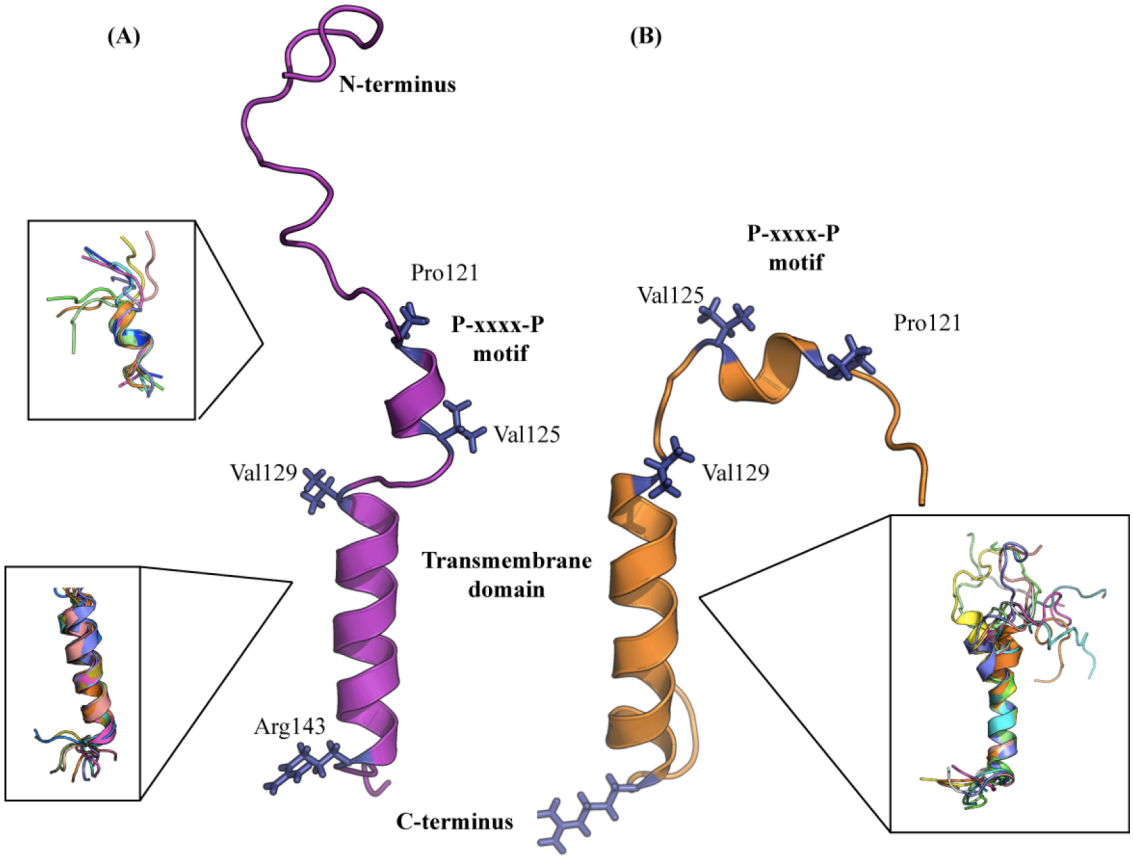

Figure 6.16: Investigation of the structure of RAMP1tm in 40 mM SDS
The best ten structures of (A) RAMP1tm(102-148) and (B) RAMP1tm(116-148) are shown. However, the disordered regions in between the helical domains made an overlay of the entire structure uninformative. The helical regions were well defined across detergents across constructs.

6.2.6.4 Evaluation of structure quality

iCing (Doreleijers et al. 2012) was used to compare experimental data with the NMR-derived structural models. Ramachandran plots assessed the quality of each structure. Both RAMP1tm constructs exhibited good Ramachandran statistics for structured regions (Figure 6.17 (A+B)). RAMP1tm(102-148) showed slightly better values for favourable Ramachandran spaces (+0.90 %) than RAMP1tm(116-148). Arg143 was the only outlier in RAMP1tm(116-148). Thr144 was located in the generously allowed region in both constructs.

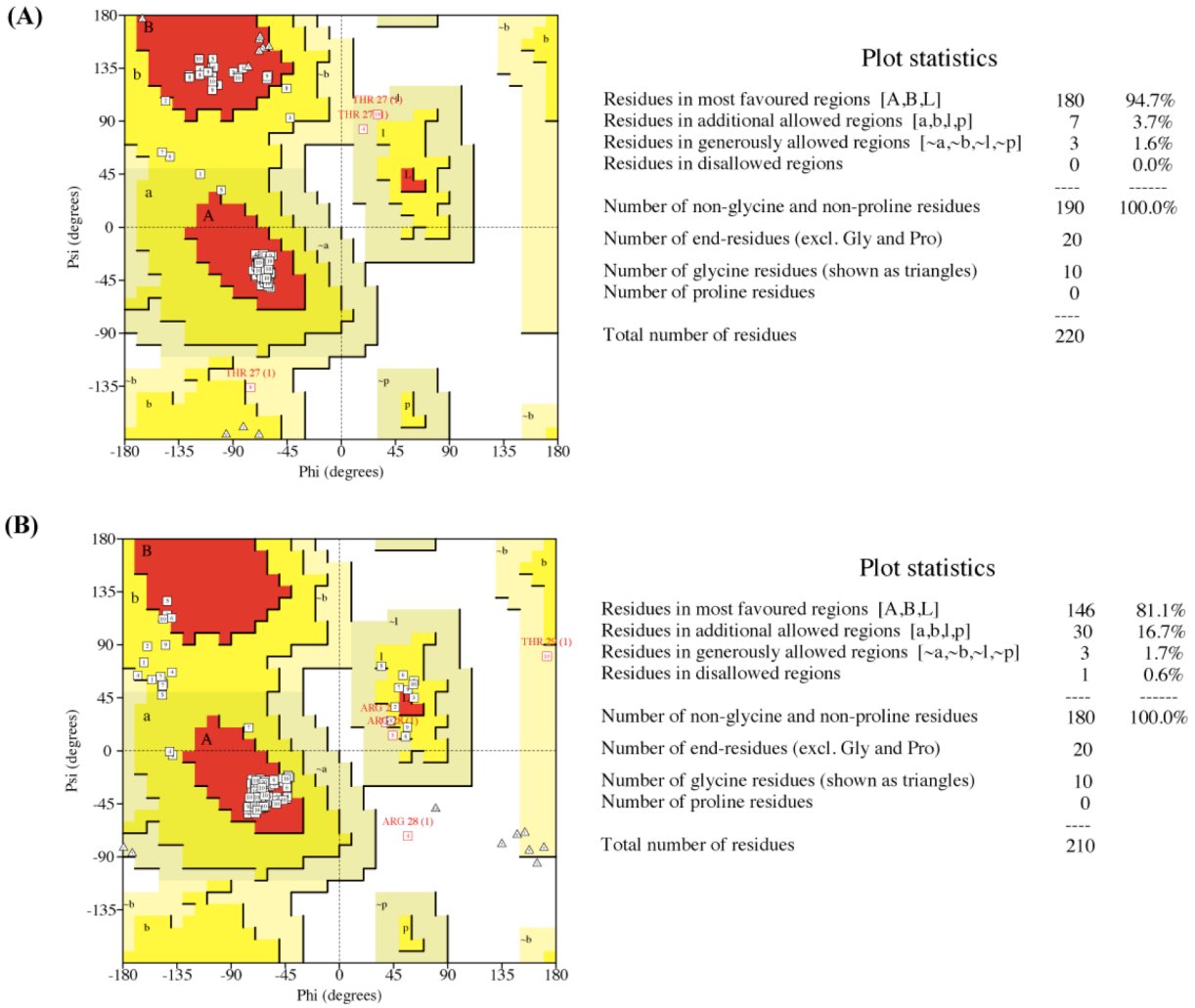

Figure 6.17: Ramachandran plot of RAMP1tm constructs in 40 mM SDS generated by iCing.
(A) Ramachandran plot of RAMP1tm(102-148)
(B) Ramachandran plot of RAMP1tm(116-148)

6.2.6.4.1 Residual dipolar coupling for evaluation

50 structures of RAMP1tm(102-148) in 40 mM SDS were refined against experimental obtained RDC restraints. RMSDs over the ten best structures illustrated good convergence (Table 6.5). In general, RMSD values decreased only slightly after refinement with RDCs.

RMSD (Å)	*without RDCs*	*with RDCs*
Backbone (all structured regions)	*1.25 ± 0.32 Å*	*1.22 ± 0.28 Å*
Heavy (all structured regions)	*1.86 ± 0.30 Å*	*1.76 ± 0.22 Å*

Table 6.5: RMSD assessment for structures calculated with and without RDC restraints

Ramachandran plot analysis was used to re-evaluate the newly refined structures of RAMP1tm(102-148). Refining the RAMP1tm structure against RDCs improved Ramachandran statistics for the structured regions.

Region assessment (%)	*without RDCs*	*with RDCs*
Most favoured regions	*94.7 %*	*100 %*
Additional allowed regions	*3.7 %*	*0 %*
Generously allowed regions	*1.6 %*	*0 %*
Disallowed regions	*0.0 %*	*0 %*

Table 6.6: Ramachandran plot assessment for structures calculated without and with RDC

Overall, the extensive agreement between structure ensembles calculated by XPLOR-NIH and obtained after refinement with RDCs gave good confidence in the quality of the experimentally NOE-derived RAMP1tm(102-148) structure.

The program MODULE (Dosset et al. 2001) was used to fit RDC constraints onto the NOE-derived RAMP1tm(102-148) structure to determine the alignment tensor parameters for individual or multiple domains within a protein. Two alignment tensors, one for the PxxxxP-motif (residue Pro121 to Pro126) and one for the transmembrane residues Leu131 to Glu145, were required to fit RDC data onto the helical region (Figure 6.18(A)).

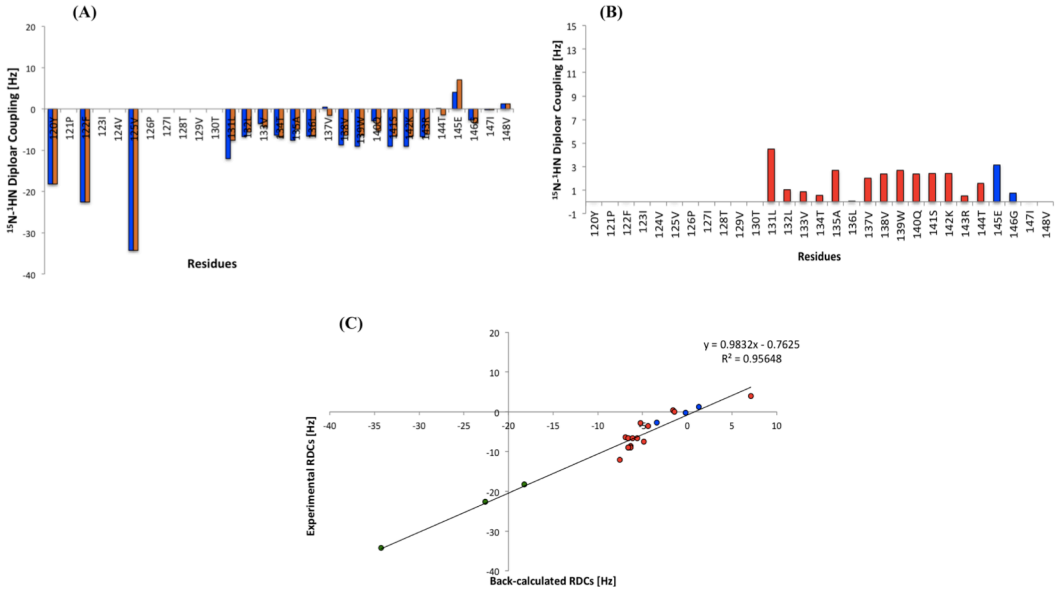

Figure 6.18: Correlation plots of experimental ^{15}N-$^{1}H_N$ Residual Dipolar Coupling data sets of RAMP1 calculated with two alignment tensors, between the PxxxxP-motif and the transmembrane region
One alignment tensor was set defining the transmembrane domain.
(A) Experimental and back-calculated ^{15}N-$^{1}H_N$ RDCs
(B) Difference between experimental and back-calculated ^{15}N-$^{1}H_N$ RDCs
(C) Correlation of experimental back-calculated RDCs

The correlation between experimental and back-calculated RDC values was high (Figure 6.18(B), with a correlation coefficient R^2 after refinement of the structure with RDCs of 0.956. The good agreement between the experimental data and the calculated values Figure 6.18(C) demonstrated that the calculated structure satisfied the RDC data.

	Alignment tensor on residues Pro121-Pro126	Alignment tensors on residues Leu131-Glu145
A_a ($1e^{-4}$)	30.06	7.14
A_r ($1e^{-4}$)	4.64	1.47
α	-38.15	-6.98
β	176.20	94.87
γ	-32.50	-30.93
χ^2 Exp	0	193.37

Table 6.7: Alignment tensors for RAMP1tm(102-148) in 40 mM SDS

The domain dependent parameters, which are listed in Table 6.7, suggested a prolate spheroid micelle shape for SDS, including the target protein. This result was based on the A_a/A_r obtained value for the transmembrane region, which was calculated to be 4.8.

A similar shape was suggested for MRAP(2-67) in DHPC micelles (A_a /A_r = 1.6) (subchapter 4.2.5.5.1). However, the difference in values suggested a more significant prolate shaped spheroid for RAMP1tm(102-148) than for MRAP(2-67).

In conclusion, collected RDCs of RAMP1tm(102-148) were consistent with the obtained structure, defining two helical regions (residues Pro121 to Val125 and residues Val129 to Arg143).

6.2.7 Comparison of chemical shift perturbation between the monomeric RAMP1tm(102-148) and RAMP1tm(116-148)

To gain insights into possible differences between the two RAMP1tm constructs chemical shift perturbation (CSP) was carried out. ^{1}H-^{15}N HSQC-experiments were recorded on 200 μM ^{15}N-labelled labelled samples in 40 mM SDS. Comparison of ^{1}H-^{15}N backbone resonances between RAMP1tm(102-148) and RAMP1tm(116-148) revealed little perturbation ($\Delta\delta \leq 0.1$) across the transmembrane domain and the PxxxxP-motif (Figure 6.18 (B)).

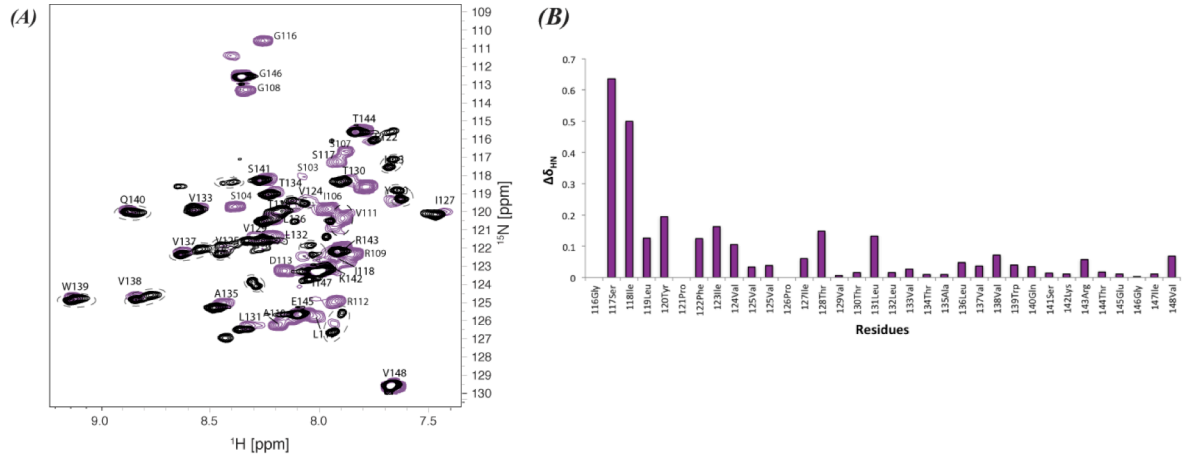

Figure 6.19: Difference between long RAMP1tm(102-148) and short RAMP1tm(116-148) in 40 mM SDS at 600 MHz at 301.15 K
(A) ^{1}H-^{15}N HSQC of RAMP1tm(102-148) [purple] and RAMP1tm(116-148) [black]
(B) Chemical shift perturbation between RAMP1tm(102-148) and short RAMP1tm(116-147)

Unsurprisingly, the flexible N-terminal residues Ser117 to Tyr120 exhibited the largest shift changes (Δδ = 0.21 – 0.64). Since only very few shift perturbations were observed, this finding gave confidence in a similar secondary structure between the two constructs.

6.2.8 Establishing a dimeric interface

6.2.8.1 Crosslinking of RAMP1tm(116-148) in SDS and DMPC

RAMP1tm(116-148) was chemically crosslinked in 40 mM SDS and DMPC liposomes to evaluate its oligomerisaiton properties. Samples in SDS micelles were prepared by simple reconstitution as described previously. Liposomes were formed by dissolving DMPC in 100 % TFE in a glass vial and rotating the vial under a weak nitrogen stream until a thin film was created. This process was repeated twice before solubilised protein was added. Formation of a thin film was repeated twice and followed by lyophilisation. After re-hydration in 50 mM sodium phosphate buffer the target sample was added. To allow the formation of covalent bonds between two or more molecules each crosslinking reaction with 7 mM DSP was enabled for 5 minutes before being quenched with 100 mM

TrisHCl.

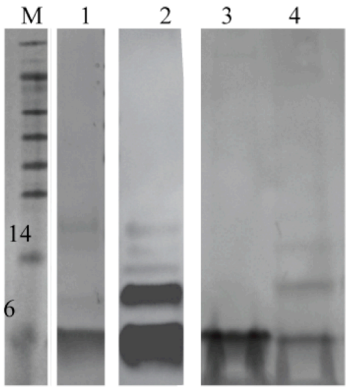

Figure 6.20: Crosslinking of RAMP1tm(116-148) in 40 mM SDS and DMPC liposomes with 7 mM DSP
1 - RAMP1tm(116-148) in 40 mM SDS
2 - RAMP1tm(116-148) in 40 mM SDS crosslinked
3 - RAMP1tm(116-148) in DMPC liposomes
4 - RAMP1tm(116-148) in DMPC liposomes crosslinked

Crosslinking in SDS micelles and DMPC liposomes indicated a monomeric and a dimeric conformation of RAMP1tm(116-148) (Figure 6.20).

6.2.8.2 Concentration dependence and peak doubling of RAMP1tm constructs

To establish whether the acquired findings in crosslinking experiments are due to specific dimerisation or rather to non-specific interactions concentration dependency and peak doubling of RAMP1tm(116-148) was examined. Peak doublings can be a consequence of oligomerisation or conformational changes; hence the existence of peak doubling could give information about a possible dimeric conformation of RAMP1tm. Additionally, RAMP1tm(102-148) was analysed to identify differences between the long and the short construct.

A protein concentration dependent titration of both samples was carried out. The protein concentration of RAMP1tm(102-148) was increased from 50 µM to 850 µM within four titration steps. Neither concentration dependent peak doubling nor oligomerisation was observed (Figure 6.20).

For RAMP1tm(116-148) the spectrum was monitored over a protein concentration range of 25 μM to 900 μM within five steps (25 μM, 50 μM, 75 μM, 250 μM, 900 μM). Peak doubling was detected at early titration steps, between 25 μM and 250 μM, in residues Ile117, Leu118, Leu119, Tyr120, Phe122, Val124, Val125, Val137, Val138, Gln140 and Ser141 (Figure 6.20). The intensity ratio of each peak doublet was compared across concentrations and normalised to Thr121, which did not show concentration dependent changes. At a concentration of 900 μM the spectrum of RAMP1tm(116-148) showed oligomerisation and aggregation.

The N-terminal residues Ile117, Leu118, Tyr120, Val124 and Val125 experienced no dramatic intensity changes between the two observed peaks of the same residue as a function of concentration. This might be due to a conformational change and interaction with the detergent. However, residue Val124 showed a dramatic change in intensity ratio at only one titration point, which might be explained by a concentration-dependent conformational change.

Doubled peaks of residues Leu119 and Phe122 displayed large concentration-dependent changes in intensity ratios. In the transmembrane domain residues Val137, Val138, Gln140 and Ser141 exhibited peak doubling. There the difference of intensity ratios showed substantial concentration dependencies.

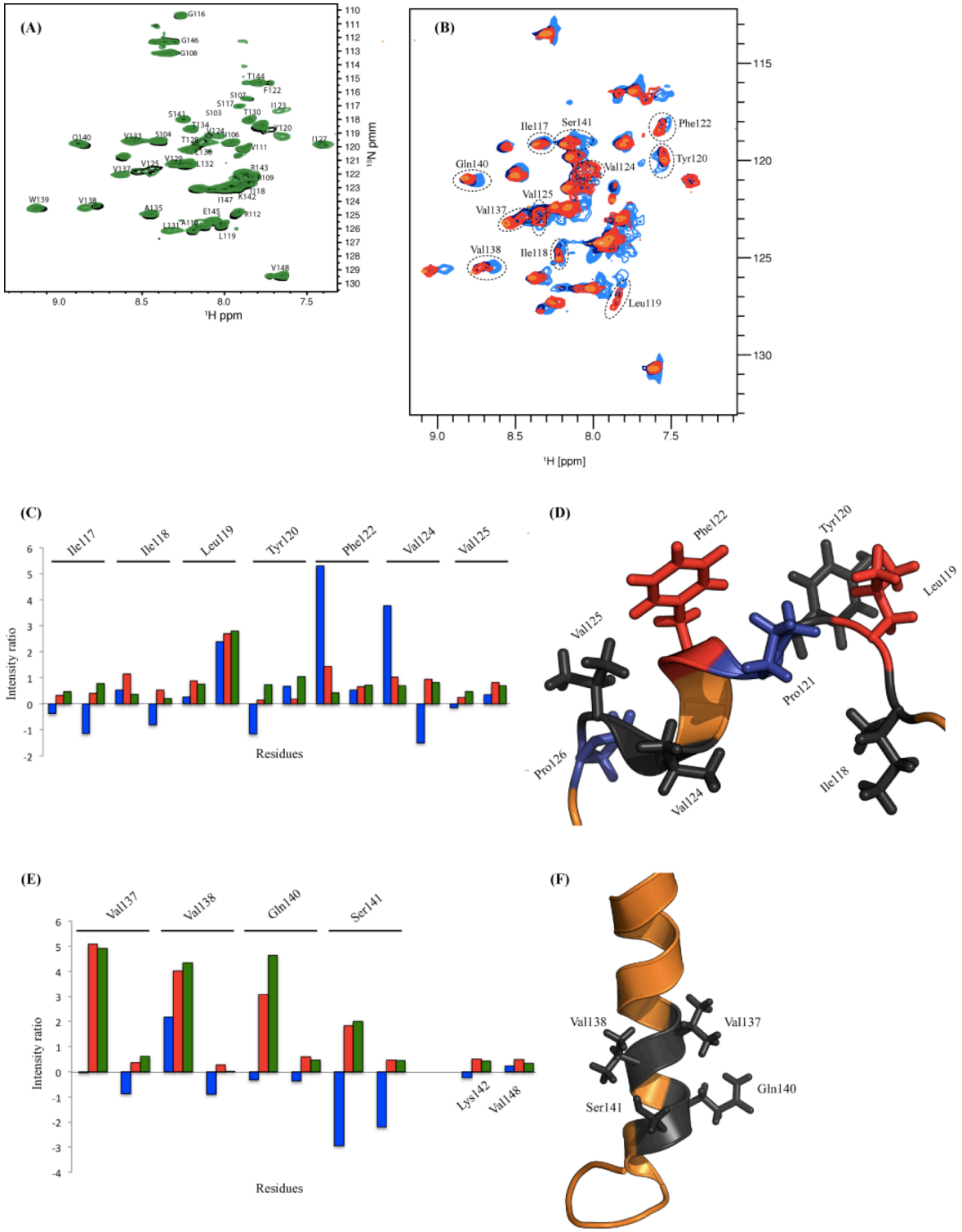

Figure 6.21: Concentration dependency and peak doubling in RAMP1tm construct.
(A) No peak doubling nor oligomerisation was detected in RAMP1tm(102-148)
Colouring: black – 250 μM; green – 800 μM
(B) Resonance doubling was observed in in RAMP1tm(116-148). Peak doublets are indicated by dashed circles.
Colouring: orange - 25 μM; red - 50 μM; dark blue - 75 μM; light blue - 250 μM
(C) The difference in intension ratio of N-terminal doubles in RAMP1tm(116-148) and their (D) position on the monomeric structure.
(E) The difference in intension ratio of transmembrane doubles in RAMP1tm(116-148) and their (F) position on the monomeric structure. Lys142 and Val148 were included as negative controls, which did not experience resonance doubling.
Colouring: blue - intensity ratio of 25 μM to 250 μM; red - intensity ratio of 50 μM to 250 μM; green - intensity ratio of 75 μM to 250 μM

Thus, the N-terminal peak doubling of RAMP1tm(116-148) did not appear to be strongly concentration dependent, and may be due to a heterogeneous population of local conformations. By contrast, the doublings in the transmembrane region were concentration dependent. This observation along with the presence of a dimer band in gels of crosslinked RAMP1tm(116-148) supported the conclusion that the protein was dimerising via the transmembrane domain, and that at high concentrations RAMP1tm(116-148) exists as a population of monomer and dimer species in slow exchange. The small chemical shift differences between the two sets of resonances, however, suggested a high structural similarity.

Notably, RAMP1tm(102-148), did not exhibit peak doubling, suggesting that the additional N-terminal residues were preventing peptide association, perhaps through interactions with SDS micelles.

6.2.8.3 Acquiring intermolecular NOEs for a dimeric RAMP1tm(116-148) interface

To confirm the obtained results on a possible dimeric conformation of RAMP1tm(116-148) and to further establish an interface by solution NMR, attempts were made to detect intermolecular NOEs. 3D ^{1}H-^{15}N-NOESY-HSQC experiments were recorded in 40 mM deuerated SDS at 750 MHz (250 ms mixing time) on samples of RAMP1tm(102-148) or RAMP1tm(116-148) that contained equimolar amounts of unlabelled and $^{2}H^{15}N$-labelled peptide. Consistent with the results described in the previous subchapter, no intermolecular NOEs were obtained for RAMP1tm(102-148). However, five intermolecular NOE-pairs were collected for shorter construct RAMP1tm(116-148) (Table

6.8). Interestingly, the obtained resonance doublets of residues Val137 and Gln140 were on the interface of a dimeric construct. Thus the peak doubling likely arose from the two different environments for the monomer and dimer conformation.

Monomer 1	*Monomer 2*
Val129 H_N	*Val129 Hγ*
Val133 H_N	*Val133 Hγ1*
Val133 H_N	*Val133 Hγ2*
Val137 H_N	*Val137 Hγ1*
Gln140 H_N	*Gln140 Hβ*

Table 6.8: Observed intermolecular NOEs of RAMP1tm(116-148)

6.2.9 Structure calculation of the parallel dimeric RAMP1tm(116-148)

The dimeric structure of RAMP1(116-148) was calculated starting from the monomeric form and calculated with the established XPLOR-NIH 2.21 protocol (Schwieters et al. 2003) with inclusion of the five experimentally acquired intermolecular NOEs.

Figure 6.22 depicts the final dimeric RAMP1tm(116-148) structure in 40 mM SDS, derived from experimentally obtained NOEs. An ensemble of the ten structures with the lowest overall energies was used to represent the dimer structure.

Evaluation of the structural regions of the dimeric structure with iCING (Doreleijers et al. 2012) showed good agreement within the Ramachandran plot (Figure 6.22(B)). The RMSD value for Cα backbone residues was computed to be 3.51 ± 1.29 Å. Considering the dimeric nature of this protein the calculated RMSD value together with the Ramachandran plot statistics gave confidence in the quality of structure. The complete statistical evaluation is presented in Table 6.9.

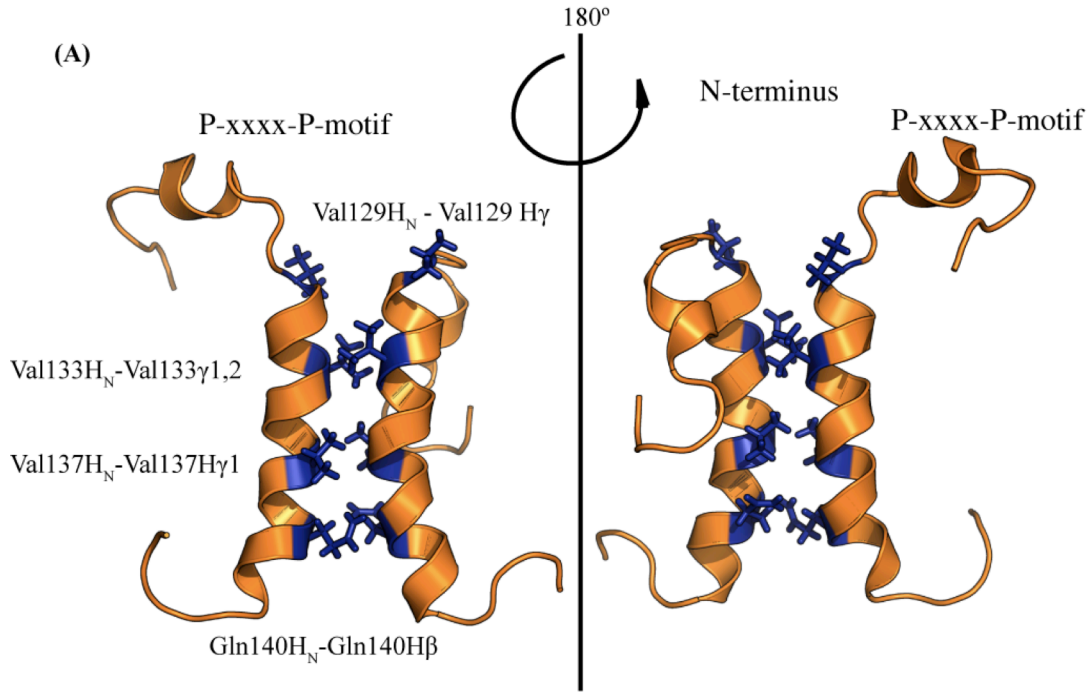

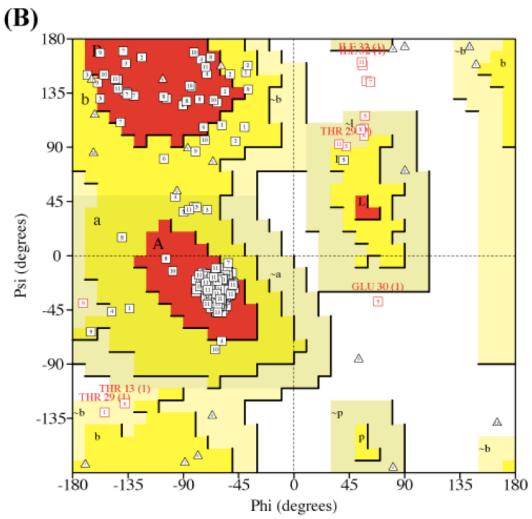

Plot statistics

Residues in most favoured regions [A,B,L]	379	90.7%
Residues in additional allowed regions [a,b,l,p]	25	6.0%
Residues in generously allowed regions [~a,~b,~l,~p]	9	2.2%
Residues in disallowed regions	5	1.2%
Number of non-glycine and non-proline residues	418	100.0%
Number of end-residues (excl. Gly and Pro)	44	
Number of glycine residues (shown as triangles)	22	
Number of proline residues	0	
Total number of residues	484	

Figure 6.22: Dimeric RAMP1tm(116-148) structure in 40 mM SDS
(A) Schematic representation of the dimeric RAMP1tm(116-148) structure. Blue indicates the residues for which the five intermolecular NOEs were observed.
(B) Ramachandran plot and statistics of the dimeric RAMP1tm(116-148)

Structure statistics	
Violations (mean ± s.d.)	**RAMP1tm(116-148)**
Distance constraints (Å)	0.90
Dihedral angle constraints (º)	0.475
Deviations from idealised geometry	
Bond length (Å)	0.000
Bond angle (º)	0.023
Impropers (º)	0.347
ϕ/ψ in most favoured or allowed regions, %	96.7 %
Average pairwise r.m.s.deviation (Å)	
RMSD (Å)	RAMP1tm(116-148)
Backbone (all structured regions)	3.51 ± 1.29 Å
Heavy (all structured regions)	3.95 ± 1.21 Å

Table 6.9: NMR refinement statistics for dimeric structure of RAMP1tm(116-148) in 40 mM SDS

6.2.10 Dynamics of RAMP1tm constructs in 40 mM SDS

The dynamics of RAMP1tm constructs were investigated by analysis of the relaxation parameters ^{15}N R_1, ^{15}N R_2 and {^1H}-^{15}N heteronuclear NOEs, which were measured at 500 MHz (303.15 K). {^1H}-^{15}N heteronuclear NOEs were determined from the ratio of peak intensities with and without an amide proton saturation period, I_{on}/I_{off}. ^{15}N R_1 and R_2 relaxation values were acquired from a series of 2D experiments with different delay times, which were chosen according to Cramer-Rao theory (Farrow et al. 1994). The obtained relaxation parameters were analysed using the program NMRPipe (Delaglio et al. 1995). The exact parameters are described in Chapter 3 (Methods and Materials).

Overall, the analyses suggested similar dynamics in both RAMP1tm constructs. Ser117 exhibited large differences in dynamics between RAMP1tm(102-148) and RAMP1tm(116-148), which was unsurprising as it is close to the site of truncation. Moreover, nine peak doublets were observed at Ile118, Leu119, Tyr120, Phe122, Val124, Val125, Val137, Val138 and Gln140 and are described in the previous subchapter. Peak doubling either

occurred as a consequence of exchange with the detergent (N-terminal residues) or as a result of dimerisation (within the transmembrane domain). These peaks were analysed separately across the entire section and are indicated in blue triangles.

In RAMP1tm(102-148) $\{^{1}H\}$-^{15}N heteronuclear NOE values > 0.50 were observed in residues Tyr120 to Arg143, whereas in RAMP1tm(116-148) values above 0.50 were observed only in the region between residues Val125 and Arg143. Residues Gly146 to Val148, in both constructs, and amino acid Ser117 in the monomeric RAMP1tm(116-148) depicted negative values and hence were very flexible. Residue Phe122 experienced a large error in all constructs, which was due to its resonance being very broad and likely undergoing slow timescale dynamics, which may be due to the nearby Pro121 (Figure 6.23). Obtained $\{^{1}H\}$-^{15}N heteronuclear NOE values for peak doublets within the N-terminal domain were less stabilised than the monomeric constructs. This was an expected result, since it was likely that the PxxxxP-motif was helix destabilising. In addition, this region contains a high proportion of β-branched amino acids, which are helix-destabilising. Doubled resonances in the transmembrane domain exhibited similar values as the monomeric conformations (Figure 6.22; indicated by blue triangles).

R_1 values were fairly constant throughout both constructs. RAMP1tm(102-148) and RAMP1tm(116-148) showed highly similar values for the transmembrane region starting at residues Leu132 up to the C-terminus. Interestingly, the PxxxxP-motif and residues Ile118, Leu119 and Tyr120, exhibited higher values in RAMP1tm(102-148) than in RAMP1tm(116-148). Similar to $\{^{1}H\}$-^{15}N heteronuclear NOE findings, N-terminal residues that experienced resonance doubling were less stabilised than in the monomeric conformation and the doubled residues in the transmembrane domain were more stable

than their monomeric ones, consistent with stabilisation of the protein in the dimeric form.

R_2 values indicated structure for both constructs between residue Val125 and Arg143, with a dramatic decrease at residue Ser142, indicating a highly flexible C-terminus. Ile127 exhibited a significantly higher R_2 value than any other residues, indicating the likely presence of conformational exchange on the microsecond to millisecond timescale, which may have been due to the adjacent proline. Residues within the PxxxxP-motif increased gradually until residue Val125. R_2 values for peak doublets confirmed the findings in R_2 relaxation measurements, with the transmembrane doublets showing higher stabilisation than in monomeric conformations.

The average for RAMP1tm(102-148) value for R_1 values was 1.22 ± 0.03 s^{-1} and for R_2 values it was 12.74 ± 0.42 s^{-1}. Obtained values for RAMP1tm(116-148) were highly similar with an average R_1 value of 1.20 ± 0.10 s^{-1} and an average R_2 value of 13.22 ± 0.70 s^{-1}. Values for mean and standard deviation of R_1 and R_2 in all constructs are displayed in table 6.10.

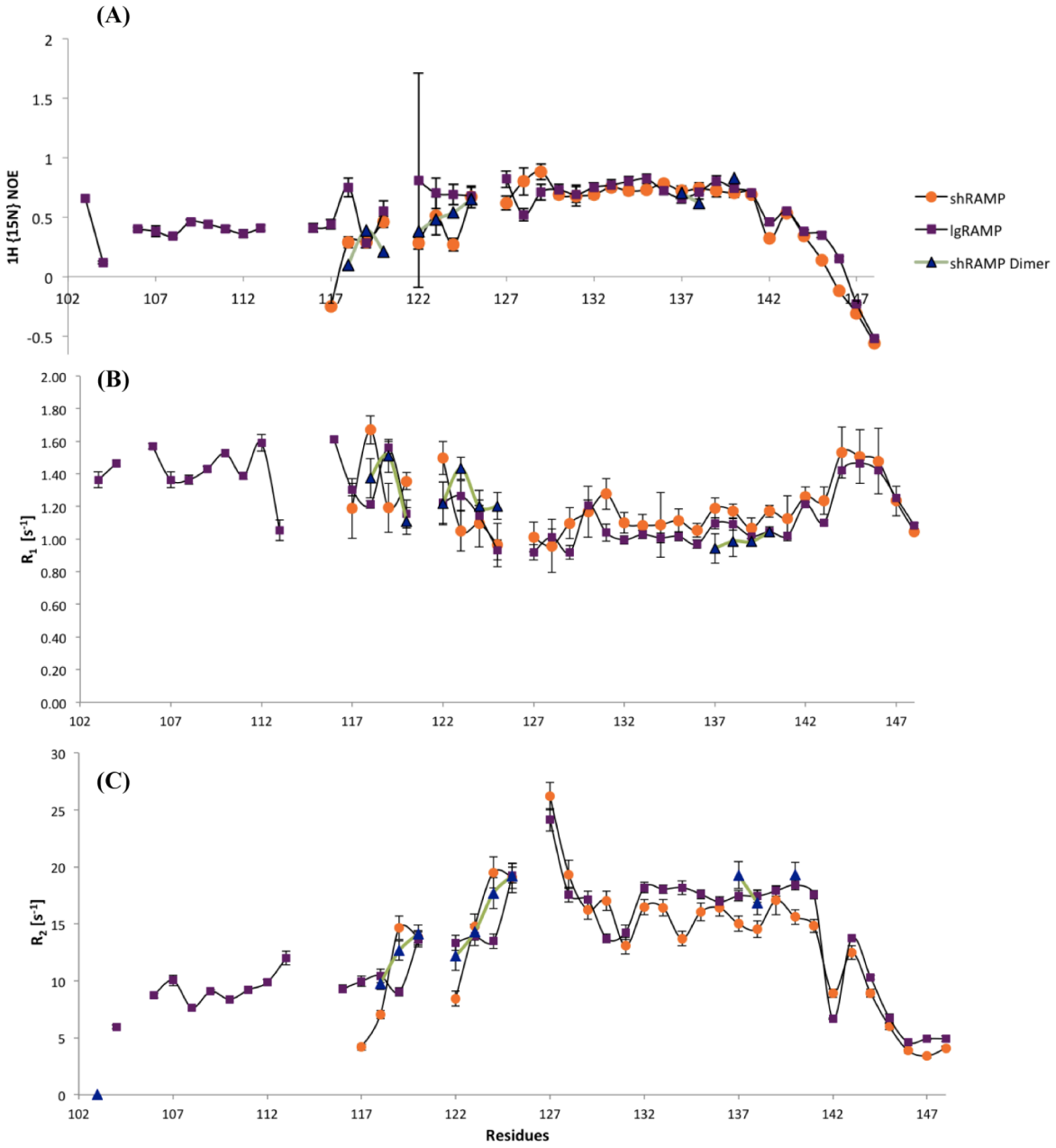

Figure 6.23: Dynamics of RAMP1tm(102-148) and RAMP1tm(116-148) in 40 mM SDS at 600MHz
(A) {^{1}H}-^{15}N heteronuclear NOE of RAMP1tm
(B) R_1 of RAMP1tm
(C) R_2 of RAMP1tm
Colouring: purple - RAMP1tm(102-148);orange - monomeric RAMP1tm(116-148); blue- resonance doublets of RAMP1tm(116-148)

The ratio R_2/R_1 and R_1*R_2 for each residue provided initial estimations for structured regions of RAMP1tm constructs and those that undergo chemical shift exchange on the microsecond to millisecond timescale. R_1*R_2 was used to distinguish between motional anisotropy and chemical exchange (Kneller et al. 2002). R_1*R_2 showed low values (R_1*R_2 <

10 s^{-2}) at the C-terminus. No significant difference outside the error range was observed between RAMP1tm(102-148) and RAMP1tm(116-148). The average R_1*R_2 ratio for RAMP1tm(102-148) was calculated to be 14.69 ± 0.99 s^{-2}. For RAMP1tm(116-148) average R_1*R_2 ratio was 15.25 ± 2.15 s^{-2} (Figure 6.23).

	R_1	R_2	R_2/R_1
RAMP1tm(102-148)			
Average	1.22 ± 0.03 s^{-1}	12.74 ± 0.42 s^{-1}	11.36 ± 0.79 s^{-2}
Standard deviation	0.21 s^{-1}	4.89 s^{-1}	
RAMP1tm(116-148)			
Average	1.20 ± 0.10 s^{-1}	13.22 ± 0.70 s^{-1}	11.64 ± 1.69 s^{-2}
Standard deviation	0.18 s^{-1}	5.47 s^{-1}	

Table 6.10: R_2/R_1 ratio values for RAMP1tm constructs in 40 mM SDS

High R_2/R_1 values for residues Leu132 to Ser141 delimited the core transmembrane domain in both constructs. Overall, the R_2/R_1 ratio for the longer construct, RAMP1tm(102-148), indicated a comparatively more stable secondary structure of the transmembrane region than RAMP1tm(116-148) (Figure 5.32(B)). The average R_2/R_1 ratio over RAMP1tm(102-148) was calculated to be 11.35 ± 0.79 s^{-2} and over RAMP1tm(116-148) it computed to be 11.64 ± 1.69 s^{-2} (Figure 6.23). Interestingly, the difference in ratios between RAMP1tm(102-148) and RAMP1tm(116-148) was small, although the error in RAMP1tm(116-148) was higher.

Separate investigation of the motional anisotropy and chemical exchange was performed by display of R_1*R_2 versus R_1/R_2 (Kneller et al. 2002). For both monomeric constructs the distribution of ^{15}N relaxation rates suggested a strong bias in the orientation of the H_N bond vectors and a motionally anisotropic transmembrane region. The N-terminal helix was suggested to be moving on a fast timescale (Figure 6.23(C); in blue), whereas the PxxxxP-motif was located close to the trimmed mean (Figure 6.23 (CD)- in green).

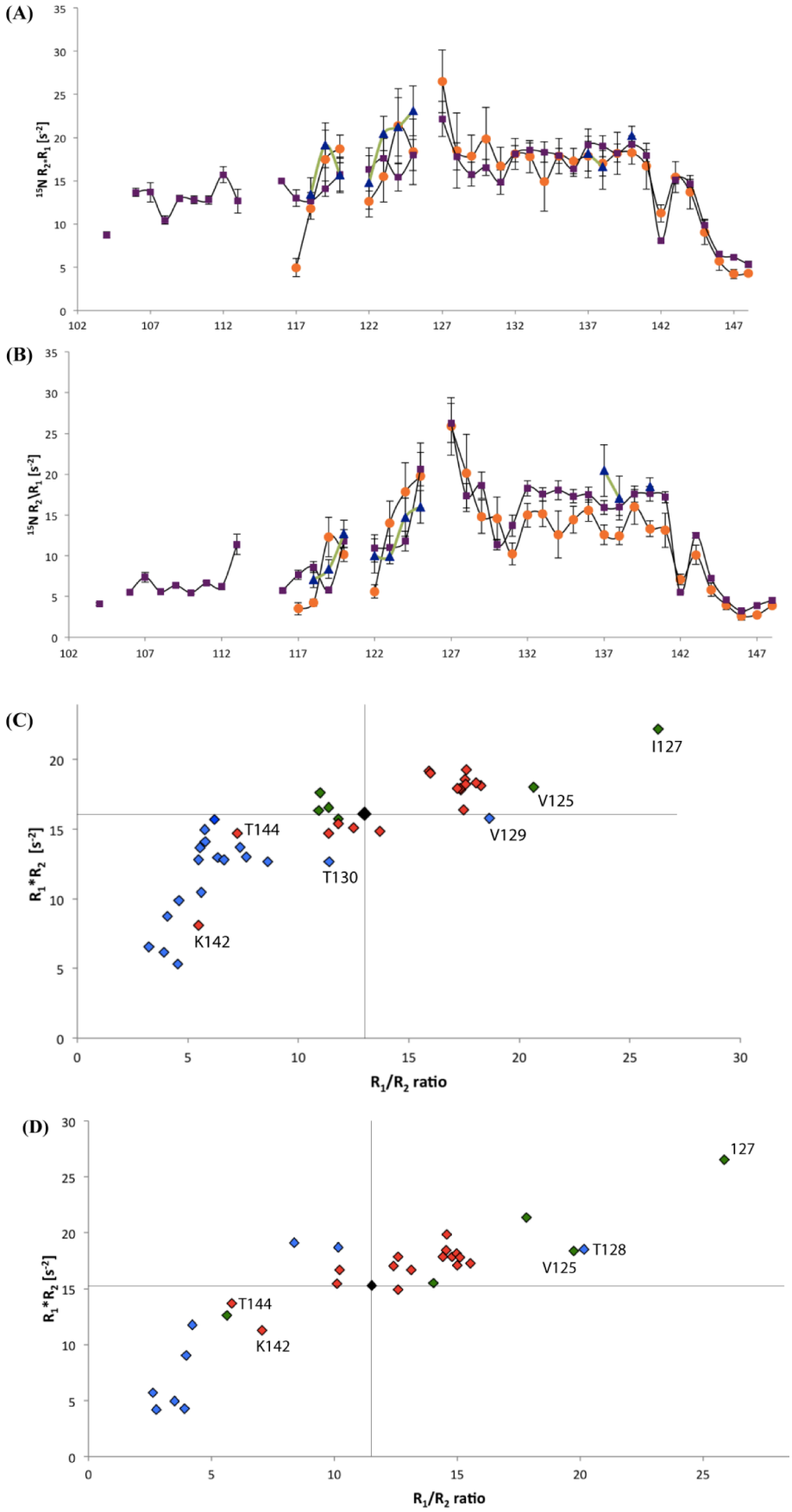

Figure 6.24: Motional Anisotropy of RAMP1tm in 40 mM SDS
*(A) R1*R2 of RAMP1tm constructs; (B) R2/R1 of RAMP1tm constructs; (C) Motional Anisotropy of RAMP1tm(102-148); (D) Motional Anisotropy of RAMP1tm(116-148)*
Colouring: purple - RAMP1tm(102-148); orange - RAMP1tm(116-148); blue peak doublets of RAMP1tm(116-148)

Surprisingly, residues Val125 and Ile127 showed slow timescale exchange. This might indicate slow motions of Pro126. Most transmembrane residues "clustered" slightly above the trimmed mean. Residue Lys142 and Tyr144 were located at the border of the micelles, thus may have dynamic interactions with the detergent headgroup region.

The overall rotational correlation time, τ_c, was calculated for different RAMP1tm regions and provided further useful insights into tumbling times and structural features. τ_c-values are stated in Tables 6.11.

	RAMP1tm(102-148)	RAMP1tm(116-148)	Dimeric
τ_c of the entire construct	10 ns	10 ns	11 ns
τ_c of the transmembrane region	11 ns	11 ns	11 ns
τ_c of the PxxxxP-motif	11 ns	12 ns	11 ns

Table 6.11: Rotational correlation time τ_c of RAMP1tm constructs

τ_c values of both monomeric constructs were highly similar. Interestingly, no significant difference in the tumbling time between transmembrane domain and PxxxxP-motif was observed. This is likely due to the N-terminal addition in RAMP1tm(102-148) being highly flexible and not contributing to the overall molecular tumbling time.

Summarising, R_1 and R_2 values for both constructs were highly similar and suggested a similar monomeric secondary structure. Additionally, the PxxxxP-motif appeared to be more stabilised within the dimeric than a monomeric RAMP1tm construct.

6.2.11 Investigation of the depth of insertion of RAMP1tm(102-148) in 40mM SDS micelles

6.2.11.1 By water-soluble PRE

The water-soluble paramagnetic broadening agent $Mn^{2+}EDDA^{2-}$ was used to explore which residues are protected by the SDS micelles from the environment (Lau et al. 2008).

Since the monomeric conformation of both constructs behaved similar only RAMP1tm(102-148) was investigated.

A clear steep increase in I/I_0 values defined the protected transmembrane region between residues Ile123 and Trp139. The central positions between these boundaries were residues Tyr130 and Leu132. The N-terminal domain, in general, experienced strong line broadening in presence of the paramagnetic spin label indicating water accessibility. These results were in good agreement with the predicted transmembrane domain from PSI-PRED, TMHMM and (SP)Octopus.

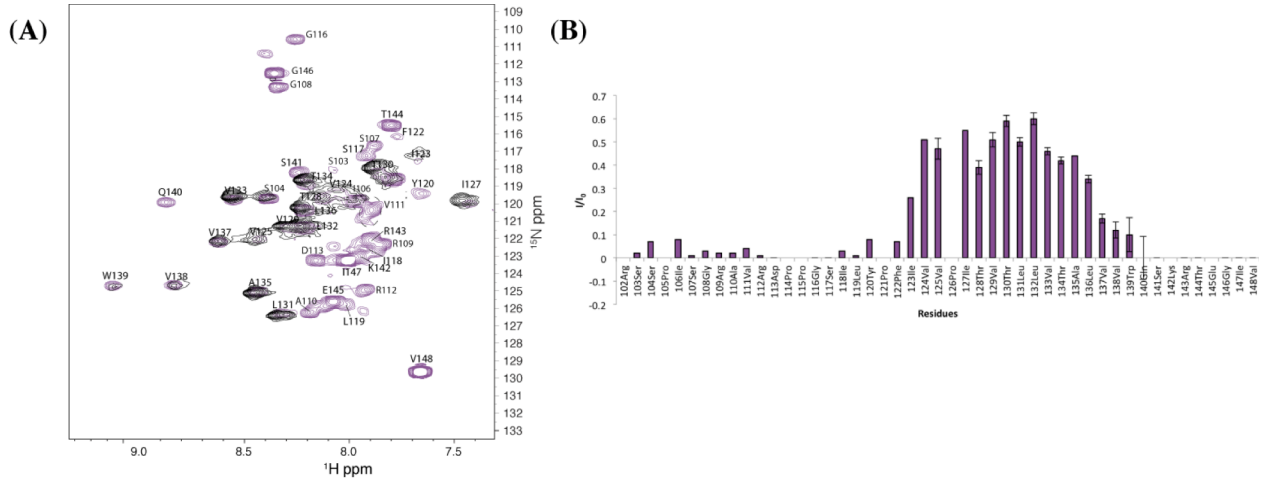

Figure 6.25: Water-soluble paramagnetic broadening enhancement of the backbone 1H-15N groups of RAMP1tm(102-148) (A) Signal broadening is due to paramagnetic relaxation enhancement arising from the presence of Mn2+ EDDA2=. The normalised ratio of 1H-15N HSQC signal intensities in the presence (black) and absence (purple) of 1 mM of Mn2+ EDDA2=.
(B) Exchange rate of backbone NH with water. I/Io is used to quantify signal broadening for each residue.

6.2.11.2 Hydrogen-deuterium (H/D) exchange

To further explore the unusual dynamics observed in the N-terminal portion of the transmembrane domain, the exchange rates of the target protein with water were measured by collecting a range of 2D ^{1}H-^{15}N SOFAST-HMQC experiments after solubilisation in D_2O. The experimental data were obtained by lyophilising the initial NMR sample, which was purified in H_2O, and reconstituting into detergent solution

containing 100 % D_2O (Figure 6.26). The exchange rate was then monitored by comparing peak intensities, I/I_0, as a function of time. H/D exchange rates were measured at previously established conditions for RAMP1tm(102-148).

The result corresponded well with the paramagnetic broadening experiments. The exchange-rates of the N-terminal domain were very fast. Residue Ile123 to residue Gln140 experienced detectable exchange. However, only residues Leu132 until Trp139 appeared to be highly protected. Interestingly, Tyr130, which was indicated by water-soluble paramagnetic broadening experiments to be deeply buried within the SDS micelles, experienced relatively fast exchange with D_2O. Results obtained for Leu132, however, were in agreement with the water-soluble PRE experiments and showed the lowest exchange rate with D_2O.

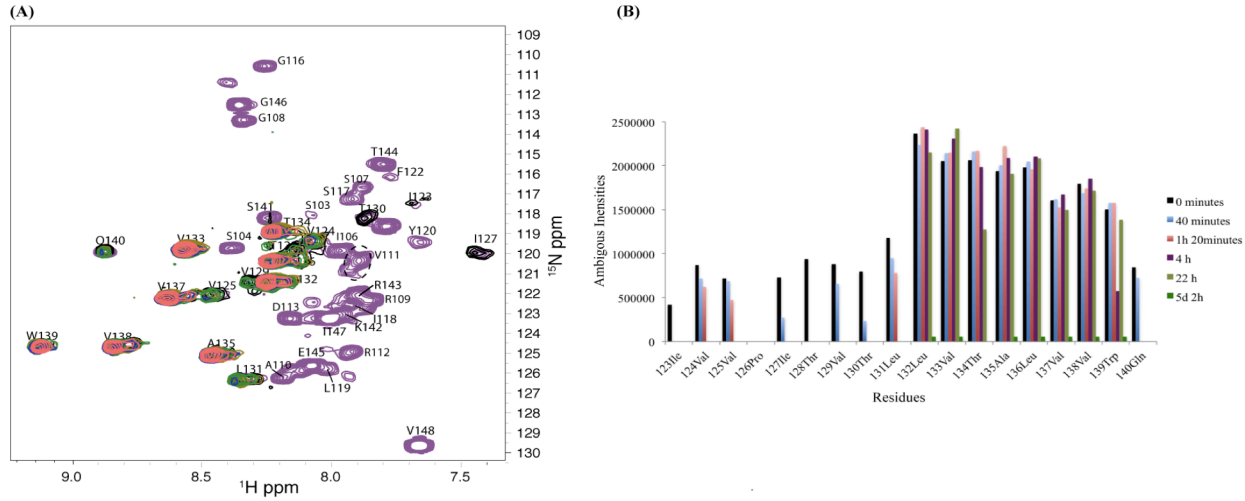

Figure 6.26: Hydrogen/deuterium exchange of the backbone ^{15}N-^{1}H groups of RAMP1tm(101-148) in 40 mM SDS Colouring: black – 0 min, green – 40 min; brown – 80 min; blue – 120 min; red – 160 min

Summarising, both experiments showed that residue Ile132 was the first residue in the transmembrane region, which is protected by the micelles. Interestingly, residues within the PxxxxP-motif, shown in both experiments to moderate exchange, suggest that this

region is highly destabilised. The C-terminal boundary was well defined by Trp139, with Gln140 experienced some exchange with D_2O.

6.2.12 Mutational studies and close examination of the dimeric interface

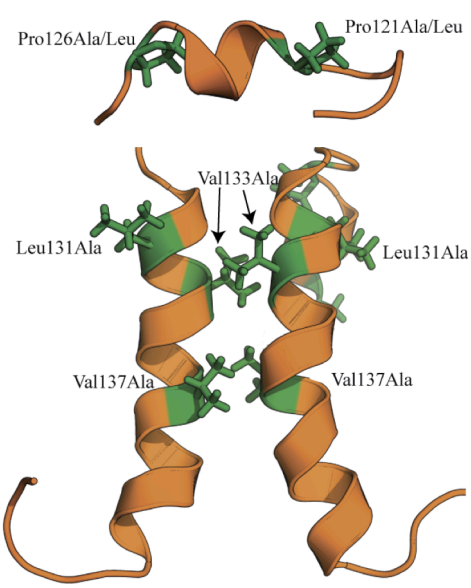

Figure 6.27: Dimeric RAMP1tm(116.148) structure with displayed mutations

To investigate which amino acids are involved in stabilising the dimeric conformation of RAMP1, and whether the prolines have some role in facilitating the interaction, mutations were introduced at residues Pro121, Pro126, Leu131, Val133 and Val137. Leu131 was introduced as a possible negative control. RAMP1tm(102-148) was shown not to dimerise hence all mutations were only studied on the shorter construct RAMP1tm(116-148). Figure 6.27 displays all mutants and their position within the dimer. CD was performed on all mutants to examine the effect on their secondary structure. Additionally, chemical crosslinking and NMR were used to investigate whether mutation of these residues affected dimerisation.

6.2.12.1 Investigation by circular dichroism

As an initial step, all mutations were examined by CD in 40 mM SDS to establish changes in secondary structure and folding properties. Similar to wild-type, all mutants experienced negative maxima at ~220 nm and ~210 nm indicating a high α-helical content (Figure 2.28).

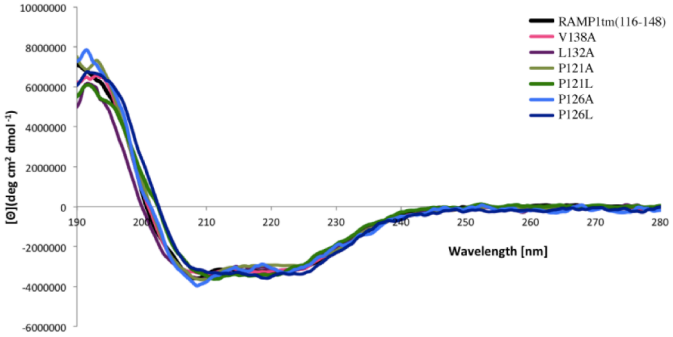

Figure 6.28: Circular dichroism spectra of RAMP1tm(116-148) wild-type and mutants

To assess the degree of α-helicity the ratio $\theta_{222}/\theta_{208}$ was calculated (Libich et al. 2009) for each mutant (Table 6.12).

Construct	$\theta_{222}/\theta_{208}$	Conclusion
RAMP1tm(116-148)	0.905	α-helical
V137A	0.971	α-helical
L131A	0.945	α-helical
P121A	0.827	α-helical
P121L	1.033	Coiled-coil
P126A	0.866	α-helical
P126L	1.100	Coiled-coil

Table 6.12: Examination of the α-helical ratio of RAMP1tm(116-148) and mutants (Libich et al.

Circular dichroism displayed marginal differences in secondary structure conformation between each mutant and the wild-type. Thus it indicated a stable secondary structure of each mutant. Interestingly, P121L and P126L displayed coiled-coil features in CD.

6.2.12.2 Investigation of the interfacial residues

Chemical crosslinking in SDS micelles was performed on V133A and V137A to analyse whether it is possible to disrupt the dimeric interface. L131A served as a negative control. The formation of covalent bonds was enabled by 7 mM DSP for 5 minutes, before the reaction was stopped with 100 mM Tris HCl.

Un-crosslinked constructs exhibited a strong monomeric band on SDS-PAGE (Figure 6.28). All three constructs showed impurities of the fusion-protein with trpLE. Therefore all constructs were purified a second time by HPLC before crosslinking was continued. V133A behaved like the wild-type, whereas V137A oligomerised at higher molecular weight. L131A showed a ladder of oligomers, which was unexpected.

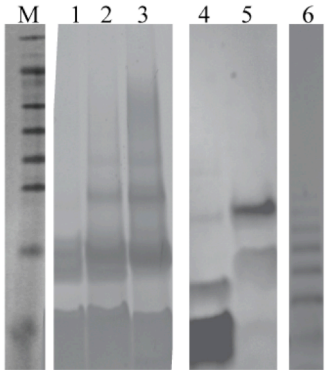

Figure 6.29: Crosslinking of V133A, V137A and the negative control L131A in 40 mM SDS with 7 mM DSP

Constructs before crosslinking	*Constructs after crosslinking*
1 - V133A	*4 - V133A*
2 - V137A	*5 - V137A*
3 - L131A	*6 - L131A*

Additionally, V133A and V137A were examined by ^{1}H-^{15}N HSQCs in 40 mM SDS to establish chemical shift perturbation and possible effects on peak doubling, thus dimerisation (Figure 6.30). Each mutated residue lead to substantial chemical shift perturbations, which made it impossible to create a CSP map without recording 3D spectra for re-assignment of the resonances. Although time limitations prevented re-assignment of all variants, visual examination of the spectra permitted some insight into the effects of the substitutions.

The V133A substitution displayed unusual peak broadening and no resonance doubling. Similar results were found for mutation V137A. However, peak doubling was observed for residue Tyr120, Ile123 and Leu131.

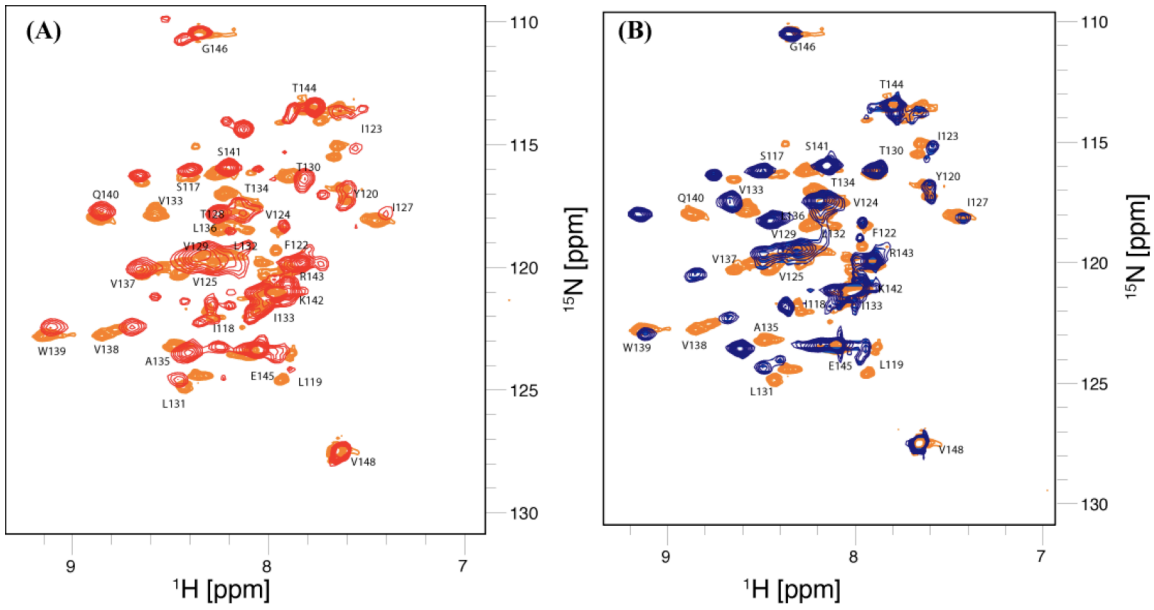

Figure 6.30: Mutational studies of RAMP1tm(116-148) and mutation V133A and V137A by solution NMR
(A) ^{1}H-^{15}N HSQC overlay of RAMP1tm(116-148) and its mutants V133A
(B) ^{1}H-^{15}N HSQC overlay of RAMP1tm(116-148) and its mutants V137A
Colouring: orange - WT, red - V133A, navy - V137A

More experimental data are needed to gain confidence in these findings, since the negative control showed unexpected oligomerisation, and V133A and V137A by themselves did not completely disrupt the dimeric conformation.

6.2.12.3 Investigation of the PxxxxP-motif

Since unusual dynamics were observed around the prolines in the transmembrane domain, the chemical shifts of the proline sidechains were used to evaluate the conformation of the preceding peptide bond and whether isomerisation may account for some of the behaviour of this region of the protein. The chemical shifts of the Cβ and Cγ resonances of prolines can be used to identify whether the proline peptide bond is in the *cis* or *trans* conformation. For *cis*-conformations Cβ are located at 33.8 ±1.2 ppm and Cγ at 24.4 ± 0.7 ppm. When prolines occupy a *trans*-conformation they values for Cβ are at 31.8 ± 1 ppm and for Cγ 27.4 ± 0.9 ppm (Shen & Bax 2009). For RAMP1tm, the chemical shift of the proline was analysed by using a 3D CBCA(CO)NH experiment. In RAMP1tm

constructs the Cβ atoms suggested that the prolines were present in a *trans* conformation, with Pro121 Cβ being located at 31.36 ppm and Pro126 Cβ at 31.95 ppm.

To explore the structural role of the PxxxxP-motif and its conformation further Pro121 and Pro126 were mutated to alanines and leucines and crosslinked in 40 mM SDS and DMPC liposomes. Crosslinking was executed according to that described for wild-type construct (subchapter 6.3.8.1).

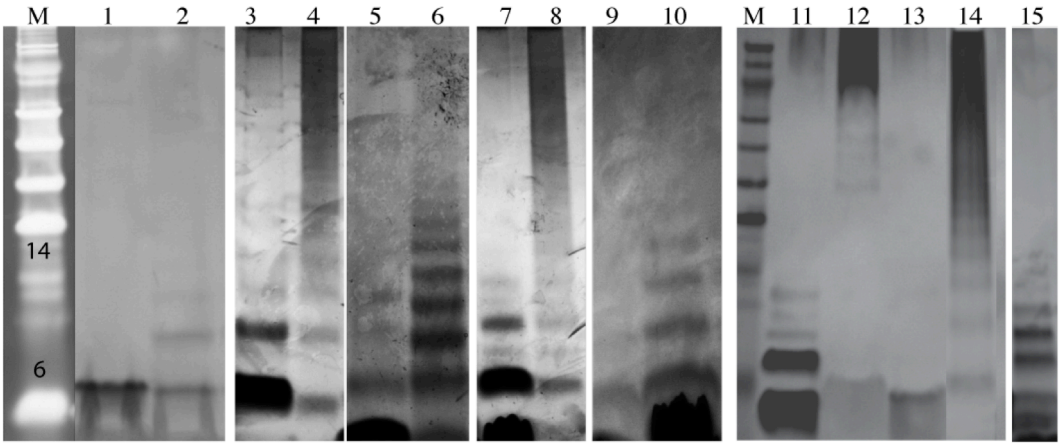

Figure 6.31: Crosslinking of P121A/L and P126A/L in DMPC liposomes and in SDS micelles with 7 mM DSP

1 - RAMP1tm(116-148)
2 - RAMP1tm(116-148) crosslinked in liposomes
3 - P121A
4 - P121A crosslinked in liposomes
5 - P121L
6 - P121L crosslinked in liposomes
7 - P126A
8 - P126A crosslinked in liposomes
9 - P126L
10 - P126L crosslinked in liposomes
11 - RAMP1tm(116-147) WT
12 - P121L crosslinked in SDS
13 - P126L crosslinked in SDS
14 - P121A crosslinked in SDS
15 - P126A crosslinked in SDS

The obtained results were rather surprising. Crosslinking in SDS micelles and DMPC liposomes displayed an expected monomeric and a dimeric band, as well as some trimeric bands for wild-type. Crosslinked P121L and P126L in SDS (Figure 6.31 – lane 5, 9, 12, 13) exhibited a monomeric band. In contrast, both mutants crosslinked in liposomes formed a ladder of oligomeric states on the gel (Figure 6.31 – lane 6, 10) while P121A and P126A led to high molecular weight (> 100 kDa) aggregation Surprisingly, P126A displayed a ladder of oligomeric states on the gel. Overall, chemical crosslinking

in both environments gave little indications, whether the PxxxxP-motif was directly responsible for dimerisation, since only P126L crosslinked in SDS showed a dominated monomeric conformation.

In addition, mutations P121A/L and P126A/L were examined by ^{1}H-^{15}N HSQCs in 40 mM SDS to observe chemical shift perturbations and any effects on peak doubling (Figure 6.31). However, similar to V133A and V137A, it was not possible to create a CSP-map, due to substantial chemical shift perturbations.

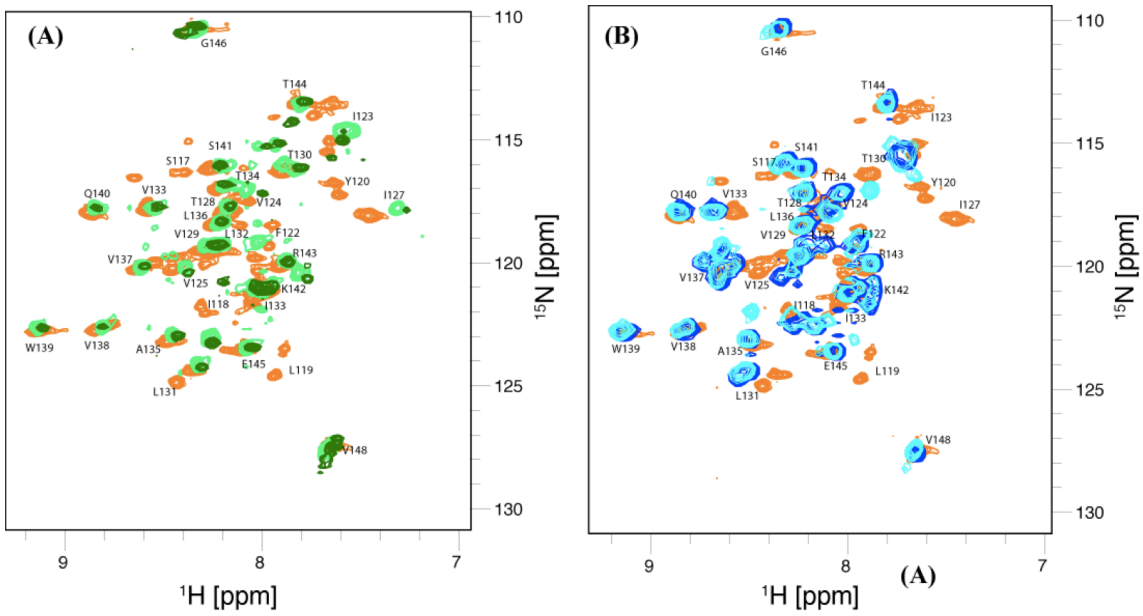

Figure 6.32: Mutational studies of RAMP1tm(116-148) by solution NMR
(A) ^{1}H-^{15}N HSQC overlay of RAMP1tm(116-148) and its mutants P121L and P121A
(B) ^{1}H-^{15}N HSQC overlay of RAMP1tm(116-148) and its mutants P126L and P126A
Colouring: orange - WT, dark green - P121L, light green - P121A, blue - P126L, light blue - P126A

Mutations of Pro121 behaved similar. Dramatic shift changes relative to wild-type RAMP1tm(116-148) and the widespread disappearance of peaks were observed (Figure 6.31 (A)). N-terminal residues disappeared and peak doubling was no longer observed. Similar results were acquired for mutations in Pro126 (Figure 6.31 (B)). The difference in chemical shift perturbation between Pro126L and Pro126A was small. Visual examination indicated the loss of peak doubling and unobservable N-terminal peaks.

Summarising, chemical crosslinking gave little indication of whether the PxxxxP-motif was directly responsible for dimerisation and what the role of Val133 and Val137 have on their own. However, a correlation was observed between the results in CD and chemical crosslinking in DMPC liposomes. P121A and P126A, which appeared to be less α-helical than wild-type, showed aggregation at high order and clear monomeric and dimeric bands. In comparison, P121L and P126L exhibited oligomerisation in crosslinking and coiled-coil signatures by CD, consistent with a high degree of self-association.

Furthermore, the proline Cβ chemical shifts were consistent with a *trans* conformation of the prolines, with no indication of partial *cis* character that may lead to increased dynamics in the regions around the prolines.

6.3 DISCUSSION

Udawela *et al*. (Udawela et al. 2004) and Héroux *et al.* (Héroux et al. 2007) first described dimerisation of the small accessory protein RAMP1 in transfected cells. Since the isolated ectodomain of RAMP1 does not dimerise, it was proposed that the transmembrane region may be responsible for this feature (Koth et al. 2010; Moore & Salvatore 2012). I used solution-state NMR as the main technique to gain deeper insights into the transmembrane region of RAMP1 and its ability to form homodimers. The established NMR-compatible detergent and membrane mimetic SDS (Chill 2006; King et al. 2011) was used to investigate the concentration-dependent oligomerisation and structural features of the RAMP1 transmembrane domain. First the monomeric structure of the RAMP transmembrane domain was determined, then the homodimeric interface was identified. In addition, the PxxxxP-motif was identified as undergoing unusual dynamics that may contribute indirectly to the dimeric state.

6.3.1 How robust is the structure of the transmembrane region of RAMP1?

Two constructs of different length were examined. Dynamics and circular dichroism established a strong consistency in secondary structure between the two constructs. Chemical shifts indicated that the structured transmembrane domain was consistent in both constructs between residues Val129 and Arg143. Additionally, a second small helix between residues Pro121 and Val125, which enclosed the PxxxxP-motif, was identified in both constructs by NOEs and RDCs. Moreover, a similar rotational correlation time τ_c of ~11 ns was calculated for both constructs, indicating that the N-terminal extension

contains mostly flexible residues. Therefore it was concluded that the obtained structure between residue Ser117 and Val148 was not strongly dependent on the construct size.

6.3.2 What is the impact of the N-terminal domain on dimerisation?

The longer construct RAMP1tm(102-148) consisted of an additional 14 N-terminal residues in comparison to RAMP1tm(116-148). Non-detectable concentration dependency and the lack of observed intermolecular NOEs lead to the conclusion that even though the secondary structure of the transmembrane region was similar in both, the additional residues interfered with dimerisation of the transmembrane region of RAMP1. One possible explanation for a solely monomeric RAMP1tm(102-148) construct could be an interference from SDS. SDS has been shown to preserve secondary and tertiary structures of transmembrane domains if they contain only short extramembrane segments (Chill 2006; King et al. 2011). Thus, the extended long RAMP1tm construct RAMP1tm(102-148) could have been to long, leading to SDS micelle binding that promoted dissociation of the dimer. However, the full-length RAMP1 construct was not tested, and therefore it is not possible to conclude whether the same observed dimeric interaction occurs in the full-length RAMP1.

6.3.3 What is the role of the PxxxxP-motif?

The PxxxxP-motif was investigated by mutagenesis studies to examine its role in dimerisation. Prolines are known to be important for the function and structure of integral membrane proteins. Their five-membered pyrolidine ring imparts special conformational characteristics. Generally, a proline residue can be either highly stabilising when located in the first position of an α-helix (helix 'cap') or de-stabilising

when internal to a helix. The reason for this is the lack of an amide proton, which would normally form a hydrogen bond to a carbonyl at position i–4 within a helix (Schimmel & Flory 1968; Senes et al. 2004). This results in an increased local backbone flexibility and thus can affect hinge-bending motions (Tieleman et al. 2001; Sansom & Weinstein 2000). Interestingly, a similar PxxxxP-motif was shown to stabilise helix–helix packing with TOXCAT (Russ & Engelman 2000). Using this approach on a large number of variant constructs, Dawson et al. (Dawson et al. 2002) observed that this motif and similar ones that were rich in serine, threonine or proline residues could self-associate. With this prior knowledge, it was hypothesised that the RAMP1 PxxxxP-motif could be responsible for RAMP1 dimerisation. However, mutations of both prolines to alanines and leucines and their subsequent crosslinking in presence of SDS and liposomes showed aggregation and oligomerisation. The PxxxxP motif was found to be quite dynamic in RAMP1, and another region at the C-terminal end of the transmembrane domain was found to be responsible for specific dimeric contacts (see below). Therefore, it was concluded that the PxxxxP-motif might be indirectly involved in allowing the formation of dimers by preventing non-specific oligomerisation.

6.3.4 What drives dimerisation?

The RAMP1 transmembrane domain dimer appeared to adapt a coiled-coil secondary structure, with the amino acids Val129, Val133, Val137 and Gln140 on the dimeric interface. Concentration-dependent resonance doubling confirmed that the transmembrane domain of RAMP1 stabilised the parallel homodimeric conformation of the protein. Although not all positions were tested, a single mutation was not found that completely disrupted the RAMP1tm dimer, suggesting that most of the interactions observed at the interface may be necessary for dimerisation. Experimental validation of this hypothesis is required.

CHAPTER 7

CONCLUSION AND OUTLOOK

"Nothing has such power to broaden the mind as the ability to investigate system systematically and truly all that comes under the observation in life."

(Marcus Aurelius)

The work I present in this thesis examines in detail the two GPCR accessory proteins, MRAP and RAMP1. The studies ranged from atomic level structural details, via structural determinations of each accessory protein, and included a range of biophysical approaches to study their overall secondary structure (e.g., CD) and hydrodynamic properties (e.g., PFG-NMR and DLS), as well as molecular dynamic simulations in lipid bilayers. Guided by solution-state NMR, the main goal of my research was to learn as much as possible about the structure of these two different accessory proteins and their dimerisation at an atomic level. Structure determination of membrane proteins by solution-state NMR spectroscopy is an important aspect of contemporary structural biology. Membrane proteins require the presence of lipids and/or detergents to maintain their structural and functional integrity. However, the presence of lipids can prevent experimental measurements to high resolution. As a result, when possible, the structural properties of the membrane proteins in different types of detergents were compared to evaluate the robustness of the results.

7.1 Findings concerning MRAP in general

The monomeric structure of MRAP was studied in Chapter 4 by solution-state NMR, which provides insights into the structure and behaviour of MRAP in micelle and mixed micelle environments. I was able to establish that the structure is robust and detergent-independent. The presence of a previously unidentified N-terminal helix was established, which includes a region

previously shown to be critical for receptor activation. RDC measurements of a weakly aligned MRAP sample in polyacrylamide gels and the following dipolar wave analysis determined the relative orientation within a gel and gave confidence in obtained helical regions. In addition to the structure, the region of the protein that was solvent inaccessible was consistent across micelle mixtures, and thus is likely to indicate the region that is embedded in membranes. Investigation of dynamics suggested that the KH-rich region, which is critical for dual topology in cells, as well as several residues N-terminal to the KH-rich region are highly flexible. This part of MRAP may act as a flexible linker to allow free movement of the α-helical N-terminal LDY(L/I) motif, possibly to enable interactions with the GPCR class A melanocortin receptors and/or the receptor ligands to modulate their activity.

Chapter 5 concentrated on efforts to establish the previously proposed unique antiparallel homodimeric interface of MRAP. However, after much effort that included multiple biophysical and computational approaches, it was not possible to demonstrate dimer formation of MRAP *in vitro*. Although, essentially a negative result indicating the need for further studies, my results have lead to the hypothesis that an unidentified component or feature of endogenous membranes is required for MRAP dimerisation. Possible factors influencing dimerisation *in vivo* are membrane asymmetry or the presence of another component that mediates or stabilises the dimer. This could be

another protein or possibly a specific lipid interaction, similar to what has been shown for the transmembrane domain of the COPI protein p24 (Contreras et al. 2012).

7.2 Findings concerning RAMP

Chapter 6 describes structural studies of the transmembrane domain of the GPCR accessory protein, RAMP1. Like MRAP, RAMP1 can be isolated from cells in a dimeric conformation, which has been suggested to be due to the transmembrane domain since the ectodomain does not oligomerise. A high resolution structure of the RAMP1 transmembrane domain was determined by solution NMR, and measurements of dynamics and RDCs gave confidence in the structure. Furthermore, it was possible to determine a specific dimeric interface by solution-NMR. Additional investigation focused on the PxxxxP-motif, its unusual dynamic properties, and its possible role in disallowing the formation of oligomers. By contrast, a construct containing additional N-terminal residues disrupted RAMP1 dimerisation, which was speculated to be due to either the structural attributes of the N-terminal domain itself or due to its interactions with SDS. In general, investigation of RAMP1 supported previously reported biochemical analysis.

7.3 Future directions and experiments in progress

This thesis tried to provide molecular insights into two quite diverse GPCR accessory proteins, however it is a timely snapshot of a quickly advancing

field. The atomic-level structural information on MRAP and RAMP1 are the first to be reported on the transmembrane domain of any of the growing collection of membrane-embedded GPCR accessory proteins. Through detailed structural and biophysical studies, this work has furthered our understanding of this unique protein type. It is likely that this work will provide a foundation for further studies on these systems, whether to better understand the role of the PxxxxP-motif on RAMP1 function in cells, or in seeking out unrecognised cellular interaction partners of MRAP.

7.3.1 Future directions for studies of MRAP

MRAP, as well as MRAP2, are unique in having no signal peptide, a dual topology and the ability to bidirectionally modulate receptor trafficking and function, distinguishing them from the other families of accessory proteins. Much more has yet to be learnt about MRAP in the years to come. The following experiments are suggestions or on-going work to extend the current findings:

Membrane–Rosetta is a de novo structure prediction method for prediction of helical transmembrane protein structures. The membrane is a multi-layered environment, and this is modelled in Membrane-Rosetta by parallel planes defining a hydrophobic core, an interface, and a polar lipid headgroup layer. This python-based protocol uses the Rosetta fragment assembly method and calculates whole structures using this membrane-mimicking force field, in which residue-residue and residue-environment interactions are functions of

the region of the membrane layer in addition to amino acid identity, distance, and density. Initial simulations for MRAP have been set up for monomeric MRAP, and will ultimately be applied to test whether Membrane-Rosetta calculations can converge on a unique MRAP dimer conformation.

A further possibility is that the MRAP dimer is stabilised in membranes, but our assay was not sensitive enough to detect the association. The TOXCAT assay, which uses the dimerisation dependent transcription factor ToxR fused to the transmembrane domains of interest was established to study such interactions (Russ & Engelman 2000). In TOXCAT, activation of the encoding chloramphenicol acetyltransferase (CAT) quantitatively reports on the association of the transmembrane regions in membranes, and thus may provide a more accurate insight into whether MRAP on its own has a propensity to associate.

Based on recent findings showing that the MRAP homology MRAP2 is critical in regulating MC4R, a receptor involved in hereditary obesity and therefore of great biomedical interest, an important future direction would be structural studies of MRAP2. It is of great interest to compare the structural features of MRAP2 in order to understand what regions may be responsible for differential regulation of melanocortin receptors by MRAP and MRAP2.

A further possible direction would be the investigation of the heterodimerisation of MRAP with MRAP2. MRAP/MRAP2 heterodimers have been shown to regulate MCRs in a bidirectional manner and to

subsequently stimulate MC2R. Little is known so far about this interaction, but examination of the MRAP/MRAP2 complex in isolation could lead to a deeper understanding of the melanocortin system.

Finally, investigations into the potential interaction of MRAP with the MC2R ligand ACTH (Appendix) were begun based on the role of RAMP1 in binding receptor ligands. However time prevented a thorough study. A complete investigation of ACTH with MRAP and possibly also the receptor, would certainly be of great help in understanding the regulation of MC2R by MRAP.

7.3.2 Future directions for studies of RAMP

The research presented in this dissertation has shed light on the homodimerisation of RAMP1. While these studies provide evidence for its dimeric conformation, ongoing experiments focus on finding mutants that completely disrupt the dimer. It is hoped that via collaboration these mutants can then be tested *in vivo* on the role of dimer in regulating receptor maturation.

Also of interest are studies of RAMP2. The transmembrane region of RAMP3 is highly similar to the one in RAMP1. However, in RAMP2, the PxxxxP-motif is located in the core transmembrane domain, and thus it would be interesting to establish whether or not the motif experiences heightened dynamics also in this context, and whether RAMP2 retains the ability to homodimerise. In addition, studies of RAMP3 would help to establish whether the RAMPs have adopted a general mechanism for dimerisation across the protein family.

Of course, as with MRAP, an exciting future direction would be to study RAMP1 in the presence of receptor. These studies remain extremely difficult, but are ultimately necessary to fully understand the regulation of GPCRs by these accessory proteins.

The findings presented in this dissertation have advanced our molecular understanding of small GPCR accessory proteins and their dimerisation. This thesis has shown the power of modern solution-state NMR in the field of structural biology and that this biophysical technique is a highly useful tool for unravelling the intricate interplay between structure, stability, dynamics and interactions of proteins.

BIBLIOGRAPHY

"If I have seen further than others, it is by standing upon the shoulders of giants."

(Isaac Newton)

Abdel-Malek, Z.A., 2001. Melanocortin receptors: their functions and regulation by physiological agonists and antagonists. *Cellular and Molecular Life Sciences*, 58(3), pp.434–441.

Abràmoff, M.D., et al., 2004. Image processing with ImageJ. *Biophotonics International*, 11(7), pp.36–42.

Achour, L. et al., 2008. An escort for GPCRs: implications for regulation of receptor density at the cell surface. *Trends in Pharmacological Sciences*, 29(10), pp.8–8.

Adamian, L. & Liang, J., 2002. Interhelical hydrogen bonds and spatial motifs in membrane proteins: polar clamps and serine zippers. *Proteins*, 47(2), pp.209–218.

Adams, R.R. et al., 2012. Binding sites in membrane proteins--diversity, druggability and prospects. *European Journal of Cell Biology*, 91(4), pp.326–339.

Adcock, S.A. & McCammon, J.A., 2006. Molecular dynamics: survey of methods for simulating the activity of proteins. *Chemical Reviews*, 106(5), pp.1589–1615.

Ader, C.C. et al., 2010. Protein dynamics detected in a membrane-embedded potassium channel using two-dimensional solid-state NMR spectroscopy. *Biochimica et Biophysica Acta -Biomembranes*, 1798(2), pp.5–5.

Agulleiro, M.J. et al., 2010. Role of melanocortin receptor accessory proteins in the function of zebrafish melanocortin receptor type 2. *Molecular and Cellular Endocrinology*, 320(1-2), pp.145–152.

Aiyar, N. et al., 2000. Involvement of G protein-coupled receptor kinase-6 in desensitization of CGRP receptors. *European Journal of Pharmacology*, 403, pp 1-7.

Alberts, B., 2008. *Molecular Biology of the Cell*, Garland Pub.

Alder, N.N. & Johnson, A.E., 2004. Cotranslational membrane protein biogenesis at the endoplasmic reticulum. *Journal of Biological Chemistry*, 279(22), pp.22787–22790.

Almén, M.S. et al., 2009. Mapping the human membrane proteome: a majority of the human membrane proteins can be classified according to function and evolutionary origin. *BioMed Central Biology*, 7, pp.50–50.

Altenbach, C.C. et al., 1994. A collision gradient method to determine the immersion depth of nitroxides in lipid bilayers: application to spin-labeled mutants of bacteriorhodopsin. *Proceeding of the National Academy of Science*, 91(5), pp.1667–1671.

Aluru, N.N. & Vijayan, M.M., 2008. Molecular characterization, tissue-specific expression, and regulation of melanocortin 2 receptor in rainbow trout. *Journal of Endocrinology*, 149(9), pp.4577–4588.

Alvares, R.D. et al., 2013. Effects of a polar amino acid substitution on helix formation and aggregate size along the detergent-induced peptide folding pathway. *Biochimica et Biophysica Acta - Biomembranes*, 1828(2), pp.373–381.

Andersson, A.A. & Mäler, L.L., 2005. Magnetic resonance investigations of lipid motion in isotropic bicelles. *Langmuir*, 21(17), pp.7702–7709.

Arkin, I.T. & Brunger, A.T., 1998. Statistical analysis of predicted transmembrane alpha-helices. *Biochimica et biophysica acta*, 1429(1), pp.113–128.

Asai, M. et al., 2013. Loss of Function of the Melanocortin 2 Receptor Accessory Protein 2 Is Associated with Mammalian Obesity. *Science*, 341(6143), pp.275–278.

Arsham, H. & Kahn, A.B., 1990. "What-if" analysis in computer simulation models: A comparative survey with some extensions. *Mathematical and Computer Modelling*, 14, pp.101–106.

Attwood, T.K. & Findlay, J.B., 1994. Fingerprinting G-protein-coupled receptors. *Protein Engineering, Design and Selection*, 7(2), pp.195–203.

Auffray, I. et al., 2001. Glycophorin A dimerization and band 3 interaction during erythroid membrane biogenesis: in vivo studies in human glycophorin A transgenic mice. *Blood*, 97(9), pp.2872–2878.

Baas, B.J., et al., 2004. Homotropic cooperativity of monomeric cytochrome P450 3A4 in a nanoscale native bilayer environment. *Archives of Biochemistry and Biophysics*, 430(2), pp.218–228.

Bai, X.C. et al., 2012. Ribosome structures to near-atomic resolution from thirty thousand cryo-EM particles. *eLife*, 2, pp.e00461–e00461.

Baier, C.J. et al., 2010. Cholesterol modulation of nicotinic acetylcholine receptor surface mobility. *European Biophysics Journal*, 39(2), pp.213–227.

Baron, A. et al., 2009. Modeling the evolution of the MC2R and MC5R genes: Studies on the cartilaginous fish, Heterondotus francisci. *General and comparative Endocrinology*, 161(1), pp.13–19.

Barwell, J. et al., 2012. Calcitonin and calcitonin receptor-like receptors: common themes with family B GPCRs? *British Journal of Pharmacology*, 166(1), pp.51–65.

Baskaran, K. et al., 2010. Mapping of protein structural ensembles by chemical shifts. *Journal of Biomolecular NMR*, 48(2), pp.71–83.

Battiste, J., 2000. Utilization of site-directed spin labeling and high-resolution heteronuclear nuclear magnetic resonance for global fold determination of large proteins with limited nuclear Overhauser effect data. *Journal of Biochemistry*, 39, pp.5355-5365.

Bay, D.C. & Turner, R.J., 2013. Membrane composition influences the topology bias of bacterial integral membrane proteins. *Biochimica et biophysica acta*, 1828(2), pp.260–270.

Bayburt, T.H. & Sligar, S.G., 2002. Single-molecule height measurements on microsomal cytochrome P450 in nanometer-scale phospholipid bilayer disks. *Proceeding of the National Academy of Science*, 99(10), pp.6725–6730.

Beevers, A.J. & Dixon, A.M., 2010. Helical membrane peptides to modulate cell function. *Chemical Society Reviews*, 39(6), pp.2146–2157.

Bellot, G. et al., 2013. DNA nanotubes for NMR structure determination of membrane proteins. *Nature Protocols*, 8(4), pp.755–770.

Benemei, S.S. et al., 2007. Pain pharmacology in migraine: focus on CGRP and CGRP receptors. *Neurological Sciences*, 28, pp.S89–S93.

Berg, B.V. et al., 2003. X-ray structure of a protein-conducting channel. *Nature*, 427(6969), pp.36–44.

Blackledge, 2005. Recent progress in the study of biomolecular structure and dynamics in solution from residual dipolar couplings. *Progress in Nuclear Magnetic Resonance Spectroscopy*, 46(1), pp.23-61.

Blom, N. et al., 2004. Prediction of post-translational glycosylation and phosphorylation of proteins from the amino acid sequence. *Proteomics*, 4(6), pp.1633–1649.

Bockaert, J., et al., 2010. GPCR interacting proteins (GIPs) in the nervous system: roles in physiology and pathologies. *Annual review of Pharmacological Toxicology, 50,* pp.89-109

Bodenhausen, G. & Ruben, D.J., 1980. Natural abundance nitrogen-15 NMR by enhanced heteronuclear spectroscopy. *Chemical Physics Letters*, 69(1), pp 185-189.

Bodenhausen, G., et al., 1984. Selection of coherence-transfer pathways in NMR pulse experiments. *Journal of Magnetic Resonance*, 58(3), pp.370–388.

Bond, P. et al., 2007. Coarse-grained molecular dynamics simulations of membrane proteins and peptides. *Journal of Structural Biology*, 157(1), pp.593-605.

Bond, P.J. & Sansom, M.S.P., 2006. Insertion and assembly of membrane proteins via simulation. *Journal of the American Chemical Society*, 137(5), pp.2697–2704.

Boston, B.A. & Cone, R.D., 1996. Characterization of melanocortin receptor subtype expression in murine adipose tissues and in the 3T3-L1 cell line. *Journal of Endocrinology*, 96, pp.2043–2050.

Bouschet, T.T., et al., 2005. Receptor-activity-modifying proteins are required for forward trafficking of the calcium-sensing receptor to the plasma membrane. *Journal of Cell Science*, 118(Pt 20), pp.4709–4720.

Bowes, J.H. & Cater, C.W.C 1968. The interaction of aldehydes with collagen. *Biochimica et Biophysica Acta - Bioenergetics*, 168(2), pp.341–352.

Brändén, C.-I. & Tooze, J., 1999. *Introduction to Protein Structure*, Garland Pub.

Braun, P.P. & Heijne, von, G.G., 1999. The aromatic residues Trp and Phe have different effects on the positioning of a transmembrane helix in the microsomal membrane. *Biochemistry*, 38(30), pp.9778–9782.

Brewer, M.R. et al., 2009. The juxtamembrane region of the EGF receptor functions as an activation domain. *Molecular cell*, 34(6), pp.641–651.

Broughman, J.R. et al., 2002. Structural implications of placing cationic residues at either the NH2- or COOH-terminus in a pore-forming synthetic peptide. *Journal of Membrane Biology*, 190(2), pp.93–103.

Buchan, D.W. et al., 2010. Protein annotation and modelling servers at University College London. *Nucleic Acids Research*, 38, pp.W563–W568.

Bulenger, S.S., Marullo, S.S. & Bouvier, M.M., 2005. Emerging role of homo- and heterodimerization in G-protein-coupled receptor biosynthesis and maturation. *Trends in Pharmacological Sciences*, 26(3), pp.7–7.

Butler, P., et al., 2004. The Escherichia coli multidrug transporter EmrE is a dimer in the detergent-solubilised state. *Journal of Molecular Biology*, 340, pp. 797–808

Call, M.E. et al., 2006. The Structure of the ζζ-Transmembrane Dimer Reveals Features Essential for Its Assembly with the T Cell Receptor. *Cell*, 127(2), pp.355–368.

Campbell, I., 2012. *Biophysical Techniques*, Oxford University Press.

Cantor, R.S., 1999. Lipid Composition and the Lateral Pressure Profile in Bilayers. *Biophysical journal*, 76(5), pp.15–15.

Caravatti, P., et al., 1983. Heteronuclear correlation spectroscopy in rotating solids. *Chemical Physics Letters*, 100(4), pp.305–310.

Carpenter, E.P. et al., 2008. Overcoming the challenges of membrane protein crystallography. *Current opinion in structural biology*, 18(5), pp.6–6.

Cavanagh, J., 2007. *Protein NMR Spectroscopy*,

Cerdá-Reverter, J.M. et al., 2013. Involvement of melanocortin receptor accessory proteins (MRAPs) in the function of melanocortin receptors. *General and comparative Endocrinology, 188, pp. 133-136*.

Chan, L. & Metherell, L., 2008. Familial glucocorticoid deficiency: advances in the molecular understanding of ACTH action. *Hormone Research,* 69,pp. 75-82.

Chan, L. et al., 2009. MRAP and MRAP2 are bidirectional regulators of the melanocortin receptor family. *Proceedings of the National Academy of Sciences*, 106(15), pp.6146–6151.

Chan, L., et al., 2011. Effects of melanocortins on adrenal gland physiology. *European journal of pharmacology*, 660(1), pp.171–180.

Chen, A.S. et al., 2000. Inactivation of the mouse melanocortin-3 receptor results in increased fat mass and reduced lean body mass. *Nature genetics*, 26(1), pp.97–102.

Chen, M.M. et al., 2007. Molecular identification of the human melanocortin-2 receptor responsible for ligand binding and signaling. *Biochemistry*, 46(40), pp.11389–11397.

Chen, W. et al., 1997. Exocrine gland dysfunction in MC5-R-deficient mice: evidence for coordinated regulation of exocrine gland function by melanocortin peptides. *Cell*, 91(6), pp.789–798.

Chen, L. et al., 2011. Glycogen Synthase Kinase-3{beta} Is a Functional Modulator of Serotonin-1B Receptors. *Molecular pharmacology*, 79(6), pp.974–986.

Cherezov, V. et al., 2007. High-resolution crystal structure of an engineered human beta2-adrenergic G protein-coupled receptor. *Science,* 318(5854), pp.1258–1265.

Chhajlani, V.V. & Wikberg, J.E.J., 1992. Molecular cloning and expression of the human melanocyte stimulating hormone receptor cDNA. *Federation of European Biochemical Societies letters*, 309(3), pp.417–420.

Chida, D. et al., 2007. Melanocortin 2 receptor is required for adrenal gland development, steroidogenesis, and neonatal gluconeogenesis. *Proceedings of the National Academy of Sciences*, pp.18205–18210.

Chill, J.H., 2006. NMR study of the tetrameric KcsA potassium channel in detergent micelles. *Protein Science*, 15(4), pp.684–698.

Chothia, C.C., et al., 1977. Structure of proteins: packing of alpha-helices and pleated sheets. *Proceeding of the National Academy of Science*, 74(10), pp. 4130-3134

Chou, J.J. et al., 2001. A simple apparatus for generating stretched polyacrylamide gels, yielding uniform alignment of proteins and detergent micelles. *Journal of Biomolecular NMR*, 21(4), pp.377–382.

Christopoulos, A. et al., 2003. Novel Receptor Partners and Function of Receptor Activity-modifying Proteins. *Journal of Biological Chemistry*, 278(5), pp.3293–3297.

Christopoulos, G.G. et al., 1999. Multiple amylin receptors arise from receptor activity-modifying protein interaction with the calcitonin receptor gene product. *Molecular pharmacology*, 56(1), pp.235–242.

Chun, L., et al., 2012. Structure and ligand recognition of class C GPCRs. *Acta pharmacologica Sinica*, 33(3), pp.312–323.

Chung, T.T. et al., 2008. The majority of adrenocorticotropin receptor (melanocortin 2 receptor) mutations found in familial glucocorticoid deficiency type 1 lead to defective trafficking of the receptor to the cell surface. *Journal of Clinical & Metabolism*, 93(12), pp.4948–4954.

Chung, T.T. et al., 2010. Phenotypic characteristics of familial glucocorticoid deficiency (FGD) type 1 and 2. *Clinical endocrinology*, 72(5), pp.589–594.

Claridge, J.K. & Schnell, J.R., 2011. Bacterial Production and Solution NMR Studies of a Viral Membrane Ion Channel. *Methods in Molecular Biology*, 831, pp. 165–179.

Clark, A.J. et al., 2003. Expression, desensitization, and internalization of the ACTH receptor (MC2R). *Annuals of the New York Academy of Sciences*, 994, pp.111–117.

Clark, A.J. et al., 2005. Inherited ACTH insensitivity illuminates the mechanisms of ACTH action. *Trends in Endocrinology and Metabolism*, 16(10), pp.451–457.

Clore, G.M., et al., 1998. Direct Structure Refinement against Residual Dipolar Couplings in the Presence of Rhombicity of Unknown Magnitude. *Journal of Magnetic Resonance*, 131(1), pp.4–4.

Cocquerel, L., 2002. Topological changes in the transmembrane domains of hepatitis C virus envelope glycoproteins. *The EMBO journal*, 21(12), pp.2893–2902.

Cohen, C. & Parry, D.A.D., 1986. α-Helical coiled coils — a widespread motif in proteins. *Trends in biochemical sciences*, 11(6), pp.245–248.

Columbus, L. et al., 2009. Mixing and matching detergents for membrane protein NMR structure determination. *Journal of the American Chemical Society*, 131(21), pp.7320–7326.

Cone, R.D. et al., 1993. Cloning and functional characterization of a family of receptors for the melanotropic peptides. *Annals of the New York Academy of Sciences*, 680, pp.342–363.

Cone, R.D., 2006. Studies on the physiological functions of the melanocortin system. *Endocrine Reviews*, 27(7), pp.736–749.

Contreras, F.X. et al., 2012. Molecular recognition of a single sphingolipid species by a protein's transmembrane domain. *Nature*, 481(7382), pp.525–529.

Cooray, S.N. et al., 2008. The melanocortin 2 receptor accessory protein exists as a homodimer and is essential for the function of the melanocortin 2 receptor in the mouse y1 cell line. *Journal of Endocrinology*, 149(4), pp.1935–1941.

Cooray, S.N. & Clark, A.J., 2011. Melanocortin receptors and their accessory proteins. *Molecular and Cellular Endocrinology*, 331(2), pp.7–7.

Cooray, S.N. et al., 2011. Bioluminescence Resonance Energy Transfer Reveals the Adrenocorticotropin (ACTH)-Induced Conformational Change of the Activated ACTH Receptor Complex in Living Cells. *Journal of Endocrinology*, 152(2), pp.495–502.

Cueille, C.C. et al., 2002. Increased myocardial expression of RAMP1 and RAMP3 in rats with chronic heart failure. *Biochemical and biophysical research communications*, 294(2), pp.340–346.

Dam, J. & Schuck, P., 2004. Calculating Sedimentation Coefficient Distributions by Direct Modeling of Sedimentation Velocity Concentration Profiles. In *Methods in enzymology*. Methods in Enzymology. Elsevier, pp. 185–212.

Davis, D.G. & Bax, A., 1985. Simplification of proton NMR spectra by selective excitation of experimental subspectra. *Journal of the American Chemical Society*, 107(24), pp.7197–7198.

Dawson, J.P.J., et al., 2002. Motifs of serine and threonine can drive association of transmembrane helices. *Journal of Molecular Biology*, 316(3), pp.7–7.

Delaglio, F. et al., 1995. NMRPipe: a multidimensional spectral processing system based on UNIX pipes. *Journal of Biomolecular NMR*, 6(3), pp.277–293.

Deng, Y. & Roux, B., 2009. Computations of standard binding free energies with molecular dynamics simulations. *The journal of physical chemistry B*, 113(8), pp.2234–2246.

de Jong, D.H. et al., 2013. Improved Parameters for the Martini Coarse-Grained Protein Force Field. *Journal of Chemical Theory and Computation*, 9(1), pp.687–697.

de Planque, M.R. et al., 2003. Interfacial anchor properties of tryptophan residues in transmembrane peptides can dominate over hydrophobic matching effects in peptide-lipid interactions. *Biochemistry*, 42(18), pp.5341–5348.

Derst, C.C. et al., 2000. Genomic structure and chromosome mapping of human and mouse RAMP genes. *Cytogenetics and Cell Genetics*, 90(1-2), pp.115–118.

Devaux, P.F., 1988. Phospholipid flippases. *Federation of European Biochemical Societies letters*, 234(1), pp.8–12.

Doods, H. et al., 2000. Pharmacological profile of BIBN4096BS, the first selective small molecule CGRP antagonist. *British Journal of Pharmacology*, 129(3), pp.420–423.

Doreleijers, J.F. et al., 2012. CING: an integrated residue-based structure validation program suite. *Journal of Biomolecular NMR*, 54(3), pp.267–283.

Dores, R.M., 2009. Adrenocorticotropic hormone, melanocyte-stimulating hormone, and the melanocortin receptors: revisiting the work of Robert Schwyzer: a thirty-year retrospective. *Annals of the New York Academy of Sciences*, 1163, pp.93–100.

Dores, R.M. & Baron, A.J., 2011. Evolution of POMC: origin, phylogeny, posttranslational processing, and the melanocortins. *Annals of the New York Academy of Sciences*, 1220(1), pp.34–48.

Dosset, P.P. et al., 2001. A novel interactive tool for rigid-body modeling of multi-domain macromolecules using residual dipolar couplings. *Journal of Biomolecular NMR*, 20(3), pp.223–231.

Douglas, S.M., et al., 2007. DNA-nanotube-induced alignment of membrane proteins for NMR structure determination. *Proceeding of the National Academy of Science*, pp.6644–6648.

Doura, A.K. et al., 2004. Sequence Context Modulates the Stability of a GxxxG-mediated Transmembrane Helix-Helix Dimer. *Journal of Molecular Biology*, 341(4), pp.8–8.

Doura, A.K. & Fleming, K.G., 2004. Complex Interactions at the Helix-Helix Interface Stabilize the Glycophorin A Transmembrane Dimer. *Journal of Molecular Biology*, 343(5), pp.11–11.

Dowhan, W., 1997. Molecular basis for membrane phospholipid diversity: why are there so many lipids? *Annual review of biochemistry*, 66, pp.199–232.

Driessen, A.J., et al., 1998. The Sec system. *Current Opinion in Microbiology*, 1(2), pp.216–222.

Dunlop, J., et al., 1995. Membrane insertion and assembly of ductin: a polytopic channel with dual orientations. *The EMBO journal*, 14(15), pp.3609–3616.

Dürr, U.H., et al., 2012. The magic of bicelles lights up membrane protein structure. *Chemical reviews*, 112(11), pp.6054–6074.

Eilers, M. et al., 2000. Internal packing of helical membrane proteins. *Proceeding of the National Academy of Science*, pp.5796–5801.

Eilers, M. et al., 2005. Comparison of class A and D G protein-coupled receptors: common features in structure and activation. *Biochemistry*, 44(25), pp.8959–8975.

Ellgaard, L. & Helenius, A., 2003. Quality control in the endoplasmic reticulum. *Nature Reviews: Molecular Cell Biology*, 4(3), pp.181–191.

Fairman, J.W., et al., 2011. The structural biology of β-barrel membrane proteins: a summary of recent reports. *Current opinion in structural biology*, 21(4), pp.523–531.

Fanucci, G., 2006. Recent advances and applications of site-directed spin labeling. *Current opinion in structural biology*.

Farooqi, I.S. et al., 2003. Clinical spectrum of obesity and mutations in the melanocortin 4 receptor gene. *New England Journal of Medicine*, 348(12), pp.1085–1095.

Farrow, N.A. et al., 1994. Backbone dynamics of a free and phosphopeptide-complexed Src homology 2 domain studied by 15N NMR relaxation. *Biochemistry*, 33(19), pp.5984–6003.

Feigenson, G.W., 2007. Phase boundaries and biological membranes. *Biophysics and Biomolecular Structure*, 36, pp.63–77.

Ferguson, S.S. et al., 1996. G-protein-coupled receptor regulation: role of G-protein-coupled receptor kinases and arrestins. *Canadian Journal of Physiology and Pharmacology/Revue Canadienne de Physiologie et Pharmacologie*, 74(10), pp.1095–1110.

Finbow, M.E. & Pitts, J.D., 1998. Structure of the ductin channel. *Bioscience reports*, 18(6), pp.287–297.

Finger, C.C., et al., 2009. The single transmembrane domains of human receptor tyrosine kinases encode self-interactions. *Audio, Transactions of the IRE Professional Group on*, 2(89), pp.ra56–ra56.

Fitzsimmons, T.J., et al., 2003. The extracellular domain of receptor activity-modifying protein 1 is sufficient for calcitonin receptor-like receptor function. *Journal of Biological Chemistry*, 278(16), pp.14313–14320.

Foord, S.M. & Marshall, F.H., 1999. RAMPs: accessory proteins for seven transmembrane domain receptors. *Trends in Pharmacological Sciences*, 20(5), pp.184–187.

Franco, R. et al., 2007. Basic Concepts in G-Protein-Coupled Receptor Homo- and Heterodimerization. *The Scientific World journal*, 7, pp.48–57.

Frank, J., 2006. *Three-Dimensional Electron Microscopy of Macromolecular Assemblies : Visualization of Biological Molecules in Their Native State*, Oxford University Press.

Fraser, N.J. et al., 1999. The amino terminus of receptor activity modifying proteins is a critical determinant of glycosylation state and ligand binding of calcitonin receptor-like receptor. *Molecular pharmacology*, 55(6), pp.1054–1059.

Fredriksson, R.R. et al., 2003. The G-protein-coupled receptors in the human genome form five main families. Phylogenetic analysis, paralogon groups, and fingerprints. *Molecular pharmacology*, 63(6), pp.1256–1272.

Fridmanis, D. et al., 2010. Identification of domains responsible for specific membrane transport and ligand specificity of the ACTH receptor (MC2R). *Molecular and Cellular Endocrinology*, 321(2), pp.9–9.

Gabriel, N.E. & Roberts, M.F.M., 1984. Spontaneous formation of stable unilamellar vesicles. *Biochemistry*, 23(18), pp.4011–4015.

Gangula, P.R. et al., 2003. Mechanisms involved in calcitonin gene-related Peptide-induced relaxation in pregnant rat uterine artery. *Biology of Reproduction*, 69(5), pp.1635–1641.

Gantz, I. et al., 1993. Molecular cloning, expression, and gene localization of a fourth melanocortin receptor. *Journal of Biological Chemistry*, 268(20), pp.15174–15179.

Gantz, I. & Fong, T.M., 2003. The melanocortin system. *American journal of Physiology. Endocrinology and Metabolism*, 284(3), pp.E468–74.

Gardiner, K.K. et al., 2002. Annotation of Human Chromosome 21 for Relevance to Down Syndrome: Gene Structure and Expression Analysis. *Genomics*, 79(6), pp.11–11.

Gaponenko, V.V. et al., 2000. Protein global fold determination using site-directed spin and isotope labeling. *Protein Science: A Publication of the Protein Society*, 9(2), pp.302–309.

Gautier, A. et al., 2010. Structure determination of the seven-helix transmembrane receptor sensory rhodopsin II by solution NMR spectroscopy. *Nature structural & molecular biology*, 17(6), pp.768–774.

Getting, S.J. et al., 2008. A role for MC3R in modulating lung inflammation. *Pulmonary Pharmacology & Therapeutics*, 21(6), pp.8–8.

Gilman, A.G., 1987. G proteins: transducers of receptor-generated signals. *Annual review of biochemistry*.

Gineau, L. et al., 2012. Partial MCM4 deficiency in patients with growth retardation, adrenal insufficiency, and natural killer cell deficiency. *The Journal of clinical investigation*, 122(3), pp.821–832.

Giraldo, J. & Pin, J.-P., 2011. *G Protein-Coupled Receptors*, Royal Society of Chemistry.

Glatter, O. & Kratky, O., 1982. Small angle x-ray scattering. *Academic Press*.

Glover, K.J. et al., 2001. Structural Evaluation of Phospholipid Bicelles for Solution-State Studies of Membrane-Associated Biomolecules. *Biophysical Journal*.

Gluck et al., 2011. Solution NMR Spectroscopy and Protein Interaction Studies of Membrane Proteins in Nanodiscs. *Biophysical journal*, 100(3), pp.0–0.

Goncalves, J.A. et al., 2010. Structure and function of G protein-coupled receptors using NMR spectroscopy. *Progress in Nuclear Magnetic Resonance Spectroscopy*, 57(2), pp.22–22.

Gorrigan, R.J. et al., 2011. Localisation of the melanocortin-2-receptor and its accessory proteins in the developing and adult adrenal gland. *Journal of Molecular Endocrinology*, 46(3), pp.227–232.

Granseth, E.E., et al., 2005. A Study of the Membrane-Water Interface Region of Membrane Proteins. *Journal of Molecular Biology*, 346(1), pp.9–9.

Gratkowski, H., et al., 2001. Polar side chains drive the association of model transmembrane peptides. *Proceeding of the National Academy of Science*, pp.880–885.

Grecco, H.E., et al., 2011. Signaling from the Living Plasma Membrane. *Cell*, 144(6), pp.13–13.

Greenfield, J.J. & High, S., 1999. The Sec61 complex is located in both the ER and the ER-Golgi intermediate compartment. *Journal of Cell Science*.

Grieco, P. et al., 2002. Synthesis and biological evaluation on hMC3, hMC4 and hMC5 receptors of gamma-MSH analogs substituted with L-alanine. *The journal of peptide research : Official Journal of the American Peptide Society*, 59(5), pp.203–210.

Griffiths, G., 2007. Cell evolution and the problem of membrane topology. *Nature Reviews: Molecular Cell Biology*, 8(12), pp.1018–1024.

Grzesiek, S.S., et al., 1993. A simple and sensitive experiment for measurement of JCC couplings between backbone carbonyl and methyl carbons in isotopically enriched proteins. *Journal of Biomolecular NMR*, 3(4), pp.487–493.

Guvench, O.O. & MacKerell, A.D., 2008. Comparison of protein force fields for molecular dynamics simulations. *Methods in Molecular Biology*, 443, pp.63–88.

Gurevich, V.V. & Gurevich, E.V., 2006. The structural basis of arrestin-mediated regulation of G-protein-coupled receptors. *Pharmacology & therapeutics*, 110(3), pp.38–38.

Haar, ter, E. et al., 2010. Crystal Structure of the Ectodomain Complex of the CGRP Receptor, a Class-B GPCR, Reveals the Site of Drug Antagonism. *Structure/Folding and Design*, 18(9), pp.1083–1093.

Hadley, M.E.M. et al., 1996. Melanocortin receptors: identification and characterization by melanotropic peptide agonists and antagonists. *Pigment Cell Research*, 9(5), pp.213–234.

Hansen, M.R., et al., 1998. Tunable alignment of macromolecules by filamentous phage yields dipolar coupling interactions. *Nature structural & molecular biology*, 5(12), pp.1065–1074.

Harikumar, K.G. et al., 2009. The molecular basis of association of receptor activitymodifying protein 3 with the family B G-protein-coupled secretin receptor. *Biochemistry*, 48(49), pp.11773–11785.

Hartmann, E., et al., 1989. Predicting the orientation of eukaryotic membrane-spanning proteins. *Proceeding of the National Academy of Science*, pp. 5786–5790.

Hauser, H.H., 2000. Short-chain phospholipids as detergents. *Biochimica et Biophysica Acta - Bioenergetics*, 1508(1-2), pp.164–181.

Hay, D.L. et al., 2003. CL/RAMP2 and CL/RAMP3 produce pharmacologically distinct adrenomedullin receptors: a comparison of effects of adrenomedullin22-52, CGRP8-37 and BIBN4096BS. *British Journal of Pharmacology*, 140(3), pp.477–486.

Hay, D. & Poyner, D., 2006. GPCR modulation by RAMPs. *Pharmacology & therapeutics*.

Heijne, von, G.G., 1981. Membrane proteins: the amino acid composition of membrane-penetrating segments. *Federation of European Biochemical Societies Journal*, 120(2), pp.275–278.

Heijne, von, G., 1986. The distribution of positively charged residues in bacterial inner membrane proteins correlates with the trans-membrane topology. *The EMBO journal*, 5(11), pp.3021–3027.

Heijne, von, G. & Gavel, Y., 1988. Topogenic signals in integral membrane proteins. *European journal of biochemistry / Federation of European Biochemical Societies Journal*, 174(4), pp.671–678.

Heijne, von, G., 1992. Membrane protein structure prediction: Hydrophobicity analysis and the positive-inside rule. *Journal of Molecular Biology*.

Heijne, von, G., 2006. Membrane-protein topology. *Nature Reviews: Molecular Cell Biology*, 7(12), pp.909–918.

Heng, B.C., et al., 2013. An overview of the diverse roles of G-protein coupled receptors (GPCRs) in the pathophysiology of various human diseases. *Biotechnology advances*.

Henry, G.D. & Sykes, B.D., 1994. Methods to study membrane protein structure in solution. *Methods in enzymology*, 239, pp.515–535.

Héroux, M. et al., 2007. Assembly and Signaling of CRLR and RAMP1 Complexes Assessed by BRET †. *Biochemistry*, 46(23), pp.7022–7033.

Higy, M., Junne, T. & Spiess, M., 2004. Topogenesis of Membrane Proteins at the Endoplasmic Reticulum †. *Biochemistry*, 43(40), pp.12716–12722.

Hilairet, S., 2001. Agonist-promoted Internalization of a Ternary Complex between Calcitonin Receptor-like Receptor, Receptor Activity-modifying Protein 1 (RAMP1), and beta -Arrestin. *Journal of Biological Chemistry*, 276(45), pp.42182–42190.

Hiller, S. et al., 2009. Coupled Decomposition of Four-Dimensional NOESY Spectra. *Journal of the American Chemical Society*, 131(36), pp.12970–12978.

Hinkle, P. & Sebag, J., 2009. Structure and function of the melanocortin2 receptor accessory protein (MRAP). *Molecular and Cellular Endocrinology*, 300, pp.25-31.

Hinkle, P.M. et al., 2011. Use of chimeric melanocortin-2 and -4 receptors to identify regions responsible for ligand specificity and dependence on melanocortin 2 receptor accessory protein. *European journal of pharmacology*, 660, pp. 94-102.

Hiragushi, K. et al., 2004. The role of adrenomedullin and receptors in glomerular hyperfiltration in streptozotocin-induced diabetic rats. *Kidney international*, 65(2), pp.540–550.

Hirsch, A. et al., 2011. Loss of the C terminus of melanocortin receptor 2 (MC2R) results in impaired cell surface expression and ACTH insensitivity. *The Journal of Clinical Endocrinology and Metabolism*, 96(1), pp.65–72.

Hoare, S., 2005. Mechanisms of peptide and nonpeptide ligand binding to Class B G-protein-coupled receptors. *Drug Discovery Today*, 10(6), pp.417–427.

Hollenstein, K. et al., 2013. Structure of class B GPCR corticotropin-releasing factor receptor 1: Nature. Nature Publishing Group. *Nature*, 00, pp.1-7.

Holte, L.L. et al., 1995. 2H nuclear magnetic resonance order parameter profiles suggest a change of molecular shape for phosphatidylcholines containing a polyunsaturated acyl chain. *Biophysical Journal*, 68(6), pp.8–8.

Hopwood, D.D., et al., 1970. The reactions between glutaraldehyde and various proteins. An investigation of their kinetics. *The Histochemical Journal*, 2(2), pp.137–150.

Hou, Q. et al., 2011. Keratinocyte expression of calcitonin gene-related peptide β: Implications for neuropathic and inflammatory pain mechanisms. *PAIN*, 152(9), pp.2036–2051.

Hughes, C.R. et al., 2010. Missense Mutations in the Melanocortin 2 Receptor Accessory Protein That Lead to Late Onset Familial Glucocorticoid Deficiency Type 2. *The Journal of Clinical Endocrinology and Metabolism*, 95(7), pp.3501.

Huschilt, J.C., et al., 1989. Orientation of alpha-helical peptides in a lipid bilayer. *Biochimica et Biophysica Acta - Bioenergetics*, 979(1), pp.139–141.

Husmann, K.K. et al., 2000. Mouse receptor-activity-modifying proteins 1, -2 and -3: amino acid sequence, expression and function. *Molecular and Cellular Endocrinology*, 162(1-2), pp.35–43.

Ikeda, M., et al., 2006. Lipid asymmetry of the eukaryotic plasma membrane: functions and related enzymes. *Biological & Pharmaceutical Bulletin*, 29(8), pp.1542–1546.

Jean-Alphonse, F. & Hanyaloglu, A.C., 2010. Regulation of GPCR signal networks via membrane trafficking. *Molecular and Cellular Endocrinology*, 2, pp.205-214.

Jeannin, P.P. et al., 2005. Complexity and Complementarity of Outer Membrane Protein A Recognition by Cellular and Humoral Innate Immunity Receptors. *Journal of Immunity*, 22(5), pp.10–10.

Jenei, Z.A. et al., 2011. Packing of transmembrane domain 2 of carnitine palmitoyltransferase-1A affects oligomerization and malonyl-CoA sensitivity of the mitochondrial outer membrane protein. *Federation of American Societies for Experimental Biology Journal*, 25(12), pp.4522–4530.

Jones, J.A. et al., 1996. Optimal Sampling Strategies for the Measurement of Spin-Spin Relaxation Times. *Journal of Magnetic Resonance, Series B*, 113(1), pp.10–10.

Jones, J.A. et al., 1997. Characterisation of protein unfolding by NMR diffusion measurements. *Journal of Biomolecular NMR*, 10(2), pp.199–203.

Jones, D.T., 1999. Protein secondary structure prediction based on position-specific scoring matrices. *Journal of Molecular Biology*, 292(2), pp.8–8.

Jones, D.H. & Opella, S.J., 2004. Weak alignment of membrane proteins in stressed polyacrylamide gels. *Journal of Magnetic Resonance*, 171,pp. 25-269.

Karplus, M. & Kuriyan, J., 2005. Molecular dynamics and protein function. *Proceeding of the National Academy of Science*, 102(19), pp.6679–6685.

Katritch, V.V., et al., 2012. Diversity and modularity of G protein-coupled receptor structures. *Trends in Pharmacological Sciences*, 33(1), pp.17–27.

Kay, E.I., et al., 2013a. hMRAPa increases αMSH-induced hMC1R and hMC3R functional coupling and hMC4R constitutive activity. *Journal of Molecular Endocrinology*, 50(2), pp.203–215.

Kay, E.I., et al., 2013b. hMRAPa specifically alters hMC4R molecular mass and N-linked complex glycosylation in HEK293 cells. *Journal of Molecular Endocrinology*, 50(2), pp.217–227.

Kay, L.E. & Prestegard, J.H., 1986. An application of pulse-gradient double-quantum spin echoes to diffusion measurements on molecules with scalar-coupled spins. *Journal of Magnetic Resonance*, 67(1), pp.103–113.

Kay, L.E., et al., 1989. Backbone dynamics of proteins as studied by 15N inverse detected heteronuclear NMR spectroscopy: application to staphylococcal nuclease. *Journal of Biochemistry*, 28(23), pp.8972–8979.

Keeler, J., 2011. *Understanding NMR Spectroscopy*, Wiley.

Keller R, Wuthrich.K., *Computer-aided resonance assignment (CARA)*,

Kelly, S.M., et al., 2005. How to study proteins by circular dichroism. *Biochimica et Biophysica Acta - Proteins & Proteomics*, 1751(2), pp.119–139.

Kendrew, J.C. et al., 1958. Nature physics portal - looking back - X-ray crystallography - the first image of myoglobin. *Nature*, 133, pp.794-795.

Kilianova, Z. et al., 2006. Human Melanocortin Receptor 2 Expression and Functionality: Effects of Protein Kinase A and Protein Kinase C on Desensitization and Internalization. *Journal of Endocrinology*, 147(5), pp.2325–2337.

Kim, N.S. et al., 2013. Transcriptional activation of melanocortin 2 receptor accessory protein by PPARÎ³ in adipocytes. *Biochemical and biophysical research communications*, 439(3), pp.401-406.

King, G. et al., 2011. Towards a structural understanding of the smallest known oncoprotein: investigation of the bovine papillomavirus E5 protein using solution-state NMR. *Biochimica et Biophysica Acta - Bioenergetics*, 1808(6), pp.1493–1501.

Klein, P.S. et al., 1988. A chemoattractant receptor controls development in Dictyostelium discoideum. *Science*, 241(4872), pp.1467–1472.

Kluger, R.R. & Alagic, A.A., 2004. Chemical cross-linking and protein-protein interactions-a review with illustrative protocols. *Bioorganic Chemistry*, 32(6), pp.451–472.

Kneller, J.M., et al., 2002. An Effective Method for the Discrimination of Motional Anisotropy and Chemical Exchange. *Journal of the American Chemical Society*, 124(9), pp.1852–1853.

Kolakowski L.F., 1994. GCRDb: a G-protein-coupled receptor database. *Receptors & channels*, 2(1), pp.1–7.

Korkhov, V., 2009. An emerging consensus for the structure of EmrE. *Acta Crystallographica Section D: Biological Crystallography*, D65, pp.186-192.

Korukottu, J.J. et al., 2008. High-resolution 3D structure determination of kaliotoxin by solid-state NMR spectroscopy. *PLoS ONE*, 3(6), pp.2359–2359.

Koth, C.M. et al., 2010. Refolding and characterization of a soluble ectodomain complex of the calcitonin gene-related peptide receptor. *Biochemistry*, 49(9), pp.1862–1872.

Kroeze, W.K., et al., 2003. G-protein-coupled receptors at a glance. *Journal of Cell Science*, 116(24), pp.4867–4869.

Krogh, A.A. et al., 2001. Predicting transmembrane protein topology with a hidden Markov model: application to complete genomes. *Journal of Molecular Biology*, 305(3), pp.567–580.

Krueger-Koplin, R.D. et al., 2004. An evaluation of detergents for NMR structural studies of membrane proteins. *Journal of Biomolecular NMR*, 28(1), pp.43–57.

Kruijff de B. B. et al., 2006. Striated domains: self-organizing ordered assemblies of transmembrane alpha-helical peptides and lipids in bilayers. *Biological Chemistry*, 387(3), pp.235–241.

Kubatzky, K.F. et al., 2001. Self assembly of the transmembrane domain promotes signal transduction through the erythropoietin receptor. *Current Biology*, 11(2), pp.6–6.

Kuhn, A., 1987. Bacteriophage M13 procoat protein inserts into the plasma membrane as a loop structure. *Science*, 238(4832), pp.1413–1415.

Kukić, P. & Nielsen, J.E., 2010. Electrostatics in proteins and protein–ligand complexes. *Future Medicinal Chemistry*, 2(4), pp.647–666.

Kumar, A., et al., 1981. Buildup rates of the nuclear Overhauser effect measured by two-dimensional proton magnetic resonance spectroscopy: implications for studies of protein conformation. *Journal of the American Chemical Society*, 103, pp.3654-3658.

Kusano, S. et al., 2008. Crystal structure of the human receptor activity-modifying protein 1 extracellular domain. *Protein Science: A Publication of the Protein Society*, 17(11), pp.1907–1914.

Kuszewski, J., et al., 1997. Improvements and extensions in the conformational database potential for the refinement of NMR and X-ray structures of proteins and nucleic acids. *Journal of magnetic resonance*, 125(1), pp.171–177.

Kuwasako, K. et al., 2003. Novel calcitonin-(8–32)-sensitive adrenomedullin receptors derived from co-expression of calcitonin receptor with receptor activity-modifying proteins. *Biochemical and biophysical research communications*, 301(2), pp.460–464.

Kuwasako, K. et al., 2000. Visualization of the calcitonin receptor-like receptor and its receptor activity-modifying proteins during internalization and recycling. *Journal of Biological Chemistry*, 275(38), pp.29602–29609.

Kuwasako, K.K. et al., 2004. Adrenomedullin receptors: pharmacological features and possible pathophysiological roles. *Peptides*, 25(11), pp.2003–2012.

Lacapère, J.J. et al., 2007. Determining membrane protein structures: still a challenge! *Trends in Biochemical Sciences*, 32(6), pp.259–270.

Lagerström, M.C. & Schiöth, H.B., 2008. Structural diversity of G protein-coupled receptors and significance for drug discovery. *Nature reviews. Drug discovery*, 7(4), pp.339–357.

Lander, G.C., Saibil, H.R. & Nogales, E., 2012. Go hybrid: EM, crystallography, and beyond. *Current Opinion in Structural Biology*, 22(5), pp.627–635.

Lambert, C. & Prange, R., 2001. Dual topology of the hepatitis B virus large envelope protein: determinants influencing post-translational pre-S translocation. *Journal of Biological Chemistry*, 276(25), pp.22265–22272.

Larkin, M.A. et al., 2007. Clustal W and Clustal X version 2.0.

Laskowski, R. et al., 1996. AQUA and PROCHECK-NMR: Programs for checking the quality of protein structures solved by NMR. *Journal of Biomolecular NMR*, 8(4), pp.477–486.

Lau, T.L., et al., 2008. Structure of the integrin alphaIIb transmembrane segment. *Journal of Biological Chemistry*, 283(23), pp.16162–16168.

Lau, T.L., et al., 2009. The structure of the integrin αIIbβ3 transmembrane complex explains integrin transmembrane signalling. *The EMBO journal*, 28(9), pp.1351–1361.

Leach, A.R., 2001. Molecular Modelling: Principles and Applications. *Pearson* College Division.

Lear, J.D., et al., 1988. Synthetic amphiphilic peptide models for protein ion channels. *Science*, 240(4856), pp.1177–1181.

Lee, S., et al., 2003. Structure and dynamics of a membrane protein in micelles from three solution NMR experiments. *Journal of Biomolecular NMR*, 26(4), pp.327–334.

le Maire, M.M., et al., 2000. Interaction of membrane proteins and lipids with solubilizing detergents. *Biochimica et Biophysica Acta - Bioenergetics*, 1508(1-2), pp.86–111.

Lemmon, M.A. et al., 1992. Sequence specificity in the dimerization of transmembrane alpha-helices. *Journal of Biochemistry*, 31(51), pp.12719–12725.

Lemmon, M.A., 2009. Ligand-induced ErbB receptor dimerization. *Experimental Cell Research*, 315(4), pp.638–648.

Leuthäuser, K. et al., 2000. Receptor-activity-modifying protein 1 forms heterodimers with two G-protein-coupled receptors to define ligand recognition. *Biochemical Journal*, 351(2), pp. 347-351.

Levitt, M.H., 2013. *Spin Dynamics*, John Wiley & Sons.

Li, Wimley Hristova, 2012. Transmembrane helix dimerization: Beyond the search for sequence motifs. *Biochimica et Biophysica Acta -Biomembranes*, 1818(2), pp.183-193.

Liang, B., et al., 2006. Site-directed parallel spin-labeling and paramagnetic relaxation enhancement in structure determination of membrane proteins by solution NMR spectroscopy. *Journal of the American Chemical Society*, 128(13), pp.4389–4397.

Liang, L. et al., 2011. Functional expression of frog and rainbow trout melanocortin 2 receptors using heterologous MRAP1s. *General and Comparative Endocrinology*, 174(1), pp.5–14.

Liao, M. et al., 2013. Structure of the TRPV1 ion channel determined by electron cryo-microscopy. *Nature*, 504(7478), pp.107–112.

Libich, D.S. et al., 2009. Intrinsic disorder and coiled-coil formation in prostate apoptosis response factor 4. *Federation of European Biochemical Societies Journal*, 276(14), pp.3710–3728.

Lichtenberg, D., et al., 2013a. The mechanism of detergent solubilization of lipid bilayers. *Biophysical journal*, 105(2), pp.289–299.

Lichtenberg, D.D., et al., 2013b. Detergent solubilization of lipid bilayers: a balance of driving forces. *Trends in biochemical sciences*, 38(2), pp.85–93.

Lingwood, D. & Simons, K., 2009. Lipid Rafts As a Membrane-Organizing Principle. *Science*, 327(5961), pp.46–50.

Lipsitz, R.S. & Tjandra, N., 2004. Residual dipolar couplings in NMR structure analysis. *Biophysics and Biomolecular Structure*, 33, pp. 387-413.

Löhr, F. et al., 2012. Combinatorial triple-selective labeling as a tool to assist membrane protein backbone resonance assignment. *Journal of Biomolecular NMR*, 52(3), pp.197–210.

Loura, L.M., et al. 2010. Membrane microheterogeneity: Förster resonance energy transfer characterization of lateral membrane domains. *European Biophysics Journal*, 39(4), pp.589–607.

Lu, D.D. et al., 1994. Agouti protein is an antagonist of the melanocyte-stimulating-hormone receptor. *Nature*, 371(6500), pp.799–802.

Lu, H., et al., 2001. Proline residues in transmembrane alpha helices affect the folding of bacteriorhodopsin. *Journal of Molecular Biology*, 308(2), pp.437–446.

Luchette, P.A. et al., 2001. Morphology of fast-tumbling bicelles: a small angle neutron scattering and NMR study. *Biochimica et Biophysica Acta - Biomembranes*, 1513(2), pp.83–94.

Lupas, A., 1996. Coiled coils: new structures and new functions. *Trends in biochemical sciences*, 21(10), pp.375–382.

MacKenzie, K.R. & Prestegard, J., 1996. Leucine side-chain rotamers in a glycophorin A transmembrane peptide as revealed by three-bond carbon—carbon couplings and 13 C chemical shifts. *Journal of Biomolecular NMR*, 7, pp. 256-260.

MacKenzie, K.R., et al., 1997. A transmembrane helix dimer: structure and implications. *Science*, 276(5309), pp.131–133.

Magalhaes, A.C., et al., 2012. Regulation of GPCR activity, trafficking and localization by GPCR-interacting proteins. *British Journal of Pharmacology*, 165(6), pp.1717–1736.

Mainz, A. et al., 2013. NMR spectroscopy of soluble protein complexes at one mega-dalton and beyond. *Angewandte Chemie International Edition*, 52(33), pp.8746–8751.

Mall, S.S. et al., 2001. Self-association of model transmembrane alpha-helices is modulated by lipid structure. *Journal of Biochemistry*, 40(41), pp.12379–12386.

Mallee, J.J. et al., 2002. Receptor activity-modifying protein 1 determines the species selectivity of non-peptide CGRP receptor antagonists. *Journal of Biological Chemistry*, 277(16), pp.14294–14298.

Manning, G. et al., 2002. Evolution of protein kinase signaling from yeast to man. *Trends in biochemical sciences*, 27(10), pp.514–520.

Marrink, S.J., et al., 2004. Coarse Grained Model for Semiquantitative Lipid Simulations. *The journal of physical chemistry B*, 108(2), pp.750–760.

Marrink, S.J. et al., 2007. The MARTINI Force Field: Coarse Grained Model for Biomolecular Simulations. *The Journal of Physical Chemistry*, 111(27), pp.7812–7824.

Marsh, D., 2013. *Handbook of Lipid Bilayers*, CRC Press.

Mascioni, A. & Veglia, G., 2003. Theoretical Analysis of Residual Dipolar Coupling Patterns in Regular Secondary Structures of Proteins. *Journal of the American Chemical Society*, 125(41), pp.12520–12526.

Maslennikov, A.A., et al., 2007. [Immunological correction in progressive pulmonary tuberculosis]. *Problemy tuberkuleza i bolezneĭ legkikh*, 9, pp.30–33.

Mattson, G. et al., 1993. A practical approach to crosslinking. *Molecular Biology Reports*, 17(3), pp.167–183.

McLatchie, L.M. et al., 1998. RAMPs regulate the transport and ligand specificity of the calcitonin-receptor-like receptor. *Nature*, 393(6683), pp.333–339.

Meiboom, S. & Gill, D., 1958. Modified Spin-Echo Method for Measuring Nuclear Relaxation Times. *Review of Scientific Instruments*, 29(8), pp.688–691.

Meimaridou, E. et al., 2012. Familial glucocorticoid deficiency: New genes and mechanisms. *Molecular and Cellular Endocrinology*, 371(1-2), pp. 195-200.

Mendes, H.F. et al., 2005. Mechanisms of cell death in rhodopsin retinitis pigmentosa: implications for therapy. *Trends in Molecular Medicine*, 11(4), pp.9–9.

Mesleh, M.F. et al., 2002. Dipolar waves as NMR maps of protein structure. *Journal of the American Chemical Society*, 124(16), pp.4206–4207.

Metherell, L.A. et al., 2005. Mutations in MRAP, encoding a new interacting partner of the ACTH receptor, cause familial glucocorticoid deficiency type 2. *Nature genetics*, 37(2), pp.166–170.

Metherell, L.A., et al., 2006. The genetics of ACTH resistance syndromes. *Best Practice & Research Clinical Endocrinology & Metabolism*, 20(4), pp.547–560.

Metherell, L.A. et al., 2009. Nonclassic lipoid congenital adrenal hyperplasia masquerading as familial glucocorticoid deficiency. *The Journal of clinical Endocrinology and Metabolism*, 94(10), pp.3865–3871.

Micelli, S.S. et al., 2004. Effect of nanomolar concentrations of sodium dodecyl sulfate, a catalytic inductor of alpha-helices, on human calcitonin incorporation and channel formation in planar lipid membranes. *Biophysical Journal*, 87(2), pp.1065–1075.

Migneault, I.I. et al., 2004. Glutaraldehyde: behavior in aqueous solution, reaction with proteins, and application to enzyme crosslinking. *BioTechniques*, 37(5), pp.790–802.

Modan-Moses, D.D. et al., 2006. Unusual presentation of familial glucocorticoid deficiency with a novel MRAP mutation. *Journal of Clinical Endocrinology & Metabolism*, 91(10), pp.3713–3717.

Moore, E.L. & Salvatore, C.A., 2012. Targeting a family B GPCR/RAMP receptor complex: CGRP receptor antagonists and migraine. *British Journal of Pharmacology*, 166(1), pp.66–78.

Morfis, M., et al., 2003. RAMPs: 5 years on, where to now? *Trends in Pharmacological Sciences*, 24(11), pp.596–601.

Morris, D.G. et al., 2003. Identification of adrenocorticotropin receptor messenger ribonucleic acid in the human pituitary and its loss of expression in pituitary adenomas. *Journal of Clinical Endocrinology & Metabolism*, 88(12), pp.6080–6087.

Mountjoy, K.G. et al., 1994. ACTH induces up-regulation of ACTH receptor mRNA in mouse and human adrenocortical cell lines. *Molecular and Cellular Endocrinology*, 99(1), pp.17–20.

Mueller, L., 1979. Sensitivity enhanced detection of weak nuclei using heteronuclear multiple quantum coherence. *Journal of the American Chemical Society*, 101(16), pp.4481–4484.

Murakami, M.M. & Kouyama, T.T., 2008. Crystal structure of squid rhodopsin. *Nature*, 453(7193), pp.363–367.

Muthuswamy, S.K., Gilman, M. & Brugge, J.S., 1999. Controlled dimerization of ErbB receptors provides evidence for differential signaling by homo- and heterodimers. *Molecular and Cellular Biology*, 19(10), pp.6845–6857.

Naarmann, N.N. et al., 2005. Controlling association of vesicle embedded peptides by alteration of the physical state of the lipid matrix. *Biochemistry*, 44(13), pp.5188–5195.

Nagle, J.F. et al., 1996. X-ray structure determination of fully hydrated L alpha phase dipalmitoylphosphatidylcholine bilayers. *Biophysical Journal*, 70(3), pp.1419-1431.

Nankova, B.B., et al., 2003. Adrenocorticotropic hormone (MC-2) receptor mRNA is expressed in rat sympathetic ganglia and up-regulated by stress. *Neuroscience Letters*, 344(3), pp.149–152.

Naville, D.D. et al., 1997. Genomic Structure and Promoter Characterization of the Human ACTH Receptor Gene. *Biochemical and biophysical research communications*, 230(1), pp.6–6.

Neal, S.S. et al., 2003. Rapid and accurate calculation of protein 1H, 13C and 15N chemical shifts. *Journal of Biomolecular NMR*, 26(3), pp.215–240.

Neale, C. et al., 2013. Detergent-mediated protein aggregation. *Chemistry and Physics of Lipids*, 169, pp.72–84.

Neri, D. et al., 1989. Stereospecific nuclear magnetic resonance assignments of the methyl groups of valine and leucine in the DNA-binding domain of the 434 repressor by biosynthetically directed fractional 13C labeling. *Journal of Biochemistry*, 28(19), pp.7510–7516.

Nishikimi, T. et al., 2005. Alteration of renal adrenomedullin and its receptor system in the severely hypertensive rat: effect of diuretic. *Regulatory Peptides*, 124(1-3), pp.89–98.

Nilsson, J.J., et al., 2005. Comparative analysis of amino acid distributions in integral membrane proteins from 107 genomes. *Proteins*, 60(4), pp.606–616.

Noon, L.A. et al., 2002. Failed export of the adrenocorticotrophin receptor from the endoplasmic reticulum in non-adrenal cells: evidence in support of a requirement for a specific adrenal accessory factor. *Journal of Endocrinology*, 174(1), pp.17–25.

North, B.B. et al., 2006. Characterization of a Membrane Protein Folding Motif, the Ser Zipper, Using Designed Peptides. *Journal of Molecular Biology*, 359(4), pp.930-939.

North, C.L. & Blacklow, S.C., 1999. Structural independence of ligand-binding modules five and six of the LDL receptor. *Biochemistry*, 38(13), pp.3926–3935.

Nyholm, T.K., et al., 2007. How protein transmembrane segments sense the lipid environment. *Biochemistry*, 46(6), pp.1457–1465.

Oie, E. et al., 2000. Induction of a myocardial adrenomedullin signaling system during ischemic heart failure in rats. *Journal of the American Heart Association*, 101(4), pp.415–422.

Oliver, K.R. et al., 2001. Cloning, characterization and central nervous system distribution of receptor activity modifying proteins in the rat. *European Journal of Neuroscience*, 14(4), pp.618–628.

Oliver, R.C. et al., 2013. Dependence of micelle size and shape on detergent alkyl chain length and head group. *PLoS ONE*, 8(5), pp.62488–62488.

Opella, S.J. & Marassi, F.M., 2004. Structure Determination of Membrane Proteins by NMR Spectroscopy. *Chemical reviews*, 104(8), pp.3587–3606.

Orlova, E.V. & Saibil, H.R., 2011. Structural analysis of macromolecular assemblies by electron microscopy. *Chemical reviews*, 111, pp. 7710-7748.

Ott, C.M. & Lingappa, V.R., 2004. Signal sequences influence membrane integration of the prion protein. *Journal of Biochemistry*, 43(38), pp.11973–11982.

Ottiger, M.M. & Bax, A.A., 1998. Characterization of magnetically oriented phospholipid micelles for measurement of dipolar couplings in macromolecules. *Journal of Biomolecular NMR*, 12(3), pp.361–372.

Otzen, D.E., 2002. Protein unfolding in detergents: Effect of micelle structure, ionic strength, pH, and temperature. *Biophysical Journal*, 83(4), pp.2219–2230.

Palczewski, K.K. et al., 2000. Crystal structure of rhodopsin: A G protein-coupled receptor. *Science*, 289(5480), pp.739–745.

Pan, J. et al., 2012. Molecular structures of fluid phase phosphatidylglycerol bilayers as determined by small angle neutron and X-ray scattering. *Biochimica et Biophysica Acta -Biomembranes*, 1818(9), pp.2135–2148.

Parameswaran, N. & Spielman, W.S., 2006. RAMPs: the past, present and future. *Trends in biochemical sciences*, 31(11), pp.631–638.

Prestegard, J.H., et al., 2004. Residual dipolar couplings in structure determination of biomolecules. *Chemical reviews*, 104(8), pp.3519–3540.

Pascal, S.M., 2008. NMR Primer, *IM Publications*.

Pascual, J. et al., 1997. Solution structure of the spectrin repeat: a left-handed antiparallel triple-helical coiled-coil. *Journal of Molecular Biology*, 273(3), pp.740–751.

Paulsen, I.T. et al., 1996. The SMR family: a novel family of multidrug efflux proteins involved with the efflux of lipophilic drugs. *Molecular Microbiology*, 19(6), pp.1167–1175.

Pearlman, S.M., et al., 2011. A mechanism for the evolution of phosphorylation sites. *Cell*, 147(4), pp.934–946.

Pecora, R., 1985. *Dynamic Light Scattering*, Plenum Publishing Corporation.

Perez, D.M., 2005. From plants to man: the GPCR "tree of life". *Molecular pharmacology*, 67(5), pp.1383–1384.

Pervushin, K. et al., 1997. Attenuated T2 relaxation by mutual cancellation of dipole–dipole coupling and chemical shift anisotropy indicates an avenue to NMR structures of very large biological macromolecules in solution. *Proceeding of the National Academy of Science* , 94, pp.12366-12371.

Pi, M. et al., 2005. Identification of a novel extracellular cation-sensing G-protein-coupled receptor. *Journal of Biological Chemistry*, 280(48), pp.40201–40209.

Pluhackova, K., Wassenaar, T.A. & Böckmann, R.A., 2012. Molecular dynamics simulations of membrane proteins. *Methods in Molecular Biology*, 1033, pp.85–101.

Popot, J.L. & Engelman, D.M., 2000. Helical membrane protein folding, stability, and evolution. *Annual review of Biochemistry*, 69(1), pp.881–922.

Poyner, D.R. et al., 2002. International Union of Pharmacology. XXXII. The mammalian calcitonin gene-related peptides, adrenomedullin, amylin, and calcitonin receptors. *Pharmacological Reviews*, 54(2), pp.233–246.

Preininger, A.M., et al., 2013. Conformational Flexibility and Structural Dynamics in GPCR-Mediated G Protein Activation: A Perspective. *Journal of Molecular Biology*, 425(13), pp.2288–2298.

Prestegard, J.H., et al., 2004. Residual dipolar couplings in structure determination of biomolecules. *Chemical reviews*, 104(8), pp.3519–3540.

Qi, T. et al., 2011. Structure-function analysis of amino acid 74 of human RAMP1 and RAMP3 and its role in peptide interactions with adrenomedullin and calcitonin gene-related peptide receptors. *Peptides*, 32(5), pp.1060–1067.

Qin, L. et al., 2007. Conserved lipid-binding sites in membrane proteins: a focus on cytochrome c oxidase. *Current Opinion in Structural Biology*, 17(4), pp.444–450.

Rana, B.K., 2003. New insights into G-protein-coupled receptor signaling from the melanocortin receptor system. *Molecular Pharmacology*, 64(1), pp.1–4.

Rapp, M. et al., 2006. Identification and evolution of dual-topology membrane proteins. *Nature Structural &Mmolecular Biology*, 13(2), pp.112–116.

Rapp, M. et al., 2007. Emulating membrane protein evolution by rational design. *Science (New York, NY)*, 315(5816), pp.1282–1284.

Rasband, W.S., 2012. ImageJ: Image processing and analysis in Java. *Astrophysics Source Code Library*, p.06013.

Raschle, T. et al., 2010. Nonmicellar systems for solution NMR spectroscopy of membrane proteins. *Current opinion in structural biology*, 20(4), pp.471–479.

Rath, A. et al., 2009. Detergent binding explains anomalous SDS-PAGE migration of membrane proteins. *Proceeding of the National Academy of Science*, 106 (6), pp.1760–1765.

Rath, A. & Deber, C.M., 2013. Correction factors for membrane protein molecular weight readouts on sodium dodecyl sulfate-polyacrylamide gel electrophoresis. *Analytical biochemistry*, 434(1), pp.67–72.

Raymond S & Weintraub L., 1959. Acrylamide gel as a supporting medium for zone electrophoresis. *Science*, 130(3377), p.711.

Reinick, C.L. et al., 2012. Functional expression of Squalus acanthias melanocortin-5 receptor in CHO cells: ligand selectivity and interaction with MRAP. *European journal of pharmacology*, 161, pp.13-19.

Religa, T. & Sprangers, R., 2010. Dynamic regulation of archaeal proteasome gate opening as studied by TROSY NMR. *Science*, 328(98), pp. 97-100.

Rösner, H.I. & Kragelund, B.B., 2011. *Structure and Dynamic Properties of Membrane Proteins using NMR*, Hoboken, NJ, USA: John Wiley & Sons, Inc.

Roy, S., et al., 2010. Role of asparagine-linked glycosylation in cell surface expression and function of the human adrenocorticotropin receptor (melanocortin 2 receptor) in 293/FRT cells. *Journal of Endocrinology*, 151(2), pp.660–670.

Roy, S. et al., 2011. Adrenocorticotropin hormone (ACTH) effects on MAPK phosphorylation in human fasciculata cells and in embryonic kidney 293 cells expressing human melanocortin 2 receptor (MC2R) and MC2R accessory protein (MRAP)β. *Journal of Molecular and Cellular Endocrinology*, 336(1-2), pp.31–40.

Roy, S. et al., 2012. The C-terminal domains of melanocortin-2 receptor (MC2R) accessory proteins (MRAP1) influence their localization and ACTH-induced cAMP production. *General and comparative Endocrinology*, 176(2), pp.265–274.

Rudd, R. & Broughton, J., 1998. Coarse-grained molecular dynamics and the atomic limit of finite elements. *Physical Review B*, 58(10), pp.R5893–R5896.

Russ, W.P. & Engelman, D.M.D 2000. The GxxxG motif: A framework for transmembrane helix-helix association. *Journal of Molecular Biology*, 296(3), pp. 911-919.

Sadlish, H.H. & Skach, W.R., 2004. Biogenesis of CFTR and other polytopic membrane proteins: new roles for the ribosome-translocon complex. *Journal of Membrane Biology*, 202(3), pp.115–126.

Salvatore, C.A. et al., 2006. Identification and pharmacological characterization of domains involved in binding of CGRP receptor antagonists to the calcitonin-like receptor. *Biochemistry*, 45(6), pp.1881–1887.

Salvatore, C.A. et al., 2008. Pharmacological Characterization of MK-0974 [N-[(3R,6S)-6-(2,3-Difluorophenyl)-2-oxo-1-(2,2,2-trifluoroethyl)azepan-3-yl]-4-(2-oxo-2,3-dihydro-1H-imidazo[4,5-b]pyridin-1-yl)piperidine-1-carboxamide], a Potent and Orally Active Calcitonin Gene-Related Peptide Receptor Antagonist for the Treatment of Migraine. *The Journal of Pharmacology and and experimental Therapeutics,* 324, pp. 416-421.

Salvatore, C.A. et al., 2010. Pharmacological Properties of MK-3207, a Potent and Orally Active Calcitonin Gene-Related Peptide Receptor Antagonist. *Journal of Pharmacology and Experimental Therapeutics*, 333(1), pp.152–160.

Sal-Man, N.N., et al., 2004. The composition rather than position of polar residues (QxxS) drives aspartate receptor transmembrane domain dimerization in vivo. *Biochemistry*, 43(8), pp.2309–2313.

Salahpour, A.A. et al., 2004. Homodimerization of the beta2-adrenergic receptor as a prerequisite for cell surface targeting. *Journal of Biological Chemistry*, 279(32), pp.33390–33397.

Sanchez, G. et al., 2004. Capsid region involved in hepatitis A virus binding to glycophorin A of the erythrocyte membrane. *Journal of Virology*, 78(18), pp.9807–9813.

Sanders, C.R. & Landis, G.C., 1995. Reconstitution of membrane proteins into lipid-rich bilayered mixed micelles for NMR studies. *Journal of Biochemistry*, 34(12), pp.4030–4040.

Sanders, C.R. & Mittendorf, K.F., 2011. Tolerance to changes in membrane lipid composition as a selected trait of membrane proteins. *Journal of Biochemistry*, 50(37), pp.7858–7867.

Sansom, M.S.P. & Weinstein, H.H., 2000. Hinges, swivels and switches: the role of prolines in signalling via transmembrane alpha-helices. *Trends in Pharmacological Sciences*, 21(11), pp.445–451.

Sansom, M.S.P. & Biggin, P.C., 2010. *Molecular Simulations and Biomembranes*, Royal Society of Chemistry.

Sass, H.J. et al., 2000. Solution NMR of proteins within polyacrylamide gels: diffusional properties and residual alignment by mechanical stress or embedding of oriented purple membranes. *Journal of Biomolecular NMR*, 18(4), pp.303–309.

Sato, M. et al., 2006. Accessory proteins for G-Proteins: Partners in Signaling. *Annual Review of Pharmacology and Toxicology*, 46(1), pp.151–187.

Schanda, P.P., et al., 2005. SOFAST-HMQC experiments for recording two-dimensional heteronuclear correlation spectra of proteins within a few seconds. *Journal of Biomolecular NMR*, 33(4), pp.199–211.

Schimmel, P.R. & Flory, P.J., 1968. Conformational energies and configurational statistics of copolypeptides containing L-proline. *Journal of Molecular Biology*, 34(1), pp.105–120.

Schiöth, H.B. & Fredriksson, R., 2005. The GRAFS classification system of G-protein coupled receptors in comparative perspective. *General and comperative Endocrinology*, 142(1-2), pp.94-101.

Schuck, P.P., 2000. Size-Distribution Analysis of Macromolecules by Sedimentation Velocity Ultracentrifugation and Lamm Equation Modeling. *Biophysical Journal*, 78(3), pp.1606-1619.

Schuldiner, S., 2009. EmrE, a model for studying evolution and mechanism of ion-coupled transporters. *Biochimica et biophysica acta*, 1794(5), pp.748–762.

Schwieters, C.D. et al., 2003. The Xplor-NIH NMR molecular structure determination package. *Journal of magnetic resonance (San Diego, Calif : 1997)*, 160(1), pp.65–73.

Sebag, J.A. & Hinkle, P.M., 2007. Melanocortin-2 receptor accessory protein MRAP forms antiparallel homodimers. *Proceedings of the National Academy of Sciences of the United States of America*, 104(51), pp.20244–20249.

Sebag, J. & Hinkle, P., 2009a. Opposite effects of the melanocortin-2 (MC2) receptor accessory protein MRAP on MC2 and MC5 receptor dimerization and trafficking. *Journal of Biological Chemistry*, 284(34), pp.22641–22648.

Sebag, J. & Hinkle, P., 2009b. Regions of Melanocortin 2 (MC2) Receptor Accessory Protein Necessary for Dual Topology and MC2 Receptor Trafficking and Signaling. *Journal of Biological Chemistry*, 284(1), pp. 610-618.

Sebag, J.A. & Hinkle, P.M., 2010. Regulation of G protein-coupled receptor signaling: specific dominant-negative effects of melanocortin 2 receptor accessory protein 2. *Science signaling*, 3(116), ra.28-35.

Sebag, J.A. et al., 2013. Developmental Control of the Melanocortin-4 Receptor by MRAP2 Proteins in Zebrafish. *Science*, 341(6143), pp.278–281.

Seddon, A.M., et al., 2004. Membrane proteins, lipids and detergents: not just a soap opera. *Biochimica et Biophysica Acta - Bioenergetics*, 1666(1-2), pp.105–117.

Senes, A., et al., 2000. Statistical analysis of amino acid patterns in transmembrane helices: the GxxxG motif occurs frequently and in association with β-branched residues at neighboring positions. *Journal of Molecular Biology*, 296, pp. 912-936.

Senes, A.A., et al., 2004. Folding of helical membrane proteins: the role of polar, GxxxG-like and proline motifs. *Current opinion in structural biology*, 14(4), pp.465-479.

Senn, H.M. & Thiel, W., 2007. QM/MM Methods for Biological Systems. In *Atomistic approaches in modern biology*. Topics in Current Chemistry. Springer Berlin Heidelberg, pp. 173–290.

Seppälä, S. et al., 2010. Control of membrane protein topology by a single C-terminal residue. *Science*, 328(5986), pp.1698–1700.

Sexton, P.M. et al., 2001. Receptor activity modifying proteins. *Cellular signalling*, 13(2), pp.73–83.

Sexton, P.M. & Wootten, D., 2013. Structural biology: meet the B family. *Nature*, 499(7459), pp.417–418.

Shaikh, S.A. et al., 2013. Visualizing functional motions of membrane transporters with molecular dynamics simulations. *Biochemistry*, 52(4), pp.569–587.

Shapiro, A.L., et al., 1967. Molecular weight estimation of polypeptide chains by electrophoresis in SDS-polyacrylamide gels. *Biochemical and biophysical research communications*, 28(5), pp.815–820.

Sharman, J.L. et al., 2012. IUPHAR-DB: updated database content and new features. *Nucleic Acids Research*.

Shelley, J.C. et al., 2001. A Coarse Grain Model for Phospholipid Simulations. *The Journal of Physical Chemistry*, 105(19), pp.4464–4470.

Shen, Y. et al., 2008. Consistent blind protein structure generation from NMR chemical shift data. *Proceedings of the National Academy of Sciences of the United States of America*, 105(12), pp.4685–4690.

Shen, Y. & Bax, A., 2009. Prediction of Xaa-Pro peptide bond conformation from sequence and chemical shifts. *Journal of Biomolecular NMR*, 46(3), pp.199–204.

Shen, Y. et al., 2009. TALOS+: a hybrid method for predicting protein backbone torsion angles from NMR chemical shifts. *Journal of Biomolecular NMR*, 44(4), pp.213–223.

Shepard, T.H., et al., 1959. Familial Addison's disease; case reports of two sisters with corticoid deficiency unassociated with hypoaldosteronism. *A.M.A. journal of diseases of children*, 97(2), pp.154–162.

Singer, S.J. & Nicolson, G.L., 1972. The fluid mosaic model of the structure of cell membranes. *Science*, 175(23), pp.720–731.

Sipos, L. & Heijne, von, G., 1993. Predicting the topology of eukaryotic membrane proteins. *European Journal of Biochemistry*, 213, pp. 1333-1340.

Skrynnikov, N.R. et al., 2000. Orienting domains in proteins using dipolar couplings measured by liquid-state NMR: differences in solution and crystal forms of maltodextrin binding protein loaded with b-cyclodextrin. *Journal of Molecular Biology*, 295(5), pp.9–9.

Slominski, A., et al., 1996. ACTH receptor, CYP11A1, CYP17 and CYP21A2 genes are expressed in skin. *Journal of Clinical Endocrinology & Metabolism*, 81(7), pp.2746–2749.

Soffe N., et al., 1995. The Construction of a High-Resolution 750 MHz Probehead. *Journal of Magnetic Resonance, Series A*, 116(1), pp.117-121.

Sonnhammer, E.L., et al., 1998. A hidden Markov model for predicting transmembrane helices in protein sequences. *Proceedings International Conference on Intelligent Systems for Molecular Biology*, 6, pp.175–182.

Sparr, E.E. et al., 2005. Self-association of transmembrane alpha-helices in model membranes: importance of helix orientation and role of hydrophobic mismatch. *Journal of Biological Chemistry*, 280(47), pp.39324–39331.

Spelbrink, R.E., 2005. Detection and Identification of Stable Oligomeric Protein Complexes in Escherichi coli Inner Membranes: A PROTEOMICS APPROACH. *Journal of Biological Chemistry*, 280(31), pp.28742–28748.

Staley, J.P., 1992. Complete folding of bovine pancreatic trypsin inhibitor with only a single disulfide bond. *Proceedings of the National Academy of Sciences of the United States of America*, 89(5), p.1519-1523.

Staley, J.P. & Kim, P.S., 1994. Formation of a native-like subdomain in a partially folded intermediate of bovine pancreatic trypsin inhibitor. *Protein Science*, 3(10), pp.1822–1832.

Stansfeld, P.J. & Sansom, M.S.P., 2011. From Coarse Grained to Atomistic: A Serial Multiscale Approach to Membrane Protein Simulations. *Journal of Chemical Theory and Computation*, 7(4), pp.1157–1166.

Steiner, S. et al., 2002. The Transmembrane Domain of Receptor-Activity-Modifying Protein 1 Is Essential for the Functional Expression of a Calcitonin Gene-Related Peptide Receptor. *Biochemistry*, 41(38), pp.11398–11404.

Stevens, T.J., et al., 2008. Distinct protein interfaces in transmembrane domains suggest an in vivo folding model. *Protein Science*, 13(11), pp.3028–3037.

Suk, J.-E., et al., 2012. Construction of Covalent Membrane Protein Complexes and High-Throughput Selection of Membrane Mimics. *Journal of the American Chemical Society*, 134(22), pp.9030–9033.

Sutton, G.M. et al., 2008. The Melanocortin-3 Receptor Is Required for Entrainment to Meal Intake. *The Journal of Neuroscience,* 28(48), pp. 12946-12955.

Swiatecka-Urban, A., 2012. Membrane trafficking in podocyte health and disease. *Pediatric Nephrology*, 28(9), pp.1723–1737.

Szyperski, T. et al., 1992. Support of 1H NMR assignments in proteins by biosynthetically directed fractional 13C-labeling. *Journal of Biomolecular NMR*, 2(4), pp.323–334.

Tanford, C., et al., 1974. Molecular characterization of proteins in detergent solutions. *Biochemistry*, 13(11), pp. 2369-2375.

Tanford, C. & Reynolds, J.A., 1976. Characterization of membrane proteins in detergent solutions. *Biochimica et biophysica acta*, 457(2), pp.133–170.

Tao, Y.X., 2010. The Melanocortin-4 Receptor: Physiology, Pharmacology, and Pathophysiology. *Endocrine Reviews*, 31(4), pp.506–543.

Tapaneeyakorn, S. et al., 2011. Solution- and solid-state NMR studies of GPCRs and their ligands. *Biochimica et Biophysica Acta -Biomembranes*, 1808(6), pp.1462–1475.

Taylor, A.W. & Namba, K., 2001. In vitro induction of CD25+ CD4+ regulatory T cells by the neuropeptide alpha-melanocyte stimulating hormone (alpha-MSH). *Immunology and Cell Biology*, 79(4), pp.358–367.

Thota, C.C. et al., 2003. Changes in the expression of calcitonin receptor-like receptor, receptor activity-modifying protein (RAMP) 1, RAMP2, and RAMP3 in rat uterus during pregnancy, labor, and by steroid hormone treatments. *Biology of Reproduction*, 69(4), pp.1432–1437.

Tieleman, D.P. et al., 2001. Proline-induced hinges in transmembrane helices: Possible roles in ion channel gating. *Proteins*, 44(2), pp.63–72.

Tilakaratne, N.N. et al., 2000. Amylin receptor phenotypes derived from human calcitonin receptor/RAMP coexpression exhibit pharmacological differences dependent on receptor isoform and host cell environment. *Journal of Pharmacology and Experimental Therapeutics*, 294(1), pp.61–72.

Treutlein, H.R. et al., 1992. The glycophorin A transmembrane domain dimer: Sequence-specific propensity for a right-handed supercoil of helixes. *Biochemistry*, 31(51), pp.12726–12732.

Tontonoz, P., et al., 1994. Stimulation of adipogenesis in fibroblasts by PPAR gamma 2, a lipid-activated transcription factor. *Cell*, 79(7), pp.1147–1156.

Tugarinov, V. & Kay, L.E., 2005. Methyl Groups as Probes of Structure and Dynamics in NMR Studies of High-Molecular-Weight Proteins. *European Journal of Chemical Biology*, 6(9), pp.1567–1577.

Tugarinov, V., et al., 2006. Isotope labeling strategies for the study of high-molecular-weight proteins by solution NMR spectroscopy. *Nature Protocols*, 1(2), pp.749–754.

Tulumello, D.V. & Deber, C.M., 2012. Efficiency of detergents at maintaining membrane protein structures in their biologically relevant forms. *Biochimica et Biophysica Acta -Biomembranes*, 1818(5), pp.1351-1358.

Turner, D.L., 1980. The measurement of coupling constants from two-dimensional NMR spectra. *Journal of Magnetic Resonance (1969)*, 39(3), pp.391–398.

Udawela, M., et al., 2004. The receptor activity modifying protein family of G protein coupled receptor accessory proteins. *Seminars in Cell & Developmental Biology*, 15(3), pp.299–308.

Udawela, M., et al., 2006a. A critical role for the short intracellular C terminus in receptor activity-modifying protein function. *Molecular pharmacology*, 70(5), pp.1750–1760.

Udawela, M., et al., et al., 2006b. Distinct Receptor Activity-Modifying Protein Domains Differentially Modulate Interaction with Calcitonin Receptors. *Molecular pharmacology*, 69(6), pp.1984–1989.

Ulmschneider, M.B., et al., 2001. Amino acid distributions in integral membrane protein structures. *Biochimica et Biophysica Acta - Bioenergetics*, 1512(1), pp.1–14.

Ulmschneider, M.B., et al., 2005. Properties of integral membrane protein structures: derivation of an implicit membrane potential. *Proteins*, 59(2), pp.252–265.

Unal, H. & Karnik, S.S., 2012. Domain coupling in GPCRs: the engine for induced conformational changes. *Trends in Pharmacological Sciences*, 33(2), pp.79–88.

Urwyler, S., 2011. Allosteric modulation of family C G-protein-coupled receptors: from molecular insights to therapeutic perspectives. *Pharmacological Reviews*, 63(1), pp.59–126.

Vaisse, C.C. et al., 1998. A frameshift mutation in human MC4R is associated with a dominant form of obesity. *Nature genetics*, 20(2), pp.113–114.

Valsalan, R. et al., 2013. Early vertebrate origin of melanocortin 2 receptor accessory proteins (MRAPs). *General and Comperative Endocrinology,* 188, pp.123-132.

Van den Ouweland, A.M. et al., 1992. Mutations in the vasopressin type 2 receptor gene (AVPR2) associated with nephrogenic diabetes insipidus. *Nature genetics*, 2(2), pp.99–102.

Van Der Spoel, D., et al., 2005. GROMACS: Fast, flexible, and free - Van Der Spoel - 2005 - Journal of Computational Chemistry - Wiley Online Library *Journal of Computational Chemistry,* 26, pp. 1701-1718.

Van der Wel, P.C. et al., 2000. Tryptophan-anchored transmembrane peptides promote formation of nonlamellar phases in phosphatidylethanolamine model membranes in a mismatch-dependent manner. *Journal of Biochemistry*, 39(11), pp.3124–3133.

Van Horn, W.D. et al., 2009. Solution nuclear magnetic resonance structure of membrane-integral diacylglycerol kinase. *Science*, 324(5935), pp.1726–1729.

van Meer, G.G., et al., 2008. Membrane lipids: where they are and how they behave. *Nature Reviews: Molecular Cell Biology*, 9(2), pp.112–124.

van Meer, G.G. & de Kroon, A.I.P.M., 2011. Lipid map of the mammalian cell. *Journal of Cell Science,* 124, pp. 5-8.

Västermark, Å. & Schiöth, H.B., 2011. The early origin of melanocortin receptors, agouti-related peptide, agouti signalling peptide, and melanocortin receptor-accessory proteins, with emphasis on pufferfishes, elephant shark, lampreys, and amphioxus. *European Journal of Pharmacology*, 660(1), pp.61–69.

Venkatakrishnan, A.J. et al., 2013. Molecular signatures of G-protein-coupled receptors. *Nature*, 494(7436), pp.185–194.

Viklund, H. & Elofsson, A., 2004. Best alpha-helical transmembrane protein topology predictions are achieved using hidden Markov models and evolutionary information. *Protein Science: A Publication of the Protein Society*, 13(7), pp.1908–1917.

Viklund, H. & Elofsson, A., 2008. OCTOPUS: improving topology prediction by two-track ANN-based preference scores and an extended topological grammar. *Bioinformatics*, 24(15), pp.1662–1668.

Viklund, H. et al., 2008. SPOCTOPUS: a combined predictor of signal peptides and membrane protein topology. *Bioinformatics*, 24(24), pp.2928–2929.

Vuister, G. & Wang, A., 1993. Measurement of three-bond nitrogen-carbon J couplings in proteins uniformly enriched in nitrogen-15 and carbon-13. *Journal of the American Chemical Society,* 115, pp.5334-5335.

Wallin, E.E. et al., 1997. Architecture of helix bundle membrane proteins: an analysis of cytochrome c oxidase from bovine mitochondria. *Protein Science: A Publication of the Protein Society*, 6(4), pp.808–815.

Wang, G. et al., 1996. Conformations of human apolipoprotein E(263-286) and E(267-289) in aqueous solutions of sodium dodecyl sulfate by CD and 1H NMR. *Biochemistry*, 35(32), pp.10358–10366.

Wang, J. et al., 2000. Imaging Membrane Protein Helical Wheels. *Journal of Magnetic Resonance*, 144(1), pp.162–167.

Warshel, A. et al., 2006. Modeling electrostatic effects in proteins. *Biochimica et Biophysica Acta,* 1764, pp.1647-1676.

Watkins, H.A. et al., 2013. Identification of Key Residues Involved in Adrenomedullin Binding to the AM1 Receptor. *British Journal of Pharmacology*, 169, pp.143-155.

Webb, T.R. et al., 2008. Distinct Melanocortin 2 receptor accessory protein domains are required for melanocortin 2 receptor interaction and promotion of receptor trafficking. *Journal of Endocrinology*, 150(2), pp.720–726.

Webb, T.R. & Clark, A.J., 2010. Minireview: The Melanocortin 2 Receptor Accessory Proteins. *Molecular Endocrinology*, 24(3), pp.475–484.

Weber, M. & Schneider, D., 2013. Six amino acids define a minimal dimerization sequence and stabilize a transmembrane helix dimer by close packing and hydrogen bonding. *Federation of European Biochemical Societies letters*, 587(11), pp.1592–1596.

Welsh G I, 1993. Glycogen synthase kinase-3 is rapidly inactivated in response to insulin and phosphorylates eukaryotic initiation factor eIF-2B. *Biochemical Journal*, 294(3), p.625.

Whiles, J.A. et al., 2002. Methods for studying transmembrane peptides in bicelles: consequences of hydrophobic mismatch and peptide sequence. *Journal of Magnetic Resonance*, 158, pp.149-156.

White, S.H. & Wimley, W.C., 1999. Membrane protein folding and stability: physical principles. *Biophysics and Biomolecular Structure*, 28(1), pp.319–365.

Wilkins, D.K. et al., 1999. Hydrodynamic radii of native and denatured proteins measured by pulse field gradient NMR techniques. *Journal of Biochemistry*, 38(50), pp.16424–16431.

Wimley, W.C. & White, S.H., 1996. Experimentally determined hydrophobicity scale for proteins at membrane interfaces. *Nature structural & molecular biology*, 3(10), pp.842–848.

Wimley, W.C. et al., 1996. Direct measurement of salt-bridge solvation energies using a peptide model system: implications for protein stability. *Proceeding of the National Academy of Science*, 93, pp.2985–2990.

Wu, C.S. & Yang, J.T., 1978. Conformation of naturally-occurring peptides in surfactant solution: its relation to the structure-forming potential of amino acid sequence. *Audio and Electroacoustics Newsletter, IEEE*, 82(1), pp.85–91.

Wu, B. et al., 2010. Structures of the CXCR4 chemokine GPCR with small-molecule and cyclic peptide antagonists. *Science*, 330(6007), pp.1066–1071.

Wüthrich, K., 1989. Protein structure determination in solution by nuclear magnetic resonance spectroscopy. *Science*, 243, pp.45-50.

Xu, A.A. et al., 2002. Identification of novel putative membrane proteins selectively expressed during adipose conversion of 3T3-L1 cells. *Biochemical and biophysical research communications*, 293(4), pp.1161–1167.

Yang, Y.K. et al., 1999. Characterization of Agouti-related protein binding to melanocortin receptors. *Journal of Molecular Endocrinology*, 13(1), pp.148–155.

Yang, Y.Y. et al., 2007. Structural insights into the role of the ACTH receptor cysteine residues on receptor function. *American Journal of Physiology - Regulatory, Integrative and Comparative Physiology*, 293(3), pp.R1120–R1126.

Yeo, G.S. et al., 2003. Mutations in the human melanocortin-4 receptor gene associated with severe familial obesity disrupts receptor function through multiple molecular mechanisms. *Human Molecular Genetics*, 12(5), pp.561–574.

Yohannan, et al., 2004a. The evolution of transmembrane helix kinks and the structural diversity of G protein-coupled receptors. *Proceeding of the National Academy of Science*, pp.959–963.

Yohannan, S., et al., 2004b. Proline Substitutions are not Easily Accommodated in a Membrane Protein. *Journal of Molecular Biology*, 101(4), pp.959-963.

Yonath, A. et al., 1978. Structural analysis of denaturant-protein interactions: Comparison between the effects of bromoethanol and SDS on denaturation and renaturation of triclinic lysozyme. *European Biophysics Journal*, 4(1), pp.27–36.

Zhou, F.X. et al., 2001. Polar residues drive association of polyleucine transmembrane helices. *Proceeding of the National Academy of Science*, 98(5), pp.2250–2255.

APPENDIX

"Life is a partial, continuous, progressive, multiform and conditionally interactive self-realisation of the potentialities of atomic electron states."

(John Desmond Bernal)

APPENDIX 1: Additional experiments

Investigation of the N-terminal Domain of MRAP(2-67) by Solution NMR

Investigation of the KH-rich region

Since the N-terminal domain was water-soluble the construct MRAP(2-27) (2.87 kDa) was tested in only 50 mM sodium phosphate buffer (pH 6.5) followed by assessment in 30 mM Fos-Choline-14 micelles and POPC/DHPC bicelles. The second construct, MRAP(2-38), was studied in 50 mM sodium phosphate buffer (pH 6.5) and in DHPC. Two-dimensional ^{1}H-^{15}N HSQC experiments were acquired to determine changes dependent on detergent and construct.

MRAP(2-28) in POPC/DHPC bicelles displayed 37 peak resonances, whereas in solely buffer only 18 resonances were visible. Juxtaposition of MRAP(2-27) in 30 mM Fos-Choline-14 micelles with no surfactants shows dramatic shift changes in every single N_H backbone residues. No CSP was detected when comparing MRAP(2-28) and MRAP(2-67) in Fos-Choline-14. This implied a stable N-terminal conformation of MRAP(2-67) in

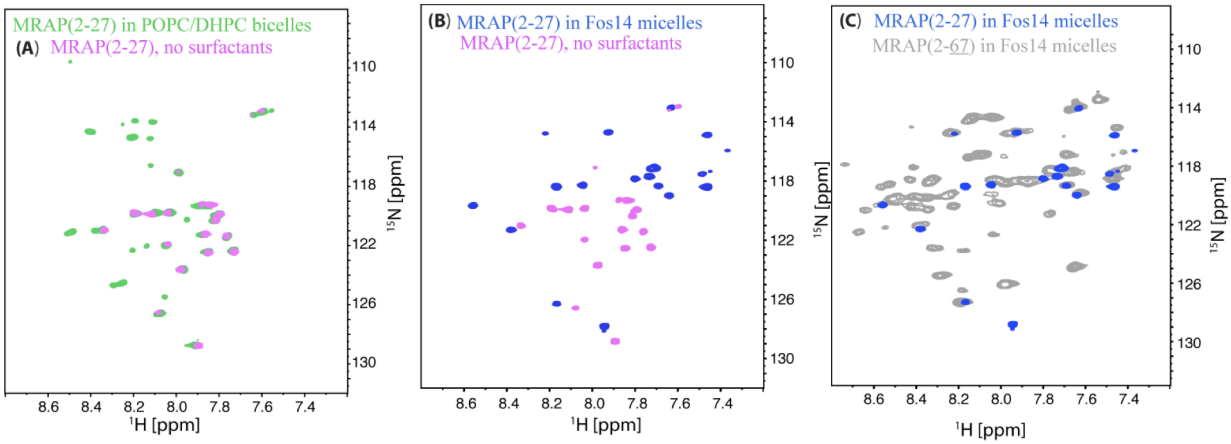

Figure Appendix 1: Investigation of the N-terminal domain of MRAP(2-27)
(A) MRAP(2-27) with and without detergent bicelles
(B) MRAP(2-27) with and without detergent micelles
(C) Difference between MRAP(2-27) and MRAP(2-67) in Fos-choline-14

presence of detergents (Figure Appendix 1).

The second construct, MRAP(2-38) (4.29 kDa), solubilised in only 50 mM sodium phosphate buffer (pH 6.5). Addition of 100 mM DHPC did not introduce visible changes to chemical shifts and a total of 35 resonances were distinguished. DHPC is a zwitterionic detergent, with a positively charged head group. Since micelles formation occurred before addition of the peptide, MRAP(2-38) would not interact with detergent since the positively charged KH-rich region and the positively charged DHPC head group would rather force themselves apart. Juxtaposition of the well-dispersed N_H backbone residues of MRAP(2-38) with MRAP(2-67) in 100 mM DHPC showed that the far N-terminal residues overlaid well, whereas residues Leu18 and onwards experienced chemical shift perturbation (Figure Appendix 5), which is attributable to interactions with the detergent micelle. Compulsory interaction of the KH-rich region with DHPC could cause intermediate flexibility and hence result in a loss of detection for residues His34 to Ser37.

Interaction of MRAP(2-67) with the ligand ACTH

DNA- subcloning for ACTH

The 39 amino acid ACTH construct contained residues Ser138 to Phe176 of the pro-opiomelanocortin protein. A single substitution of Met141Leu was introduced to enable expression with and cleavage from the trpLE protein. The sequence of the ACTH construct: SYSLEHFRWG KPVGKKRRPV KVYPNGAEDE SAEAFPLEF. It was sub-cloned into the pMM-LR6 vector as a *trpΔLE*-fusion using the same approach as for the MRAP and RAMP1 constructs.

MRAP is required for ACTH binding to the receptor MC2R and its signal transduction (Hinkle & Sebag 2009). The 4.5 kDa small ligand was expressed into inclusion bodies and

purified as MRAP(2-67), which is described in detail in Chapter 3.1.2. ACTH exhibited anomalous gel mobility, possibly a result of it being small and hydrophobic (Figure Appendix 2(A)). To investigate whether ACTH binds directly to MRAP(2-67) two separate NMR titration experiments were performed. Both titrations were conducted at 303.15 K in a mixture of 50 mM sodium phosphate buffer (pH 6.5) and mixed micelles (100 mM Fos-10, 20 mM DMPC and 5 mM DMPG) with either ^{15}N-labled MRAP or ^{15}N-labled ACTH. ^{1}H-^{15}N SOFAST-HMQCs were used to monitor the titration of uniformly ^{15}N-labled peptide.

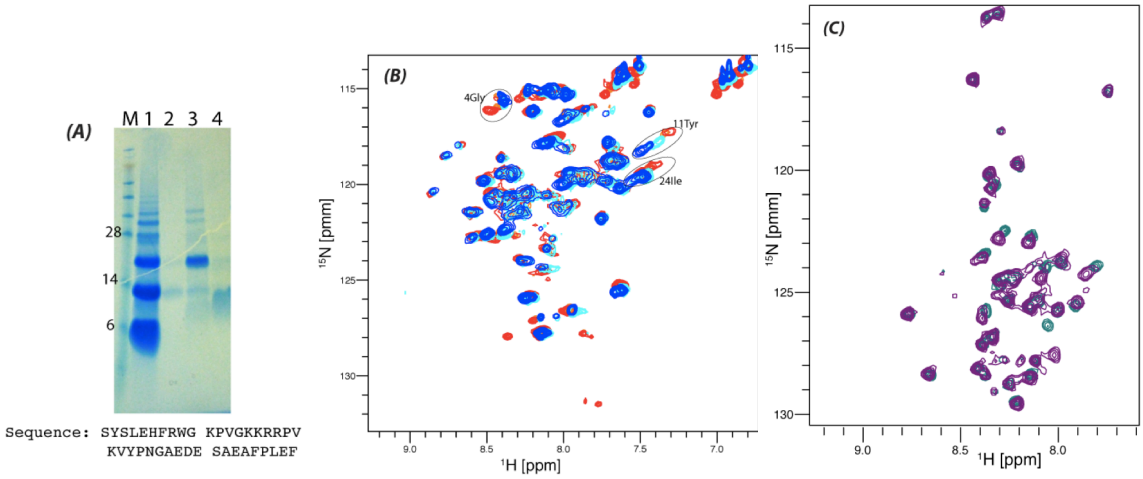

Figure Appendix 2: MRAP(2-67) - ACTH titration in mixed micelles at 600 MHz (310 K)
(A) HPLC fractions of ACTH (4.5 kDa)
(B) Soluble ^{14}N ACTH was added to 250 uM ^{15}N MRAP(2-67)
blue- 250 uM MRAP; cyan- 250 uM MRAP + 100 uM ACTH;
orange- 250 uM MRAP + 500 uM ACTH; red - 250 uM MRAP + 750 uM ACTH
(C) Soluble ^{14}N MRAP(2-67) was added to ^{15}N ACTH
blue - 500 uM ACTH, violett- 500 uM ACTH + 250 uM 14N MRAP(2-67)

The first titration included ^{15}N-labled MRAP (200 μM) and unlabelled ACTH ligand. ACTH was dissolved in the buffer mixture and added to a final concentration of 150 μM, 500 μM and 700 μM. ^{1}H-^{15}N SOFAST-HMQCs detected visible shift changes for residues Gly4, Tyr11 and Ile24 (Figure Appendix 2 (B)). To confirm shifting peaks and their possible specific interaction with MRAP(2-67) a second titration was recorded with ^{15}N isotopically labelled 400 μM ACTH and a final concentration of 200 μM unlabelled

MRAP(2-67). Only modest and non-saturable changes were recorded in backbone amide proton and nitrogen shifts, which were consistent with nonspecific or weak interaction between these two proteins.

Overall, the conclusion was that ACTH had some affinity to the micelle surface that led to nonspecific interaction between MRAP(2-67) and ACTH when both were confined to the same micelle. Additionally, the result indicated that any binding of ACTH to MRAP(2-67) in this lipid/detergent mixture was either nonspecific or weak.

Toward a PRE-based method for measuring MRAP dimerisation

Once a system is established in which MRAP self-assembles, one can obtain long-range intermolecular information by introducing site-specific paramagnetic spin labels that complements short-range NOEs, which are limited to distances up to 5 Å and can be weak for intermolecular contacts. To acquire paramagnetic relaxation enhancement (PRE) experiments the single cysteine derivative of MRAP(2-67), S65C, was expressed and purified as with wild-type, except that all buffers included DTT. After HPLC, SDS-PAGE with and without additional DTT was used to distinguish between the oxidised and disulphide-bonded states of the protein (Figure Appendix 3).

The paramagnetic nitroxide spin label (S-(2,2,5,5-tetramethyl-2,5-dihydro-1H-pyrrol-3-yl)methyl-methanesulfonothioate (MTSL) was attached to the free cysteine residue. The complete protocol for MTSL incorporation sample can be found in Chapter 3.4.7. ^{1}H-^{15}N HSQCs at 950 MHz were carried out to measure the differences in crosspeak intensity between the paramagnetic, MTSL-bound sample and the diamagnetic, reduced on with ascorbic acid. For extraction of the paramagnetic restraints peak intensities were normalised by the protein concentration.

As a test of the approach, two PRE-based experiments were conducted on MRAP constructs in both mixed micelles and 50 mM SDS. In both conditions, the first experiment included solely ^{15}N-labeled S65C bound to MTSL.

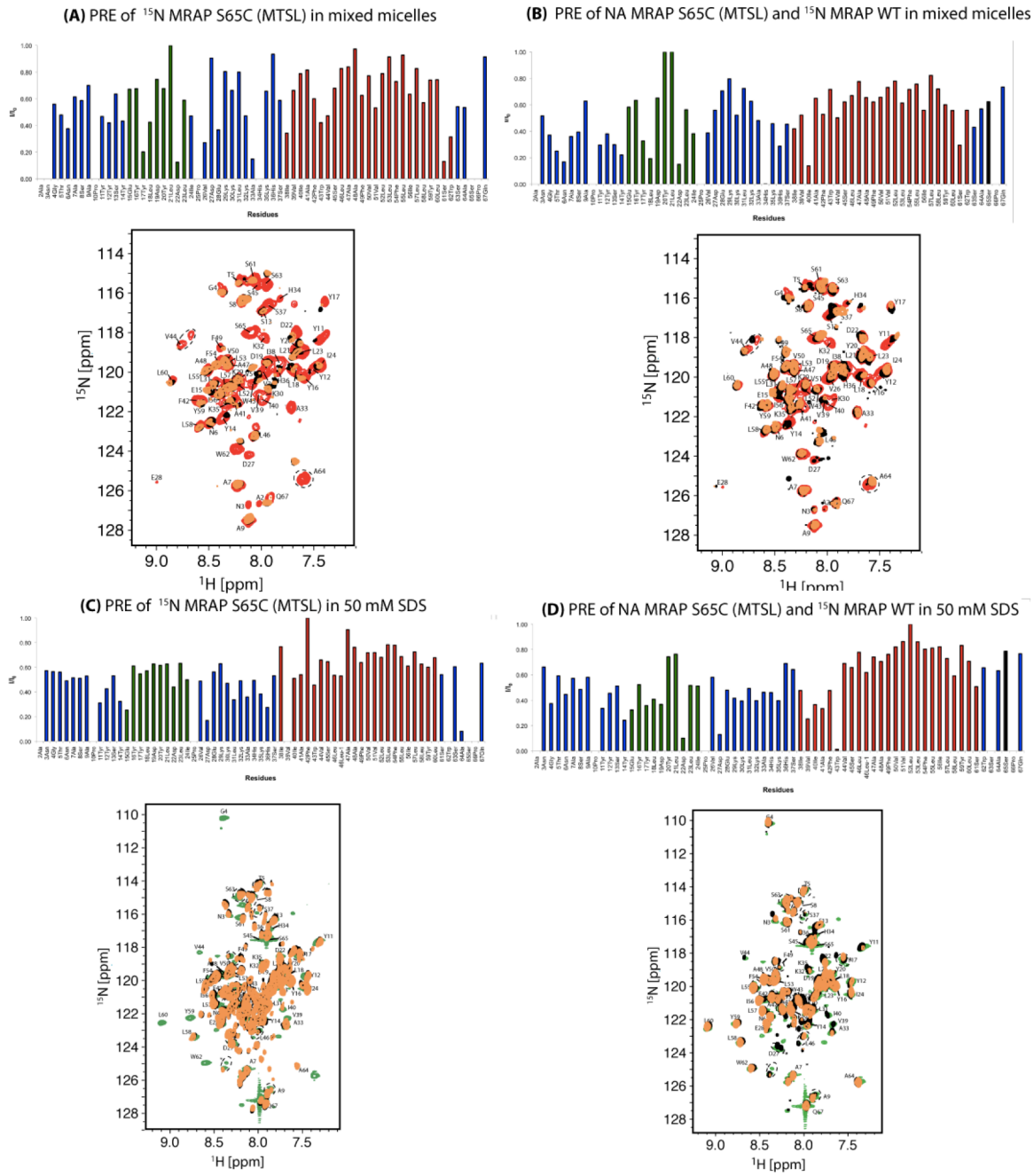

Figure Appendix 3: Paramagnetic relaxation enhancement experiments on MRAP(2-67) in mixed micelles and 50 mM SDS:
Colouring: blue - unstructured regions, green - α-helical region in the N-terminal domain, red - transmembrane domain
^{1}H-^{15}N HSQC spectra: orange - paramagnetic sample, black diamagnetic sample, red/green - WT in detergent (reference)

The second experiment included unlabelled, MTSL-bound S65C and ^{15}N-labeled MRAP(2-67) wild-type, mixed to a ratio of 1:1.

For both experiments one ^{1}H-^{15}N HSQC recorded on the paramagnetic sample and a second one the reduced, diamagnetic after addition of ascorbic acid. Unfortunately, investigation of all experiments proposed that even after much effort it was not possible to completely label S65C with MTSL and that this was likely due to rapid oxidation of the cysteines. Therefore, the PRE-results were inconclusive, but with modification of the procedure it is likely to provide a useful route toward rapid probing of MRAP self-assembly.

Study of a plausible dimeric interface of MRAP(2-67) by mutational studies

All results obtained thus far had been somewhat ambiguous in terms of the oligomeric state of MRAP *in vitro*. For example, the lack of concentration dependence of the doubled peaks excluded the possibility that the doubled peaks were attributable to a dimeric form, but did not exclude the possibility that the main peaks corresponded to a stable dimeric form. Thus, further attempts to investigate MRAP(2-67) in terms of oligomerisation, but also the structural stability and interactions with the micelles were done by studying MRAP(2-67) variants in all three detergent environments. Figure Appendix 4 illustrates all MRAP(2-67) residues that were mutated, which were Tyr17, Val26, His36, Ser37, Ala41, Trp43, Ser45L, Leu46, Leu57, Trp59, Ser61 and Pro66.

All construct were generated using the QuikChange site-directed mutagenesis protocol, expressed and purified according to the wild-type MRAP(2-67). For initial analysis

mutants V26A, A41L, W43X, S45L, L46A, L57A, and Y59A were ran on a SDS-PAGE, where they displayed comparable behaviour to the wild-type MRAP(2-67).

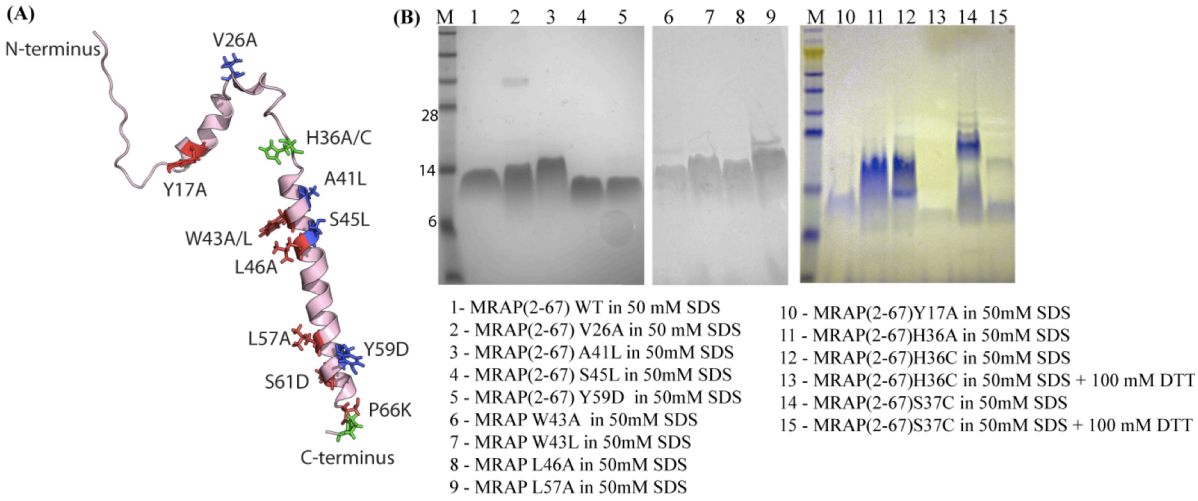

Figure Appendix 4: Mutations in MRAP (2-67)
(A) Overview of all performed mutations on MRAP (2-67)
blue- mutations in DHPC: V26A, A41L, W43A, S45L, L46A, Y59D
green - mutations in SDS: H36Y, W43A, W43L, S45L, L46A, L57A, P66K
red- mutations in mixed micelles: Y17A, W43A, L46A, L57A, S61D

In the N-terminal region Tyr17 was mutated to an alanine (Y17A) to explore the interaction of the N-terminal domain with its local environment, particularly since this residue was near to the LDY/IL region implicated in MC2R activation.

Mutating Ala41 to a leucine (A41L) resulted in residues Ile38, Ile40, Phe42, Trp43 and Ser45 experiencing intermediate to fast exchange (no visible peaks) with the detergent DHPC. This finding led to the conclusion that A41L introduced more flexibility to the transmembrane domain. Furthermore, Trp43 was investigated, to determine whether this highly aromatic amino acid is involved in the formation of a dimer. Thus, Trp43 was mutated to an alanine (W43A), a small nonpolar amino acid, and a leucine (W43L), a long-branched hydrophobic amino acid, and tested in all three detergents by 2D ^{1}H-^{15}N HSQC. Only local changes or disappearance of surrounded peaks were observed. In 100 mM DHPC residue Ala47 seemed to experience intermediate flexibility and hence was

not visible by solution-state NMR. In 50 mM SDS, W43A encountered local shift changes whereas W43L showed disappearing peaks of residues Val39 and Ala47. In mixed micelles W43A introduced local shift changes, which were explained by the dramatic change in side chain. Investigation of a leucine mutation (W43L) in mixed micelles altered the protein's conformation more than introducing an alanine at this position. Overall, since Trp43 and Ala47 were at the same interface Ala47 experienced significant, detergent-independent consequences. However it also indicated that Trp43 only affected the local environment and hence can be excluded from any possible dimeric interface (Figure Appendix 5-). Residue Ser45 was mutated to a leucine (S45L) to examine whether an introduction of a long-branched, hydrophobic amino acid, would affect the nature of MRAP(2-67)'s secondary structure. Neither in 50 mM SDS nor in 100 mM DHPC shift changes towards dimerisation were detected. However, in both detergents Phe49, which was at the same interface as Ser45 experienced dramatic shift changes of $\Delta\delta_{HN} \sim 0.6$. This might be an immediate consequence of side chain interaction at the same interface. Moreover, Leu46 and Leu57 were both mutated to alanine (L46A and L57A) and investigated in 50 mM SDS, mixed micelles and 100 mM DHPC. Only local shift changes, which were due to alteration in length of the side chain, were observed. Modification of these results did not give any conclusive insights in a likely dimeric interface of MRAP(2-67). Ser61 was mutated to an aspartate (S61D) since it was proposed to be a vulnerable post-translation modification site for phosphorylation. Possible phosphorylation will be discussed further in the following subchapter (Figure Appendix 5). In 2010 Hughes *et al.* (Hughes et al. 2010) identified Val26 and Tyr59 as homozygous missense mutations, that affect cAMP generation but not MC2R's trafficking to the

plasma membrane. To verify their findings *in vitro* the mutants V26A and Y59D were studied in 100 mM DHPC by solution-state NMR. No significant shift changes were detected, hence the impact of both mutants on MRAP(2-67)'s structure is questionable.

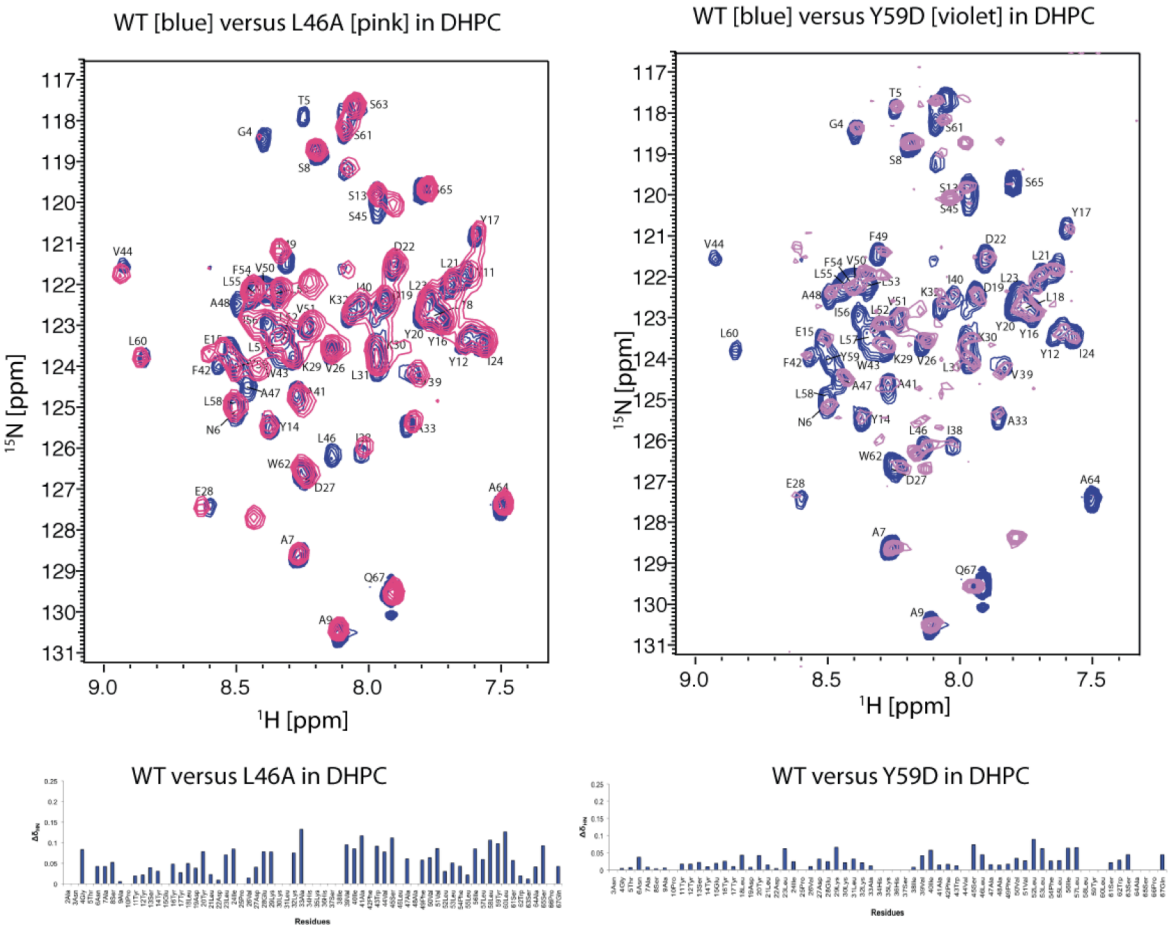

Figure Appendix 5: Mutations of MRAP (2-67) in 100 mM DHPC
Overview of all mutations on MRAP (2-67) to investigate a possible interface in DHPC

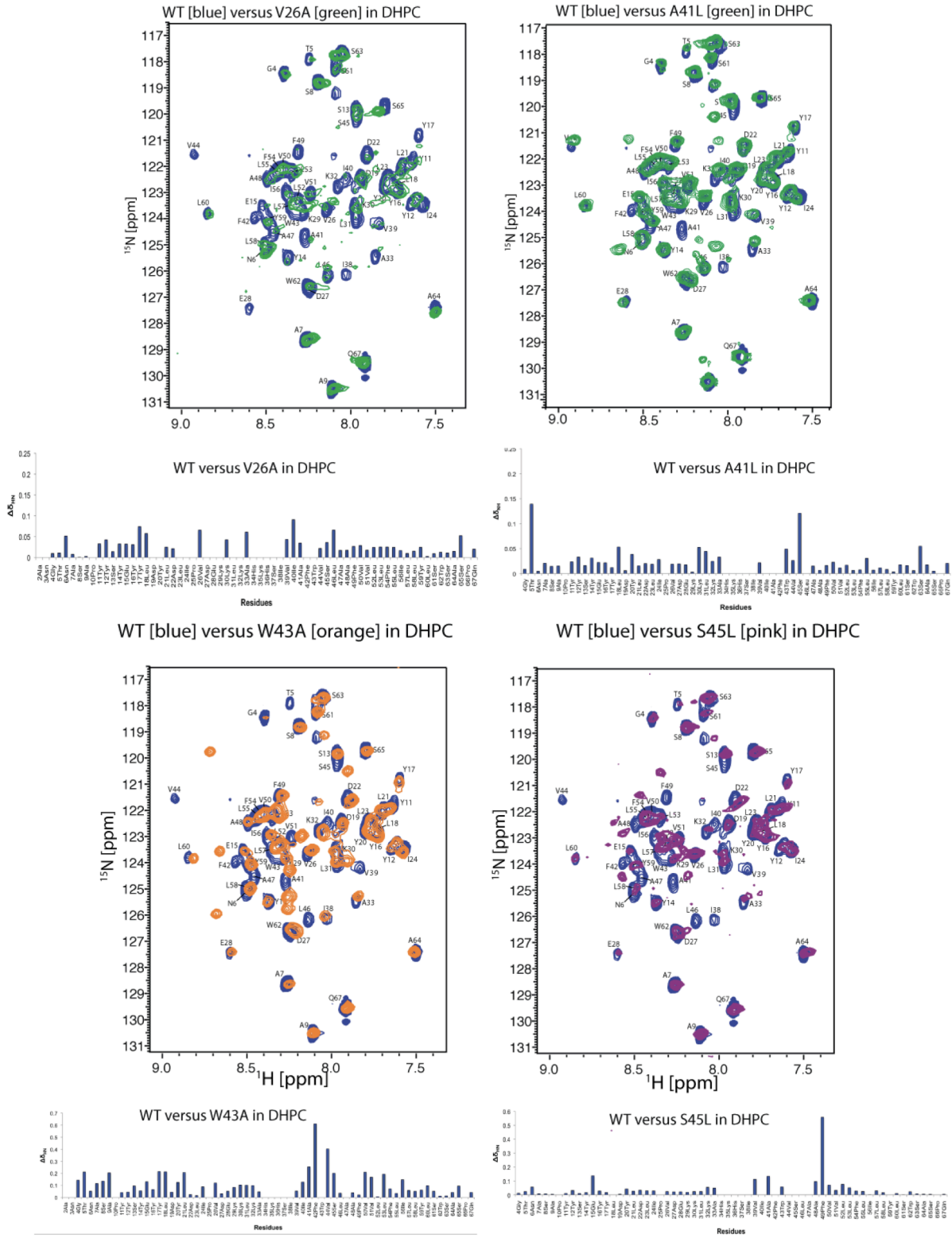

Figure Appendix 5: Mutations of MRAP (2-67) in 100 mM DHPC
Overview of all mutations on MRAP (2-67) to investigate a possible interface in DHPC

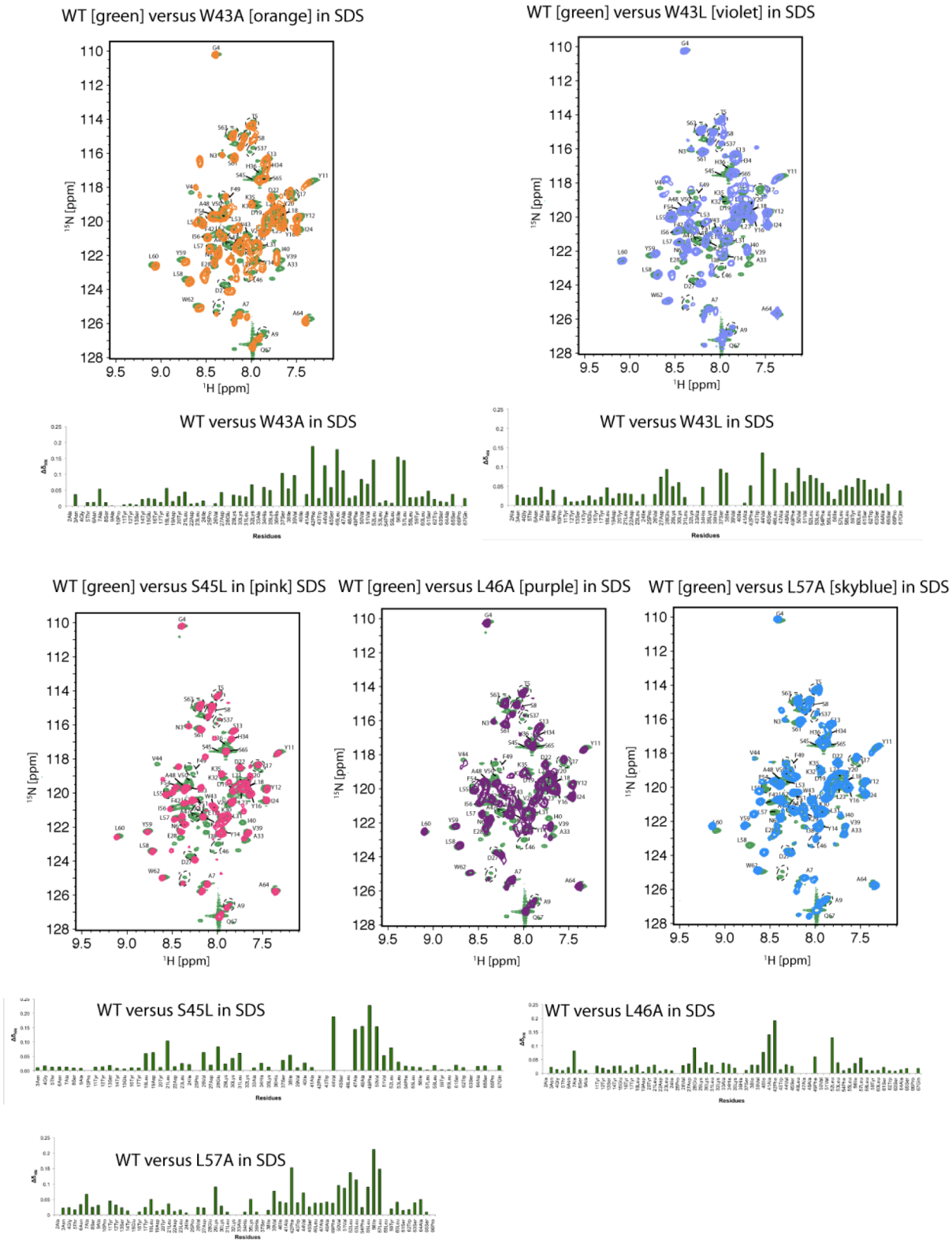

Figure Appendix 6: Mutations of MRAP (2-67) in 50 mM SDS
Overview of all mutations on MRAP (2-67) in 50 mM SDS to investigate a possible interface

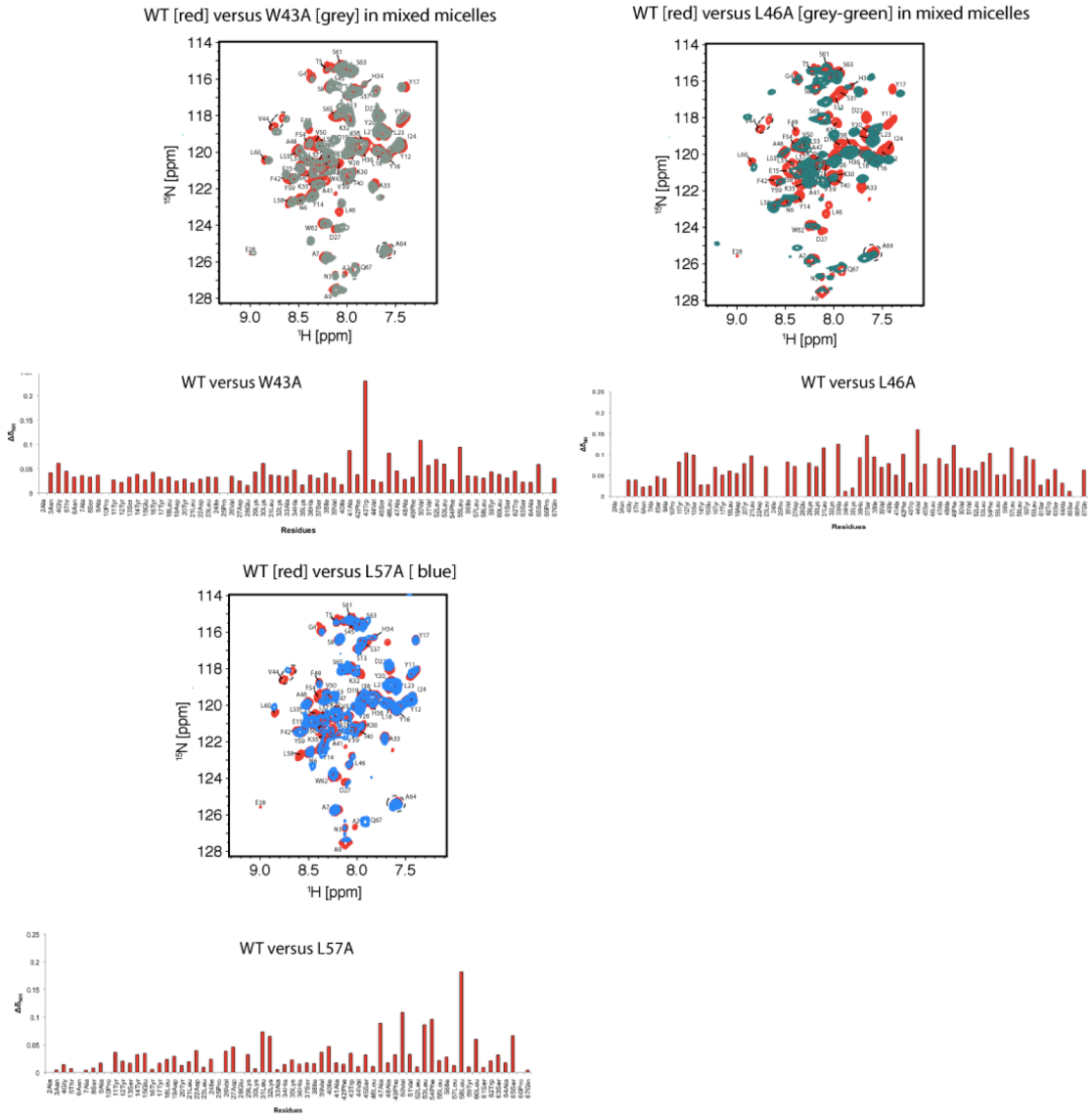

Figure Appendix 7: Mutations of MRAP (2-67) in mixed micelles
Overview of all mutations on MRAP (2-67) to investigate a possible interface in mixed micelles

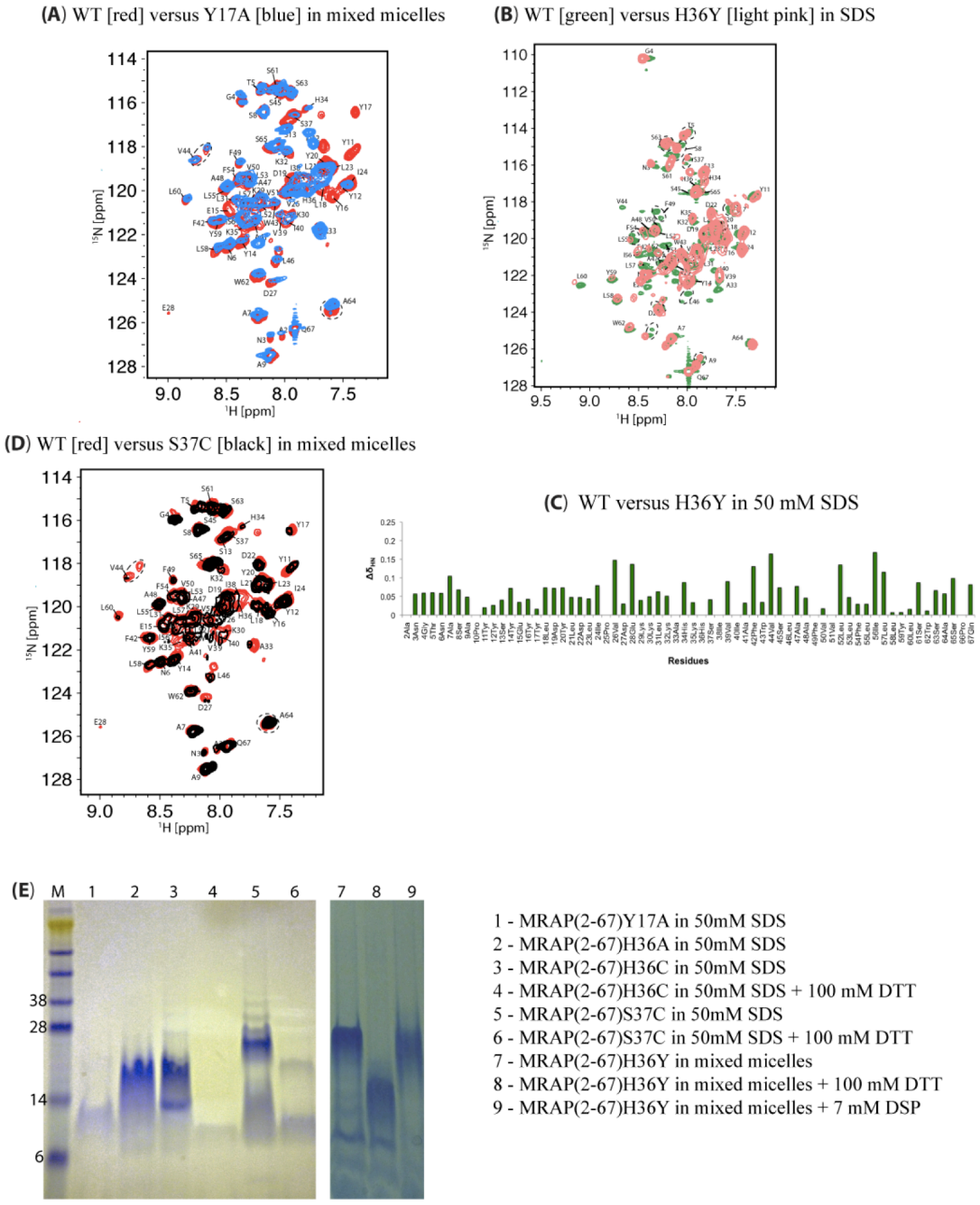

Figure Appendix 8: Further investigation of the N-terminal domain
(A) Investigation of the mutant MRAP(2-67)Y17A in mixed micelles
(B) Investigation of the mutant MRAP(2-67)H36Y in 50 mM SDS
(C) CSP of MRAP(2-67)H36Y in comparison to MRAP(2-67)WT in 50 mM SDS
(D) Investigation of the mutant MRAP(2-67)S37C in mixed micelles
(E) Investigation of MRAP(2-67) N-terminal mutants on a SDS-PAGE

Summarising, even though multiple residues were closely examined, no conclusive evidences for a possible dimeric interface of MRAP(2-67) were found.

APPENDIX 2: Cloning Protocol and Primers

The genes of interest were amplified by polymerase chain reaction (PCR) from the resource plasmids.

PCR reaction for inserts of MRAP and RAMP	PCR-Program:	
10ul 5x Reaction-buffer	5 min @ 98˚C	
2ul dNTPs	30 sec @ 98˚C	
0.5ul Primer each	30 sec @ 55˚C	
0.2ul DNA-template	45 sec @ 72˚C	25 cycles
0.5ul DNA-Polymerase	5 min @ 72˚C	
add 50 ul H2O		

Quikchange –Protocol

PCR-reaction for QuikChange -Mutagenesis	
5 ul 10x Reaction-buffer	
2 ul dNTPs	**PCR-Program:**
0.4 ul Primer each	4 min @ 98˚C
0.15 ul DNA-template	30 sec @ 98˚C
2.5 ul DMSO	1 min @ 55˚C
1 ul DNA-Polymerase	6 min @ 72˚C 15 cycles
add 50 ul H2O	7 min @ 72˚C

The PCR was followed by DpnI cleavage over night and then transformation into NEB DH5α cells.

Transformation into NEB DH5α cells

E.coli NEB DH5α competent cells were used for transforming DNA. E.coli Codon Plus BL21 (DE3) pLysS cells were used for expression purposes.

- 20-30 min incubation on ice
- Heatshock for 42 sec at 42°C
- 5 min on ice
- add 0.2 ml preheated SOC-Medium
- incubate 1 hour at 37˚C
- plate on LB-Kan plate
- incubation over night at 37˚C

Control and characterization of DNA samples

The method of choice was Colony PCR. Thereby half a colony was used and dissolved according to the protocol written below. After heating the sample up for 5 minutes at 95°C the PCR protocol, which was used for making the original DNA insert construct and the according primers were used.

- ½ colony
- 2.5ul 5xBuffer
- 1.25ul dNTPs
- 0.25ul Primer each
- 0.25ul DNA-Polymerase

Characterization, separation and crude identification of the constructs were accomplished by 1.5% agarose gel electrophoresis. SYBR Safe DNA Stain (Life Technology S33102) was added at ~0.5 ug/ml for visualizing the DNA fragments under UV radiation. Samples were mixed with 5x loading buffer and run at 96 Volts in 1x TAE buffer for 40 minutes.

Primers for MRAP

MRAP sequence:

```
catatgcatcaccatcaccatcaccatcaccataaagcaattttcgtactgaaaggttca
 H  M  H  H  H  H  H  H  H  H  H  K  A  I  F  V  L  K  G  S
ctggacagagatctcgacagccgtattgaactggaactgcgtaccgatcataaagagctg
 L  D  R  D  L  D  S  R  I  E  L  E  L  R  T  D  H  K  E  L
tctgaacatctgctgctggttgatctcgcccgtaatgatctggcacgcattgctaccccc
 S  E  H  L  L  L  V  D  L  A  R  N  D  L  A  R  I  A  T  P
ggcagccgctacgtcgccgatctcaccaaagttgaccgttattcctatgtgctgcacctc
 G  S  R  Y  V  A  D  L  T  K  V  D  R  Y  S  Y  V  L  H  L
gtctctcgcgtagtcggcgaactgcgtcacgatcttgacgccctgcacgcttatcgcgcc
 V  S  R  V  V  G  E  L  R  H  D  L  D  A  L  H  A  Y  R  A
gctctgaatctggggacgttaagcggtgcgccgaaagtacgcgctaagctttggatggcc
 A  L  N  L  G  T  L  S  G  A  P  K  V  R  A  K  L  W  M  A
aacgggaccaacgcctctgccccatactacagctatgaatactacctggactatctggac
 N  G  T  N  A  S  A  P  Y  Y  S  Y  E  Y  Y  L  D  Y  L  D
ctcattcccgtggacgagaagaagctgaaagcccacaaacattccatcgtgatcgcattc
 L  I  P  V  D  E  K  K  L  K  A  H  K  H  S  I  V  I  A  F
```

tgggttagcctggctgccttcgtggtgctgctcttcctcatcttgctctacttgtcctgg
W V S L A A F V V L L F L I L L Y L S W
tccgcctccccgcagtgaggatcc
S A S P Q - G S

Cloning Primers for MRAP

MRAP-trp-HindIII-fwd: ttcgtagcaagctttgg atggccaacgggaccaacgcctc
MRAP-trp-BamHI-rev: attgctagggatcctcatcagctctgcaattgagaggtcc

LSWSASPQ-stp-stp-BamHI-extension: MRAPsh-trp-M60L-BamHI-rev:
attgctagggatcctcactgcggggaggcggaccaggacaagtagagcaa
M60L

M60L-fwd: ctcatcttgctctacCTGtcctggtccgcctcc
M60L-rev: ggaggcggaccaggaCAGgtagagcaagatgag

QuikChange Primers

V26A
V26A-fwd:
ctggacctcattcccGCGgacgagaagaagctg
V26A-rev:
cagcttcttctcgtcCGCgggaatgcggtccag

L31C
L31C-fwd:
gtggacgagaagaagTGCaaagcccacaaacat
L31C-rev:
atgtttgtgggctttGCActtcttctcgtccac

A33C
A33C-fwd:
gagaagaagctgaaaTGCcacaaacattccatc
A33C-rev:
gatggaatgtttgtgGCAtttcagcttcttctc

H36A
H36A-fwd:
ctgaaagcccacaaaGCTtccatcgtgatcgca
H36A-rev:
tgcgatcacgatggaCGAtttgtgggctttcag

H36C
H36C-fwd:
ctgaaagcccacaaaTGTtccatcgtgatcgca
H36C-rev:
tgcgatcacgatggaACAtttgtgggctttcag

S37C
S37C-fwd:
aaagcccacaaacatTGCatcgtgatcgcattc
S37C-rev:
gaatgcgatcacgatGCAatgtttgtgggcttt

F49V
F49V-fwd:
gttagcctggctgccGTCgtggtgctgctcttc
F49V-rev:
gaagagcagcaccacGACggcagccaggctaac
V49A-fwd:
gttagcctggctgccGCCgtggtgctgctcttc
V49A-rev:
gaagagcagcaccacGGCggcagccaggctaac

F54A
F54A-fwd:
ttcgtggtgctgctcGCGctcatcttgctctac
F54A-rev:
gtagagcaagatgagCGCgagcagcaccacgaa

L57A
L57A-fwd:
ctgctcttcctcatcGCGctctacttgtcctgg
L57A-rev:
ccaggacaagtagagCGCgatgaggaagagcag

Y59D
Y59D-fwd:
ttcctcatcttgctcGATatgtcctggtccgcc
Y59D-rev:
ggcggaccaggacatATCgagcaagatgaggaa

S61D
S61D-fwd:
atcttgctctacttgGACtggtccgcctccccg
S61D-rev:
cggggaggcggaccaGTCcaagtagagcaagat

A41L
A41V-fwd:
cattccatcgtgatcGTAttctgggttagcctg
A41V-rev:
caggctaacccagaaTACgatcacgatggaatg
V41L-fwd:
cattccatcgtgatcCTAttctgggttagcctg
V41L-rev:
caggctaacccagaaTAGgatcacgatggaatg

W43L
W43L-fwd:
atcgtgatcgcattcTTGgttagcctggctgcc
W43L-rev:
ggcagccaggctaacCAAgaatgcgatcacgat

S45I
S45I-fwd:
atcgcattctgggttATCctggctgccttcgtg
S45I-rev:
cacgaaggcagccagGATaacccagaatgcgat
I45L-fwd:
atcgcattctgggttCTCctggctgccttcgtg
I45L-rev:
cacgaaggcagccagGAGaacccagaatgcgat

L46A
L46A-fwd:
gcattctgggttagcGCGgctgccttcgtggtg
L46A-rev:
caccacgaaggcagcCGCgctaacccagaatgc

F49A
F49S-fwd:
gttagcctggctgccTCCgtggtgctgctcttc
F49S-rev:
gaagagcagcaccacGGAggcagccaggctaac
S49A-fwd:
gttagcctggctgccGCCgtggtgctgctcttc
S49A-rev:
gaagagcagcaccacGGCggcagccaggctaac

S61DS65C
S65CS61D-fwd:
atcttgctctacttg*GAC*tggtccgcc*TGC*ccg
S65CS61D-rev:
cggGCAggcggaccaGTCcaagtagagcaagat

S61E
S61E-fwd:
atcttgctctacttgGAGtggtccgcctccccg
S61E-rev:
cggggaggcggaccaCTCcaagtagagcaagat

S61ES65C
S65CS61E-fwd:
atcttgctctacttgGAGtggtccgccTGCccg
S65CS61E-rev:
cggGCAggcggaccaCTCcaagtagagcaagat

P66KQ67K
P66KQ67K-fwd:
tggtccgcctccaagAAGtgaggatccgaattc
P66KQ67K-rev:
gaattcggatcctcaCTTcttggaggcggacca

Q67K
Q67K-fwd:
tggtccgcctccccgAAGtgaggatccgaattc
Q67K-rev:
gaattcggatcctcaCTTcggggaggcggacca

Primers for RAMP

RAMP sequence:

```
tacaaaaaagcaggctccaccatggcccgggccctgtgccgcctcccgcggcgcggcctc
 Y  K  K  A  G  S  T  M  A  R  A  L  C  R  L  P  R  R  G  L
tggctgctcctggcccatcacctcttcatgaccactgcctgccaggaggctaactacggt
 W  L  L  L  A  H  H  L  F  M  T  T  A  C  Q  E  A  N  Y  G
gccctcctccgggagctctgcctcacccagttccaggtagacatggaggccgtcggggag
 A  L  L  R  E  L  C  L  T  Q  F  Q  V  D  M  E  A  V  G  E
acgctgtggtgtgactggggcaggaccatcaggagctacagggagctggccgactgcacc
 T  L  W  C  D  W  G  R  T  I  R  S  Y  R  E  L  A  D  C  T
tggcacatggcggagaagctgggctgcttctggcccaatgcagaggtggacaggttcttc
 W  H  M  A  E  K  L  G  C  F  W  P  N  A  E  V  D  R  F  F
ctggcagtgcatggccgctacttcaggagctgccccatctcaggcagggccgtgcgggac
 L  A  V  H  G  R  Y  F  R  S  C  P  I  S  G  R  A  V  R  D
ccgcccggcagcatcctctacccccttcatcgtggtccccatcacggtgaccctgctggtg
 P  P  G  S  I  L  Y  P  F  I  V  V  P  I  T  V  T  L  L  V
acggcactggtggtctggcagagcaagcgcactgagggcattgtgtaggacccagctttc
 T  A  L  V  V  W  Q  S  K  R  T  E  G  I  V  -  D  P  A  F
ttgtac
 L  Y
```

Cloning Primers for RAMP

RMP1TM-trp-HindIII-fwd: ttcgtagcaagctttggatgggcagcatcctctacccccttc
RMP1TM-trp-BamHI-rev: attgctagggatccttatcacacaatgccctcagtgcgctt

RMP1-R102-C104S-trpLE-fwd:
ttcgtagcaagctttggatgaggagcagccccatctcaggc
RMP1-R102-trpLE-fwd: ttcgtagcaagctttggatgaggagctgccccatctcaggc
RMP1TM-trp-BamHI-rev: attgctagggatccttatcacacaatgccctcagtgcgctt

QuikChange Primers

P6A P6A-fwd: ggcagcatcctctacGCCttcatcgtggtcccc P6A-rev: ggggaccacgatgaaGGCgtagaggatgctgcc	**L16A** L16A-fwd: atcacggtgaccctgGCGgtgacggcactggtg L16A-rev: caccagtgccgtcacCGCcagggtcaccgtgat
P6L P6L-fwd: ggcagcatcctctacCTCttcatcgtggtcccc P6L-rev: ggggaccacgatgaaGAGgtagaggatgctgcc	**V18C** V18C-fwd: acggtgaccctgctgTGCacggcactggtggtc V18C-rev: gaccaccagtgccgtGCAcagcagggtcaccgt

P11A P11A-fwd: cccttcatcgtggtcGCCatcacggtgaccctg P11A-rev: cagggtcaccgtgatGGCgaccacgatgaaggg	**V18A** V18A-fwd: acggtgaccctgctgGCGacggcactggtggtc V18A-rev: gaccaccagtgccgtCGCcagcagggtcaccgt
P11L P11L-fwd: cccttcatcgtggtcCTCatcacggtgaccctg P11L-rev: cagggtcaccgtgatGAGgaccacgatgaaggg	**V22A** V22A-fwd: ctggtgacggcactgGCGgtctggcagagcaag V22A-rev: cttgctctgccagacCGCcagtgccgtcaccag